Working Mechanism of Organic Friction Modifiers on Steel and Paper Materials

Yasushi Onumata

Submitted in accordance with the requirements for the degree of
Doctor of Philosophy

The University of Leeds

School of Mechanical Engineering

September 2016

The candidate confirms that the work submitted is his own and that appropriate credit has been given where reference has been made to the work of others.

Acknowledgement

Firstly, I would like to express my sincere appreciation to my primary supervisor Professor Anne Neville for the continuous support of my PhD study. It must have been challenging to accept the oversea research student who is possible to stay at the University only for two and half years. Her kind guidance based on immense knowledge on the tribology field helped me all the time of research and writing of this thesis.

Besides, I would like to thank my co-supervisor Dr Hongyuan John Zhao for his insightful comments and encouragement. His technical papers were the motivation for my decision to study in Leeds, and his deep knowledge and kind advice on the tribotest procedure or the analytical techniques kept supporting my research.

My sincere thanks also for Professor Ardian Morina, Dr Chun Wang and all the group members for providing me the precious opportunities to discuss the research topics. The experience and the network connections established in Leeds must be the irreplaceable treasure for my lifetime.

I thank my sponsor JX Nippon Oil and Energy Corporation for giving me the opportunity to study in the UK as a PhD student. Their financial support for the academic and the living expenses was essential to conduct the research. I'm coming back to work with them in Japan, and the experience and knowledge obtained in Leeds will be utilised for the lubricant in future.

Finally, I would like to thank my family; my wife Maki and children. I know it was quite hard time for them to live in the different culture, especially for Maki looking after our two energetic boys. It is thanks to their spiritual and continuous support that I could finish writing up the thesis.

Abstract

The effect of organic Friction Modifiers (FMs) on friction properties at steel and paper clutch materials is investigated, and their working mechanisms are assessed by the observation of reaction and adsorption films formed on the surface.

FMs are essential additives for drivetrain lubricants to manage friction properties. Recently developed fuel efficient transmission systems such as Continuously Variable Transmission (CVT) require precise and complicated friction control. As a result it is extremely important for the detailed behaviour of the FMs and in particular their reactions with the surfaces to be elucidated.

In this study, friction properties of organic friction modifiers, oleic acid, oleyl alcohol and glycerol mono-oleate, were evaluated by TE77 and MTM using steel and paper specimens, which simulate two major components of CVT; a steel belt-pulley mechanism and a paper clutch system. The surface films on the post-test materials were studied by SEM, EDX, XPS and ATR-FTIR to assess the influence of the FMs.

The results indicate that the friction properties are strongly affected by the substrate material and test temperature as well as the chemical structure of the FMs. In addition, interactions between the FMs and the other additives play an important role for the friction modification mechanism. In order to discuss the working mechanism of the FMs, the relationship between the friction properties and the chemical nature of the surface films was considered. Furthermore, the chemical structure of the FMs and its formulation suitable for CVT fluids are discussed.

Table of Contents

List of Tables

List of Figures

List of Publications

1) Onumata, Y., Zhao, H., Wang, C., Morina, A. and Neville, A., *"Interactive Effect between Organic Friction Modifiers and Additives on Friction at Metal Pushing V-belt CVT Components"*, Tribology Transactions, *Waiting for the reviewer scores*
2) Onumata, Y., Zhao, H., Mrina, A. and Neville, A., *"Behavior of Organic Friction Modifieres at Metal Pushing V-belt CVT Components in Different Temperature Conditions"*, Tribology Letters, *Ready for submission*

Chapter 1 - Introduction

1.1. Background

Reduction of CO_2 emissions has been a worldwide concern for dealing with global warming. The total amount of CO_2 discharged from automobiles keeps increasing due to expanding demands on cars in the world, especially in emerging countries. Considering the situation in EU, the CO_2 emissions from road transport have been increased by 22.6% in the period of 1990 to 2010 and passenger cars alone are responsible for around 12% of the emissions [1]. For the purpose of reducing CO_2 emissions, legislation has been regulated all over the world as shown in Fig. 1-1. EU established the strictest target, which requires 130 grams of CO_2 per kilometre (g/km) by 2015 and 95g/km by 2021 as a fleet average of new cars [2]. In order to achieve the targets, car manufacturers need to keep developing new technologies for improving fuel efficiency.

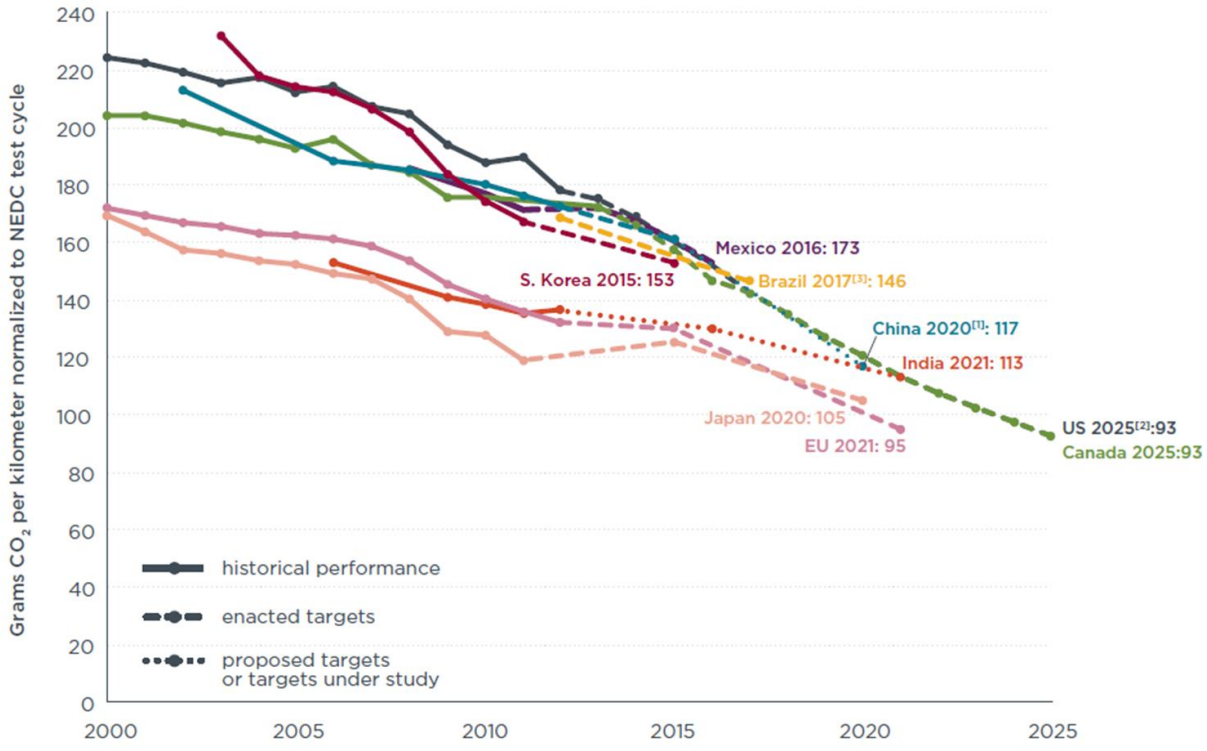

Fig. 1-1. Global CO_2 regulation for passenger cars, reprinted from [2]

The methodology for improving the efficiency can be divided into two types of approaches. The first is friction reduction at the components. The friction loss at the engine and the transmission occupies more than 10% of the energy consumption in cars as shown in Fig. 1-2. Engine oils and transmission fluids are able to contribute to decreasing the loss by reducing the viscosity as well as the friction on the substrate surface [3-5]. Although this approach has been successfully applied to a large number of commercial lubricants, the further improvement could be difficult considering negative influences on the reliability, such as wear and fatigue life [6].

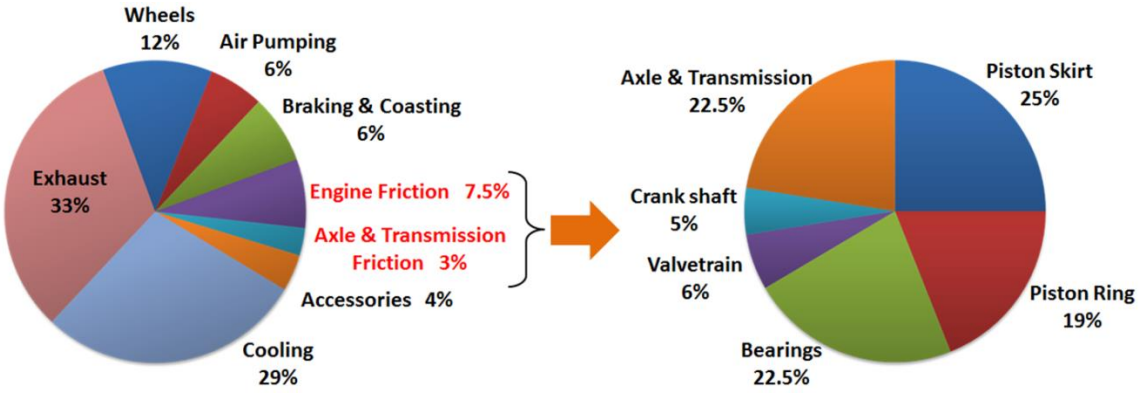

Fig. 1-2. Energy consumption in light-duty vehicles [7]

The second way is development of novel high fuel efficient systems. In case of engines, one of the recent successful examples is a combination of “downsizing” and “direct injection” technologies, which has significantly improved the engine efficiency [8, 9]. However, as a new technology usually leads to a new issue, it caused a problem of “low speed pre-ignition (LSPI)”. It has been revealed that certain additives in engine oil have influence on LSPI [10-12], and research on the new engine oil formulations dealing with LSPI is in progress all over the world. The advanced automotive systems generally require additional properties for the lubricants.

The circumstance is similar in terms of the transmission. In addition to traditional systems, Manual Transmission (MT) or conventional Automatic Transmission (AT), fuel-efficient transmission systems have been developed recently. Continuously Variable Transmission (CVT) has a steel belt-pulley gear shift mechanism, which enables the engine to run at the most efficient condition [13-15], while Dual Clutch Transmission (DCT) has two separate clutches for odd and even gear sets in order to minimise the shift time for better efficiency [16]. The issues are that they require much

more complicated and sophisticated friction control than the traditional systems as shown in Fig. 1-3. For example, the technical challenge for the CVT is the management of both steel and paper clutch frictions using only one lubricant. The steel friction at the belt-pulley should be kept higher, while the paper clutch requires friction modification. The behaviour of lubricant additives must be understood sufficiently in order to satisfy the opposite frictional requirements at the same time.

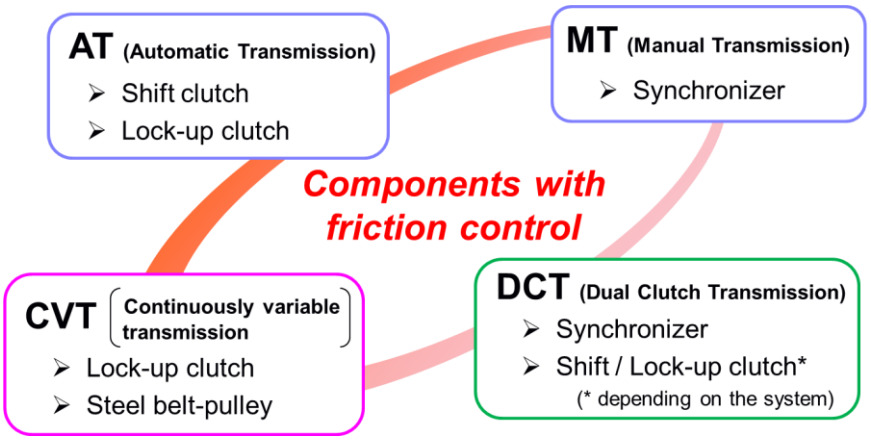

Fig. 1-3. Transmission components which requires frictional control

In summary, friction control is a key technology for improving the transmission efficiency, and the lubricants are expected to achieve it. One type of additive, so called Friction Modifier (FM), plays an important role on the friction management. Although it has been commonly and widely formulated in commercial lubricants for a long time, the working mechanism has not been understood sufficiently to satisfy the complicated friction control required by the advanced system.

This study aims to elucidate the working mechanism of FMs in a CVT fluid (CVTF). This knowledge is important for car and lubricant industries for designing high performance CVTFs whose frictional properties at steel and paper clutch material are optimised. In addition, it can also be utilised for developing other transmission fluids with the paper clutch system because the behaviour of the FMs on steel is also essential for the reliability of the steel components [17].

1.2. Objectives

The main objective of this research is to elucidate the working mechanism of Friction Modifiers (FMs). The following approaches were taken for achieving the purpose;

1) Lubricant formulation

- To investigate the relationship between the friction modification effect and the polar group structure in three types of organic FMs (oleic acid, oleyl alcohol and glycerol mono-oleate)
- To understand interactive effect between the FMs and other additives on the frictional properties

2) Sliding condition

- To observe the behaviour of the FMs on the different substrate; the steel and the paper clutch material
- To investigate the influence of test temperature and the sliding duration on the frictional performance

3) Surface analysis

- To assess the chemical nature of the adsorption and reaction film on the post-test specimen surface
- To detect the FMs on the surface, and estimate the working mechanism based on the chemical structure
- To link the assumed adsorption and reaction film structure on the surface with the frictional properties
- To elucidate the mechanism how the FMs, other additives and sliding conditions affect the frictional properties and the surface chemical nature.

1.3. Research Contribution

The knowledge gained from this study is essential for developing the CVTFs with the superior frictional performances. This technology helps to improve the efficiency and driving comfort of the CVT system, promoting a market share of the fuel-efficient cars equipped with the CVT. Therefore, it is able to contribute to reducing the CO_2 emission.

Furthermore, this research is also useful to enhance the efficiency of all the types of the lubricated systems. The FMs are capable of reducing the friction loss between the sliding surfaces, so that an appropriate formulation of the FMs can lead to a better efficiency. In this case, it is necessary to confirm if the FMs do not cause a negative effect on the other performances, such as anti-wear or anti-fatigue performance, since the FMs sometimes compete with the other additives. The insight on the interactive effect of the additives, which was investigated in this study, also contributes to the lubricant formulations satisfying both the high efficiency and the reliability.

1.4. Thesis Outline

The thesis structure is illustrated in Fig. 1-4, and the contents are summarised as follows;

Chapter 1 – Introduction

Chapter 2 – Literature Review

- CVT mechanism and the CVTF formulation are summarised
- Literature Review on the working mechanism of FMs are introduced

Chapter 3 – Experimental Procedures / Analysis of Starting Oils and Surfaces

- Test oil formulations, tribotest conditions and surface analysis techniques are explained
- ATR-FTIR spectra of the starting oils, additives and substrate surfaces are shown

Chapter 4 – Results – TE77 Steel Contact Tests

- TE77 friction test results at the steel/steel sliding configuration are presented
- The chemical nature and topography on the post-test steel surface are assessed using surface analysis techniques

Chapter 5 – Results – TE77 Paper Contact Tests

- TE77 test results at the paper/steel sliding configuration are presented for the initial and durability performances

- The chemical nature and topography on the post-test paper plates are investigated, and the post durability test oils are also assessed using ATR-FTIR

Chapter 6 – Results – MTM Paper Clutch Tests

- Friction properties of the FMs on the paper clutch are evaluated by MTM
- Post-test paper plates and lubricants are assessed

Chapter 7 – Discussion

Chapter 8 – Conclusions and Future Work

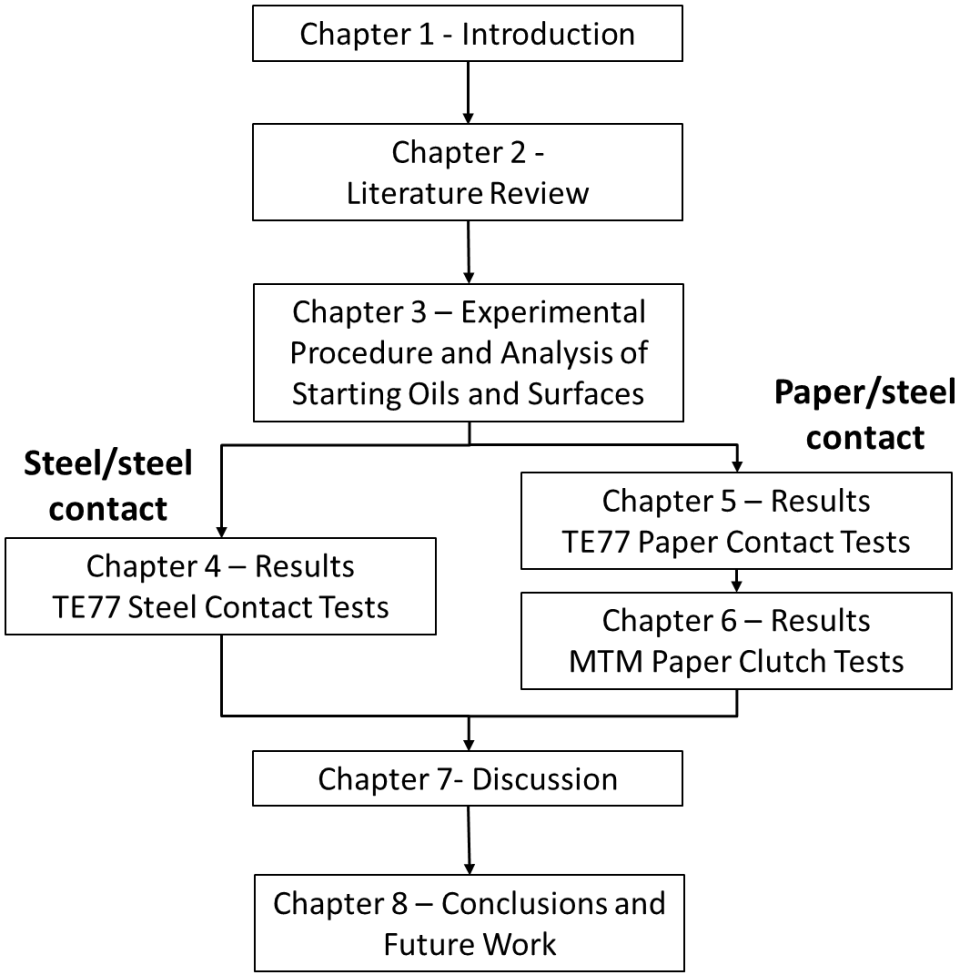

Fig. 1-4. Thesis structure

Chapter 2 – Literature Review

The basics of tribology and the application to an automotive field are introduced in this chapter. It is followed by the review of literature on the topic of this study, the friction modification at automatic transmission systems, and the originality and target of this study are presented.

2.1. Background

2.1.1. History of Tribology

Tribology is a science of interacting surfaces in relative motion, and the word origins from the Greek word "tribo" which means "rubbing". We humans have a long-term relationship with tribology because the rubbing occurs everywhere anything moves. There remains a picture in ancient Egypt, which illustrated a man pouring lubricant in front of a sledge to move a stone statue smoothly [18]. Then in middle ages, Leonardo Da Vinci studied friction and found an important observation; the force of friction is determined only by the weight of an object and doubled when the weight is doubled [18, 19].

In spite of this long history, the word "tribology" itself is relatively recent one, which was coined by the British physicist David Tabor and H Peter Jost in 1960's. Jost estimated economic loss derived from tribological phenomena (friction, corrosion and wear) and concluded that its waste reached £515 million at 1965 values [20, 21]. This report, famously known as the "Jost report", indicated the importance of tribology in industry and resulted in the foundation of several National centres of tribology in the UK and later all over the world.

2.1.2. Friction

The classical empirical friction laws in dry condition was firstly discovered by Leonardo Da Vinci in 15th century as stated above, and then rediscovered by Guillaume Amontons in 17th century [18, 19, 22-24] as follows;

- The force of friction is proportional to the applied load.
- The force of friction is independent of the apparent contact area.

This relationship is presented in the simple equation below;

$$F = \mu P$$

where F is the force of friction, μ is coefficient of friction (CoF) and P is the applied load. Later in 18th century, Charles-Augustin de Coulomb indicated additional empirical assumptions;

- The maximum static friction force is higher than dynamic friction force.
- Dynamic friction force is independent of the sliding velocity.

The friction force arises from the microscopic forces between the actual contact surfaces, which consist of molecular adhesion derived from Van der Waals and electrostatic force, and mechanical abrasion by elastic and plastic deformation. Therefore, μ, coefficient of friction, depends on wide range of parameters; composition of contacting materials, surface roughness, sliding condition (e.g. sliding velocity or contact pressure) and environment (e.g. temperature or humidity).

2.1.3. Lubrication

Dry direct rubbing between substrates possibly leads to deadly wear or adhesion. To reduce the friction for preventing the mechanical failure, fluid or solid is generally applied between the surfaces as lubricant. While refined mineral base stock is the most popular as the lubricant, various kinds of fluids or solids [25] (e.g. synthetic oils, greases, solid lubricants or gases) are applied suitable for the sliding condition and the environment. The lubricant enables to separate the surfaces of the sliding substrates completely or at least partially, resulting in achieving lower friction coefficient and longer life of mechanical parts.

The "Stribeck curve", named after Richard Stribeck, is usually used to illustrate the rubbing phases corresponded to the sliding condition as shown in Fig. 2-1 [24, 26]. According to the Stribeck curve, the sliding could be divided into four regions based on the viscosity of lubricant, sliding velocity and contact pressure. The horizontal axis of the Stribeck curve is represented as follows;

$$v\eta/p$$

where v is the relative velocity, η is the viscosity of fluid and p is the contact pressure between the surfaces. This relationship indicates that the contact mode changes to a milder phase (right side) when the sliding velocity or the lubricant's viscosity increases

or the applied load decreases. The characteristics of each regime are summarised in Table 2-1.

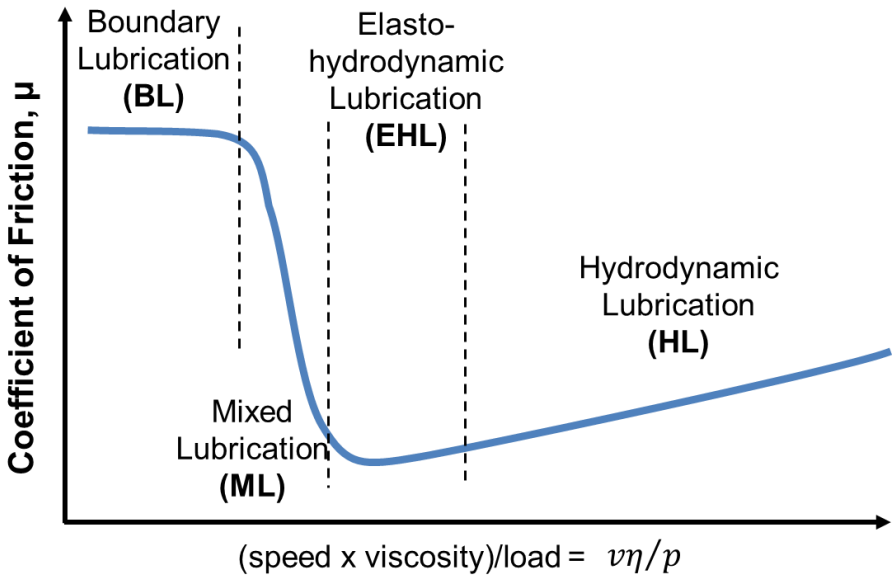

Fig. 2-1 Stribeck curve and friction regimes

Table 2-1. Characteristics of lubrication phases

Form of Lubrication	**Characteristics**
Hydrodynamic (HL)	The lubricating film is sufficiently thicker (typically 5-500μm) than the surface roughness of sliding substrates, and separates the surfaces completely. The behaviour of lubrication is determined simply by the Reynolds equation.
Elastohydrodynamic (EHL)	The film thickness is thinner than that in HL (typically 0.5-5μm), and the elastic deformation of contacting solids and the increase of lubricant's viscosity in high pressure condition play an important role to separate the surfaces.
Mixed (ML)	ML is the transition phase between HL/EHL and BL regimes in which two types of lubrication, fluid film and solid contact, affect simultaneously. The film thickness is typically 0.025-2.5μm.
Boundary (BL)	In BL phase, the coefficient of friction sharply increases (around 0.1 or higher) because of a large number of contacts between solids. The asperity, chemical composition on the substrate surface and the formulated additives in the lubricant have significant effect on the lubrication.

From a view of oil film formation and surface roughness of substrates, the lubrication phases are described based on “film thickness parameter”;

$$\Lambda = \frac{h}{\sqrt{\sigma_1^2 + \sigma_2^2}}$$

where Λ is film thickness parameter, h_{min} is the oil film thickness, σ_1 and σ_2 are roughness of relative sliding surfaces. This parameter increases along with the thicker oil film and the smoother surfaces. The relationship between the film thickness parameter and lubrication conditions are described as follows;

- $\Lambda > 3$; HL or EHL (adequate oil film thickness between substrates)
- $1 \leq \Lambda \leq 3$; ML (partially solid contact)
- $\Lambda < 1$; BL (fully solid contact)

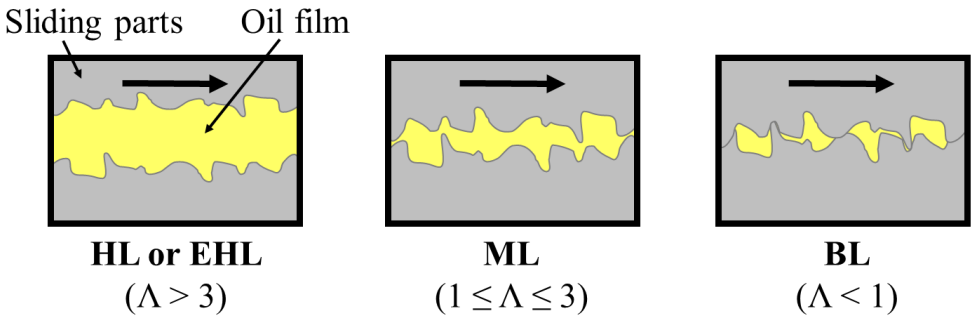

Fig. 2-2. Schematic view of lubrication phases

2.2. Lubrication Technology in Automotive Systems

There are a large number of lubricated components in automotive vehicles where a wide range of lubricants are applied to manage an appropriate lubrication, such as engine oil, transmission fluid, brake fluid, power steering fluid, refrigerating oil for the air conditioner or grease. [23, 24, 27]. Among them, the engine oil and the transmission fluid are the most major lubricants considering the roles as well as the sales volumes.

In this section, the lubrication in engines and transmissions is briefly described and compared for the better understanding of the lubrication mechanism in this study, which focuses on the Continuously Variable Transmission (CVT). The requirements for the lubricants used in the engine and the transmissions are introduced, and then the typical lubricant formulation and additives for the automatic transmission are explained.

2.2.1. Lubrication in Engines

A schematic image of a typical internal combustion engine is shown in Fig. 2-3 [24, 28-30]. There are three major rubbing parts in the engine, the valve train, the piston and the crank shaft, and they are in different friction regimes. Boundary lubrication is dominant at the valve train between the cam and a valve lifter, while an oil film separates a shaft and a bearing completely at the crank shaft. At the piston, the lubrication condition stretches from mixed to hydrodynamic lubrication because the velocity of piston changes widely in its reciprocating motion. The sliding conditions are summarised in the Stribeck curve as shown in Fig. 2-4.

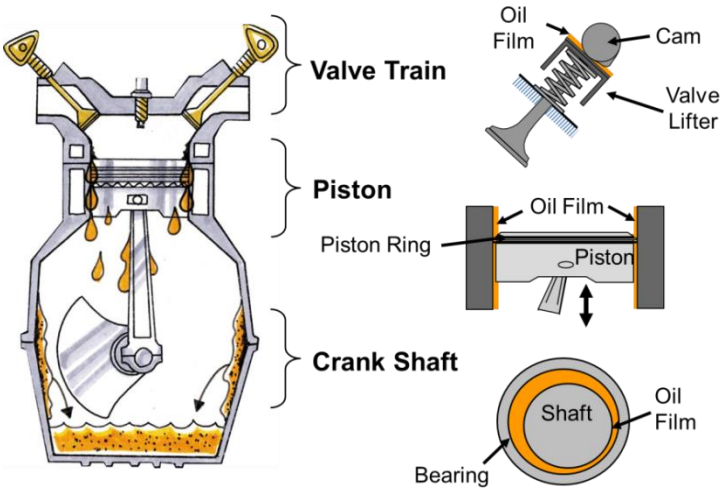

Fig. 2-3. Schematic image of the internal combustion engine
(figure courtesy of JX, JX Nippon Oil & Energy Corporation)

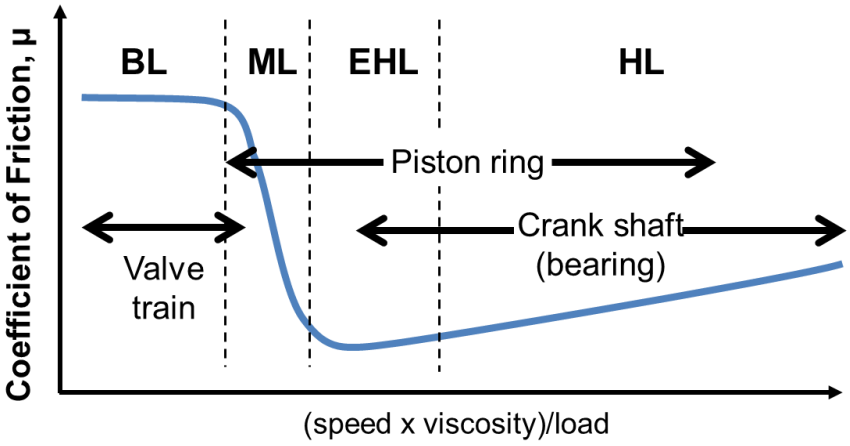

Fig. 2-4. Friction regime of engine components

The following are the major functions required from the engine oil.

- Lubrication

  Prevent wear and seizure. Considering the efficiency loss, viscosity (especially at high speed and high temperature) is important at the crank shaft and piston ring, while tribofilm compositions formed by the additives are significant at the valve train.
- Detergency/anti-oxidation

  Cleanse combustion products inside the engine and neutralize degradation products. Due to high combustion temperature, a large number of combustion and degradation products are produced in the engine. Therefore, excellent detergency and anti-oxidation performance are required for the engine oil.
- Cooling

  Adsorb and disperse the combustion heat. The heat transfer from the combustion chamber (high temperature) to the oil pan (relatively low temperature) is conducted by the engine oil.
- Sealing

  Prevent the combustion gas to diffuse through the piston. The lubricant around the piston ring enables to separate the combustion chamber and the crank case completely, which prevents compression leakage.

Global engine oil standards are managed by mainly three organizations; API (American Petroleum Institute), ILSAC (International Lubricant Standardization and Approval Committee) and ACEA (European Automobile Manufacturers' Association) [31]. It is allowed to supply an engine oil with the certain approval into the corresponding engine.

2.2.2. Lubrication in Transmission Systems

The role of the transmission systems is to convert the engine torque and rotational speed suitable for the driving condition. They can be divided into two categories, manual transmission (MT) and automatic transmission. Furthermore, the automatic transmission is classified into three major types based on its torque conversion system; conventional automatic transmission (AT), continuously variable transmission (CVT) and dual clutch transmission (DCT). The MT has a large market share in Europe, while ATs are major in the US and Japanese market probably due to the difference in the driving conditions and the car manufacture's strategies [32, 33]. The CVT has a significant share in

Japanese market, and is expanding the share mainly in Asian developing countries [34-36]. For the purpose of improving the efficiency, all the transmissions keeps to be upgraded [16] as shown in Fig. 2-5.

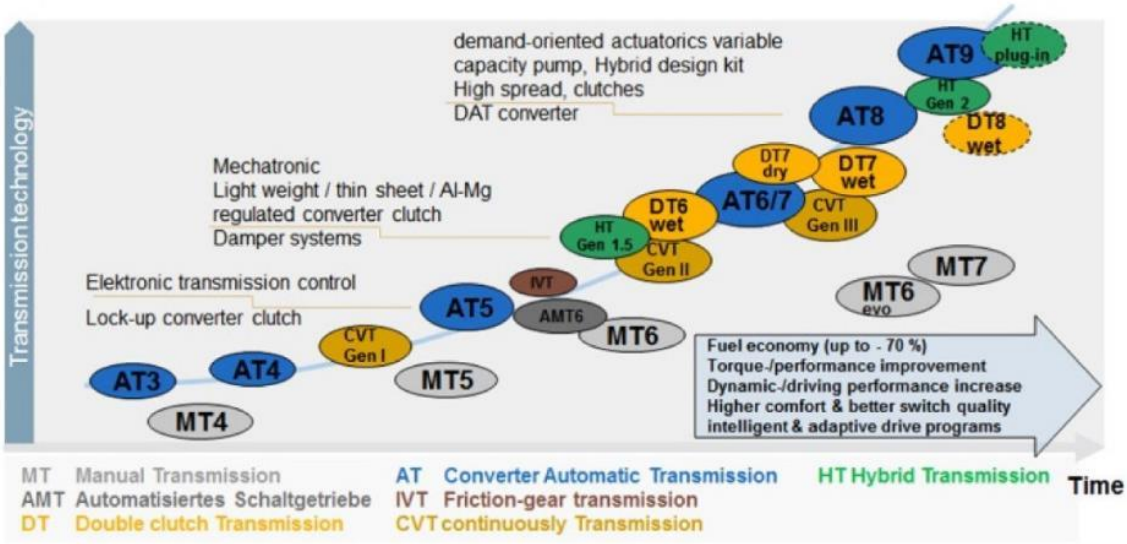

Fig. 2-5. Development of the transmission efficiency (reprinted from [16])

General requirements for transmission lubricants are compared to those of engine oils as follows;

- Lubrication

  Friction control is necessary for all the transmission systems as shown in Table 2-2. It means friction property needs to be controlled appropriately for the torque transfer mechanism, while lower friction is simply preferable for engine oils. Additionally, in some case, certain types of gears require a higher anti-wear and extreme-pressure performance than the engine components.

- Detergency/anti-oxidation

  Transmissions are operated under the milder environment than engines due to lower temperature. However, extremely longer drain interval that sometimes reaches whole car life (e.g. 200,000 km drain interval) is required.

- Cooling

  The heat generated at the sliding components is transferred by the lubricants, and released to the outside through the transmission case.

- Sealing

  Some axial shafts or components are sealed by a combinational work of oil seals and the lubricant.

Table 2-2. Friction performance commonly required by transmission systems

Transmission types	**Components and required performances**
Manual Transmission (MT)	- Synchronizer/gear (brass/steel) high torque capacity, low stick torque
Conventional Automatic Transmission (AT)	- Lock-up clutch (steel/paper) high torque capacity, μ-V characteristics - Shift clutch (steel/paper) high torque capacity, low shift shock
Continuously Variable Transmission (CVT)	- Steel belt/pulley (steel/steel) high torque capacity - Lock-up clutch (steel/paper) high torque capacity, μ-V characteristics - Shift clutch (steel/paper) high torque capacity, low shift shock
Dual Clutch Transmission (DCT)	- Shift clutch (steel/paper) high torque capacity, low shift shock - Synchronizer/gear (brass/steel) high torque capacity, low stick torque

Different from the engine oils, the automatic transmission fluids (ATF, CVTF or DCTF) do not have global standards issued by international organizations. Although some car manufactures have their original approvals, such as DEXRON by General Motors or MERCON by Ford Motor company [37], the genuine lubricants are generally designed as suitable for the specific transmissions due to the significant difference in the system layouts based on the strategies of each car company. Therefore, it is necessary to modify and adjust the transmission fluid formulations, as a made-to-order lubricant, to meet the requirements of the specific system. Deep understanding about the working mechanism of the lubricant additives is highly demanded for developing superior automatic transmission fluids quickly and efficiently.

2.2.3. Conventional Automatic Transmission (AT)

The mechanism of the AT is briefly explained before the CVT because they have same clutch systems in common; the lock-up clutch and the shift clutch [24, 32, 38]. Both systems are operated by a combination of paper clutches and counter steel plates.

The schematic layout of the AT is illustrated in Fig. 2-6. The rotational torque generated in the engine is input form the right side of the figure, and transferred through the torque converter which corresponds to a manual clutch plate in the MT. Then, the power is converted into the rotational speed and torque appropriate for the driving condition at the shift clutch and planetary gear mechanism. A suitable set of the gears can be selected automatically managed by the hydraulic control unit. The AT fluid (ATF) lubricates all the components inside the AT and also works as hydraulic fluid for the shift control.

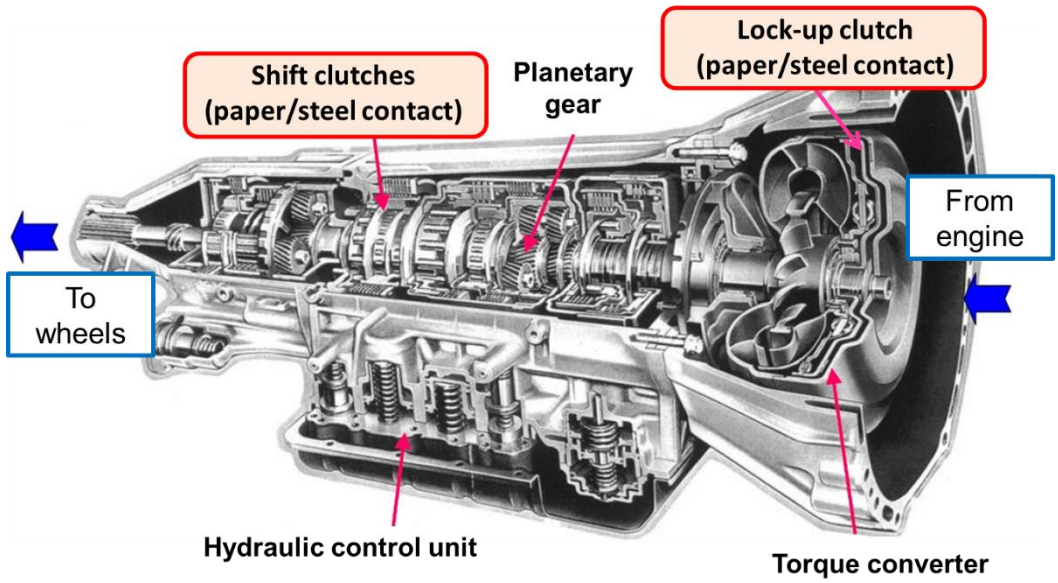

Fig. 2-6. Schematic layout of the FR (Front engine Rear drive) AT
(figure courtesy of JX)

The lock-up clutch is installed inside the torque converter for the fuel efficient control of the torque converter as shown in Fig. 2-7. It consists of a combination of the paper clutch and the counter steel plate. The working mechanism of the lock-up clutch is explained in Fig. 2-8. The torque converter is fully filled with ATF. It works as a fluid coupling at low speed condition for amplifying the engine torque and absorbing the rotational fluctuation. Once it reaches at high speed, generally over 60 km/h, the lock-up

clutch engages (lock-up) to connect the input shaft and the gear shift mechanism directly in order to prevent churning loss caused by the ATF inside the torque converter. Furthermore, partial torque transmission through the lock-up clutch, so called “slip-control”, is operated at the intermediate speed region for additional fuel efficiency [39]. The friction management is necessary for the smooth sliding control of the lock-up clutch system, and previous studies based on mathematical approaches [40, 41] revealed that a relationship between the sliding speed and the friction coefficient, so called “μ-V characteristics”, is essential for the smooth clutch control. As shown in Fig. 2-9, a positive μ-V relationship is preferable, and a negative curve should be avoided since it tends to cause self-excited vibration at the clutch, so called “shudder”.

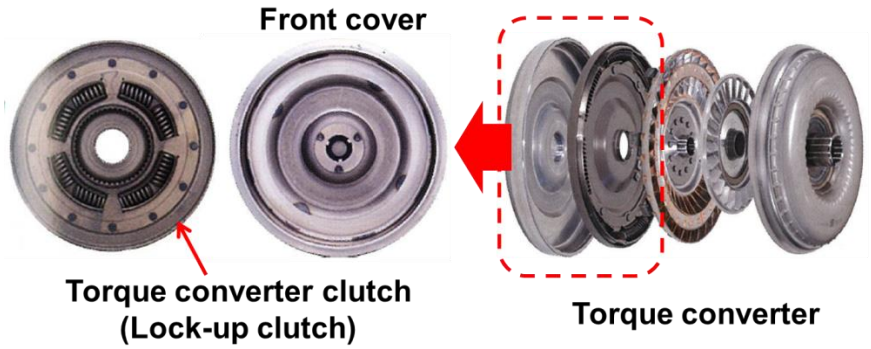

Fig. 2-7. Layout of the torque converter mechanism
(photos courtesy of JX)

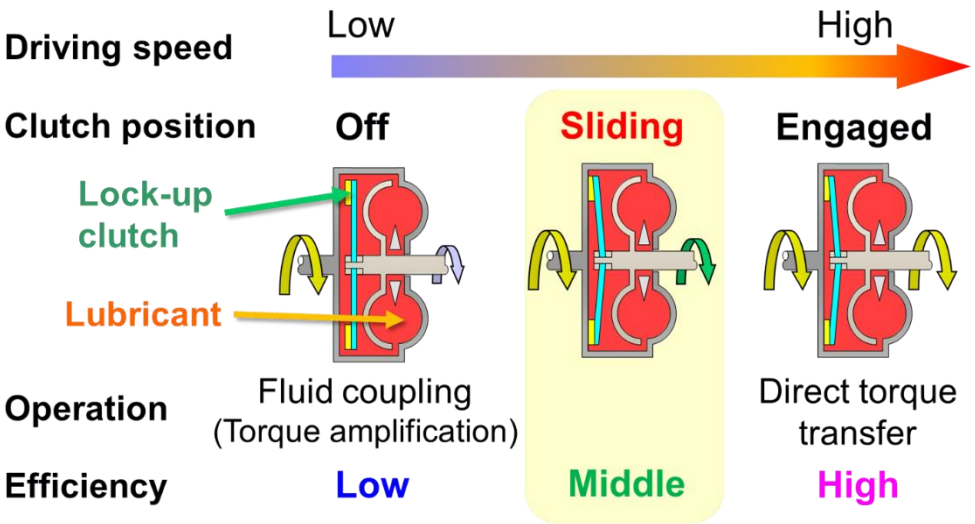

Fig. 2-8. Schematic diagram of the lock-up clutch control system

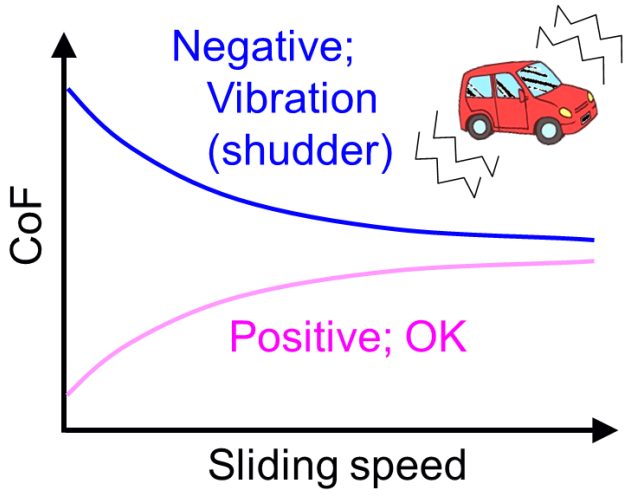

Fig. 2-9. Frictional property at the lock-up clutch (μ-V characteristics)

The second component, the shift clutch, consists of combination of paper clutches and steel plates. It enables the gears to shift automatically by connecting the certain planetary gear-set with the use of the shift clutch mechanism. In terms of the frictional control, it is necessary to prevent shift shock and shorten the gear shifting time [42]. Although the operating speed and acceleration ratio for the clutch engagement are significantly different from the lock-up clutch, the FMs generally work in the similar manner; reducing the friction at low sliding speed leading to smooth clutch engagement [43]. Therefore, this study focuses on the clutch performance at the lock-up clutch for the observation of the FM behaviour on the paper material.

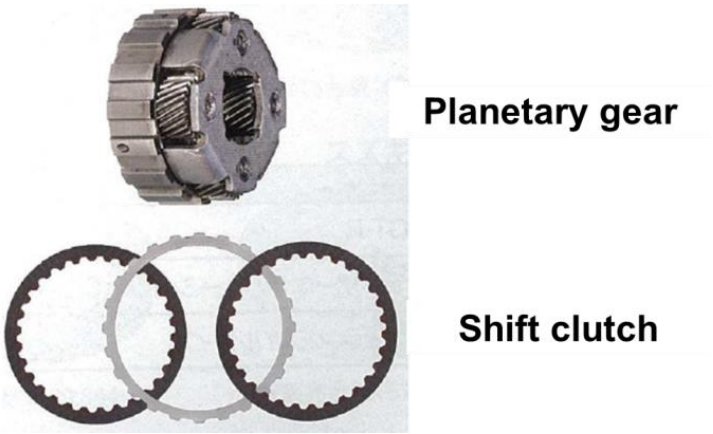

Fig. 2-10. AT gear shift mechanism (shift clutches and a planetary gear)
(photos courtesy of JX)

2.2.4. Continuously Variable Transmission (CVT)

The CVT equips a steel belt-pulley mechanism for the shift change, instead of the planetary gears in the AT. A schematic layout of the CVT and the belt-pulley mechanism are illustrated from Fig. 2-11 to Fig. 2-13. The belt-pulley mechanism works similar to the shift mechanism of a bicycle. Both the primary and the secondary pulley are able to change the wrapping radius of the steel belt independently by adjusting the distance between sheaves, which realises continuously variable gear shift. This operation has an advantage that makes it possible to run the engine in a highly efficient condition [44].

The CVT also has a torque converter and shift clutch system in addition to the belt-pulley. Therefore, the CVTF needs to satisfy the frictional requirements at the paper clutch systems as well as at the steel belt-pulley. It is challenging because higher friction coefficient is preferable at the steel belt-pulley to transfer large amount of torque, while friction modification is necessary at the clutches to prevent shudder [45, 46].

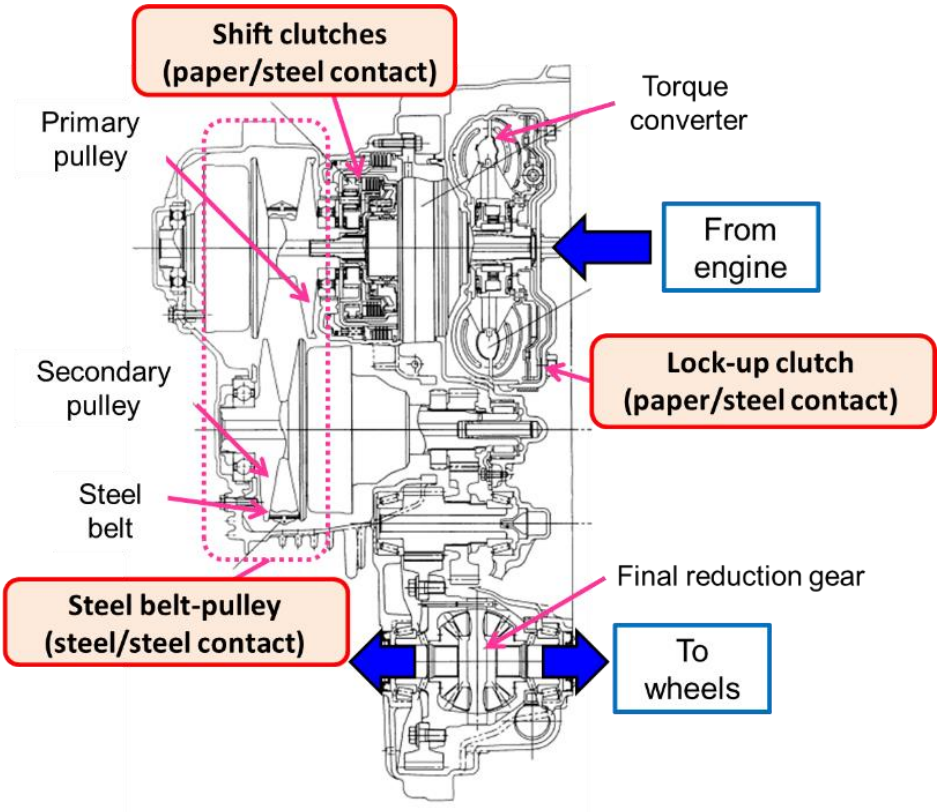

Fig. 2-11. Schematic layout of CVT (reproduced from [44])

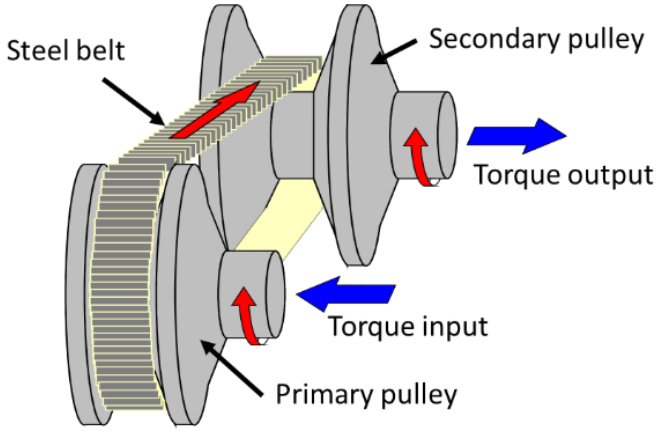

Fig. 2-12. Schematic image of the belt-pulley mechanism in CVT
(figure courtesy of JX)

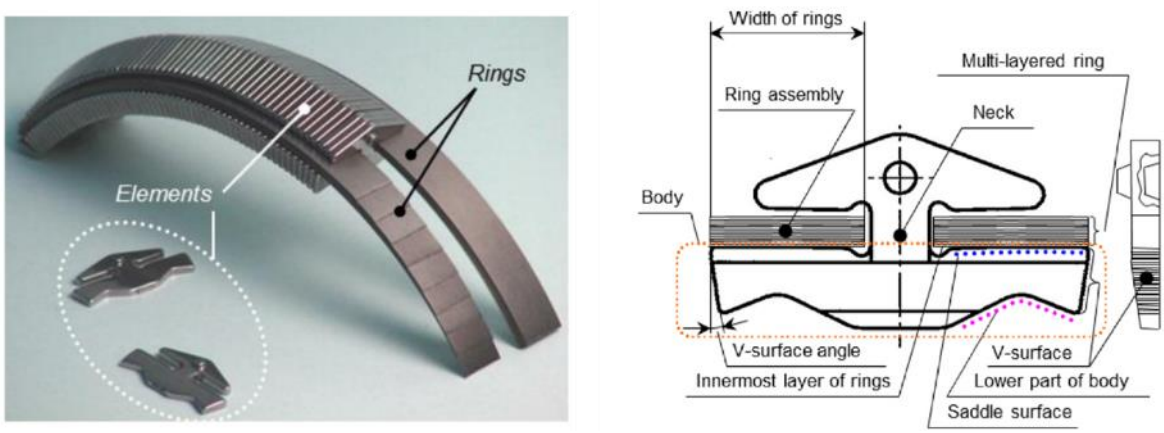

Fig. 2-13. Configuration of elements and ring assembly of CVT steel belt
(reprinted from [47])

2.3. Automatic Transmission Fluid (ATF)

2.3.1. Formulation Basis

The automotive lubricants generally consist of base oils, viscosity modifiers (VMs) and the other additives as shown in Fig. 2-14. The viscosity of the lubricants is mainly determined by the base oil and the viscosity modifier, while the additives contribute to other properties, such as anti-wear, extreme-pressure, anti-oxidation, deforming or friction modification [48]. In this section, the basis of the base oil and the other additives typically formulated in the automotive lubricants is briefly introduced for the better understanding of the test oil formulations in this study.

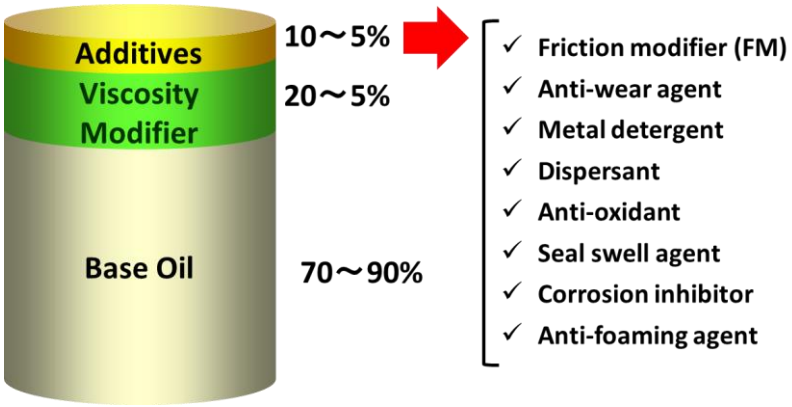

Fig. 2-14. Typical formulation of automotive lubricants

2.3.2. Base Oil

Base oils can be roughly divided into two types, refined mineral base oils and synthetic oils [25]. American Petroleum Institute (API) categorises them into 5 groups (Group I – V) as shown in Fig. 2-15. The mineral base stocks are classified as Group I to III based on their performance attributed to chemical compositions of crude oils and the refining process. Group IV and V are for synthetic oils. Group IV is Poly-α-olefin (PAO), which is generally synthesised by oligomerisation of 1-decene, and all the other synthetic stocks (such as ester or ether) are categorised as Group V.

A factor, Viscosity Index (VI), is commonly used to explain the temperature dependence of lubricant viscosity. A high VI means low temperature dependence, which is useful to improve efficiency because it enables the churning loss to be reduced at the low temperature while keeping thick oil film at high temperature [49].

Category	Sulfur, %		Saturates, %	Viscosity Index
Group I	＞ 0.03	and/or	＜ 90	80～119
Group II	≦ 0.03	and	≧ 90	80～119
Group III	≦ 0.03	and	≧ 90	≧ 120
Group IV	Poly-α-olefin（PAO）			
Group V	All others not included in Group Ⅰ,Ⅱ,Ⅲ or Ⅳ			

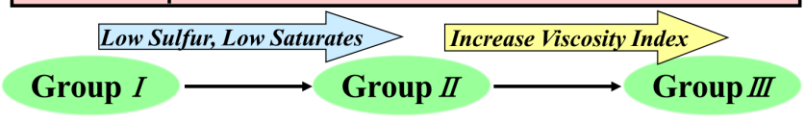

Fig. 2-15. API categories of base stocks

2.3.3. Viscosity Modifier (VM)

The VM is a polymer that enables to increase viscosity and VI of lubricants. Poly-methacrylate (PMA) is widely used for the automotive lubricants due to the superior oil film thickening and VI improving effect. The range of PMA's molecular weight is generally between 10,000 and 1,000,000, which is selected to meet the requirements of the lubricants such as viscosity, shear stability or pour point.

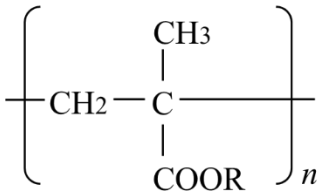

Fig. 2-16. Typical molecular structure of PMA

2.3.4. Zinc Dialkyl Dithiophosphate (ZDDP)

ZDDP is one of the oldest and probably the most famous additives [50]. Initially, it was formulated as an anti-oxidant, and later the superior anti-wear was known. It is commonly used in the engine oils, and the working mechanism and the reaction film formed by the ZDDP have been intensively studied. However, in spite of the excellent performances, the ZDDP is not generally formulated in the automatic transmission fluids due to the negative effect on the paper clutch performance. ZDDP tends to damage the paper clutch material leading to the shorter life [51].

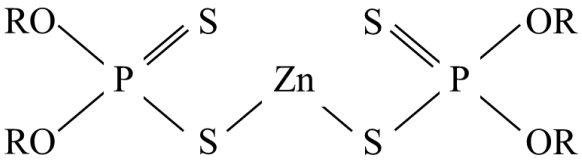

Fig. 2-17. Typical molecular structure of ZDDP

2.3.5. Molybdenum Dithiocarbamate (MoDTC)

MoDTC is categorised as the friction modifier and essential for the engine oil to improve the fuel efficiency. It is able to form molybdenum disulphide (MoS_2) solid laminar films with extremely low friction coefficient on the metal structure. Same as the

ZDDP, the MoDTC is also difficult to be formulated into transmission fluids because the MoS_2 film decreases the clutch torque capacity significantly.

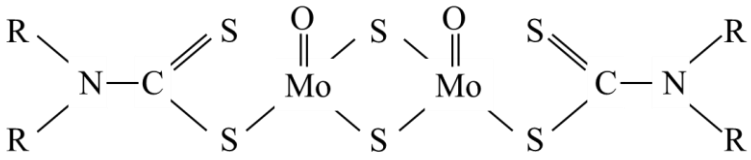

Fig. 2-18. Typical molecular structure of MoDTC

2.3.6. Organic Friction Modifier (FM)

The organic FMs are friction-reducing agents that do not contain metal elements, such as Mo, Zn or Ca. The chemical structure of the FM is the same as surfactants, which consists of one or multiple polar groups (e.g. acid, ester, alcohol, amine or amide) and one or multiple hydrocarbon chains. It is supposed to form the adsorption film attaching its polar groups onto substrate. The film works as a cushion and enables to prevent the solid contact between the sliding surfaces, resulting in low friction coefficient.

The working mechanism of the organic FMs is the main topic of this research, and relevant theories and previous studies are introduced in detail at next section, "2.4. Literature Review on Working Mechanism of FMs".

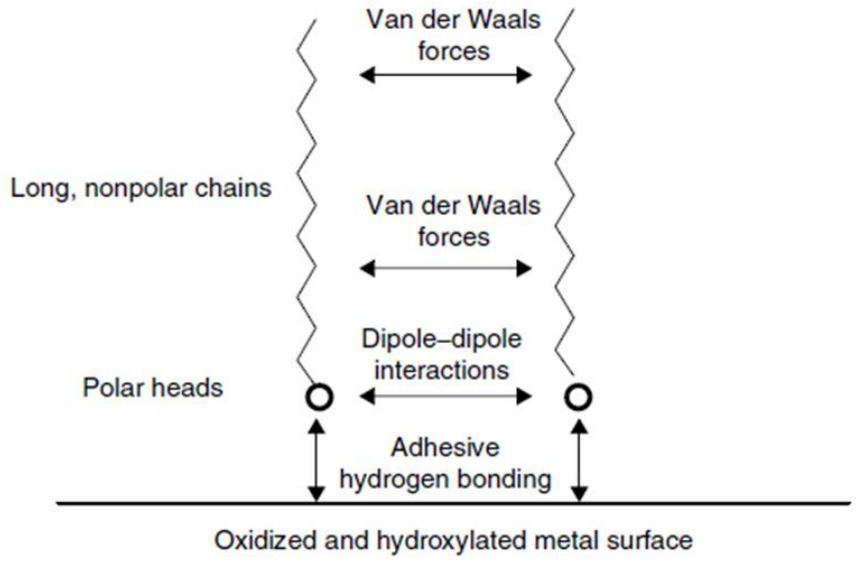

Fig. 2-19. Schematic image of organic FM adsorption (reprinted from [52])

2.3.7. Phosphorous Anti-wear Agent

Organic phosphorous components (e.g. phosphate, phosphite or thiophosphate) are generally formulated as an anti-wear agent. They are able to react on the substrate surface together with the other additives, forming a reaction film including phosphorous. The reaction film tends to be harder than the film without P, so that good at improving the anti-wear performance of lubricants.

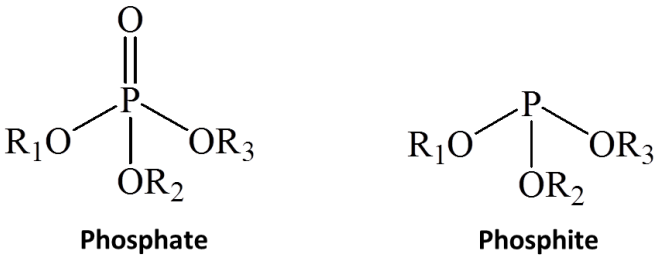

Fig. 2-20. Typical molecular structures of phosphorous anti-wear agent

2.3.8. Metal Detergent

The role of the metal detergent is to neutralise and disperse degradation products. The major chemical structures are selected from sulfonate, salicylate or phenate, while the metal element is basically calcium or magnesium. For the better neutralisation performance, a metal carbonate core is usually applied to increase the base number, which is called as an over-based metal detergent. The core is dispersed by metal detergent molecules as shown in Fig. 2-22.

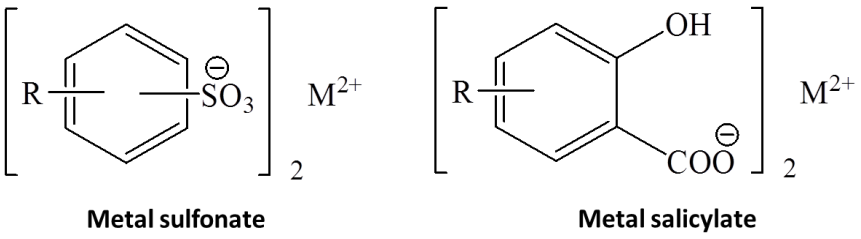

Fig. 2-21. Typical molecular structure of metal detergent

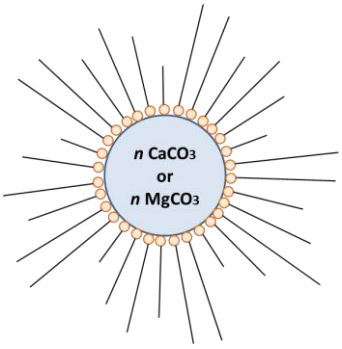

Fig. 2-22. Schematic image of over-based detergent

2.3.9. Dispersant

The dispersant is formulated for dispersing sludge into the lubricant in order to prevent sediment formation. Poly-isobutylene succinimide (PIBSI) is widely used due to the excellent dispersing performance as well as the low production cost. In addition, it is commonly known that the dispersant also has an influence on the frictional performance [53]. It tends to affect forming an adsorption film at the higher sliding velocity region than the FMs, because the molecular weight of the dispersant is considerably larger than the FM.

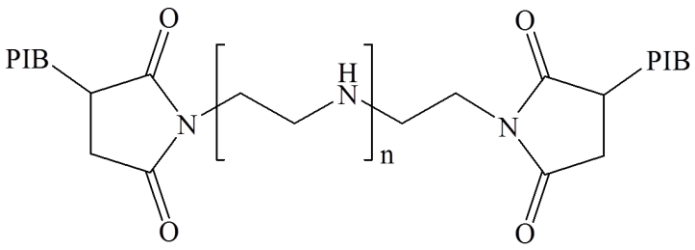

Fig. 2-23. Typical molecular structure of dispersant
(Poly-isobutylene succinimide, PIBSI)

2.3.10. Anti-oxidant

The anti-oxidants prevent oxidation of lubricants by acting as a radical scavenger. An aromatic amine and a hindered phenol types are generally used for the automotive lubricants. They are able to trap and stabilise harmful radicals, which are produced under severe thermal condition, by donating a proton at the amine or the phenol group.

It is considered that the anti-oxidants do not have a significant effect on the friction or the reaction film formation due to the low polar chemical structure [54].

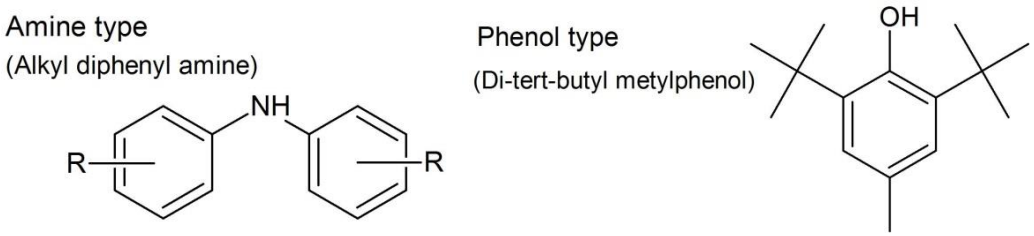

Fig. 2-24. Typical molecular structure of anti-oxidants

2.4. Literature Review on Working Mechanism of FMs

2.4.1. Adsorption Film Formation

Friction reduction has been of interest of engineers in order to decrease frictional loss as well as to prevent damage of tools or machines. The history of the studies on the adsorption film formed by the FMs is summarised in this section for the better understanding of the application to the transmission fluids [55-57].

In the 1920s, the presence of “oiliness” in certain lubricants, independent of the viscosity, was noticed. The lubricants possessing long-chain oxygenated compounds, such as vegetable oils, showed better lubrication at low sliding speed [58]. Hardy [59, 60] studied this phenomenon and indicated that the effect of oiliness depends on a type of polar group and molecular weight of the component as shown in Fig. 2-25. Based on the results, he suggested a monolayer theory at boundary lubrication condition (Fig. 2-26). It insisted that polar molecules are capable of forming monolayer with low shear strength on sliding surfaces, which is effective to reduce friction. Moreover, Bowden [61] studied the durability of the adsorbed film by the use of Langmuir-Blodgett films of stearic acid deposited on steel. The result showed that a single layer was effective only at initial, then the friction started to increase just after a few cycles (Fig. 2-27). This result implied that the FMs need to be constantly supplied onto the surface in order to keep low friction, because the adsorption film on the surface could be consumed by sliding.

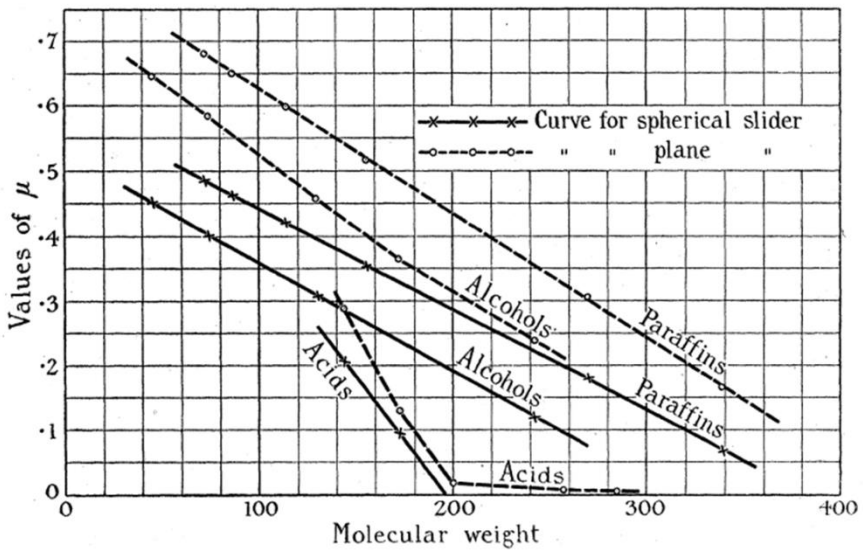

Fig. 2-25. Dependence of friction coefficient on polar group and molecular weight (reprinted from [60])

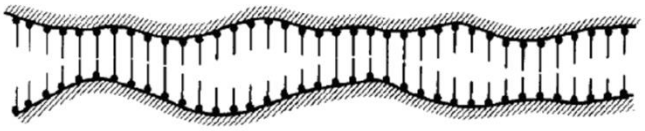

Fig. 2-26. Hardy monolayer boundary model (reprinted from [55, 62])

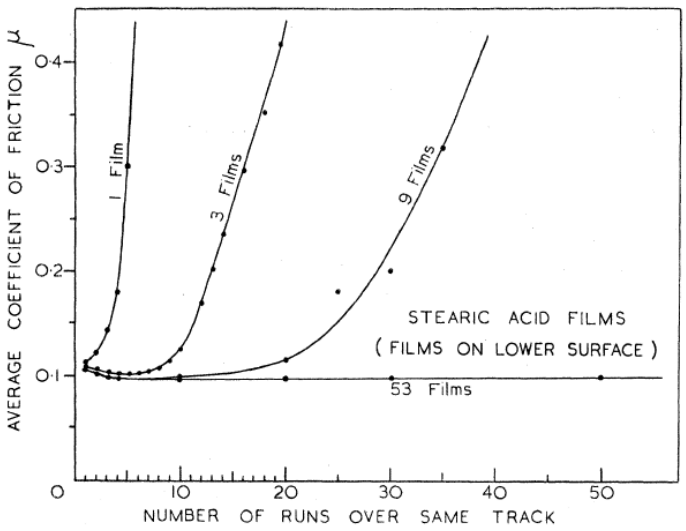

Fig. 2-27. The friction of stearic acid films formed on steel surface (reprinted from [61])

On the other hand, there have been some reports indicating the presence of multilayer adsorption. Fuks [63] measured the film thickness formed by naphthenic mineral oil (MS-20) and cyclohexane on steel and observed the stable film ranging between 50 and 350 nm as shown in Fig. 2-28. It is much thicker than expected from monolayer film formation, therefore, it implied the existence of multilayer. Interestingly, the thickness increased significantly when stearic acid was added into the oils. Allen [56] examined the previous studies and proposed "ordered liquid model" shown in Fig. 2-29. This model also indicated the multilayer adsorption; rod-like dimers are formed by a hydrogen bond between polar groups of the additive, and they stack onto the surface monolayer to construct multilayer films.

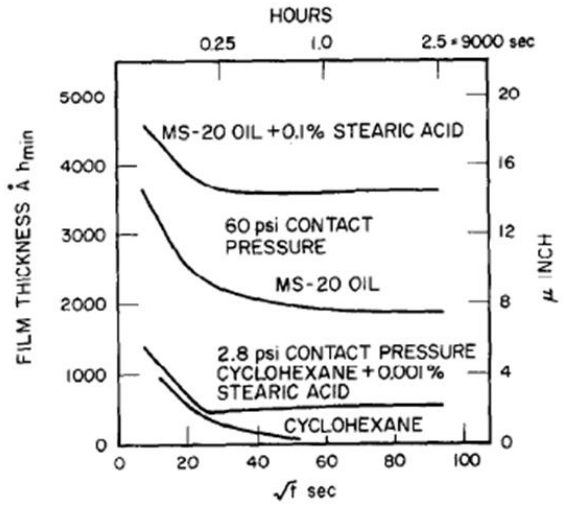

Fig. 2-28. Residual film formed by mineral oil and cyclohexane solutions [63], (reprinted from [56])

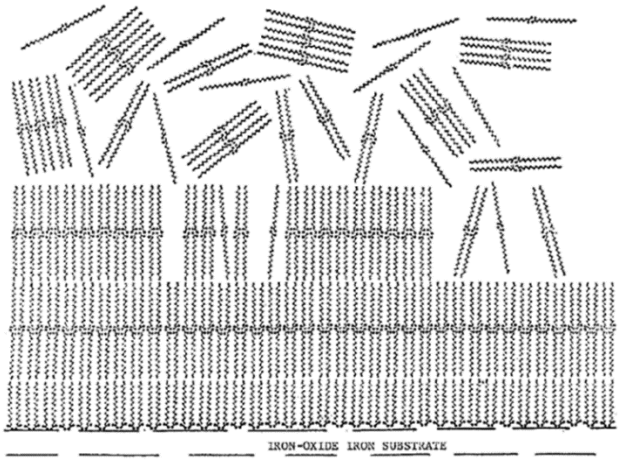

Fig. 2-29. Schematic image of stearic acid films according to the ordered liquid model [56]

Recently, Spikes [64-66] performed *in-situ* measurement of the adsorption film thickness on steel using ultrathin film interferometry. The observed film thickness ranged from a few nanometres (monolayer) to tens of nanometres (multilayers) influenced by various factors; the chemical structure or the purity of the FMs, test temperature or humidity. Fig. 2-30 shows the effect of humidity on the adsorption film formation of stearic acid. The linear line in the graph is the film thickness calculated based on the EHL theory. Although stearic acid was capable of forming the adsorption film even in dry conditions as the film thickness is above the theoretical value, the humidity promoted the film formation up to 10 nm. This result could be a reasonable insight for the argument on "monolayer vs multilayer". The formation of the adsorption film is significantly affected by external factors. Therefore, the film thickness should stretch from the monolayer to the multilayer regions even formed with the same FM.

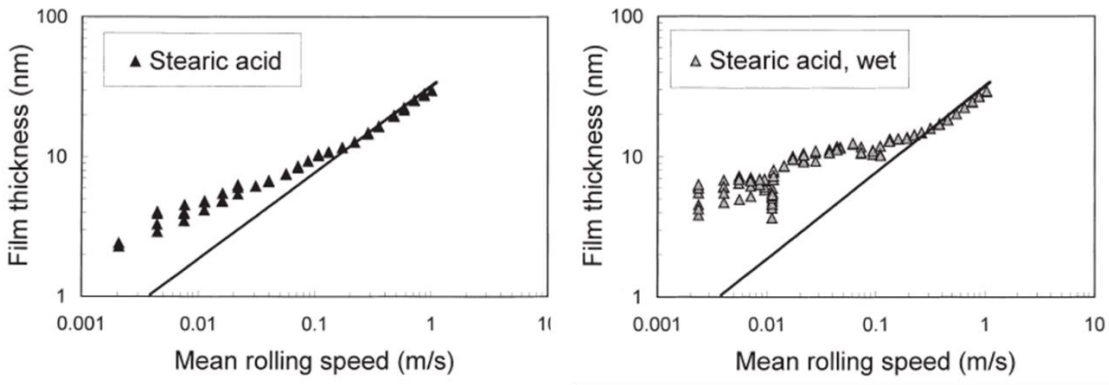

Fig. 2-30. EHD film thickness vs speed for 0.1wt% stearic acid in hexadecane
left; dry condition, right; wet condition (reprinted from [66])

The working mechanism and the chemical nature of the FMs on the substrate surface have been discussed intensively. Yoshida [67] investigated the friction of oleic acid and oleyl alcohol on different substrates; bearing steel, a-C:H DLC and ta-C DLC, and concluded that the type of the substrates has a significant effect on the friction reduction as shown in Fig. 2-31. Kalin [68] also reported the similar results in the research evaluating the effect of an alcohol FM on steel and DLC substrates. Atomic Force Microscopy (AFM) was utilised to detect the adsorption film of the alcohol on the surface, and the correspondence with the friction coefficient was successfully explained. Kano [69] studied the mechanism of ultralow friction caused by glycerol monooleate (GMO) on DLC surfaces. The Time of Flight Secondary Ion Mass Spectrometry (TOF-

SIMS) analysis of the post-test DLC specimen detected carboxylic acid only on the wear track (Fig. 2-32), and they concluded the tribochemical decomposition of GMO should be the reason of the ultralow friction. Furthermore, there are a large number of attempts to observe the detailed chemical nature on the surface with the use of latest surface analysis techniques, such as neutron reflectometry [70, 71], sum frequency generation spectroscopy [72] or temperature-programmed desorption and reflection-adsorption infrared spectroscopy [73].

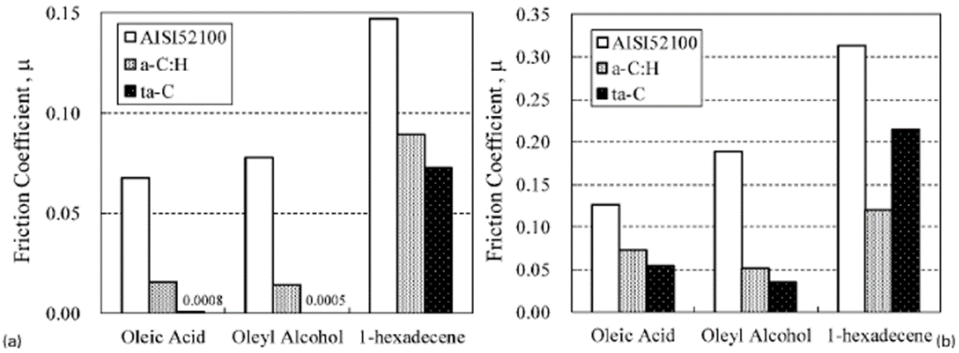

Fig. 2-31. Friction coefficient of three types of specimen lubricated with three types of lubricants, (a) at 50 mm/s, (b) 0.01 mm/s (reprinted from [67])

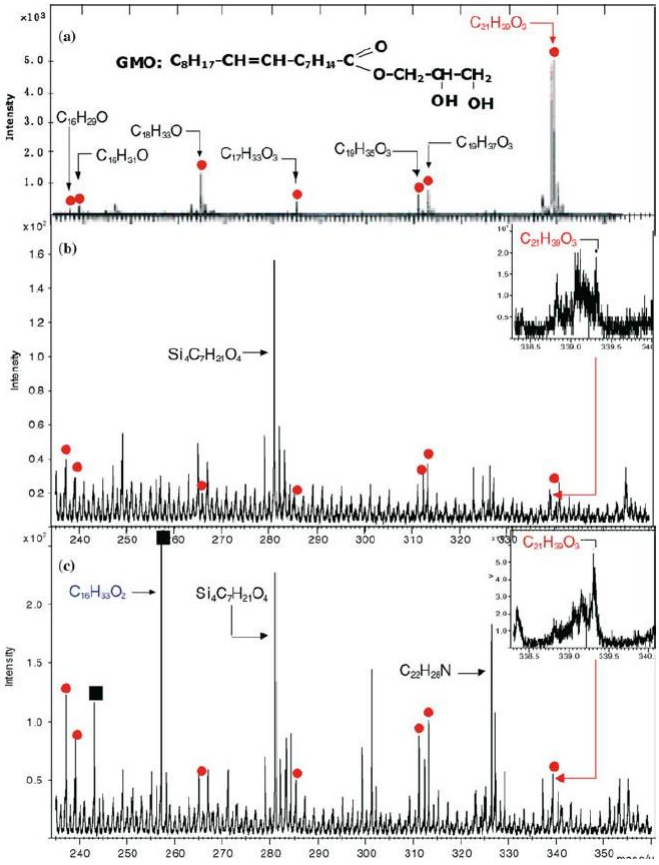

Fig. 2-32. TOF-SIMS analysis, (a) GMO and the post-test DLC specimen (b) outside wear track and (c) on the wear track (reprinted from [69])

2.4.2. Interaction with Other Additives

In commercial lubricants, various kinds of additives are formulated together with FMs. Some of the additives form the adsorption or the reaction film on the substrate surface, which possibly has synergistic or antagonistic influence on the effect of the FMs. Therefore, the lubricants are necessary to be designed taking into account the interactions between the FMs and the other additives.

A large number of reports have focused on the interaction with the ZDDP reaction films due to the wide range of the ZDDP application to the commercial lubricants represented by the engine oils. The chemical composition and geometry of the ZDDP reaction film and the chemical reaction mechanism have been of interest of many researchers [50, 74-78]. It is generally confirmed that the ZDDP forms the characteristic reaction film with pad-like structure which mainly consists of Fe/Zn phosphate structures as shown in Fig. 2-33.

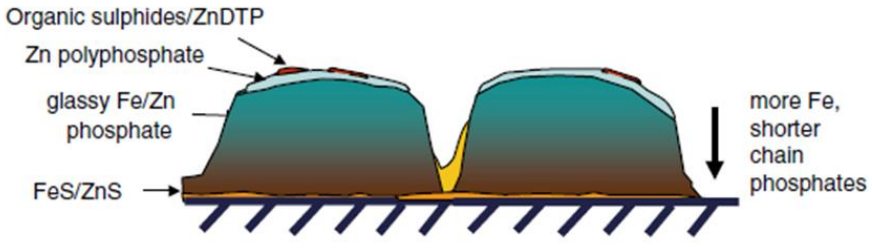

Fig. 2-33. Schematic diagram of ZDDP reaction film composition (reprinted from [50])

Miklozic [79] investigated interactions between several FMs and ZDDP. The friction results depended on the chemical structure of the FMs; while alkenyl amide or octadecylamine presented consistent friction reduction effect, polycondensed fatty acid/ester (PFA) lost the effect completely in the presence of ZDDP as shown in Fig. 2-34. In addition to the friction coefficient, the reaction film thickness and surface roughness were also affected by the interaction. Ratoi [80] formulated polyamidoalcohol, alkenoic ester and oleylamine in the fully-formulated engine oil including ZDDP, and the influence on the film formation and the friction was investigated. Interestingly, the results showed an opposite trend to the study by Miklozic; the ester FM was able to reduce the friction even with ZDDP while the amide and the amine FM decreased the effect. Moreover, Tasdemir [81, 82] reported the influence of ZDDP and the test temperature on the FM effect of GMO using a

Diamond-Like Carbon (DLC) coated specimen. Although competitive interactions between ZDDP and GMO were not observed in most of the test conditions, the ZDDP appeared to inhibit the FM effect of GMO only at 40°C.

On the other hand, Murase [83] studied the interaction between the FMs and phosphites. The test oil systems are relatively similar to the typical automatic transmission fluid because the phosphites were applied as an anti-wear agent instead of the ZDDP. The chemical nature of the FMs assessed using TOF-SIMS suggested that the adsorption of palmitic acid and GMO were strongly inhibited by the phosphite, while oleyl amine presented a synergetic effect on the adsorption with the specific phosphite, TBPi as shown in Fig. 2-35.

As a result of overviewing previous works, it is clear that the interaction mechanism of the FM is very complicated and affected by various factors; the other additives, substrate materials or the test environment.

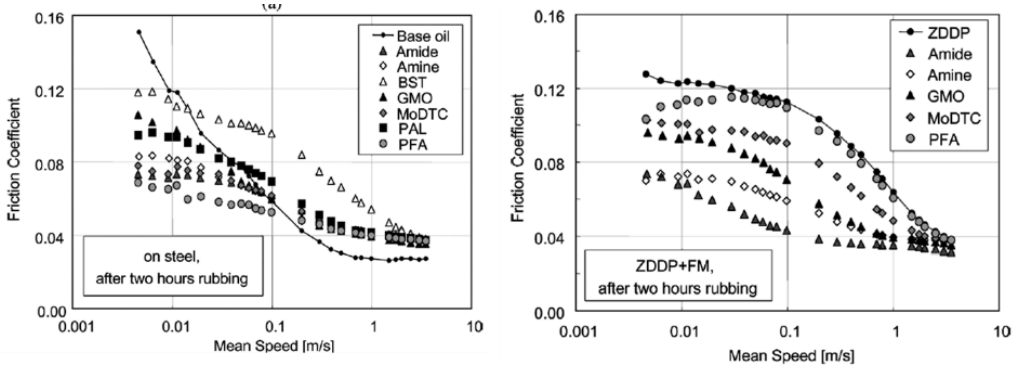

Fig. 2-34. Stribeck curves for friction modifiers, left; in base oil, right; ZDDP blends (reprinted from [79])

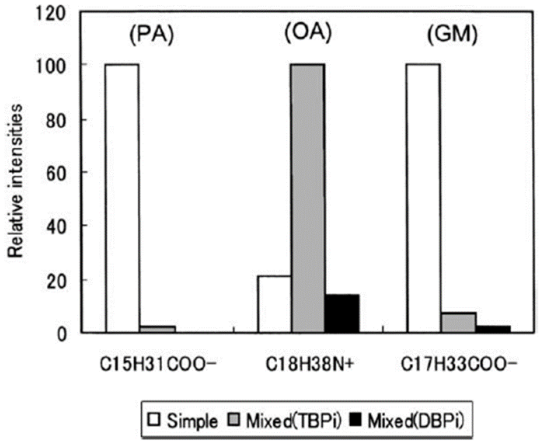

Fig. 2-35. Relative TOF-SIMS intensities derived from the FMs, PA; palmitic acid, OA; oleyl amine, GM; GMO, TBPi/DBPi; Tri/di-n-butylphosphite (reprinted from [83])

2.4.3. Application to ATF and CVTF

The friction properties need to be satisfied for designing ATFs or CVTFs. For example, a positive μ-V characteristic is required for the lock-up clutch system as mentioned in "2.2.3. Conventional Automatic Transmission (AT)".

Kugimiya [54] investigated the effect of the typical ATF additives on the μ-V performance, and the trend of each additive was summarised as shown below;

- Viscosity modifiers (VMs) or anti-oxidants; Minor impact on the performance
- Dispersants or metal detergents; Increase the friction at high sliding speed region
- FMs and P anti-wear agents; Decrease the friction at low sliding speed region

Further study focusing on the dispersants and the metal detergents was followed, which suggested that the dispersant with long poly isobutylene chains and the over-based calcium sulfonate with large $CaCO_3$ core crystals are effective to improve the friction coefficient at high sliding velocity for the better μ-V characteristics [53]. The effect of the chemical structure of the calcium sulfonate was also reported by Tohyama [84], implying that the $CaCO_3$ core was capable of keeping the surface roughness of the paper clutch, which seemed to be a key factor to keep high friction coefficient at the high sliding speed.

In terms of the effect of the FMs, Ingram [85] discussed the effect of the FMs on the frictional properties using a Mini Traction Machine (MTM). The μ-V characteristics of acid, amide and amine FM with different lengths of saturated carbon chain (C_6 – C_{18}) were evaluated, and confirmed that the longer chain led to the lower friction coefficient at low speed as expected from the classical reports. It is notable that a negative μ-V relationship appeared when the FM with C_{18} and C_6 chains were mixed as shown in Fig. 2-36, suggesting that the homogeneity of the adsorption film is essential for low-speed friction behaviour. The mechanism achieving the positive μ-V curve was also investigated by Ingram [86, 87], and implied that the rough surface asperity of the paper clutch is one of the key factors, which enables the system to stay in the boundary lubrication condition through a wide range of operating speeds. There are several studies that support this assumption [88-90].

The working mechanism and the chemical nature of the FMs on the paper surface were investigated in detail by Zhao [51, 91-93] with the use of several surface analysis

techniques; X-ray Photoelectron Spectroscopy (XPS), Attenuated Total Reflectance Fourier Transform Infrared spectroscopy (ATR-FTIR), Energy-Dispersive X-ray spectroscopy (EDX) and TOF-SIMS. The specimen after the sliding test were assessed, and the observed chemical nature was discussed related with the friction results. The durability of three FMs, a fatty amide, a fatty imidazoline and a fatty amide, on the μ-V characteristics was investigated, and the surface chemical nature was assumed as shown in Fig. 2-37 based on the friction and surface analysis results. The mechanism of the excellent frictional durability of the amide FM could be explained.

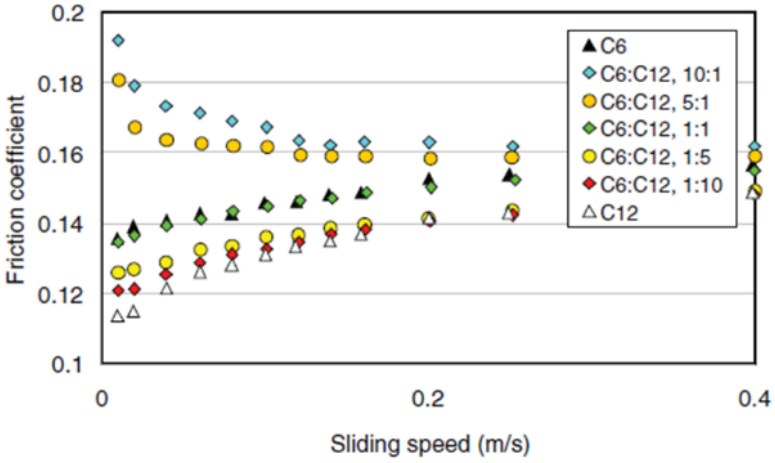

Fig. 2-36. μ-V characteristics for blends of dodecanoic acid (C_{12}) and hexanoic acid (C_6) (reprinted from [85])

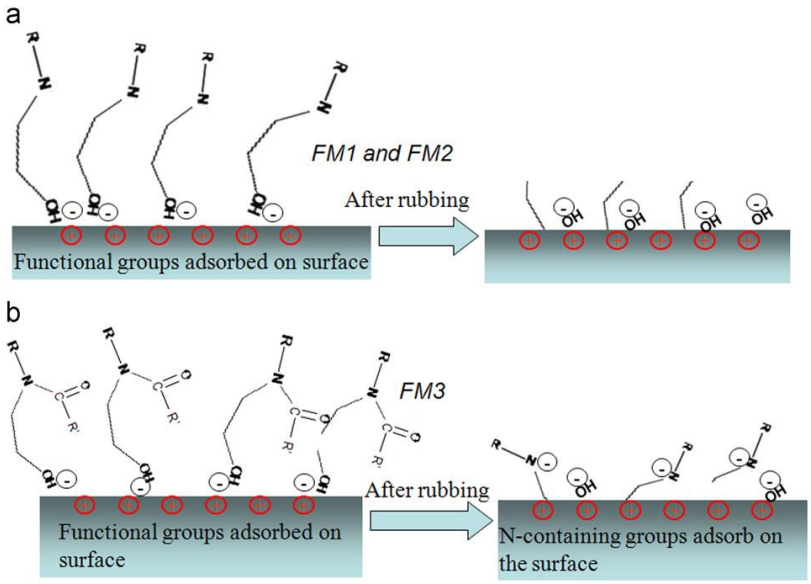

Fig. 2-37. Schematic illustration of the proposed decomposition and adsorption process FM1; fatty amine, FM2; fatty imidazoline, FM3; fatty amide (reprinted from [92])

The friction at steel/steel contact is also important for the application to CVTFs. Derevjanik [94] reported an influence of the FMs and the detergents on the steel/steel and paper clutch/steel frictional performances. Table 2-3 shows the steel/steel friction results. Although FMs generally reduce steel friction, some combinations present a synergistic effect; for example, FM-I promotes the friction reduction effect significantly in the presence of the detergents. The clutch μ-V performance also shows interactive effects between the additives.

Narita [95-98] investigated the effects of the anti-wear agent and the metal detergent on the steel/steel friction aiming for the application to CVTFs. The friction results showed that the combination of the hydrogen phosphite and the over-based calcium sulfonate increased the friction coefficient by 8% synergistically compared to when they were added independently. The XPS analysis of the post-test specimen detected formation of pyrophosphate on the surface as shown in Fig. 2-38, which is considered as the reason of the high steel friction.

Table 2-3. Steel/steel friction coefficient results (reprinted from [94])

	DET					
	NONE	A	B	C	D	E
FM						
NONE	0.130	0.126	0.125	0.124	0.129	0.128
F	0.123	0.111	0.116	0.116	0.124	0.125
G	0.123	0.120	0.121	0.125	0.123	0.123
H	0.113	0.121	0.112	0.116	0.120	0.119
I	0.125	0.117	0.117	0.117	0.121	0.120
J	0.128	0.121	0.121	0.125	0.126	0.128

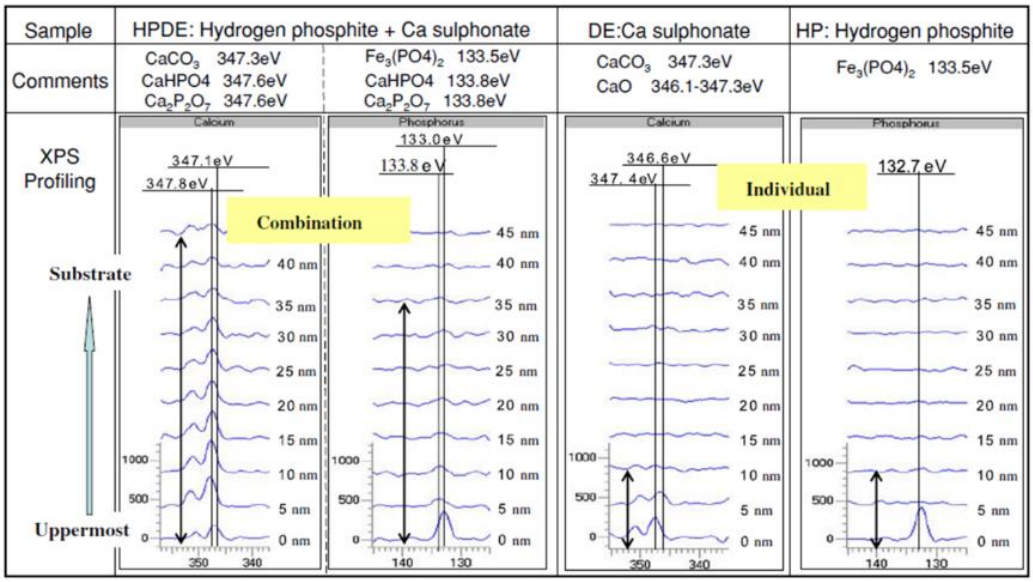

Fig. 2-38. XPS spectra of tribofilm on the post-test specimens (reprinted from [97])

2.5. Research Target

This study aims to develop CVTFs with excellent frictional performance which is capable of improving fuel efficiency. The formulation of the additives is important, and they must be designed appropriately and precisely to meet the advanced frictional requirements.

The independent effect of the additives on the frictional properties of the CVT is summarised in Table 2-4. The FM is essential to achieve a positive μ-V property. However, it generally conversely reduces the steel friction required at the belt-pulley. In addition, it seems to be difficult to cover the steel friction sufficiently by simply adding the other additives, because they can compete with the FM, worsening the μ-V characteristics. Therefore, it is necessary to optimise the interactions between the FMs and the other additives to simultaneously satisfy both of the requirements. The ideal solution should be the control of the FM to work only on the paper clutch material.

Table 2-4. Effect of the additives on the frictional performances of CVTF

	FM	Metal detergent	Anti-wear agent	Dispersant
Steel/steel friction (belt-pulley)	--	-	-	+
μ-V characteristics (lock-up clutch)	+++ low speed	+ high speed	+ low speed	+ high speed

+++; essential effect, +; positive effect, -; negative effect, --; signififant negative effect

Looking at previous work, it seems the topics can be separated into two types as shown in Fig. 2-39. The first, pattern-A are the studies focusing on the effect of the additives on the frictional performance of the paper clutch, which is represented well by the series of reports by Zhao [91-93]. The post-test specimens were assessed to evaluate the chemical nature on the paper surface, and the behaviour of the additives was assumed based on the tribotest and the surface analysis results. However, the discussion on the steel friction is necessary considering the application to the CVTFs. On the other hand, the target of pattern B is CVTFs as in the work by Derevjanik [94]. The frictional properties were evaluated using both steel and paper specimens, and the effect of the additives on the CVTF components was investigated. In this case, further information

on the surface chemical nature is essential in order to discuss the interactions among the additives.

Therefore, this study combines these two approaches. The frictional performance of the FMs are evaluated on both paper and steel substrates, then the surface of the post-test specimens is assessed in order to observe the chemical nature of the additives on the tribofilm. The friction and surface analysis results are discussed to elucidate the chemistry of interactions among the FMs and the other additives, and the working mechanism of the FMs and the optimal formulations for the CVTF are proposed.

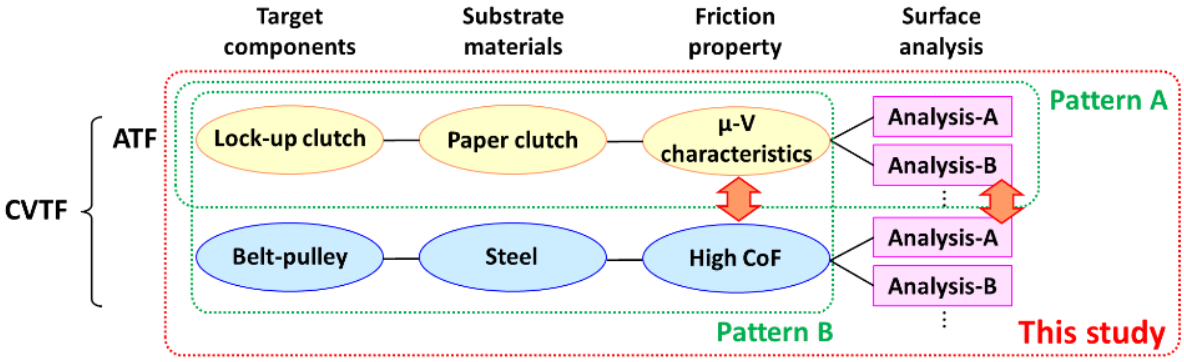

Fig. 2-39. Schematic illustration for the research target

Chapter 3 – Experimental Procedures and Analysis of Starting Oils and Surfaces

In this chapter, experimental procedures applied in this research are introduced. It aims to elucidate the behaviour of organic Friction Modifiers (FMs) on steel and the paper clutch for the purpose of formulating CVTFs with superior frictional performance. TE77 reciprocating tester and Mini Traction Machine (MTM) were used to simulate the sliding contact at the steel belt-pulley mechanism and the lock-up clutch system in the CVT. The post-test materials were assessed using a white light interferometer (WLI) and SEM for the observation of the surface morphology, XPS, EDX and ATR-FTIR to investigate the chemical nature on the substrate surface. The IR spectra of the fresh test oils and additives and the fresh specimen surfaces are also shown in this chapter to prepare for the discussion on the post-test samples.

3.1. Operating Conditions of the CVT Components

This research focuses on the working mechanism of the FMs at the steel belt-pulley and the lock-up clutch in the CVT. They are the major components which require the friction control [99, 100]. The belt-pulley mechanism is a heart of the CVT system, which realises the continuously variable gear shift effective to improve fuel efficiency of the transmission [44]. On the other hand, the lock-up clutch system is equipped inside the torque converter, and working to reduce the churning loss at high speed driving condition [101, 102]. The friction at the steel belt-pulley is preferably kept higher because the torque is transferred through the steel/steel contact between the belt and the pulley. Low steel friction possibly leads to macroscopic slip of the belt [47, 103, 104]. On the other hand, the friction at the paper clutch needs to be modified to achieve the positive μ-V characteristics, otherwise noise and vibration so called shudder would arise [43]. The issue is that the opposite requirements need to be satisfied simultaneously using only one lubricant [45, 46, 105]. It is necessary to optimise the formulation of FMs for controlling these frictional properties.

The tribotests need to simulate the actual sliding condition at the belt-pulley and the lock-up clutch. The typical materials and the operating conditions are summarised in

Table 3-1. In terms of the belt-pulley mechanism, the belt and pulley are often made from bearing steel (Cr high carbon steel) and Cr/Mo carburised steel considering a balance of hardness and anti-fatigue performance, though, there are the other options depending on the CVT systems [106-109]. The contact pressure between the belt and the pulley is generally controlled at around 1.0 GPa, and the microscopic sliding happens when the belt rotates around the pulleys due to their configuration. Narita and Priest [95-97] reported series of studies on the steel friction of CVTFs. TE77 reciprocating tests were carried out at around 1.0 GPa and 0.2 m/s using a bearing steel ball and a Cr steel plate, and it was confirmed that the friction results showed a good agreement with those acquired using an actual belt-pulley system.

On the other hand, the paper clutch material generally consists of some fibre materials (cellulose fibre, aramid fibre or carbon fibre) and diatomite earth (mainly consists of SiO_2) as a filler, compacted with phenol resin [85, 110]. The counter steel plate is made from cast iron or steel. The condition applied for the lock-up clutch sliding control is commonly less than 2.0 m/s and 3.0 MPa [93, 111, 112].

Table 3-1. Typical operating condition of the CVTF components

Component	Steel belt/pulley	Lock-up clutch
Typical material	**- Belt elements** Bearing steel (Cr high carbon) **- Pulley** Carburized steel (Cr/Mo)	**- Paper clutch** Fibre (cellulose, aramid, carbon) Filler (diatomite earth) Binder (phenol resin) **- Counter steel plate** Cast iron or steel
Operating conditions		
Sliding speed	~ 0.2 m/s	~ 2.0 m/s
Pressure	Around 1 GPa	0.5 ~ 3 MPa
Temperature	**RT ~ 150°C**	**RT ~ 150°C**

3.2. TE77 Tribotest

3.2.1. Introduction to TE77

TE77 is a reciprocating friction tester produced by Cameron-Plint, Ltd, Wokingham, UK. It enables to perform tribotests in wide ranges of sliding geometries (pin-on-flat, cylinder-on-flat, disc-on-flat or ball-on-flat), therefore, there are a large number of

literatures investigating friction or wear properties with the use of this machine [113-116]. Small dimension of the specimens is another advantage of the TE77. It is possible to perform the tribotest only with small-sized and simple-shaped specimens, which allows to prepare the modified special specimens easily (e.g. a surface coated [113], non-steel [116] or a paper plate). This feature is also a motivation for this study because the post-test specimens can be analysed without a cutting process. The post-test clutch plate used for standard lab tests, such as LVFA [111], is generally too large to be assessed in the highly vacuumed analysis chamber equipped at SEM/EDX or XPS. Because the cutting process possibly causes contamination on the surface, the specimen should be passed to surface analysis directly. In addition, a large paper plate has an issue on remaining oil inside the material because it is usually difficult to remove the oil completely when the specimen size becomes larger.

The issue is the sliding configuration at the paper/steel contact. While there is a large body of previous research applying reciprocating tribometers to measure steel friction [75, 97, 117, 118], only a few attempts have been done to evaluate the clutch friction performance [119]. The actual clutch engagement is performed under pure sliding, so that the TE77 is not the best to evaluate the μ-V property that is essential to discuss the friction performance at the clutch. Therefore, Mini Traction Machine (MTM) was also utilised using a paper coated disc in order to solve the issue, and correspondence between the TE77 and MTM was discussed. A detail of the MTM tribotest is explained in a later section.

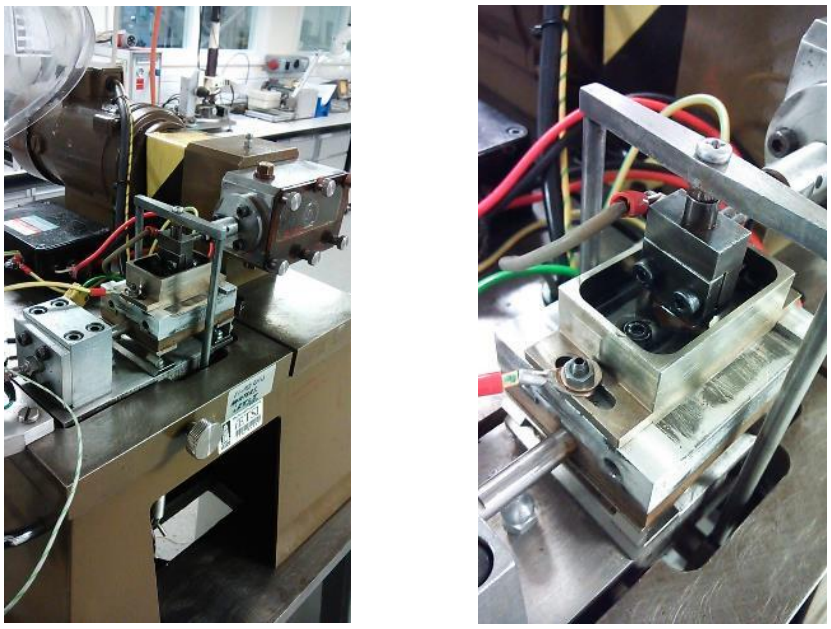

Fig. 3-1. Photos of the TE77 reciprocating tester used for this study

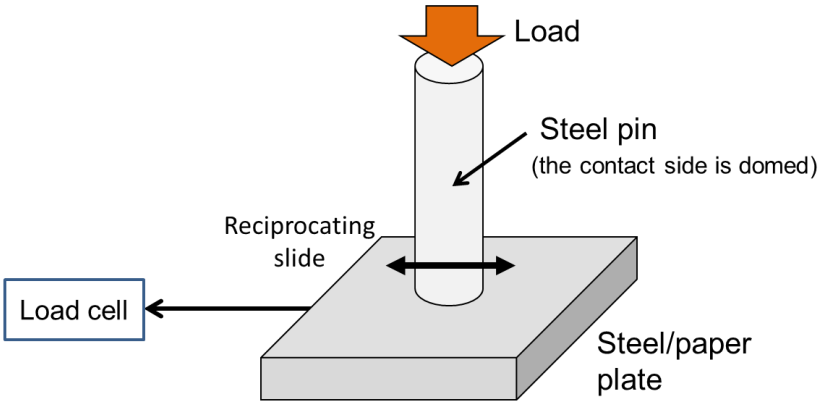

Fig. 3-2. Schematic image of the TE77 test configuration

3.2.2. TE77 Test Specimens

The detail of test specimens used for the TE77 is shown in Table 3-2 and Fig. 3-3.
The properties of the steel pin-1 and the steel plate were determined to simulate the steel belt-pulley contact. The pin made from AISI 52100 steel represents the belt, while the AISI 4140 steel plate mimic the pulley material. The end of the pin is domed at 8 mm radius achieving the typical contact pressure at 1.0 GPa.

Table 3-2. Materials and dimensions of the TE77 test specimens

	Steel Pin-1	**Steel Plate**	**Steel Pin-2**	**Paper plate**
Contact mode	Steel/steel (point contact)		Paper/steel (point contact)	
Simulated part	Steel belt-pulley		Lock-up clutch	
	Belt	Pulley	Steel plate	Wet cluch
Material	AISI 52100 Cr carbon steel	AISI 4140 Cr/Mo steel	AISI 52100 Cr carbon steel	JASO M 349 paper clutch
Dimensions	Cylinder (domed) ø = 6mm, L = 20mm r of dome = 8 mm	Plate 7 × 7 × 3 mm	Cylinder (domed) ø = 6mm, L = 20mm r of dome = 16 mm	Plate 7 × 7 × 3 mm
Hardness	H_{RC} = 58 - 62	H_{RC} = 58 - 62	H_{RC} = 58 - 62	-

On the other hand, the combination of steel pin-2 and the paper plate are prepared to simulate the lock-up clutch engagement. The JASO M 349 standard paper clutch [111] was selected as the paper material for this study. A photo and schematic image of the paper plate is shown in Fig. 3-4. The composition of the JASO paper is cellulose fibre, aramid fibre, diatomite earth and phenol resin. The standard JASO paper clutch was cut into an appropriate size as the TE77 plate specimen. The steel pin-2 with a domed end at 16 mm radius, which appears to be almost flat, was used in order to arrange the contact pressure as close as possible to the actual lock-up clutch sliding condition.

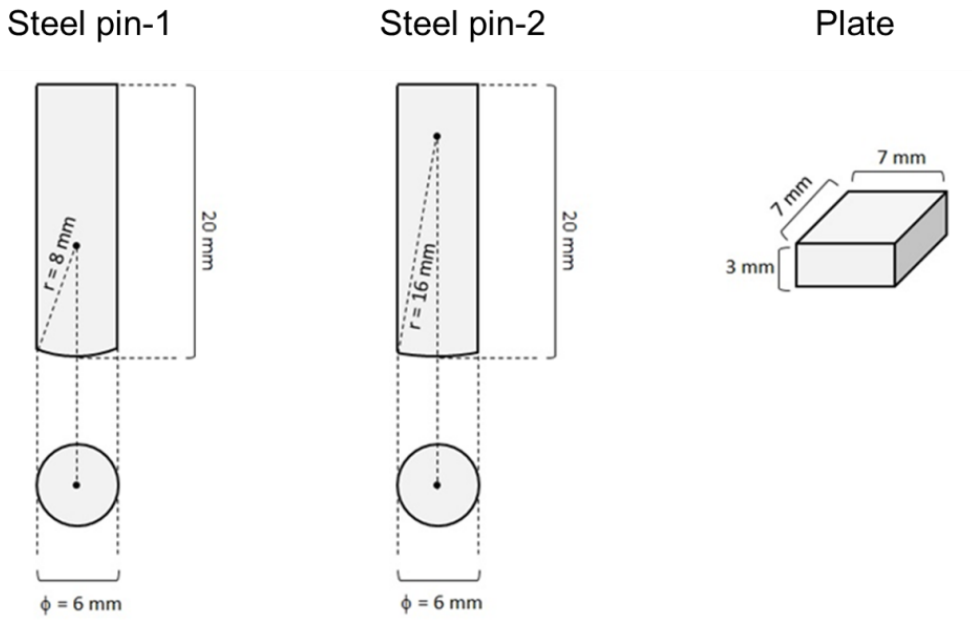

Fig. 3-3. Dimensions of the TE77 test specimens

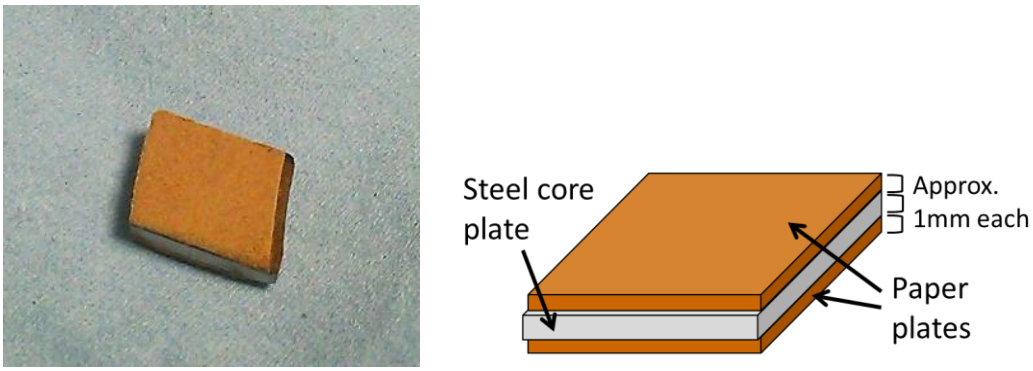

Fig. 3-4. Appearance of the TE77 paper plate
(left; photo, right; schematic image)

3.2.3. TE77 Test Conditions

The test load was determined as to simulate the typical contact pressure at the belt-pulley and the lock-up clutch at the CVT. The following equations were used to calculate the maximum Hertz contact pressure between the TE77 pin and the plate (ball-on-flat contact geometry) [19, 24];

$$P_{max} = \frac{3P}{2\pi a^2} \quad \text{(Eq. 3-1)}$$

$$a = \left\{\frac{3rP}{4}\left(\frac{1-\nu_1^2}{E_1} + \frac{1-\nu_2^2}{E_2}\right)\right\}^{1/3} \quad \text{(Eq. 3-2)}$$

where P_{max} is the maximum Hertzian contact pressure, P is the applied load, a is the contact radius and r is the radius of the pin's domed end. E_1 and E_2, ν_1 and ν_2 represent the physical parameters of the pin and the plate, the Young's modulus and Poisson ratio respectively.

E = 206 GPa and ν = 0.3 were adopted for the steel pin and the plate [120], while E = 130 MPa and ν = 0.1 for the paper plate [121, 122]. It is notable that the parameter of the paper clutch differs significantly depending on the material and the measurement method.

Based on the equations (Eq. 3-1 and 3-2), the maximum contact pressure at the steel/steel and the paper/steel contact is calculated as shown in Table 3-3. While the steel/steel contact pressure has a good agreement with the actual belt-pulley contact, that of the steel/paper is 6.0 MPa which is slightly higher than the typical clutch engagement condition up to 3 MPa due to the point contact configuration of the TE77. However, the contact pressure at 6.0 MPa is much less than the pressure applied for the clutch durability test [123], so that it should be possible to evaluate the FM effect on the paper without any negative effects, such as physical damage, caused by the high contact pressure.

The TE77 tests were carried out at both 100°C and 40°C in order to investigate the influence of the test temperature on working mechanism of the FMs and the other additives. The sliding speed was determined at 0.20 m/s (5.0 mm stroke at 20 Hz). As mentioned in session 3.1, which is appropriate for simulating the steel belt-pulley contact [97], and also suitable to evaluate the effect of the FMs on the paper clutch. If

the test oil reduces the paper friction at low speed of 0.2 m/s, it is able to lead to a positive μ-V property preferable for smooth and comfortable clutch engagement [43].

The volume of the test oil was 15 ml, which is sufficient amount to cover the plate specimen surface. Hence, the tests were performed at "fully flooded" condition.

Table 3-3. TE77 test conditions

	Steel/steel contact	Paper/steel contact
Test specimens	Pin-1 / steel plate	Pin-2 / paper plate
Load	26.5 N	16.5 N
Pressure (P_{max})	1.0 GPa	6.0 MPa
Temperature	100°C or 40°C	
Sliding speed	0.20m/s (20Hz, 5mm)	
Test duration (initial)	60 minute	
Test duration (durability)	-	12 or 24 hour

3.2.4. Data Sampling of TE77

The test duration for the initial performance test was 60 minutes. The friction force was sampled every one minute for one second with 0.001 second sampling interval, so that 1,000 raw friction data were collected every minute of the 60 minutes sliding test. The raw data were averaged and adopted as the friction coefficient result.

For the steel/steel contact, Electrical Contact Resistance (ECR) between the steel pin and the plate was sampled together with the friction force. It was used to estimate the film formation on the steel substrate as the reaction film generally has higher resistance than steel.

Moreover, the shape of the friction force wave at the paper/steel contact was discussed aimed at the evaluation of the frictional property like μ-V characteristics. The friction wave sampled between 31 and 60 minutes were averaged, then processed to calculate the factor named Friction Force Wave Index (FFWI). Fig. 3-5 shows an example of this procedure; the paper/steel contact test at 100°C using PAO and PAO with 0.85 wt% oleic acid. The wave of PAO (Fig. 3-5(a)) shows spikes at around 10 and 30 ms when the sliding direction of the pin became opposite, while PAO with oleic acid (Fig. 3-5(b)) presents a smoother wave shape without any obvious spike. It is considered that the

force spikes arose when the paper contact was not smooth due to the absence of effective FMs. This result implies that it would be possible to discuss the paper clutch μ-V performance by the comparison of the height of the spikes.

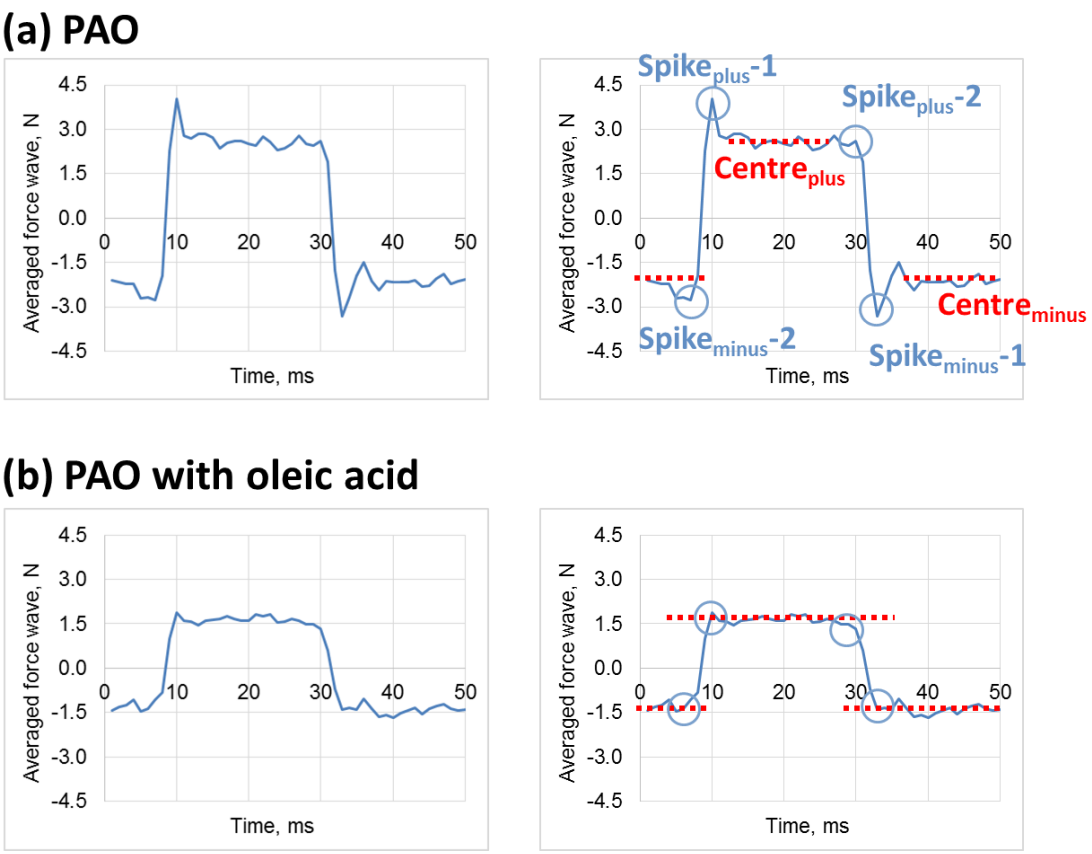

Fig. 3-5. Friction Force Wave Index (FFWI) analysis of (a) PAO and (b) PAO with oleic acid for the TE77 paper/steel contact test at 100°C
(left; averaged friction force wave, right; with factors for FFWI calculation)

For the quantitative comparison, the factor, Friction Force Wave Index (FFWI), is introduced. It represents the extent of the spike and is calculated by the division of the spike height (Spike$_{plus}$-1, Spike$_{plus}$-2, Spike$_{minus}$-1 and Spike$_{minus}$-2) by the intermediate value (Centre$_{plus}$ and Centre$_{minus}$) as shown in Fig. 3-5. The contribution from each spike is averaged as show in Eq. 3-3.

$$FFWI = \frac{1}{4}\left(\frac{Spike_{plus-1} + Spike_{plus-2}}{Centre_{plus}} + \frac{|Spike_{minus-1}| + |Spike_{minus-2}|}{|Centre_{minus}|}\right) \quad \text{(Eq. 3-3)}$$

The higher the spike, the higher the FFWI value. For example, The FFWI of PAO (Fig. 3-5(a)) is over 1.0 due to the significant spikes, while that of PAO+acid (Fig. 3-5(b)) is less than 1.0. The FFWI is calculated for all the TE77 paper/steel contact tests, and the correspondence with the μ-V characteristics measured by MTM is discussed.

Long-term performance of some test oils at paper/steel contact was investigated for the purpose of observing degradation of the FMs caused by the long-term sliding and thermal load. The durability test lasted for 12 or 24 hours, and carried out at the same condition as the initial performance test.

3.2.5. Treatment for TE77 Post-test Specimens

It is important how to treat the post-test materials in order to obtain correct and definite surface analysis results. In this research, the TE77 specimens were processed as below;

<Steel pins and steel plates>
1) Rinsed with heptane sufficiently
2) Wrapped with aluminium foil, and kept inside a resealable plastic bag

<Paper plates>
1) Rinsed with heptane continuously until oozing out of the oil from paper plate stops
2) Vacuumed in a standard vacuum chamber at 2×10^{-2} Pa for 10 hours
2') For the samples submitted to XPS analysis, higher vacuum at 1×10^{-4} Pa for 3 hours were applied additionally
3) Wrapped with aluminium foil, and kept inside a resealable plastic bag

A major concern was if it would be possible to analyse the post-test papers appropriately using SEM/EDX or XPS which requires a high vacuum condition for the measurement. As mentioned in the later section regarding the surface analysis procedure, this treatment worked well; SEM/EDX analysis was performed under the environmental mode at 30 Pa, and XPS analysis was successfully carried out at the standard vacuum condition without any issue.

3.3. Mini Traction Machine (MTM) Tribotest

3.3.1. Introduction to MTM

MTM (PCS Instruments, UK) was utilised to evaluate the frictional performance of the paper clutch. The MTM tribotest is generally performed with a steel disc and a steel ball at ball-on-disc configuration. The MTM enables the disc sliding speed and the ball rolling speed to be controlled independently, so that it is widely used to simulate the lubrication where sliding/rolling ratio has a significant influence on the reaction film formation, such as the valve train in engines [76, 79, 80].

The procedure to measure the μ-V performance of the paper clutch using MTM was established by Ingram [85, 87]. Two arrangements shown below were installed to the MTM following Ingram's reports;

1) Pin on disc mode – This mode is necessary for pure sliding control of the ball by stopping the rotational motion of the ball.

2) Zero force sampling – MTM basically calibrate the zero force using the positive and the negative traction force under the standard operation mode. This method is not possible at the pure sliding mode, so the zero force is sampled before every measurement for the calibration.

MTM configuration is shown in Fig. 3-6. A paper coated disc is attached inside the test chamber, and the chamber is filled with the test oil on the friction measurement. A schematic image of the MTM test is shown in Fig. 3-7.

Fig. 3-6. MTM tribotester (left; appearance, right; inside the test chamber)

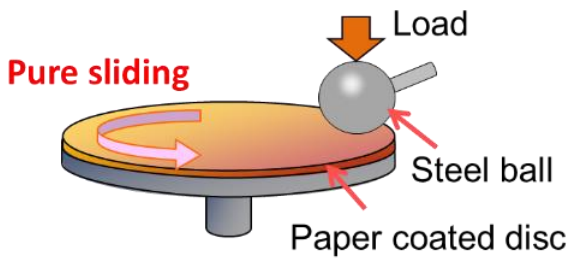

Fig. 3-7. Schematic image of MTM tribotest using the paper clutch plate

3.3.2. MTM Test Specimens

The detail of MTM test specimens is shown in Table 3-4. The 3/4'' AISI 52100 steel ball is a standard test specimen supplied by PCS Instrument. The paper coated disc was provided from the sponsor, JX Nippon Oil & Energy Corporation. The JASO M 349 paper clutch material is coated on the steel plate which is designed to be the same dimension as the MTM standard disc. A photo of the paper disc is presented in Fig. 3-8. The steel and the paper materials are the same as the TE77 specimens for the purpose of comparing the test results between the MTM and the TE77.

Table 3-4. Detail of the MTM test specimens

	Steel ball	**Paper coated disc**
Contact mode	Paper/steel (point contact)	
Simulated part	Lock-up clutch	
	Steel plate	Paper cluch
Material	AISI 52100 (Cr carbon steel)	JASO M 349 (paper clutch)
Dimensions	3/4" ball (Ra < 0.01 μm)	Plate (46 mm diameter)

Fig. 3-8. Photo image of the MTM paper coated disc

3.3.3. MTM Test Conditions

The detailed MTM test conditions are summarised in Table 3-5. The load was set at 3.0 N, which is the minimum load of MTM, in order to arrange the contact pressure close to the actual condition. The maximum contact pressure calculated based on the equations shown in "3.2.3. TE77 Test condition" was 4.8 MPa (the mean contact pressure; 3.2 MPa). This value is similar to that applied in the TE77 paper/steel contact test, and also almost the same as the pressure applied in the reference report by Ingram [85]. Therefore, it should be reasonable to evaluate the clutch μ-V characteristics at this pressure condition. The friction test was carried out at both 100°C and 40°C in order to investigate the influence of the test temperature on the effect of the FMs.

The test oil volume for the MTM test was 40 ml. This amount was sufficient to cover the paper plate surface, so that the friction tests were carried out in a "fully flooded" condition.

Table 3-5. MTM tribotest condition

	Paper/steel contact
Test specimens	Steel ball (AISI 52100) Paper coated disc (JASO M 349)
Load	3.0 N
Pressure	P_{max}; 4.8 MPa, P_{mean}; 3.2 MPa
Temperature	100°C or 40°C
Sliding speed	0.01 ~ 2.4 m/s (3 min / each speed step)
Run-in condition	30 min, 3.0 N, 1.0 m/s, 100°C or 40°C

The schematic image of the MTM test sequence is illustrated in Fig. 3-9. The μ-V measurement is proceeded by the run-in process at 1.0 m/s, 3.0 N for 30 minutes. The measurement is carried out for 3 minutes at each speed step, and the friction data sampled during the last 1 minute are used to calculate the friction coefficient. The sliding speed applied for this study is determined following the reference [85] as below;

0.01, 0.02, 0.04, 0.06, 0.08, 0.10, 0.12, 0.14, 0.16, 0.18, 0.20, 0.25, 0.30, 0.35, 0.40, 0.45, 0.50, 0.55, 0.60, 0.70, 0.80, 0.90, 1.0, 1.2, 1.4, 1.6, 1.8, 2.0, 2.2, 2.4 (m/s), 30 steps in total

The test starts from the lowest speed (0.01 m/s) to the highest speed (2.4 m/s), then goes back to 0.01 m/s considering the influence of the hysteresis.

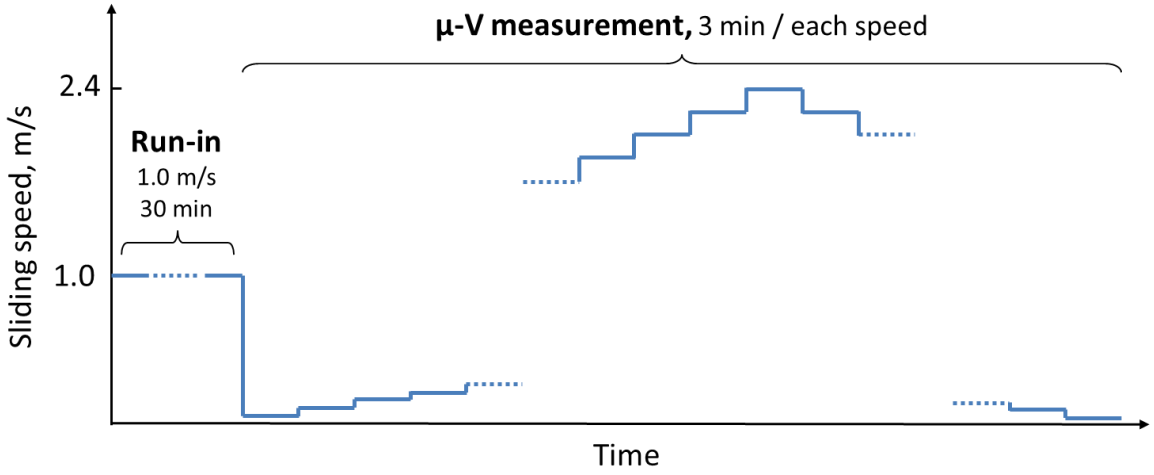

Fig. 3-9. MTM friction measurement sequence

A factor "μ ratio" is introduced for the quantitative comparison of the μ-V curves obtained from the MTM measurement. It is calculated as a division of the friction coefficient at 0.01 m/s by that at 0.50 m/s as shown below;

$$\mu\, ratio = \mu_{0.01\, m/s} \,/\, \mu_{0.50\, m/s} \qquad \text{(Eq. 3-4)}$$

As shown in the schematic image in Fig. 3-10, the μ ratio less than 1 means a positive μ-V curve, while that more than 1 means a negative curve. The lower the μ ratio, the better paper friction property. There are some attempts to use the friction ratio for the quantitative evaluation of the lock-up clutch performance as shown in previous reports [91].

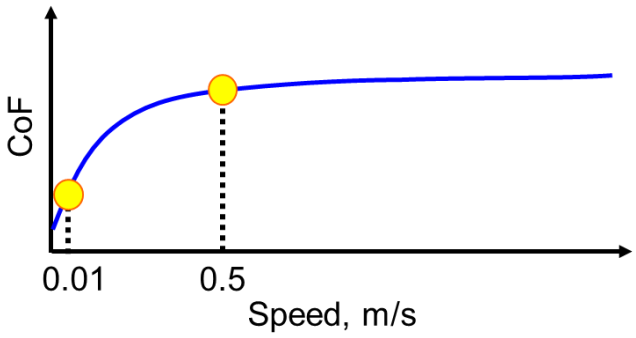

Fig. 3-10. Calculation of μ ratio from the μ-V curve

3.4. Test Oil Formulation

3.4.1. Friction Modifiers (FMs)

Three organic FMs are chosen for this study; oleic acid, oleyl alcohol and glycerol monooleate (GMO). The chemical structures are shown in Fig. 3-11. They have a same oleyl hydrocarbon chain and different type of polar groups, a carboxylic acid for oleic acid, a hydroxyl group for oleyl alcohol and an ester group and two hydroxyl groups for GMO. They are widely applied to commercial transmission fluids, and there have been a large number of reports regarding their effect on steel and paper clutch surfaces [54, 81, 83]. However, the discussion on the working mechanism in CVTFs seems to be insufficient.

Information of the FMs on the suppliers and assay is shown below;

- Oleic acid - Tokyo Chemical Industry Co., LTD (TCI), production code; O0011, assay > 85 %
- Oleyl alcohol - Sigma-Aldrich, production code; 369314, assay > 85%
- Glycerol monooleate - TCI, production code; G0082, assay > 40%

Each of the FMs is formulated at the same molar concentration, 0.03 mol/kg, in order to arrange the number of the FM molecules in the test oil to be same. The weight concentrations of oleic acid, oleyl alcohol and GMO are 0.85, 0.81 and 1.07 wt%, respectively, which are reasonable dosage levels compared with the previous studies focusing on the effect of FMs [72, 79-81, 83].

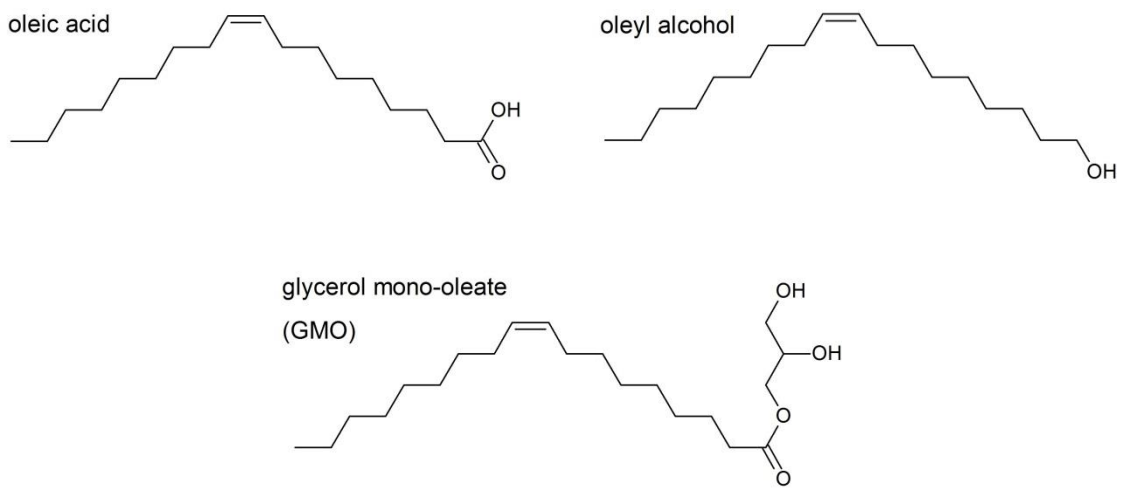

Fig. 3-11. Molecular structures of the organic friction modifiers

3.4.2. Base Fluids

Two different types of base fluid are prepared for this research; poly-α-olefin (PAO) and a model CVTF. PAO is a synthetic base stock synthesised generally by polymerization reaction of 1-decene and contains few impurities. It is chosen for the purpose of investigating the pure effect of the FMs without any influence from the other additives or contaminants. On the other hand, the CVTF base fluid consists of PAO as base oil and following typical CVTF additives [45]; a phosphorous anti-wear agent (P; 300 ppm), an overbased calcium sulfonate detergent (Ca; 300 ppm), a poly-isobutenyl succinic imide dispersant (3 wt%), a poly-methacrylate viscosity modifier (8.5 wt%) and anti-oxidants (amine and phenol types; 1.0 wt% in total). The combination effect of the FMs and the additives on the frictional properties was investigated with the use of the CVTF base fluid.

The detailed test oil formulations are shown in Table 3-6. It is expected that the behaviour of the FMs could be different between the PAO and the model CVTF formulations due to the interaction with the other additives.

Table 3-6. Test oil formulations

PAO formulation, wt%

		PAO	PAO +acid	PAO +alcohol	PAO +GMO
base oil	PAO4	100	99.15	99.19	98.93
FM	oleic acid		0.85		
	oleyl alcohol			0.81	
	GMO*				1.07

* glycerol mono-oleate

Model CVTF formulation, wt%

		CVTF	CVTF +acid	CVTF +alcohol	CVTF +GMO
base oil	PAO4	87.05	86.2	86.24	85.98
viscosity modifier	PMA*	8.5	8.5	8.5	8.5
anti-wear agent	DBP**	0.20	0.20	0.20	0.20
detergent	OB sulfonate	0.25	0.25	0.25	0.25
dispersant	PIBSI***	3.0	3.0	3.0	3.0
antioxidant	amine type	0.5	0.5	0.5	0.5
	phenol type	0.5	0.5	0.5	0.5
FM	oleic acid		0.85		
	oleyl alcohol			0.81	
	GMO				1.07

* polymethacrylate, ** dibutyl phosphite, *** poly isobutylene succinimide

3.4.3. Test Oil Preparation

PAO was purchased from ExxonMobil Chemical (product name; SpectraSyn 4), while the model CVTF base fluid was supplied by JX Nippon Oil & Energy Corporation. The FM was added into the base fluid following the procedure below;

1) Measure the precise weight of the FM and the base fluid in a 200 ml glass beaker.
2) Put a PTFE magnetic stir bar in the beaker.
3) Heat and stir the mixture on a hot plate for 1 hour. The oil temperature and the stirring are controlled at 60°C and 800 rpm.

The finished oils were clear and did not show any sediment. They were put in plastic containers and stored in an oil cabinet at room temperature.

3.5. Surface Analysis Techniques

3.5.1. White Light Interferometry

The wear scar on the post-test TE77 steel specimens was measured by a white light interferometer (WLI), NPFLEX (Bruker Corporation). The advantage of the WLI is non-contact measurement which enables to prevent physical damage on samples.

The steel pins and plates after the TE77 steel/steel contact test were assessed using WLI. Although the wear were observed on all the post-test pins, some of the steel plates did not show clear wear scar as shown in Fig. 3-12. Especially, the CVTF formulations did not have the detectable wear track on the plate in all the test conditions due to the anti-wear agent contained as the CVTF additive. The difference between the pin and the plate can be attributed to the contact configuration. Because the domed top of the pin kept contacted through the sliding test, it resulted in the clear and severe wear. Therefore, the anti-wear performance was evaluated using the post-test steel pins. The wear depth, wear volume and the 3D surface image were collected and compared.

On the other hand, the post-test TE77 paper plates and the steel pins after the paper/steel contact tests did not present any clear wear track on the both surface due to the low contact pressure.

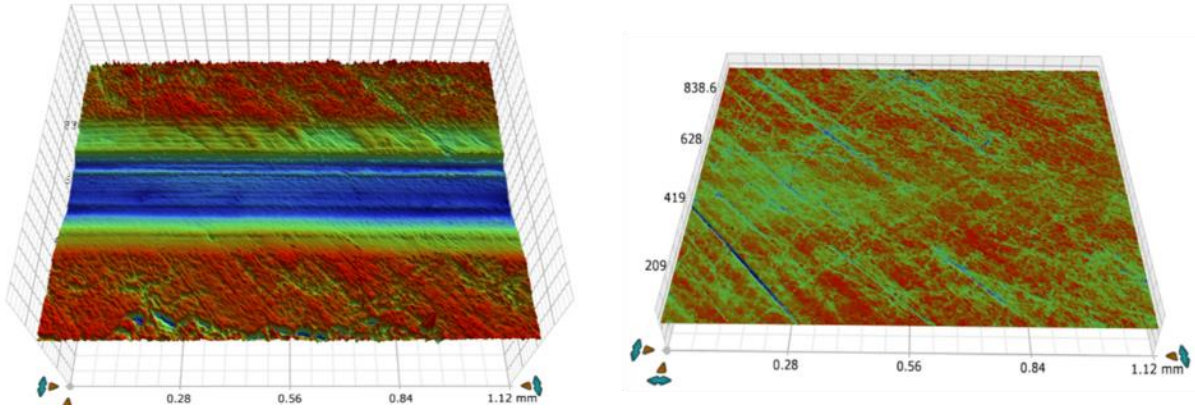

Fig. 3-12. 3D profile image of the wear track on the post-test TE77 steel plates measured by WLI (test oils, left; PAO+GMO, right; CVTF+GMO)

3.5.2. SEM/EDX

Scanning Electron Microscope (SEM) and Energy Dispersive X-ray Analysis (EDX) were performed using Carl Zeiss EVO MA 15 (Carl Zeiss AG). The post-test TE77 steel and paper plates were assessed to investigate the surface morphology and the elemental composition of the film inside the wear track.

In terms of the steel plate analysis, the plate washed by heptane was mounted on the sample holder with conductive carbon tape. The SEM/EDX analysis was carried out in standard conditions (chamber pressure of less than 10^{-3} Pa, accelerating voltage of 20 kV), and a Secondary Electron (SE) image was acquired. On the other hand, the paper samples caused charging-up at the standard condition due to the porous structure storing moisture and the remaining oil inside as well as the low electrical conductivity of the paper. In order to deal with the issue, the paper samples were pre-treated following the procedure shown in "3.2.5. Treatment for TE77 Post-test Specimens" to be cleaned intensively, and the paper surface was carbon sputtered before the analysis. In addition, SEM/EDX analysis was conducted under an environmental mode at 30 Pa of the chamber pressure, and the images were sampled using Back-Scattered Electron (BSE) mode. Fig. 3-13 shows the SEM images of the same paper plate sampled using the two methods. The right figure acquired at the environmental mode obviously shows correct paper clutch morphology [86, 110, 124-126].

The elements on the wear track were also assessed by the Energy-Dispersive X-ray spectroscopy (EDX) equipped in the SEM facility. The measurement depth of the EDX

is around 1 µm, therefore, the EDX results could reflect the chemical compositions of the tribofilm formed on the substrate surface.

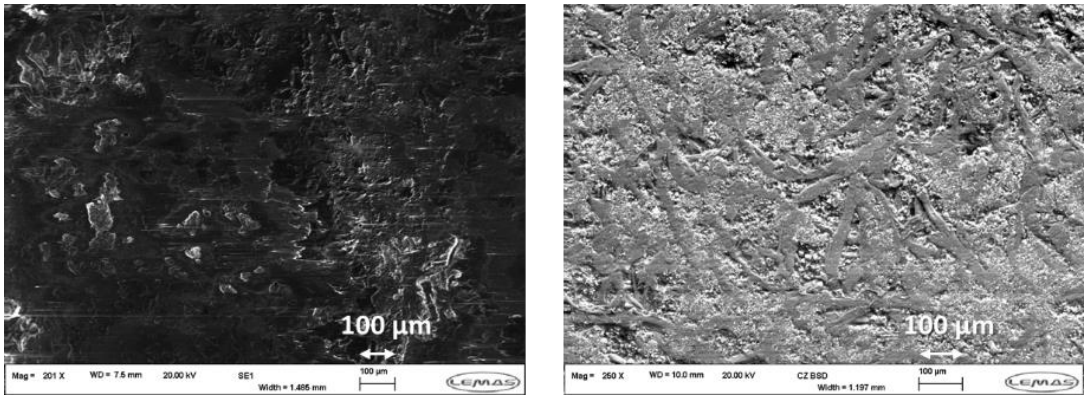

Fig. 3-13. SEM image of the TE77 paper plate after testing PAO+acid
(left; SE image at the standard mode, right; BSE image at the environmental mode)

3.5.3. XPS

X-ray Photoelectron Spectroscopy (XPS) analysis was carried out to estimate the chemical nature of the FMs and the other additives on the post-test TE77 plates. The two XPS instruments at National EPSRC XPS Users' Service (NEXUS) in New Castle, Theta Probe and K-Alpha (Thermo Fisher Scientific, Inc.), were used for this study. A sampling depth of the XPS is generally a few nm [127], therefore, the results reflect information on the uppermost steel surface, which includes the adsorption film formed by the FMs.

The XPS spectra were acquired using a monochromatic Al Kα source. The applied spot size was determined at 150 µm for the steel plate and at 400 µm for the paper plates, which was decided based on the width of the wear track. The survey scan and C 1s and O 1s detailed scans were performed, and the acquired spectra data were analysed by CasaXPS software. The peak positions were corrected by fitting the binding energy of saturated hydrocarbon detected in the C 1s detailed scan spectra at 285.0 eV [128-130]. The peak positions detected on the substrates were identified based on the previous studies; for steel [51, 92, 93, 131-143] and for the paper materials [51, 92, 93, 144-150].

Some test samples were measured twice, and good repeatability was confirmed for both steel and paper plates. For example, the XPS C 1s and O 1s spectra of the TE77 steel plate after testing CVTF at 100°C are shown in Fig. 3-14 and Fig. 3-15, respectively.

The spectra were sampled at two different positions on the wear scar of the same sample. A very good repeatability is confirmed for the peak positions and the intensities.

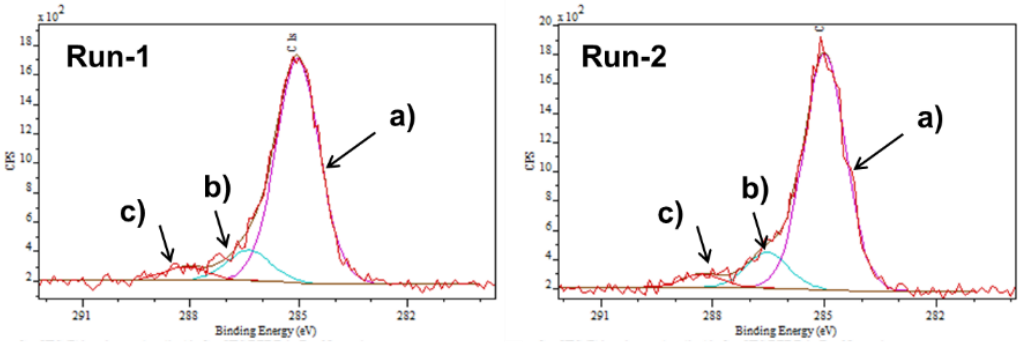

Peak #	Run-1	Run-2
a)	SHC; 285.0 eV (83.8 %Area)	SHC; 285.0 eV (82.8 %Area)
b)	286.4 eV (11.1 %Area)	286.5 eV (12.6 %Area)
c)	288.2 eV (5.1 %Area)	288.3 eV (4.7 %Area)

Fig. 3-14. XPS repeatability about C 1s detailed scan
(TE77 post-test steel plate, 100°C, Test oil; CVTF)

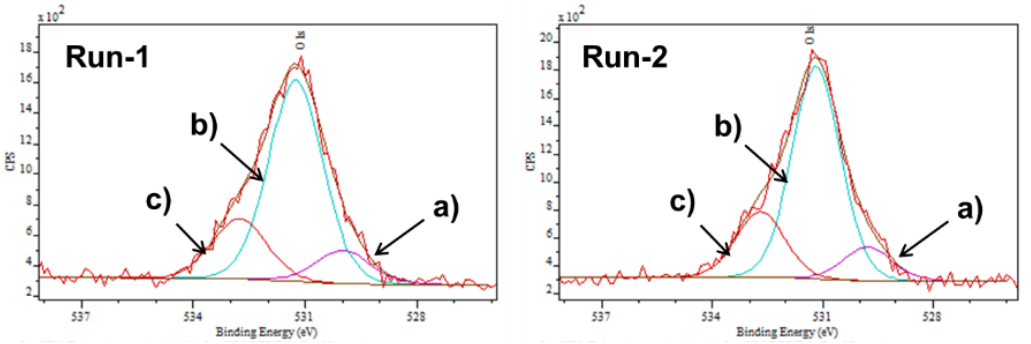

Peak #	Run-1	Run-2
a)	529.8 eV (10.7 %Area)	530.0 eV (11.2 %Area)
b)	531.2 eV (68.1 %Area)	531.2 eV (68.4 %Area)
c)	532.7 eV (21.2 %Area)	532.8 eV (20.4 %Area)

Fig. 3-15. XPS repeatability about O 1s detailed scan
(TE77 post-test steel plate, 100°C, Test oil; CVTF)

The XPS measurement for only the TE77 paper plates after testing the PAO formulations at 40°C was carried out using K-Alpha instead of Theta Probe, as summarised in Table 3-7, due to a technical trouble on Theta Probe. Theta Probe equips a high performance detector appropriate for the surface chemical nature analysis, while K-Alpha has a wider angle resolution. The same beam source and the spot size were applied for the both instruments. For the purpose of confirming the correspondence, the C 1s spectra of the post-test paper (100°C durability test, 12 hours, test oil; PAO+GMO) were compared as shown in Fig. 3-16. Although the spectrum acquired with K-Alpha shows higher 2) - 5) peaks due to the wide angle resolution, the peak positions showed a very good agreement. Therefore, it is possible to discuss the spectra measured by K-Alpha together with those by Theta Probe.

Table 3-7. XPS instruments used for the analysis

	TE77 steel plates	TE77 paper plates		
		100°C initial	40°C initial	100°C duraiblity
PAO formulations	Theta Probe	Theta Probe	K-Alpha	Theta Probe
CVTF formulations	Theta Probe	Theta Probe	Theta Probe	Theta Probe

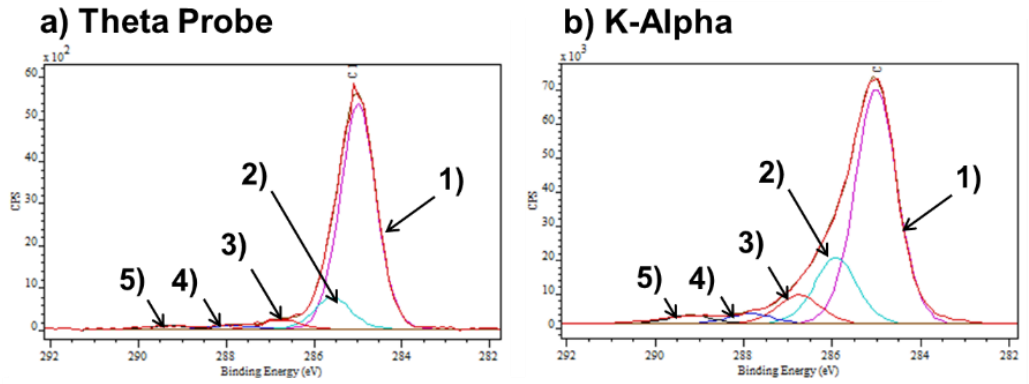

Peak #	Run-1	Run-2
1)	SHC; 285.0 eV (82.2 %Area)	SHC; 285.0 eV (67.7 %Area)
2)	285.6 eV (11.7 %Area)	285.9 eV (19.1 %Area)
3)	286.7 eV (3.4 %Area)	286.7 eV (8.1 %Area)
4)	287.9 eV (1.4 %Area)	287.9 eV (2.8 %Area)
5)	289.3 eV (1.4 %Area)	289.2 eV (2.3 %Area)

Fig. 3-16. Correspondence of the XPS spectra between Theta Probe and K-Alpha (TE77 post-test steel plate, 100°C, 12 hours durability, Test oil; PAO+GMO)

3.5.4. ATR-FTIR

Attenuated Total Reflectance-Fourier Transformed InfraRed spectroscopy (ATR-FTIR) produced by PerkinElmer, Inc. was utilised to observe the adsorption and reaction film on the surface of the post-test materials. Spectra were acquired by the use of a Perkin-Elmer Spectrum 100 FT-IR Spectrometer with a universal attenuated total reflectance (UATR) accessory. Photos of the instrument are shown in Fig. 3-17.

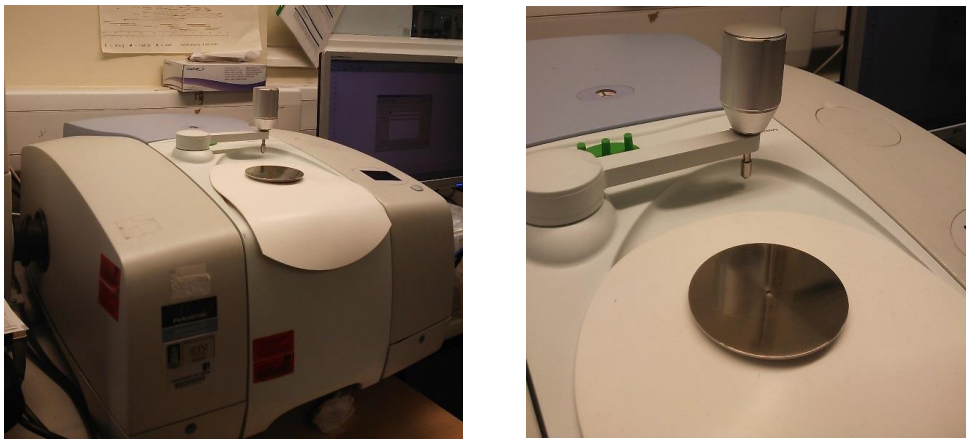

Fig. 3-17. Photo images of ATR-FTIR
(left; overall view, right; enlarged view of UATR accessory)

Fig. 3-18 shows the schematic diagram of the ATR-FTIR measurement. The ATR crystal material is germanium which is capable to collect data from 5,500 cm^{-1} to 600 cm^{-1}. The crystal has a small contact area formed by the flattened point of a cone, which ensures a 100 μm diameter contact area and one-time reflection in the optical pass.

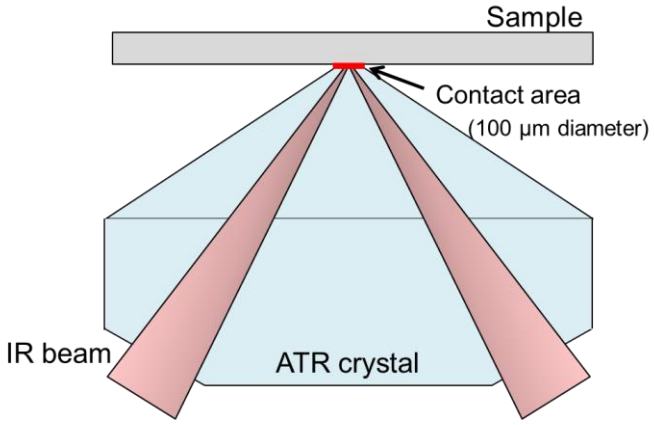

Fig. 3-18. Schematic diagram of the ATR-FTIR measurement

The spectrum was sampled between 4,000 and 650 cm^{-1} using 12 scans for the surface measurement and 4 scans for the bulk fluids/additives. Each measurement was repeated at least twice in order to confirm the reliability of acquired spectrum.

The IR spectra of the FMs, the base fluids, the other additives and the substrates are summarised in this chapter. The peak identification was done following the chart books [151-155]. Fig. 3-19 shows the IR spectra of the FMs. The prefixes ν, δ and γ mean stretching, in-plate deformation and out-of-plane deformation, respectively. The specific peaks derived from the polar groups are detected as follows;

(a) oleic acid – Strong C=O stretching bond attributed to carboxylic acid at 1,708 cm^{-1}

(b) oleyl alcohol – Medium C-O stretching bond attributed to hydroxyl group at 1,050 cm^{-1}

(c) GMO – Medium C=O stretching bond attributed to ester bond at 1,740 cm^{-1}, and medium C-O stretching bond at 1,050 cm^{-1} (primary alcohol) and at 1,170 cm^{-1} (ester and secondary alcohol)

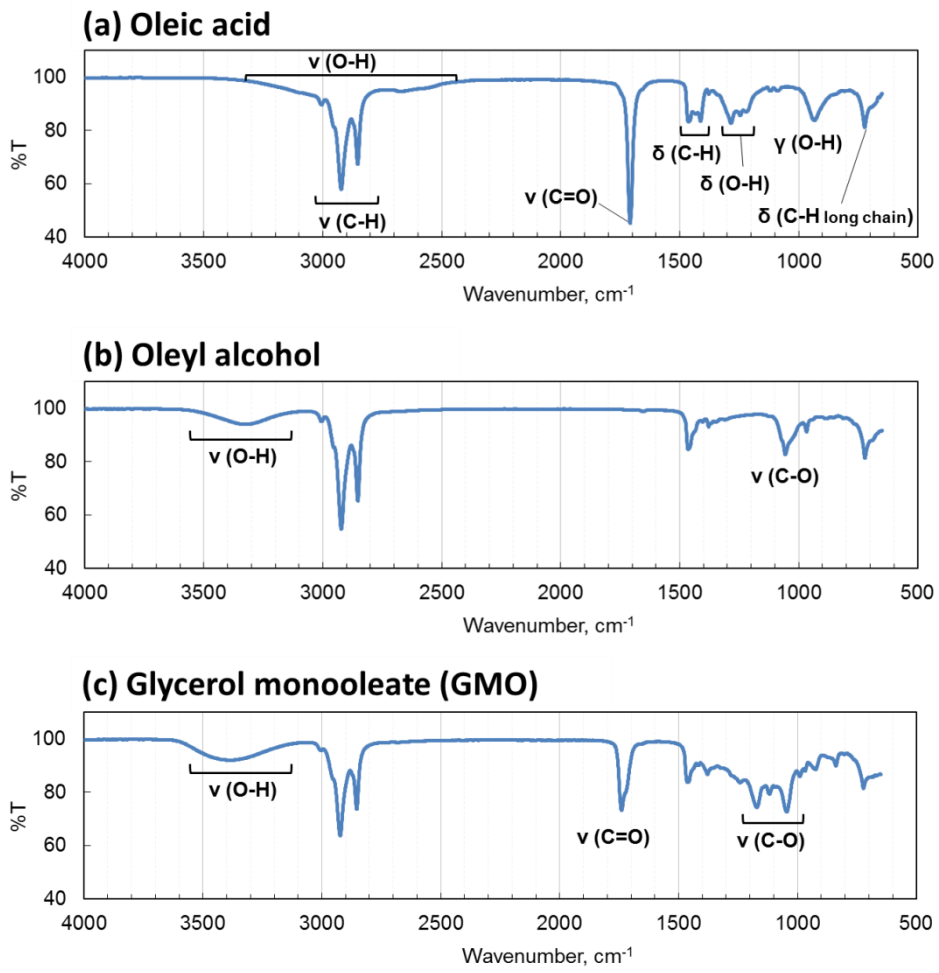

Fig. 3-19. IR spectra of the FMs, (a) oleic acid, (b) oleyl alcohol, (c) GMO

The IR spectra of the base fluids, PAO and the model CVTF, are shown in Fig. 3-20. While (a) PAO has the peaks only derived from hydrocarbon structure, (b) CVTF base fluid shows some additional peaks attributed to the CVTF additives, however, the peak intensity of the additives are weak due to the low dosage.

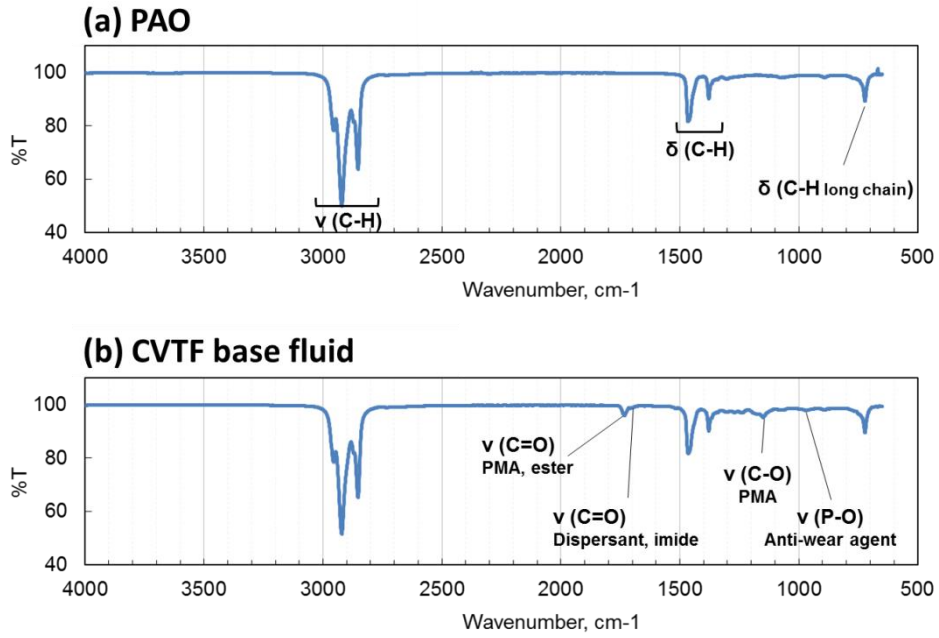

Fig. 3-20. IR spectra of the base fluids, (a) PAO, (b) CVTF base fluid

Fig. 3-21 shows the IR spectra of the CVTF additives. Considering the formulated amount and the peak intensity, the important peaks for the discussion should be as follows;

(a) viscosity modifier – C=O bond at 1,730 cm^{-1} and C-O bond at 1,150 cm^{-1}
(b) dispersant – C=O bond attributed to imide group at 1,700 cm^{-1}
(c) P anti-wear agent – P-O-C bond attributed to phosphite structure at 970 cm^{-1}

Finally, the IR spectra of the fresh tribotest specimens are presented in Fig. 3-22. The steel plate does not have any peaks, while the paper plates shows some specific peaks attributed to the fibres and the diatomite earth (silica). It is notable that a wide and strong peak derived from C-O group (cellulose fibre) and Si-O group (diatomite earth) stretches between 1,100 and 1,000 cm^{-1}. This adsorption makes it difficult to detect hydroxyl group adsorption on the paper surface, so that it is necessary to focus on the adsorption of carbonyl group between 1,750 and 1700 cm^{-1}.

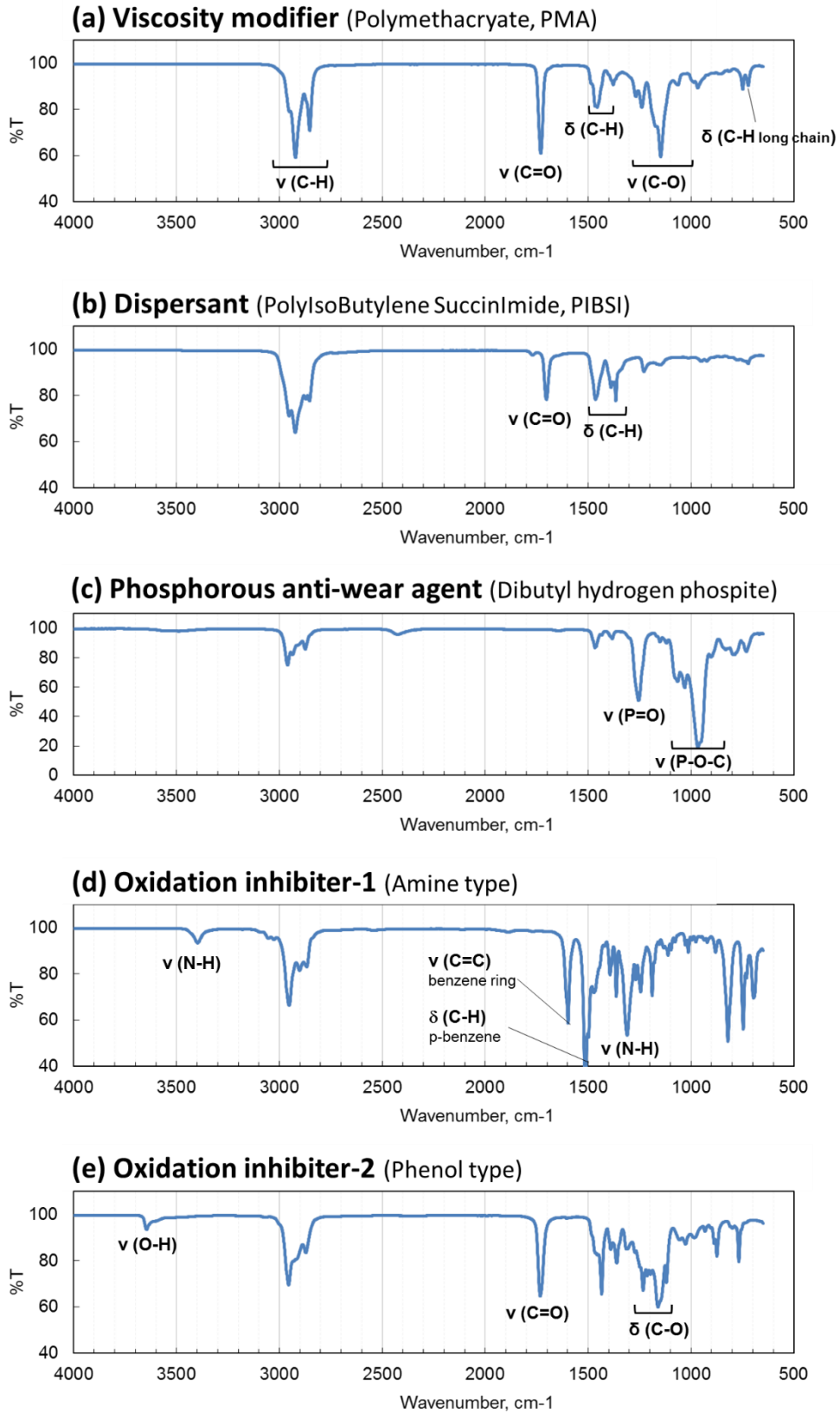

Fig. 3-21. IR spectra of the CVTF additives, (a) viscosity modifier, (b) dispersant, (c) P anti-wear agent, (d) and (e) oxidation inhibiter

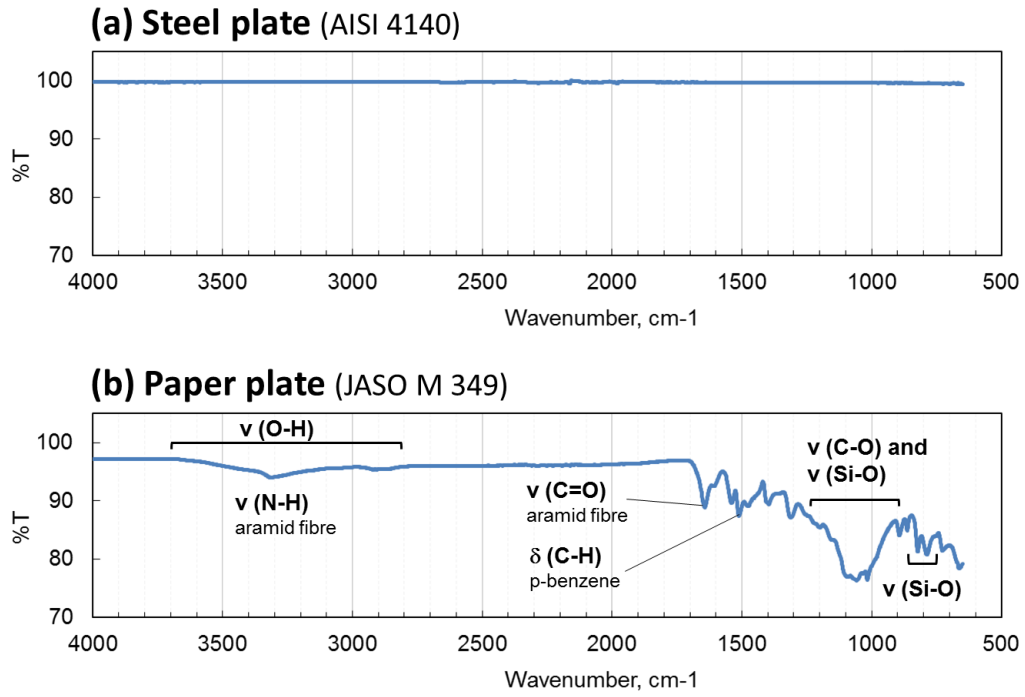

Fig. 3-22. IR spectra of the tribotest substrates
(a) steel plate (AISI 4140), (b) paper plate (JASO M 349)

In order to detect a minor difference in IR spectra caused by adsorption of additives on the surface, difference IR spectra technique was utilised. Fig. 3-23 shows an example using test oils, the CVTF base fluid and the oleic acid formulation. Although it is difficult to identify a peak derived from oleic acid due to the overlap with the carbonyl group of PMA, the subtraction of the spectra can make the acid peak clear. The chemical structure on the substrate is discussed based on previous research [156-175].

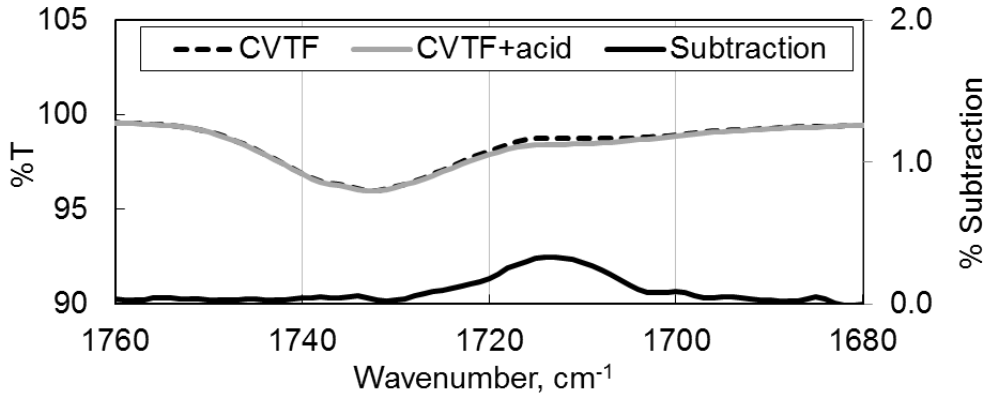

Fig. 3-23. Detection of oleic acid in the CVTF base fluid using difference IR spectra

3.5.5. Summary of Surface Analysis

Table 3-8 summarises which surface analysis technique was applied for the post tribotest specimens.

The TE77 specimens tested with the steel/steel configuration were assessed with all the instruments. Wear on the pins was measured using WLI, surface morphology on the steel plates was observed by SEM, and the chemical nature on the plates was assessed by EDX, XPS and ATR-FTIR. It is notable about the penetration depth of the instruments shown in Fig. 3-24. XPS enables to observe the uppermost surface up to around 5 nm including the adsorption film layers of the FMs, while the information acquired by EDX and ATR-FTIR mainly reflects the chemical nature of the reaction film due to the larger measurement depth at around 1 μm.

In terms of the paper specimens, the TE77 post-test papers were analysed using all the instruments except for WLI which could not detect wear on the paper. The post-test MTM paper plates were assessed only with ATR-FTIR because it was difficult to pre-treat the post-test plates appropriate for SEM/EDX and XPS measurements which require high vacuum condition. The friction properties and the ATR-FTIR results of the TE77 and MTM paper tests were compared for the discussion on the correspondence between the TE77 and MTM tribotests. The chemical information obtained using the TE77 post-test papers could be useful to understand the μ-V characteristics measured using MTM.

Table 3-8. Tribotest specimens used for the surface analyses

	TE77 steel	TE77 paper	MTM paper
WLI	✓ (pin)	-	-
SEM/EDX	✓	✓	-
XPS	✓	✓	-
ATR-FTIR	✓	✓	✓

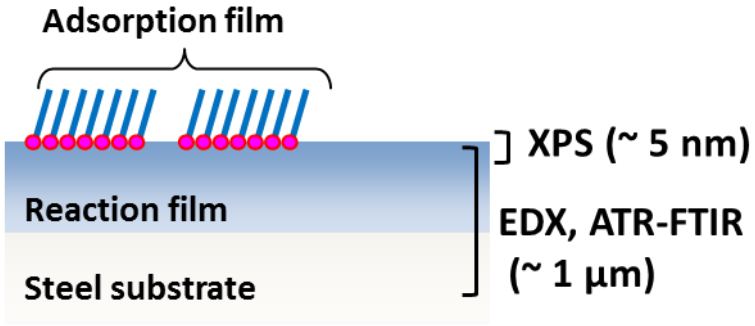

Fig. 3-24. Schematic image on the penetration depth of the instruments

Chapter 4 – Results – TE77 Steel Contact Tests

To start the chapters of results, the outline is summarised in Table 4-1. It is divided into three chapters; “Chapter 4 – Results – TE77 Steel Contact Tests”, “Chapter 5 – Results – TE77 Paper Contact Tests” and “Chapter 6 – Results – MTM Paper Clutch Tests”.

Chapter 4 and 5 shows the results for the TE77 tests at the steel/steel contact and the paper/steel contact, respectively. The effect of the FMs on the friction properties was observed using the TE77, then the post-test specimens were analysis in order to investigate the chemical and topographical condition on the surface using WLI, SEM, EDX, XPS and ATR-FTIR. The duration of the tribotests was determined at 60 minutes to observe the initial stable condition, and the performance was examined at both 100°C and 40°C to discuss the influence of the temperature. In addition, the long-term sliding tests (12 or 24 hours) at the paper/steel contact were carried out for some lubricants that showed interesting properties in the initial tests.

The effect of the FMs on μ-V characteristics is investigated using MTM in Chapter 6. Both the initial performance tests and the durability tests for 16 hours were carried out in order to assume the chemical nature of the FMs on the paper surface in detail. The post-test paper plates and lubricants were assessed using ATR-FTIR.

Table 4-1. Outline of the Results chapters (Chapter 4 - 6)

<table>
<tr><td colspan="2"></td><td>Steel/steel contact</td><td colspan="2">Paper/steel contact</td></tr>
<tr><td colspan="2">Tribometer</td><td>TE77</td><td>TE77</td><td>MTM</td></tr>
<tr><td colspan="2">Chapter</td><td>Chapter 4 - TE77
Steel Contact Tests</td><td>Chapter 5 - TE77
Paper Contact Tests</td><td>Chapter 6 - MTM
Paper Clutch Tests</td></tr>
<tr><td rowspan="2">Initial test</td><td>100°C</td><td>4.1. TE77 Steel Contact Tests at 100°C</td><td>5.1. TE77 Paper Contact Tests at 100°C</td><td rowspan="2">6.1. MTM Initial Performance Tests</td></tr>
<tr><td>40°C</td><td>4.2. TE77 Steel Contact Tests at 40°C</td><td>5.2. TE77 Paper Contact Tests at 40°C</td></tr>
<tr><td rowspan="2">Long-term test</td><td>100°C</td><td>-</td><td>5.3. TE77 Durability Tests at 100°C</td><td rowspan="2">6.2. MTM Durability Performance Tests</td></tr>
<tr><td>40°C</td><td>-</td><td>-</td></tr>
</table>

4.1. TE77 Steel Contact Tests at 100°C

4.1.1. Friction Coefficient

The friction coefficient for the test oils were evaluated using TE77 in the steel/steel contact configuration. The following sliding condition was applied as explained in detail in Chapter 3; sliding speed: 0.20 m/s (20 Hz, 5.0 mm), temperature: 100 °C, pressure: 1.0 GPa, which simulates the contact at the belt-pulley mechanism of CVT. The tribotests were repeated at least three times for each of the test oils. During the test, electrical contact resistance between the TE77 steel pin and the steel plate was collected together with the frictional force in order to estimate the growth of a tribofilm. A higher resistance generally means a thicker and more stable tribofilm is formed.

Fig. 4-1 shows the friction results for the PAO formulations. The ranking of the friction after 60 minutes was as follows; (highest) PAO = PAO+alcohol >> PAO+acid ≥ PAO+GMO (lowest). The friction was almost stable during the test except for PAO+GMO which showed a gradual friction decrease after 30 minutes.

The electrical contact resistance during the tests is summarised in Fig. 4-2. While PAO and PAO+alcohol had lower resistance, PAO+acid showed higher value meaning the presence of the tribofilm interrupting the current. The resistance of PAO+GMO sharply increased just after 30 minutes, which shows a good agreement with the frictional trend.

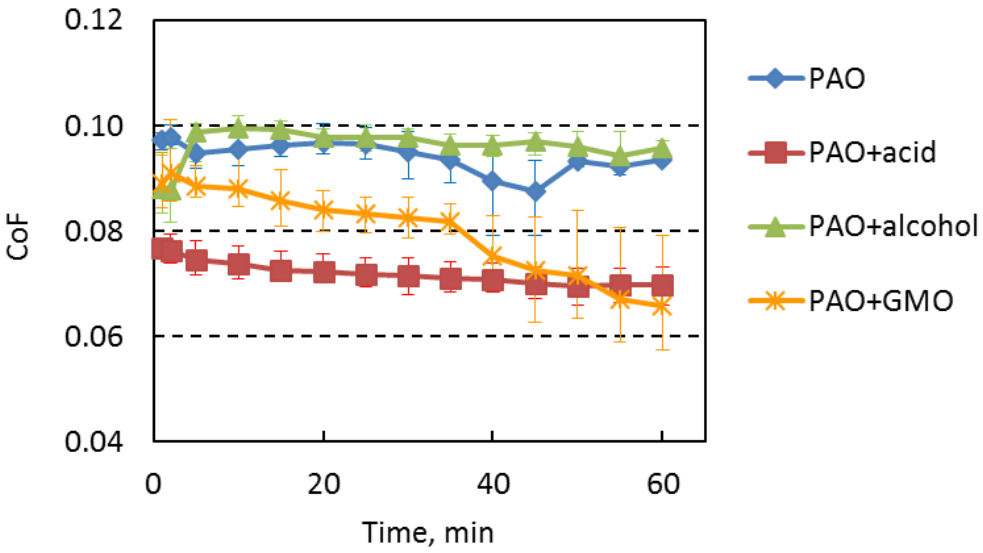

Fig. 4-1. Friction coefficient of steel/steel contact measured by TE77 (PAO formulation, 100°C, 60 min, 0.20 m/s, 1.0 GPa)

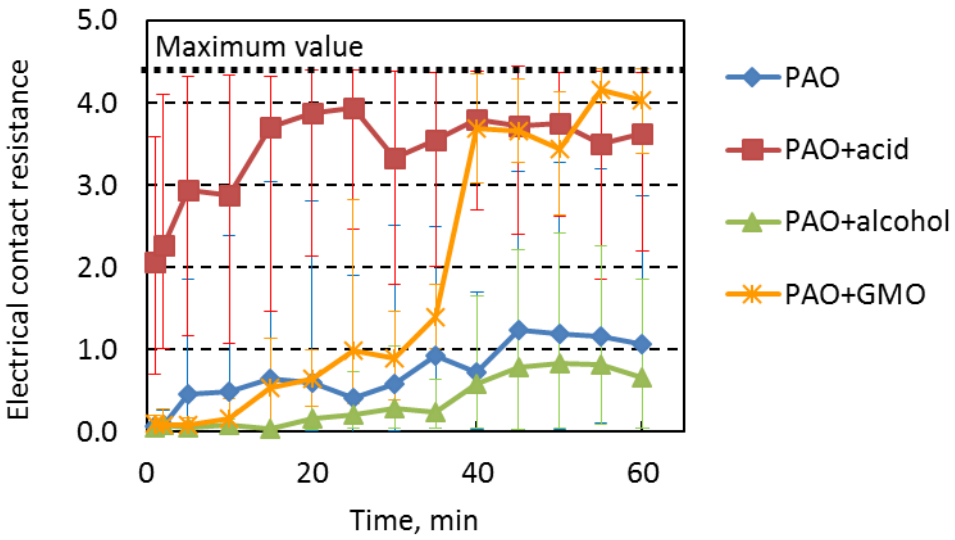

Fig. 4-2. Electrical contact resistance of steel/steel contact during the TE77 tests (PAO formulation, 100°C, 60 min, 0.20 m/s, 1.0 GPa)

The friction coefficient was also evaluated for the CVTF test oils under the same test configuration. The typical CVTF additives were formulated in the oils as introduced in the previous chapter. The results for the friction coefficient are shown in Fig. 4-3. The ranking of the friction after 60 minutes was as follows; (highest) CVTF = CVTF+acid = CVTF+alcohol > CVTF+GMO (lowest). The difference from the PAO tests is the effect of oleic acid which did not work well; suggesting that the presence of other additives poisons the effect it has in friction reduction.

The electrical contact resistance results for the CVTF oils are shown in Fig. 4-4. In contrast to the PAO results, the resistance of all the oils reached maximum just after the start of the sliding. This indicates a rapid formation of the tribofilm formed by the CVTF additives. However, only CVTF+acid took around 30 minutes to reach the stable resistance, confirming that oleic acid had an influence on the tribofilm formation.

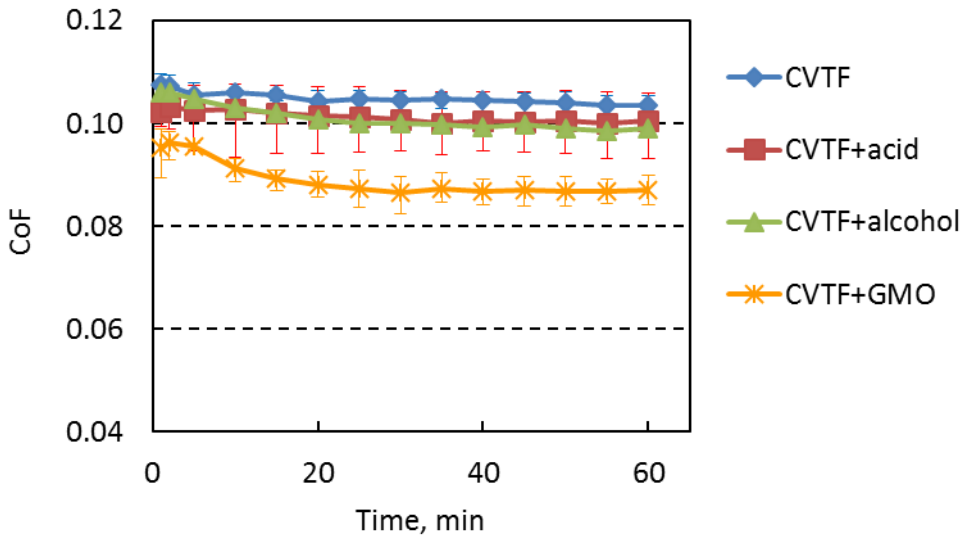

Fig. 4-3. Friction coefficient of steel/steel contact measured by TE77
(CVTF formulation, 100°C, 60 min, 0.20 m/s, 1.0 GPa)

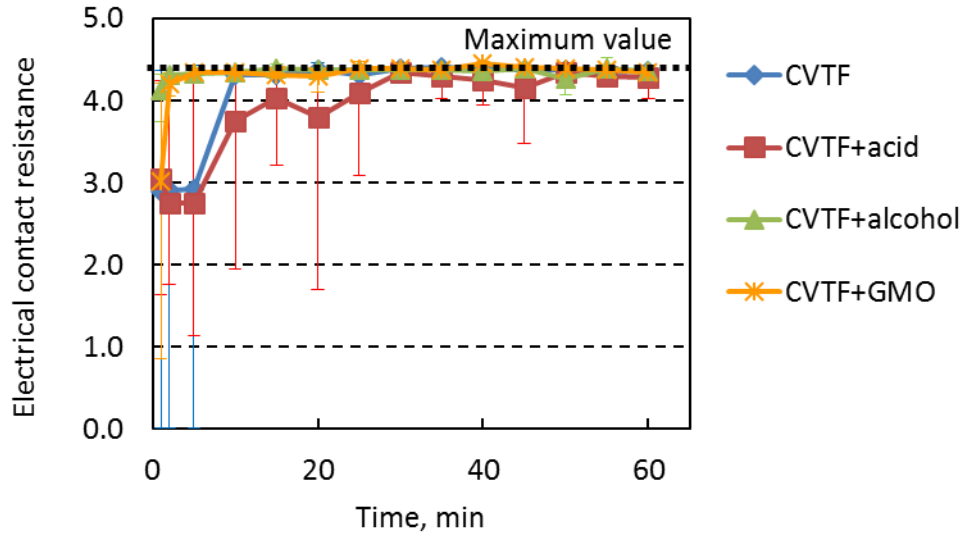

Fig. 4-4. Electrical contact resistance of steel/steel contact during the TE77 tests
(CVTF formulation, 100°C, 60 min, 0.20 m/s, 1.0 GPa)

The friction results at the end of the initial test (after 60 minutes) are summarised in Fig. 4-5. The trend of each FM in steel/steel sliding configuration was as follows;

- Oleic acid reduced the friction significantly when added in PAO, however, the effect diminished completely in the presence of the CVTF additives.
- Oleyl alcohol did not present any effect either in PAO or in the formulated oil.
- GMO showed similar trend to oleic acid; a good friction reduction in PAO and a restricted effect in the formulated CVT fluid. In contrast to oleic acid, GMO was capable of reducing the friction slightly even formulated with the CVTF additives.

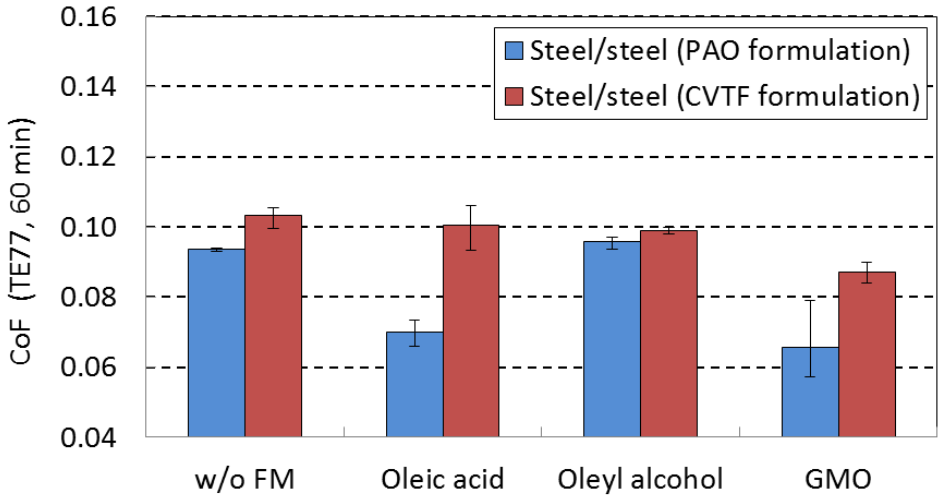

Fig. 4-5. TE77 friction coefficient of steel/steel contact (after 60 minutes, 100°C)

4.1.2. Wear Measurement by WLI

The wear on the post-test TE77 steel pins was measured using WLI, an optical interferometer. As mentioned in the previous chapter, the results focus on the wear on the steel pins because the wear scar on the plate was not obvious for most of the samples. The wear depth and volume are summarised in Fig. 4-6 and Fig. 4-7, respectively. In addition, 3D images of the wear are shown in Fig. 4-8 and Fig. 4-9. The severity of the wear was categorised as follows in this study;

Significant wear – wear depth; > 1.0 µm, wear volume; > 10,000 μm^3

Intermediate wear – wear depth; between 0.5 µm and 1.0 µm
wear volume; between 3,000 μm^3 and 10,000 μm^3

Mild wear – wear depth; < 0.5 µm, wear volume; < 3,000 μm^3

When the wear depth is over 1.0 µm ranked as significant wear, the contact area radius between the pin and the plate exceeds the theoretical value at 110 µm based on Hertzian contact theory as shown in Fig. 4-10. The mild wear could be achieved with the effect of the anti-wear agent in the CVTF formulations. The comments on the results are shown below;

- Comparing PAO and the formulated CVTF without the FM, PAO showed significant wear, around 1.0×10^5 µm^3 as average, while the CVTF presented the lowest wear volume.
- The oleic acid formulations showed an excellent anti-wear performance even with PAO. Only PAO+acid was able to achieve the mild wear among the PAO formulations, which implies that the oleic acid was capable of forming an effective film on the steel surface by itself.
- Oleyl alcohol with PAO presented the significant wear at around 2.0×10^4 µm^3, though, it is obviously smaller than PAO. It means that oleyl alcohol was able to work on the steel at some extent, however, it had no effect on the friction reduction (Fig. 4-1). In contrast, when formulated with the additives, the wear became mild comparable to that of the CVTF base fluid. In this case, oleyl alcohol appeared not to affect the chemical nature on the steel.
- GMO with PAO presented the intermediate anti-wear performance showing the wear volume at around 1.0×10^4 µm^3. It is notable that CVTF+GMO still showed the intermediate wear at around 3.0×10^3 µm^3, while the other CVTF formulations achieved the mild wear ($1.0 \times 10^3 \sim 1.5 \times 10^3$ µm^3).

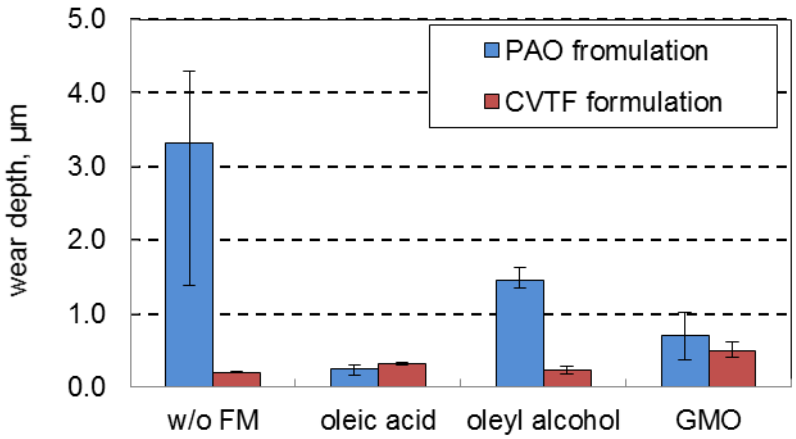

Fig. 4-6. Wear depth of the post-test TE77 steel pins
(100 °C, after 60 minutes test)

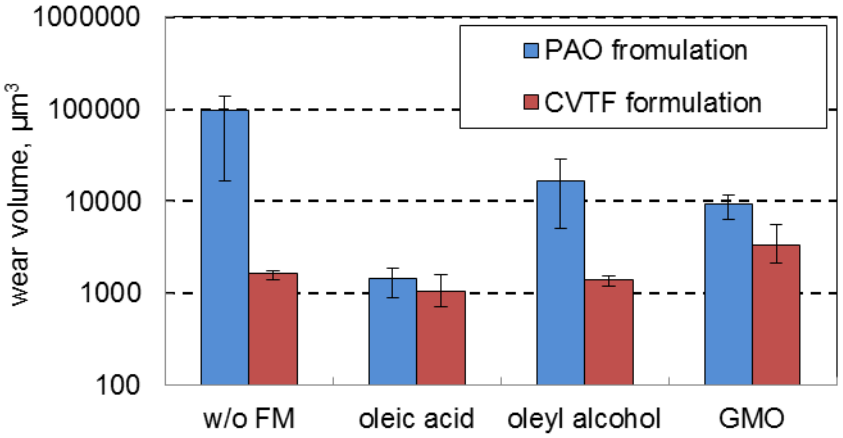

Fig. 4-7. Wear volume of the post-test TE77 steel pins
(100 °C, after 60 minutes test)

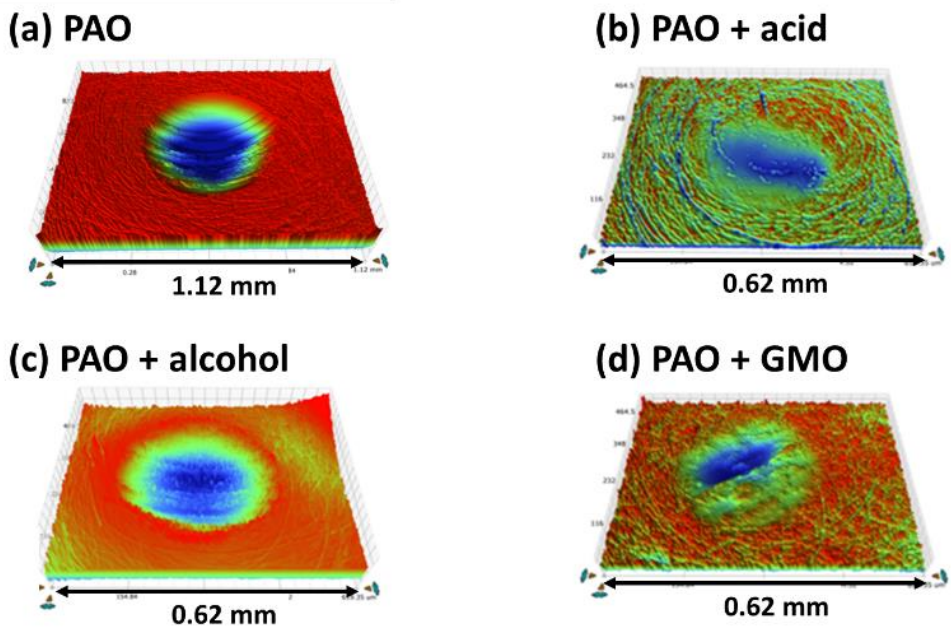

Fig. 4-8. Wear scar 3D images on the post-test TE77 steel pins
after testing PAO formulations (100 °C, 60 minutes)

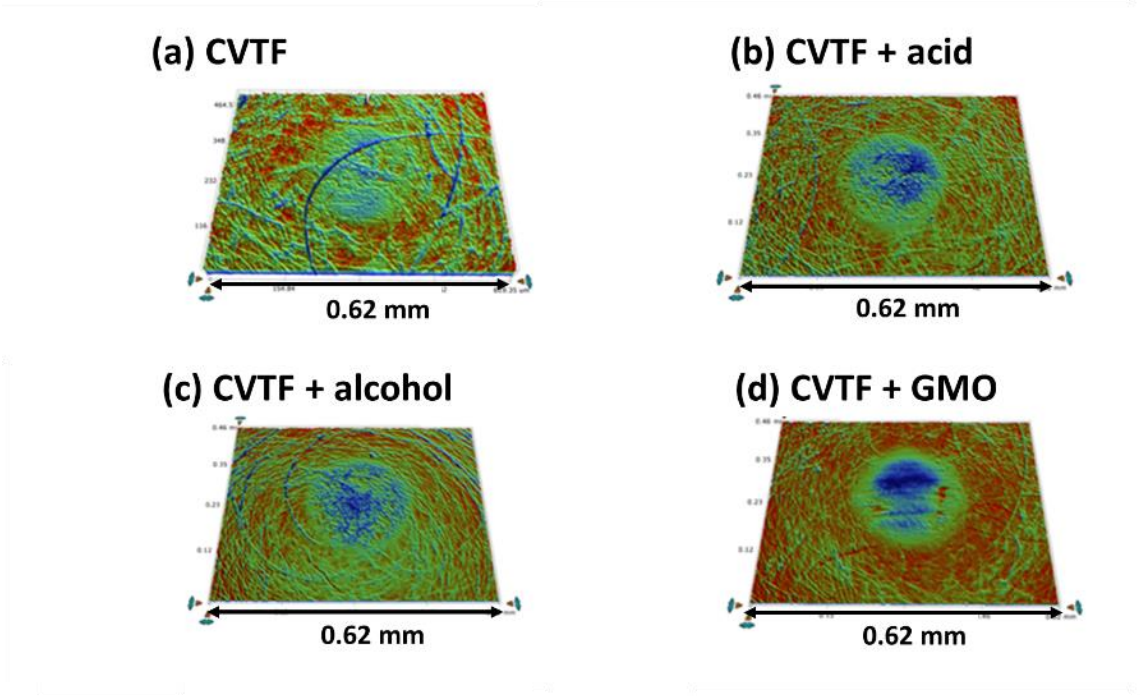

Fig. 4-9. Wear scar 3D images on the post-test TE77 steel pins after testing CVTF formulations (100 °C, 60 minutes)

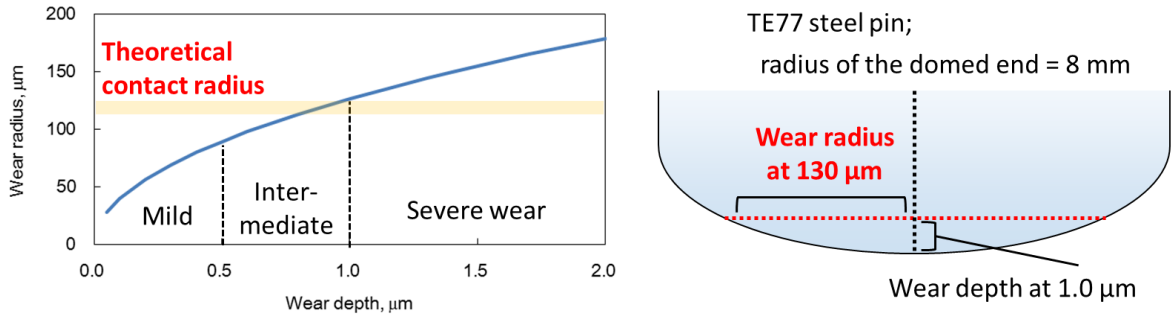

Fig. 4-10. Relationship among the wear depth, the wear radius and the theoretical contact radius based on Hertzian contact theory

4.1.3. Wear Track Observation by SEM

The wear tracks on the post-test TE77 steel plates of the PAO formulations are shown in Fig. 4-11. As expected from the WLI results, (a) PAO and (c) PAO+alcohol presented severe damage, showing the wear track partially scraped off. In contrast, significant wear was not observed in (b) PAO+acid and (d) PAO+GMO though the polish mark could be seen inside the wear track. The CVTF results did not show significant wear (Fig. 4-12). It is considered that the reaction film formed by the additives protected the steel surface.

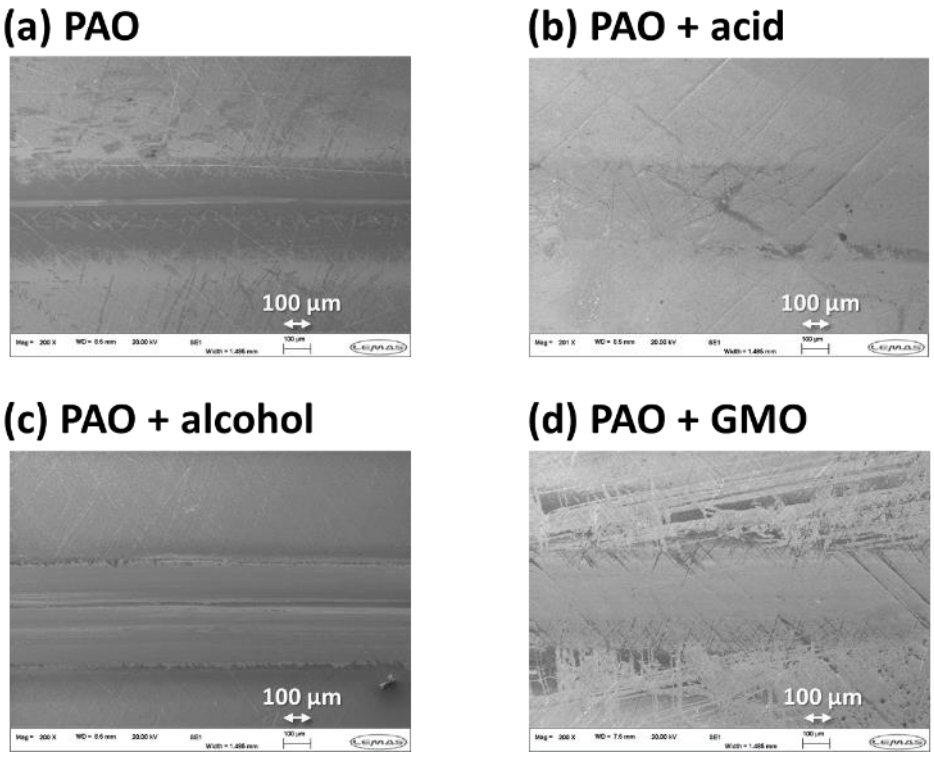

Fig. 4-11. SEM images of the post-test TE77 steel plates at 100 °C

a) PAO, b) PAO + oleic acid, c) PAO + oleyl alcohol, d) PAO + GMO

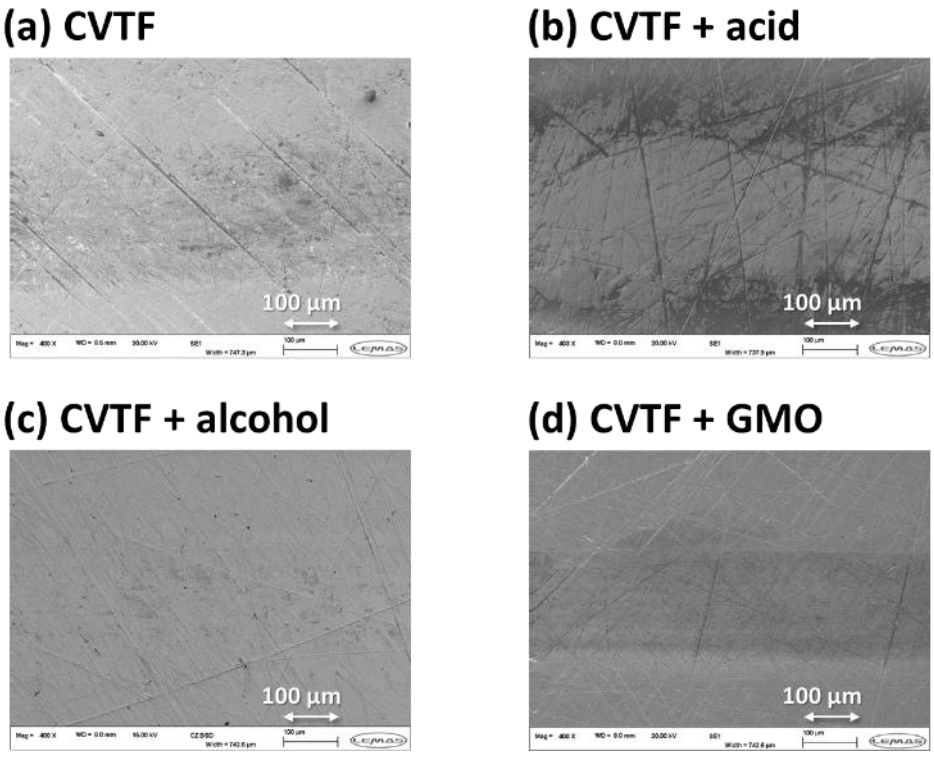

Fig. 4-12. SEM images of the post-test TE77 steel plates at 100 °C

a) CVTF, b) CVTF + oleic acid, c) CVTF + oleyl alcohol, d) CVTF + GMO

4.1.4. EDX Analysis

The wear track of the post-test TE77 steel plates was assessed using EDX in order to evaluate the element concentrations on the surface. Fig. 4-13 shows the results for the PAO formulations. As a reference, the result outside the wear track after testing PAO is shown together as "unworn surface". As mentioned in the previous chapter regarding the EDX analysis procedure, the penetration depth of EDX is considered to be approximately 1 μm. Therefore, the element concentrations obtained by EDX mainly reflect chemical information of the reaction film, rather than the adsorption film whose depth is generally less than 10 nm.

- PAO, PAO+alcohol and PAO+GMO increased the oxygen concentration. It would be derived from oxidative degradation of materials inside the wear scar as expected from the WLI wear measurements.
- The elemental concentrations of PAO+acid were quite similar to those of the unworn surface. It indicates that the oleic acid was capable of forming the FM film on the steel surface, protecting it from the wear.

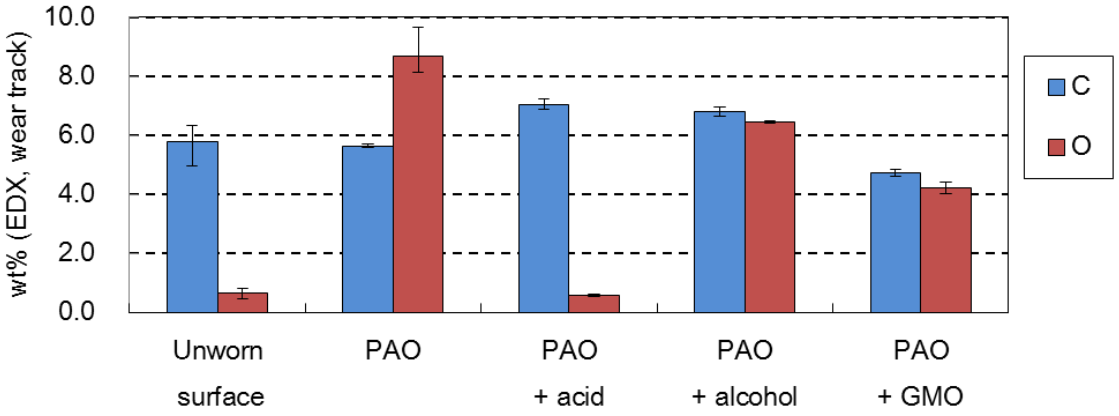

Fig. 4-13. EDX elemental analysis inside wear track of the post-test TE77 steel plates after testing PAO formulations (100 °C, 60 minutes)

* "unworn surface" data was outside the wear track of the plate after testing PAO

The EDX results of the CVTF formulations are summarised in Fig. 4-14. The bottom graph (Fig. 4-14(b)) focuses on the elements (Ca, S and P) attributed to the CVTF additives.

- While P and Ca were observed among the CVTF oils, just a slight amount of S was detected, which was almost within an error bar. The source of S is sulfonate contained in the detergent (overbased Ca sulfonate), though, it appeared not to react forming the tribofilm on the steel surface.
- The concentrations between CVTF and CVTF+alcohol were almost same. It supports the assumption that the oleyl alcohol could not adsorb on the steel surface, expected from the friction values and the other surface analysis results.
- CVTF+GMO showed a lower concentration for P or Ca. The reason is considered to be a competition between GMO and the other additives.
- CVTF+acid also presented a lower concentration of P and Ca. Interestingly, the Ca concentration was reduced much more than P, so that the ratio of P and Ca was different from the other test oils. This distinctive trend of CVTF+acid should imply a specific interaction between oleic acid and the other additives.

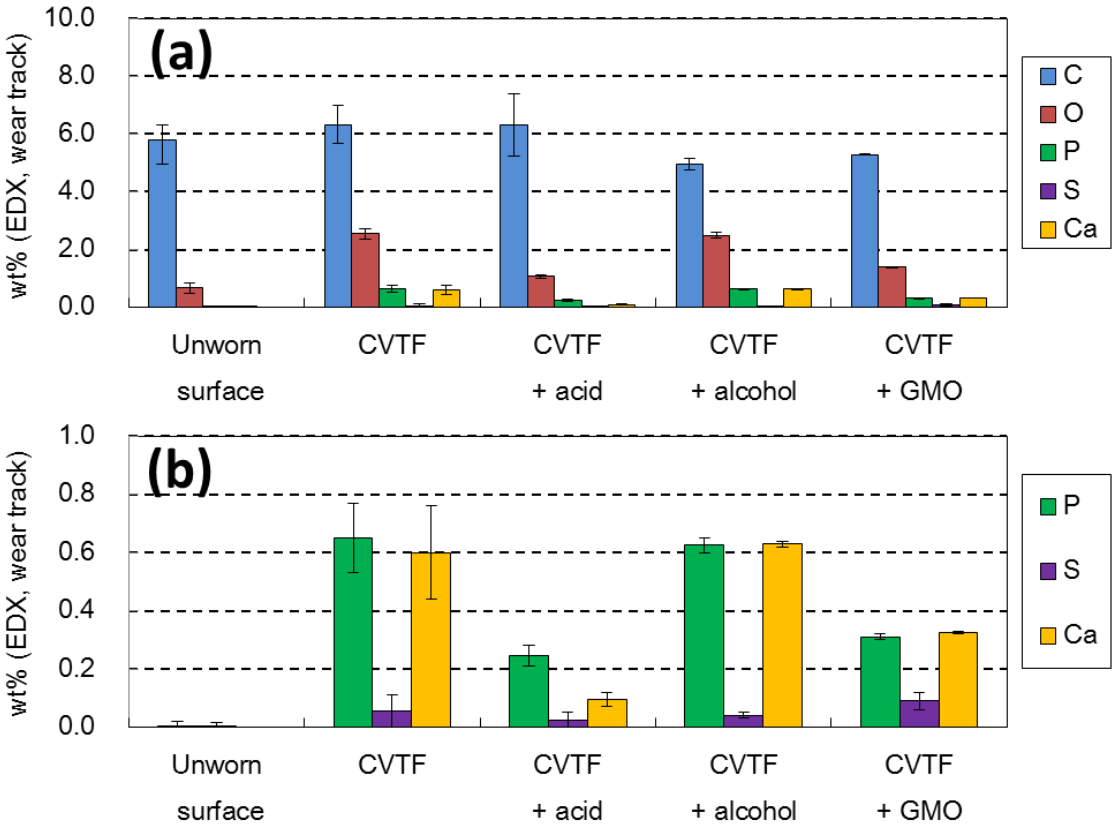

Fig. 4-14. EDX elemental analysis inside wear track of the post-test TE77 steel plates after testing CVTF formulations (100 °C, 60 minutes)

(a) all elements except for Fe, (b) focusing on P, S and Ca

* unworn surface was outside the wear track of the plate after testing PAO

4.1.5. XPS Analysis (PAO Formulations)

The chemical nature on the wear of the post-test TE77 plates was assessed using XPS. The elemental concentrations investigated using the XPS survey spectra for the PAO formulations are summarised in Table 4-2.

- Carbon, oxygen and iron were detected as expected because the chemical structure of all the contents, PAO and the FMs, consisted of only C or O.
- PAO without FM showed lower C and higher O and Fe concentrations compared to the other test oils with the FM. The reason should be the severe wear damage of PAO as shown in the wear measurement, which formed iron oxide on the steel surface.
- The other oils with FM showed a very similar trend for the elemental concentrations.

Table 4-2. XPS survey spectra inside the wear track on the post-test TE77 steel plates after testing PAO formulations (100 °C, 60 minutes)

	PAO formulations			
Element, % mass	w/o FM	oleic acid	oleyl alcohol	GMO
C 1s	61.7	69.8	69.5	69.6
O 1s	33.8	28.1	28.4	29.0
N 1s	-	-	-	-
Ca 2p	-	-	-	-
P 2p	-	-	-	-
Fe 2p	4.5	2.1	2.1	1.4

The XPS C 1s spectra of the PAO formulations are shown in Fig. 4-15. As mentioned in the previous chapter for the XPS test method, a peak attributed to saturated hydrocarbon (SHC) was fitted to 285.0 eV for all the XPS results shown afterwards.

- (a) PAO and (c) PAO+alcohol showed almost the same spectrum shape showing three peaks; at approximately 289 eV derived from a carboxyl group (O=C-O), at 286.5 eV from a C-O bond and at 285.0 eV from SHC. The former two peaks with oxygen bond should be attributed to carbon contamination because these

two formulations showed severe wear on the steel plate. The steel surface was significantly damaged, so that the film formation should be inhibited.

- On the other hand, (b) PAO+acid and (d) PAO+GMO presented an additional peak at 288.1 eV derived from O-C-O bond, and PAO+GMO showed higher peak intensity. It is considered that this peak was attributed to the adsorbed FM by taking into account the low friction coefficient of both oils.

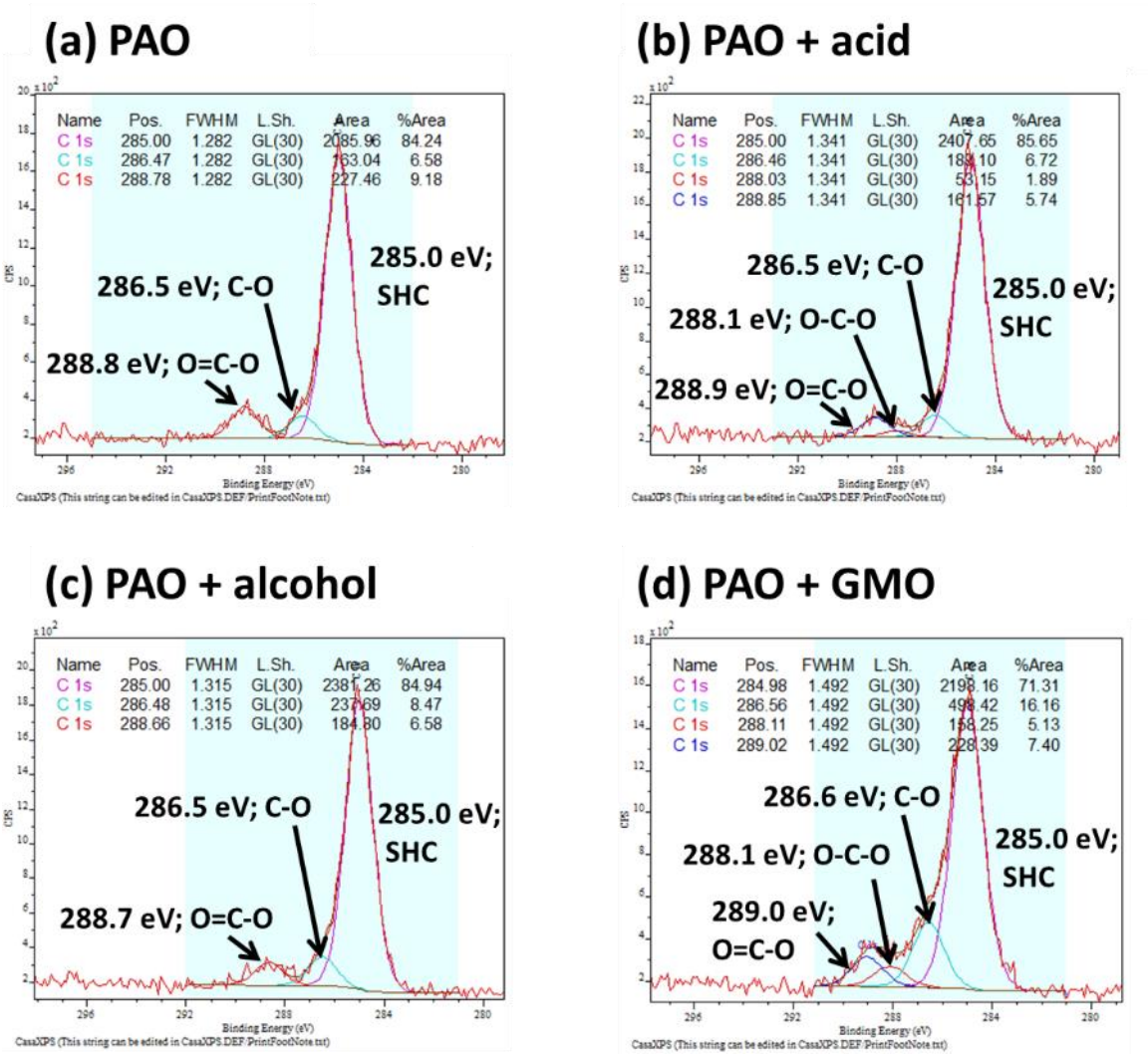

Fig. 4-15. XPS C 1s spectra inside the wear track on the post-test TE77 steel plates after testing PAO formulations (100 °C, 60 minutes)

a) PAO, b) PAO + oleic acid, c) PAO + oleyl alcohol, d) PAO + GMO

The XPS O 1s spectra of the PAO formulations are shown in Fig. 4-16. Because it is not easy to identify the peaks into an exact chemical structure due to the overlapped peaks of oxygenated chemical compounds, they were briefly divided into the three general peaks; metal oxide (MBO) approximately at 530 eV, non-bridging oxygen (NBO, C=O or C-O-M) at 532 eV and bridging oxygen (BO) at 533 eV.

While MBO was the highest peak in (a) PAO and (c) PAO+alcohol spectra, NBO was the highest for (b) PAO+acid and (d) PAO+GMO. This result implies that oleic acid and GMO were able to form a chemical bond with steel surface (C-O-Fe) as a stable adsorption film, which shows a good agreement with the C 1s spectra and the FM effect at the TE77 friction tests.

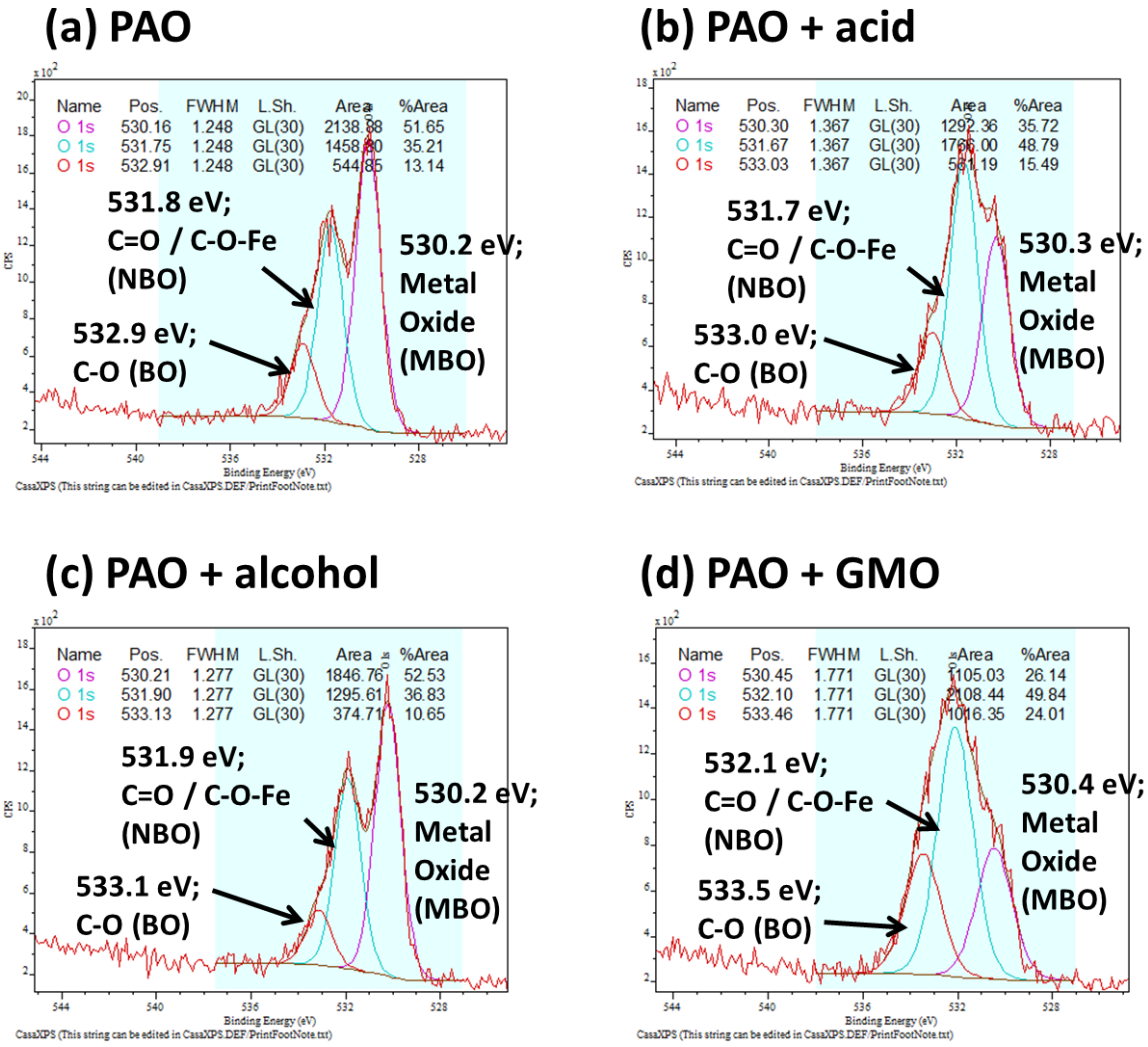

Fig. 4-16. XPS O 1s spectra inside the wear track on the post-test TE77 steel plates after testing PAO formulations (100 °C, 60 minutes)

a) PAO, b) PAO + oleic acid, c) PAO + oleyl alcohol, d) PAO + GMO

4.1.6. XPS Analysis (CVTF Formulations)

XPS survey spectra for the CVTF formulations are summarised in Table 4-3.

- The elements derived from the CVTF additives were detected. N was from the dispersant, Ca from the over-based Ca sulfonate and P from the anti-wear agent.
- Regarding Ca and P, all the samples, except for CVTF+acid, showed the similar concentrations approximately at 4 mass% for Ca and 8 mass% for P. CVTF+acid presented lower Ca concentration at 3.0 mass% and higher P at 10.8 mass%, which indicates that oleic acid had some interactions with the additives and affected the chemical nature on the steel surface.

Table 4-3. XPS survey spectra inside the wear track on the post-test TE77 steel plates after testing CVTF formulations (100 °C, 60 minutes)

	CVTF formulations			
Element, % mass	w/o FM	oleic acid	oleyl alcohol	GMO
C 1s	59.3	57.5	61.9	56.6
O 1s	23.4	24.4	21.2	27.7
N 1s	3.9	3.7	3.7	2.4
Ca 2p	4.6	3.0	5.1	4.8
P 2p	8.2	10.8	7.8	7.6
Fe 2p	0.6	0.6	0.3	0.9

The XPS C 1s spectra of the CVTF formulations are shown in Fig. 4-17.

- The spectra of (a) CVTF, (b) CVTF+acid and (c) CVTF+alcohol had a similar trend with three peaks; approximately 288.3 eV derived from N=C-O attributed to the adsorption of the dispersant, 286.5 eV from C-O or C-N and a reference 285.0 eV peak from SHC. These results indicate that the adsorption of oleic acid and oleyl alcohol was negligible in the presence of the CVTF additives.
- The peak at around 289 eV attributed to carboxylate (O=C-O) was detected only in the spectrum of (d) CVTF+GMO, which implies the adsorption of GMO on the steel surface. This result agrees with the TE77 steel friction results that only CVTF+GMO showed the friction reduction at the steel/steel contact when formulated with the CVTF additives.

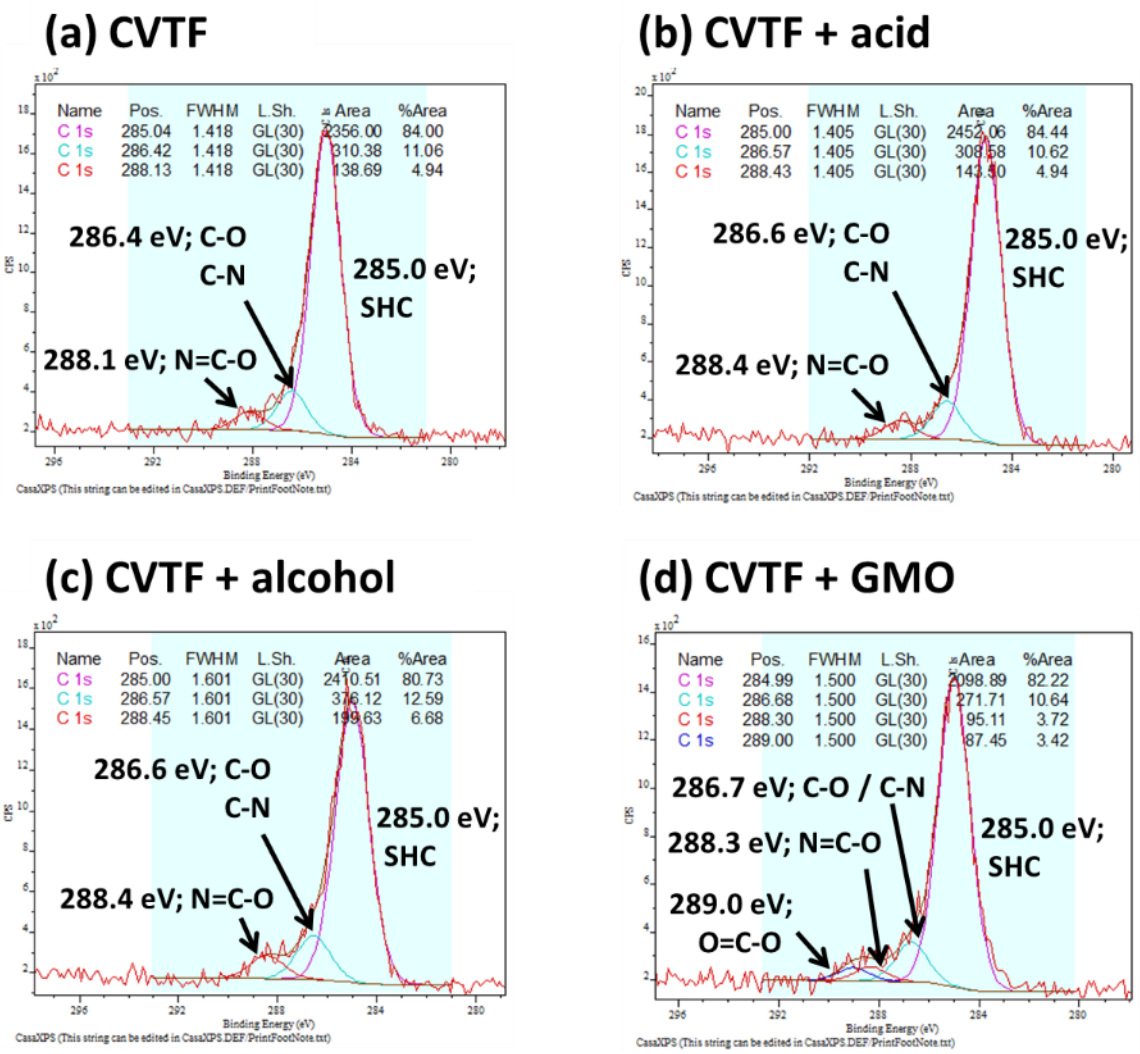

Fig. 4-17. XPS C 1s spectra inside the wear track on the post-test TE77 steel plates after testing CVTF formulations (100 °C, 60 minutes)

a) CVTF, b) CVTF + oleic acid, c) CVTF + oleyl alcohol, d) CVTF + GMO

The XPS O 1s spectra for the CVTF formulations are shown in Fig. 4-18.

- Regarding the MBO peak, all the spectra had a lower intensity compared with the PAO formulations (Fig. 4-16). It implies that the FMs and the additives formed an adsorption and a reaction film on the steel, covering the iron oxide substrate surface.

- Especially, the spectrum of (b) CVTF+acid did not have the MBO peak. This trend can be linked with the XPS survey result that CVTF+acid showed different P and Ca concentrations from the other oils.
- The peak positions of NBO are around 531.4 eV, shifted to a lower energy compared with the PAO formulations being approximately at 532 eV. This was likely as a result of the nitrogen bond (N=C-O) of the dispersant.

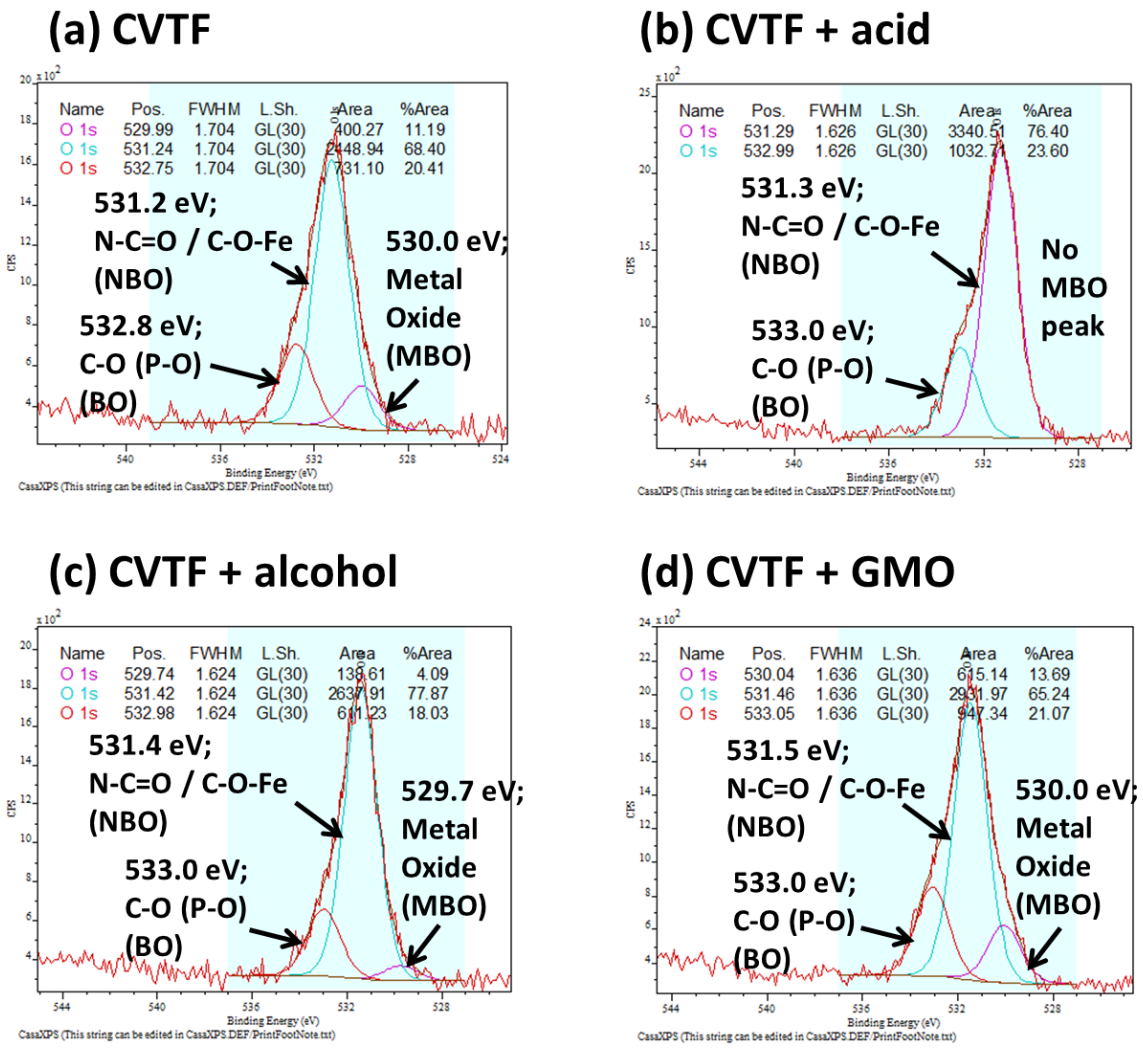

Fig. 4-18. XPS O 1s spectra inside the wear track on the post-test TE77 steel plates after testing CVTF formulations (100 °C, 60 minutes)

a) CVTF, b) CVTF + oleic acid, c) CVTF + oleyl alcohol, d) CVTF + GMO

4.1.7. ATR-FTIR Analysis

The wear track on the post-test TE77 was also analysed using ATR-FTIR. The penetration depth of the IR beam is generally at approximately 1 μm, which is comparable to EDX. Therefore, the chemical nature observed by ATR-FTIR is mainly attributed to the reaction film whose thickness is between a few tens and a few hundreds of nm.

The ATR-FTIR spectra of the PAO formulations are summarised in Fig. 4-19.

- (a) PAO and (b) PAO+acid did not show any obvious peak. It is interesting that (b) PAO+acid did not indicate the presence of the thick reaction film, while the other results, such as the wear depth of the XPS C 1s spectrum, predicted formation of the stable FM film. It means oleic acid was possible to form a thin film less than around 10 nm on the uppermost steel surface.
- (c) PAO+alcohol had many peaks derived from various organic structures, such as hydrocarbon, carbonyl group and benzene ring. They should be attributed to degradative products produced under the severe sliding conditions, which could not be removed by rinsing with heptane. (d) PAO+GMO also showed the similar peaks, although the intensity was much weaker than that of PAO+alcohol.

Then, the spectra of the CVTF formulations are summarised in Fig. 4-20.

- All the spectra presented a peak attributed to P-O stretching.
- While the peak position of (a) CVTF, (c) CVTF+alcohol and (d) CVTF+GMO was at around 1,130 cm^{-1}, that of (b) CVTF+acid was shifted to lower wave number, resulting in a wide peak stretching between 1,200 and 900 cm^{-1}.
- This difference is due to be the chemical structure of the phosphorous compounds formed in the reaction film; pyrophosphate (P_2O_7) has a relatively lower peak position compared with phosphate (PO_4). CVTF+acid did form a distinctive film consisting of P_2O_7 and PO_4, while the other test oils formed the reaction film mainly with PO_4.
- These results imply the special interaction between oleic acid and the additives as already expected form the other results.

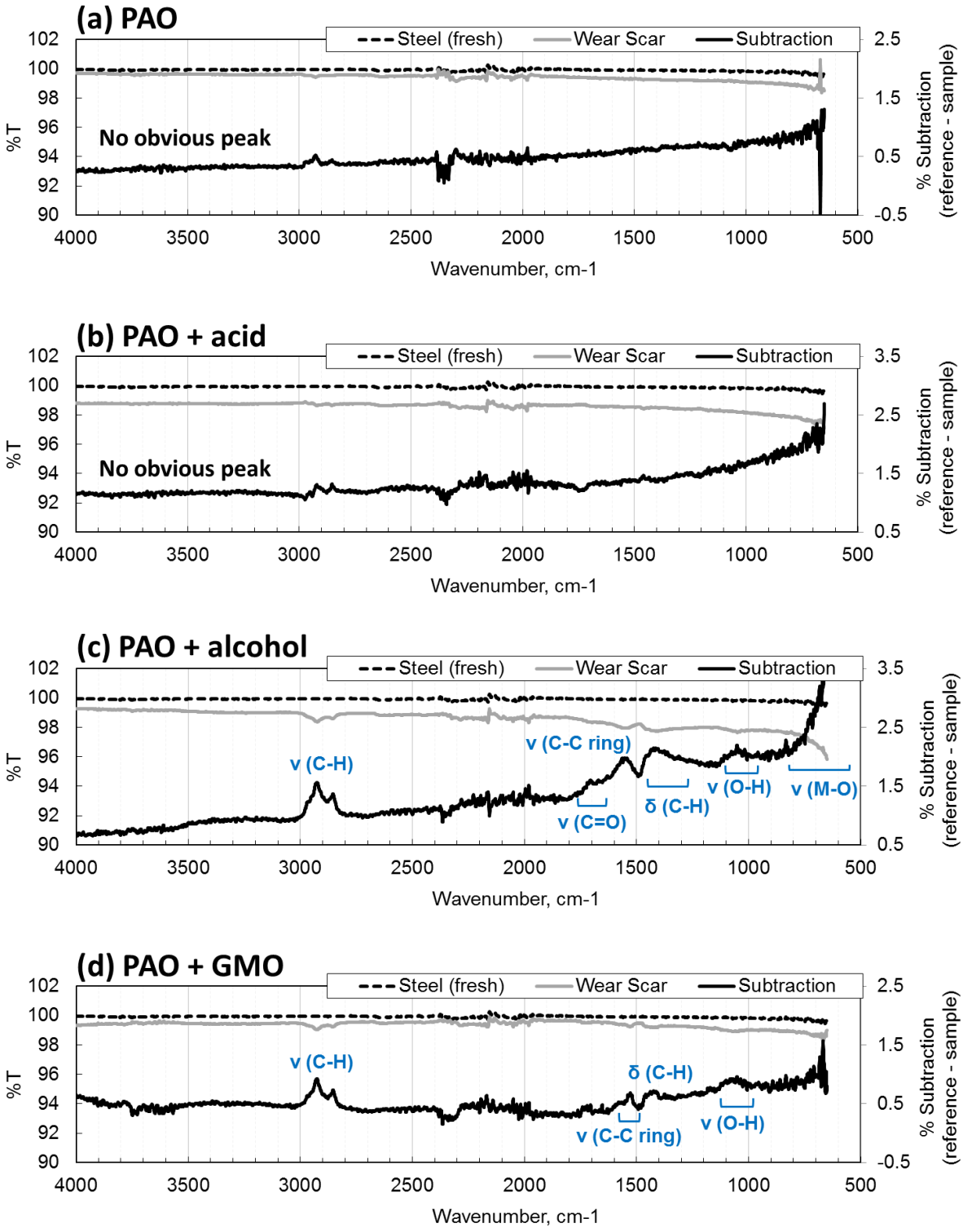

Fig. 4-19. ATR-FTIR spectra on wear track of the post-test TE77 steel plates after testing PAO formulations (100 °C, 60 minutes)

a) PAO, b) PAO + oleic acid, c) PAO + oleyl alcohol, d) PAO + GMO

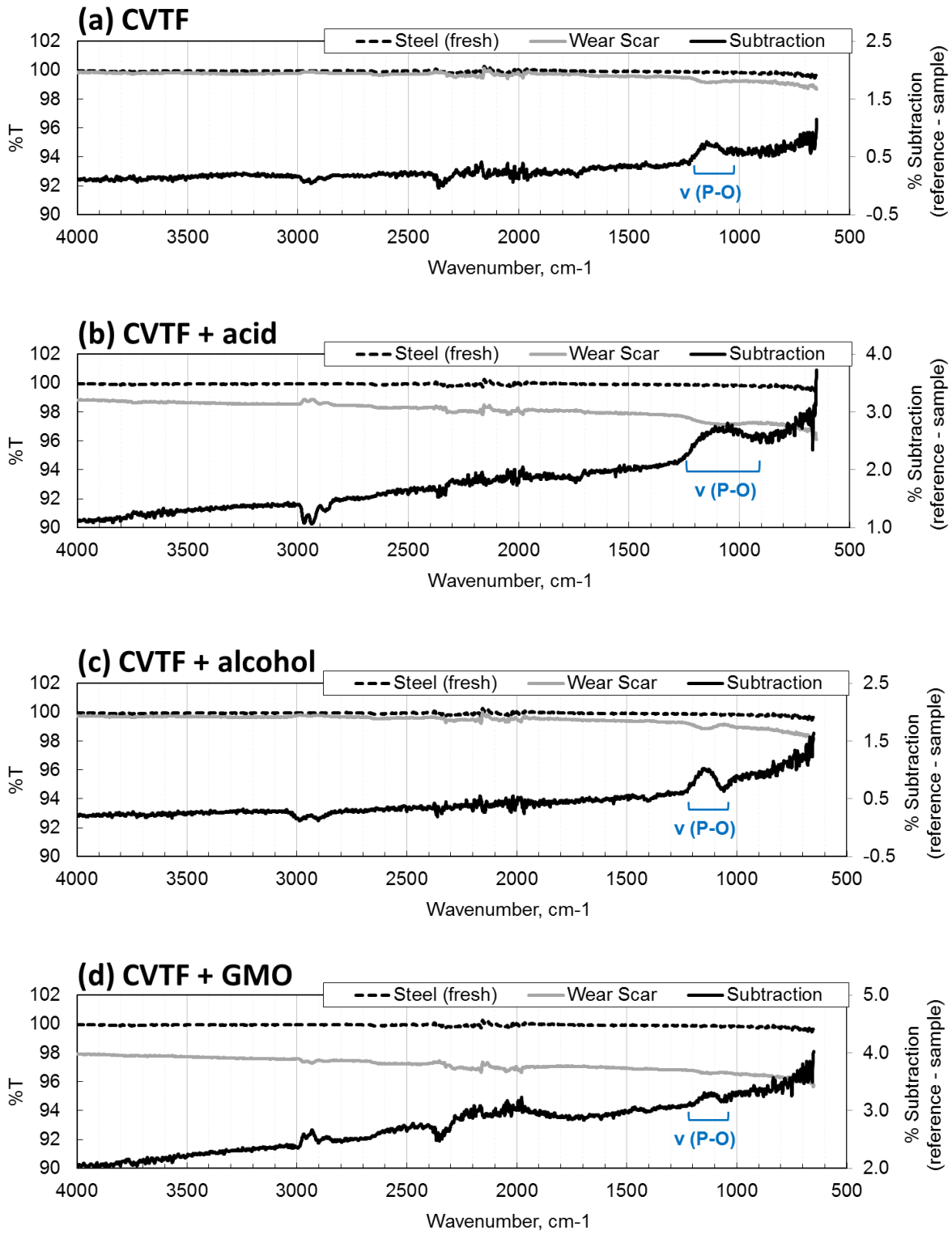

Fig. 4-20. ATR-FTIR spectra on wear track of the post-test TE77 steel plates after testing CVTF formulations (100 °C, 60 minutes)

a) CVTF, b) CVTF + oleic acid, c) CVTF + oleyl alcohol, d) CVTF + GMO

4.1.8. Summary of TE77 Steel Contact Tests at 100 °C

The results of the TE77 steel/steel sliding tests at 100°C are summarised in Table 4-4.

In terms of the PAO formulations, PAO and PAO+alcohol caused severe wear of over 1.0 μm depth, and the surface analysis of the post-test specimens detected oxidative degradation products on the surface. On the other hand, PAO+acid and PAO+GMO presented the friction reduction effect, and the XPS C 1s peak attributed to O-C-O was observed on the steel plate surface.

On the other hand, among the CVTF formulations, only GMO showed the friction reduction effect. The XPS C 1s spectrum of CVTF+GMO had a peak attributed to carboxylate (O=C-O), therefore, it was considered to be a key structure to reduce friction. CVTF+acid did not show the FM effect, and pyrophosphate was detected by ATR-FTIR. It implies an interaction between oleic acid and the CVTF additives.

Table 4- 4. Summary of TE77 steel/steel contact at 100°C

	PAO formulations			
	w/o FM	oleic acid	oleyl alcohol	GMO
CoF	0.094	0.070	0.096	0.066
Wear	Severe	Mild	Severe	Intermediate
Chemical nature				
Topmost surface (XPS)	Carbon contamination	**O-C-O**	Carbon contamination	**O-C-O**
Reaction film (EDX and ATR-FTIR)	Oxidative degradation products	N/A	Oxidative degradation products	Oxidative degradation products (slightly)

	CVTF formulations			
	w/o FM	oleic acid	oleyl alcohol	GMO
CoF	0.103	0.101	0.099	0.087
Wear	Mild	Mild	Mild	Mild
Chemical nature				
Topmost surface (XPS)	C-O / C-N N=C-O	C-O / C-N N=C-O	C-O / C-N N=C-O	C-O / C-N N=C-O **O=C-O**
Reaction film (EDX and ATR-FTIR)	Ca compound PO_4	Ca compound PO_4 and **P_2O_7** (lower P and Ca concentrations)	Ca compound PO_4	Ca compound PO_4 (lower P and Ca concentrations)

4.2. TE77 Steel Contact Tests at 40°C

The TE77 friction test was carried out in the lower temperature condition (40°C) in order to recognise the effect of the test temperature on the working mechanism of the FMs. The transmission temperature at 40°C represents the starting up condition, while the 100°C simulates the saturated temperature condition during cruise driving. Therefore, the frictional properties also need to be satisfied at 40°C, which makes some clutch test standards regulate the friction performance test at 40°C [37, 111]. In this study, all the TE77 test configurations and the conditions were arranged to be comparable to the 100°C test.

4.2.1. Friction Coefficient

The friction coefficient values measured with the PAO formulations are shown in Fig. 4-21. The ranking at the end of the 60 minute tests was as follows; (highest) PAO > PAO+acid = PAO+alcohol = PAO+GMO (lowest). The test oils with the FM presented similar friction values which were lower than the PAO base oil. In addition, the effect of the FMs appeared to be smaller than at 100°C (Fig. 4-1).

The results of the electrical contact resistance are shown in Fig. 4-22. While PAO+acid reached a maximum value after 20 minutes, the alcohol and the GMO oils had lower values. Especially, PAO+GMO showed a major difference from the 100°C result (Fig. 4-2) that reached a maximum after 40 minutes. This result implies that GMO could not form the film capable of inhibiting the direct contact between the surfaces at 40°C.

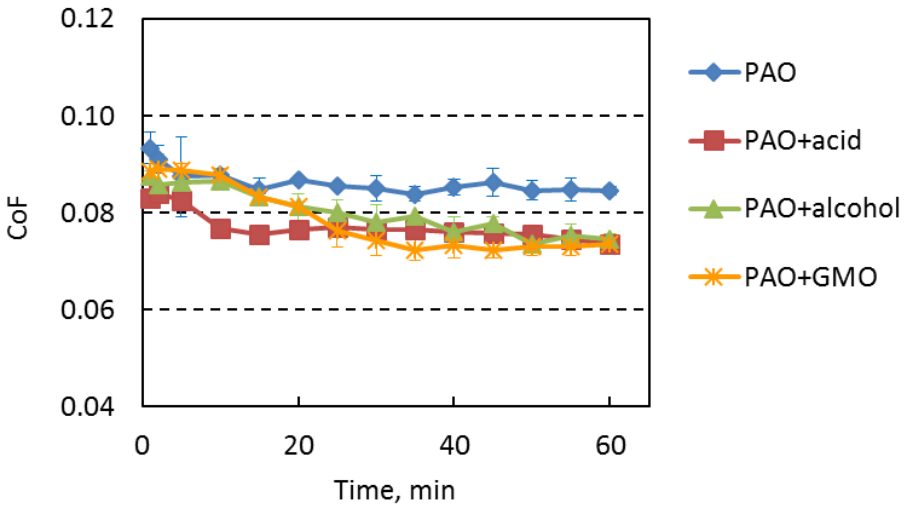

Fig. 4-21. Friction coefficient of steel/steel contact measured by TE77 (PAO formulations, 40°C, 60 min)

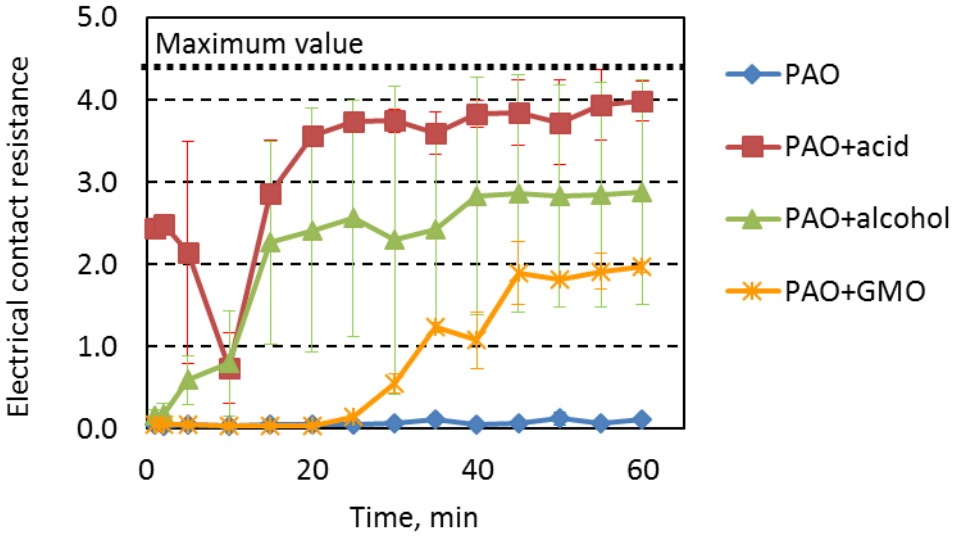

Fig. 4-22. Electrical contact resistance of steel/steel contact during the TE77 tests (PAO formulations, 40°C, 60 min)

The friction results for the CVTF formulations are summarised in Fig. 4-23. The ranking was different from that of PAO; (highest) CVTF = CVTF+alcohol > CVTF+acid > CVTF+GMO (lowest). It is notable that the oleic acid showed some extent of the friction reduction in contrast to the 100°C result (Fig. 4-3). All the test oils showed stable electrical contact resistance reaching a maximum just after starting the test as shown in Fig. 4-24. This indicates the reaction film formation by the CVTF additives was active even at 40°C.

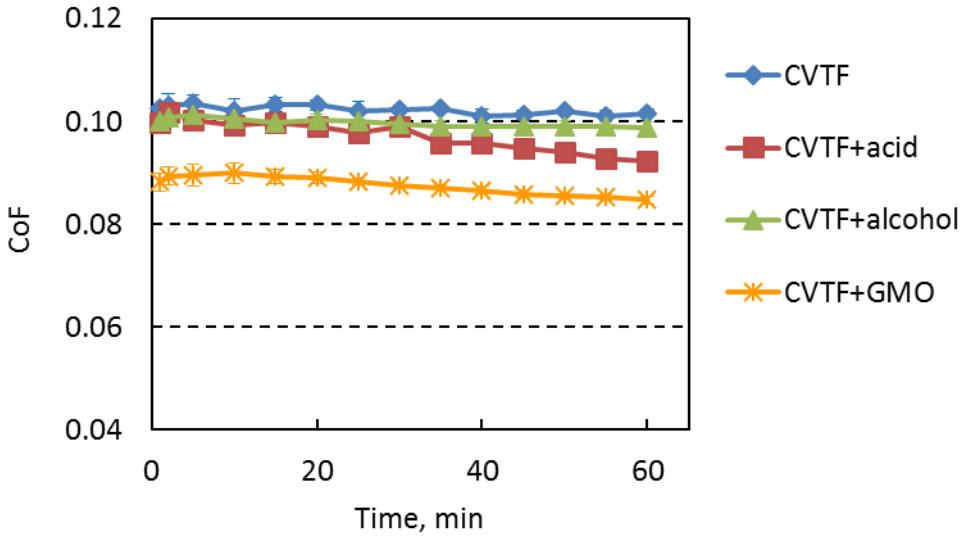

Fig. 4-23. Friction coefficient of steel/steel contact measured by TE77 (CVTF formulation, 40°C, 60 min)

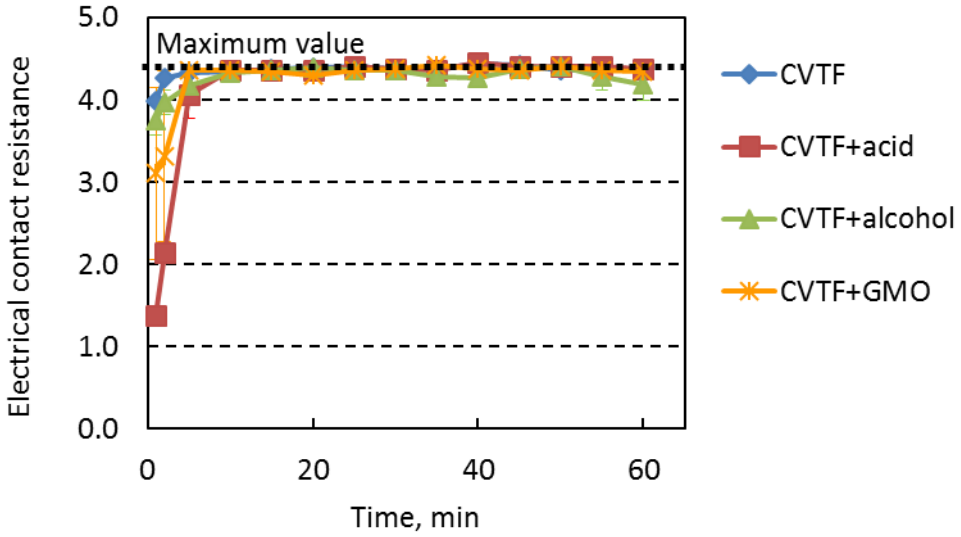

Fig. 4- 24. Electrical contact resistance of steel/steel contact during the TE77 tests (CVTF formulation, 40°C, 60 min)

The friction coefficient values at the end of the 60 minute test were summarised in Fig. 4-25. The PAO formulations appeared to be showing lower friction than the CVTFs. However, the effect from the wear damage explained in the next session should be taken into account.

Among the CVTF formulations, oleic acid and GMO presented a friction reduction effect, while oleyl alcohol did not. The effect of GMO was greater than that of oleic acid.

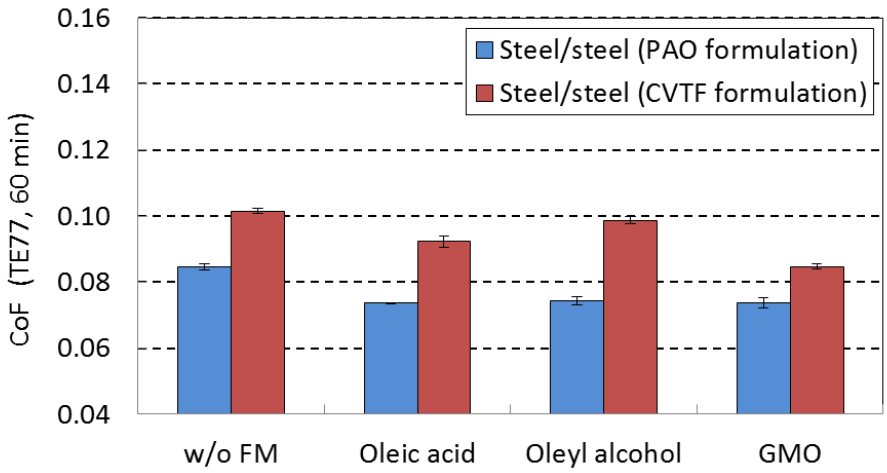

Fig. 4-25. TE77 friction coefficient of steel/steel contact (after 60 minutes, 40°C)

4.2.2. Wear Measurement by WLI

The topography on the post-test TE77 steel pins was measured by WLI as shown in Fig. 4-26 and Fig. 4-27. The 3D images of the wear scar are presented in Fig. 4-28 and Fig. 4-29.

- The overall trend was similar to the 100°C results (between Fig. 4-6 and Fig. 4-9) except that PAO+GMO indicated much more severe wear of over 1.5 µm depth.
- The results for the PAO test oils showed a good agreement with the TE77 electrical contact resistance (Fig. 4-22); the larger the wear, the lower the resistance. The severe wear over 1.0 µm depth possibly affected the friction result by increasing the contact area as explained in Fig. 4-10.
- Oleic acid indicated an excellent anti-wear effect even in PAO as seen at 100°C.
- All the CVTF formulations presented a superior anti-wear performance. It implies that the CVTF additives were also capable of forming the film at 40°C.

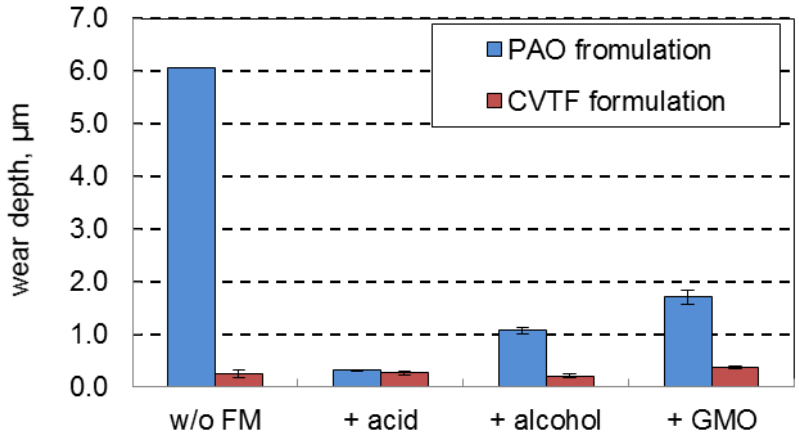

Fig. 4-26. Wear depth of the post-test TE77 steel pins (40 °C, after 60 minutes)

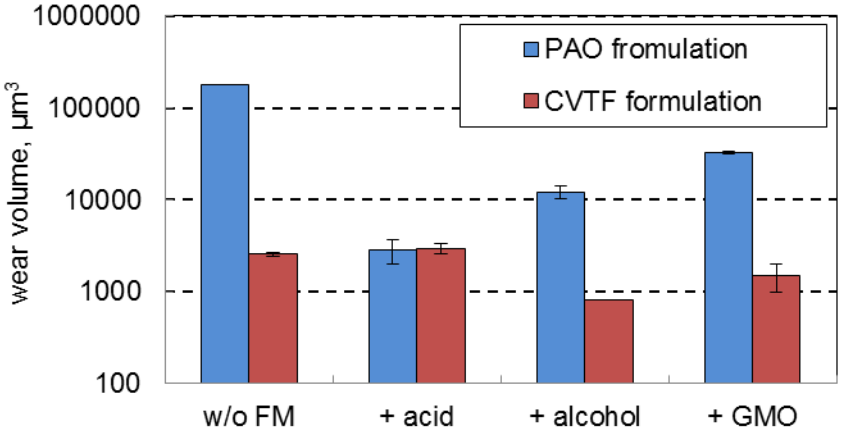

Fig. 4-27. Wear volume of the post-test TE77 steel pins (40 °C, after 60 minutes)

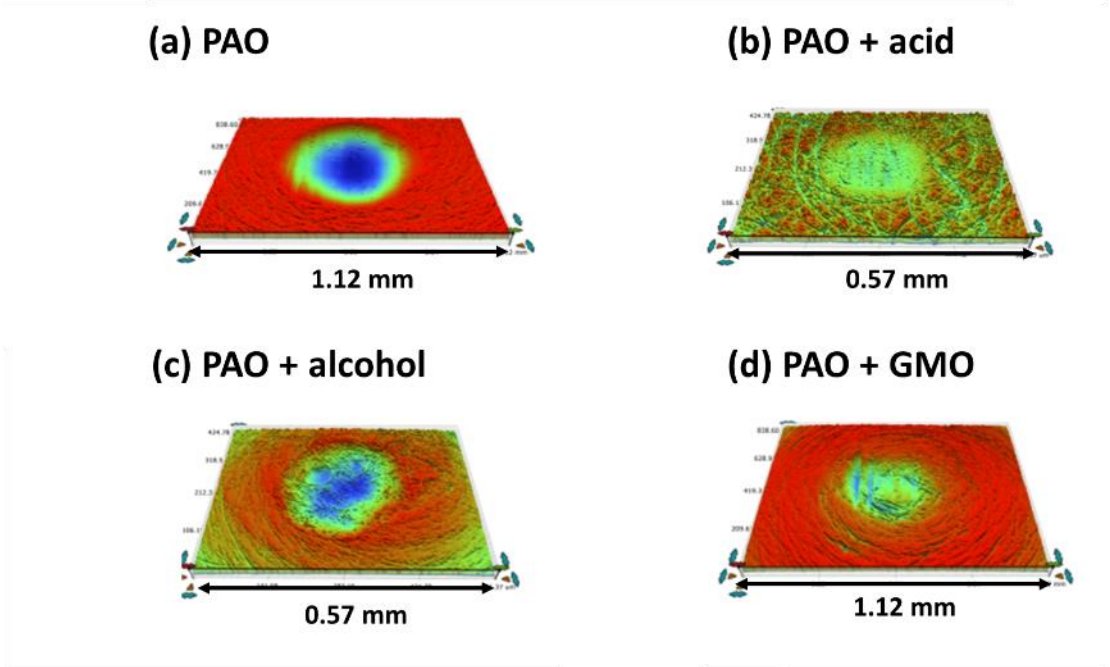

Fig. 4-28. Wear scar 3D images on the post-test TE77 steel pins after testing PAO formulations (40 °C, 60 minutes)

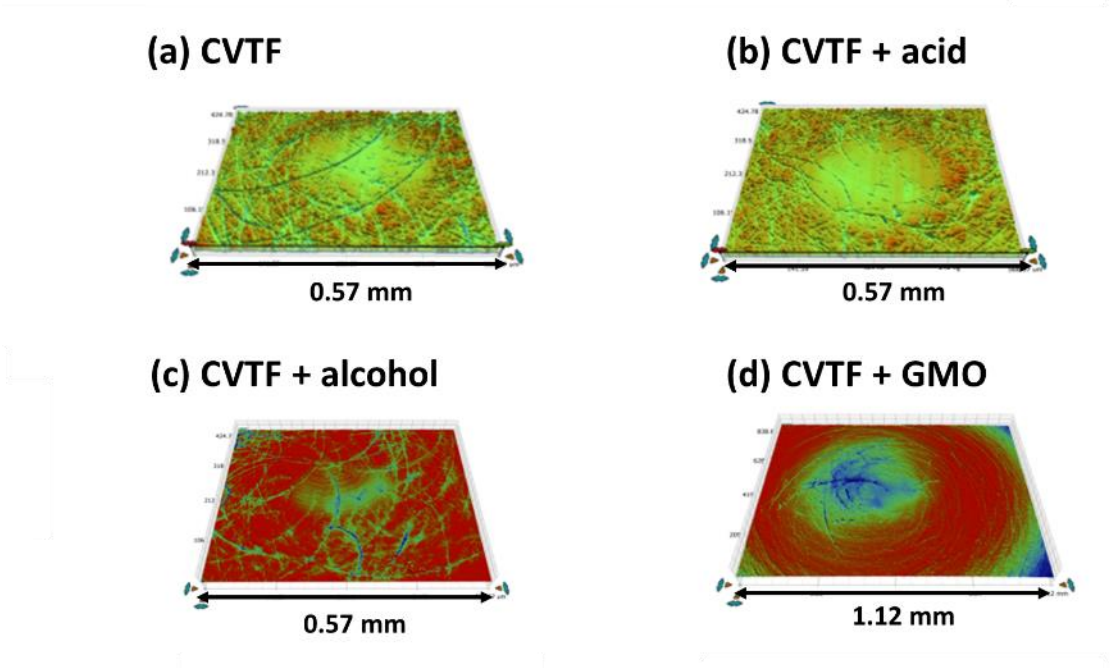

Fig. 4-29. Wear scar 3D images on the post-test TE77 steel pins after testing CVTF formulations (40 °C, 60 minutes)

4.2.3. Wear Track Observation by SEM

The SEM images on the post-test TE77 steel plates are shown in Fig. 4-30 for the PAO oils and in Fig. 4-31 for the CVTF oils.

Among the PAO test oils, (a) PAO and (d) PAO+GMO presented severe and wide wear scars corresponding to the WLI observations. (b) PAO+acid showed the narrowest wear width.

On the other hand, none of the CVTF post-test steel plates presented significant wear. Especially, the wear tracks of (a) CVTF and (c) CVTF+alcohol were difficult to be seen due to the small wear volume and the surface appearance quite similar to outside the wear track. In contrast, the wear scar was detectable for (b) CVTF+acid and (d) CVTF+GMO as the colour inside the wear was different from the outside. This trend corresponds to the friction results in which oleic acid and GMO showed the friction reduction effect (Fig. 4-23).

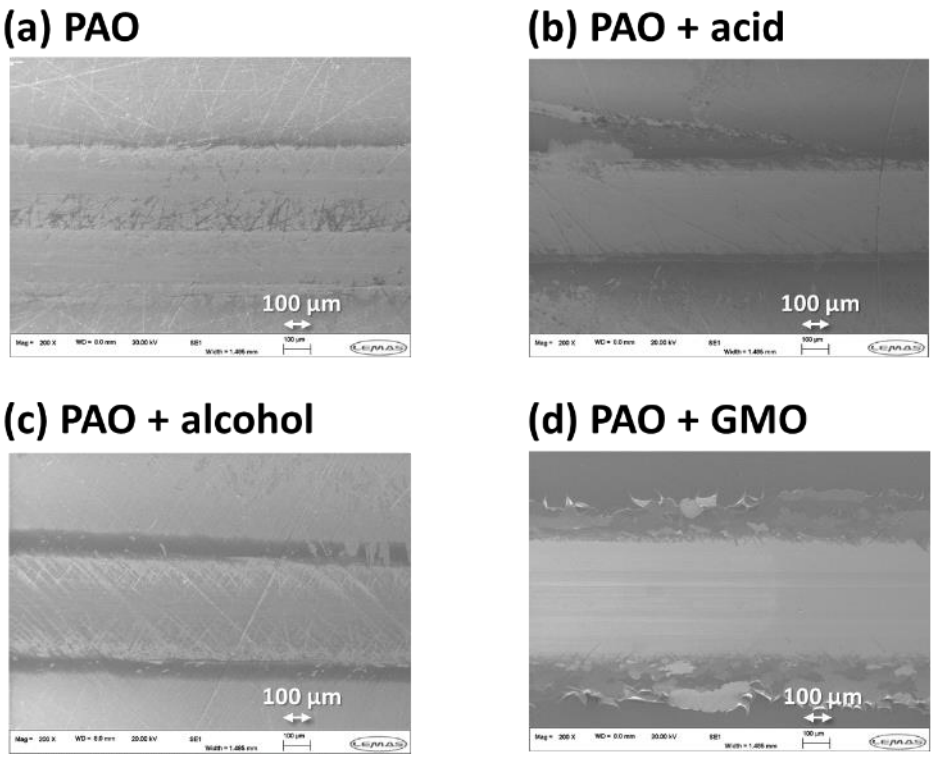

Fig. 4-30. SEM images of the post-test TE77 steel plates
after testing PAO formulations (40 °C, 60 minutes)
a) PAO, b) PAO + oleic acid, c) PAO + oleyl alcohol, d) PAO + GMO

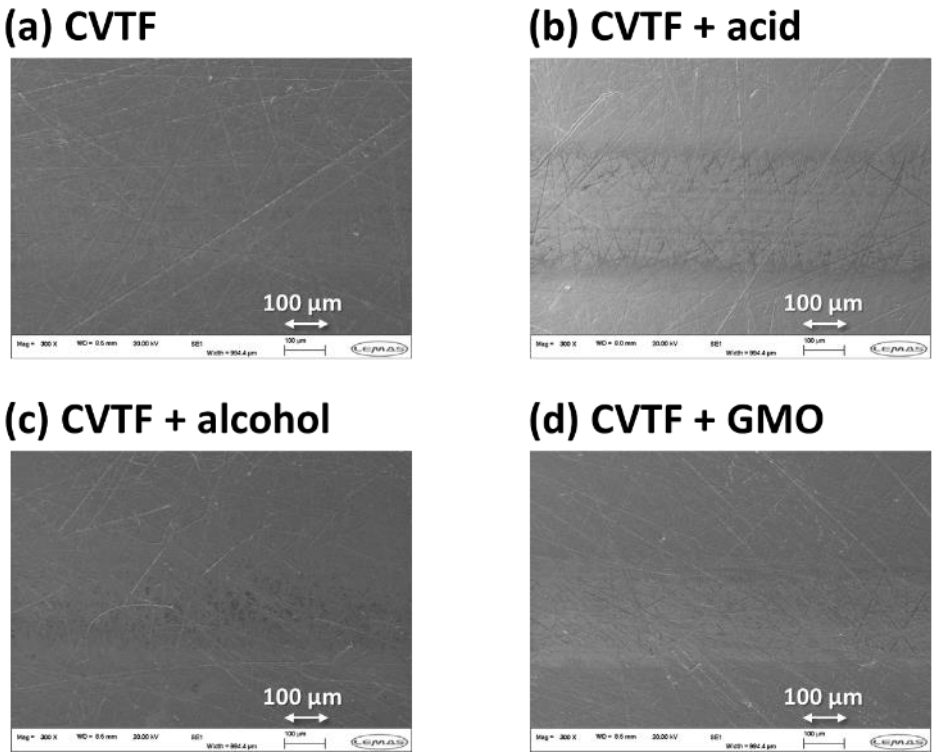

Fig. 4-31. SEM images on the post-test steel plates for the CVTF oils (40 °C, 60 minutes) a) CVTF, b) CVTF + oleic acid, c) CVTF + oleyl alcohol, d) CVTF + GMO

4.2.4. EDX Analysis

The elemental concentration on the wear track of the post-test plates was assessed using EDX. The result of the PAO formulations is shown in Fig. 4-32. Similar to the 100°C results (Fig. 4-13), the plates with the severe wear (PAO, PAO+alcohol and PAO+GMO) presented higher oxygen concentration due to oxidative degradation products or iron oxide, while PAO+acid resulted in low oxygen concentration as expected from the small wear volume.

The results of the CVTF test oils are shown in Fig. 4-33. The elements derived from the additives are summarised separately in (b). As an overall trend, the concentrations of elements from the CVTF additives were less in the reaction film compared with the 100°C results (Fig. 4-14). For example, the concentrations of P and Ca for the CVTF base without the FM were both 0.6 wt% at 100°C, thought, they dropped down to 0.25 and 0.1 wt% at 40°C.

On the other hand, CVTF+acid showed lower Ca concentration compared to the other oils. However, it was not obvious as shown at 100°C because the other oils experienced a significant decrease in the Ca concentration. The results between CVTF and CVTF+alcohol were comparable, which shows a good correspondence to the friction results indicating that oleyl alcohol could not work in the presence of the additives.

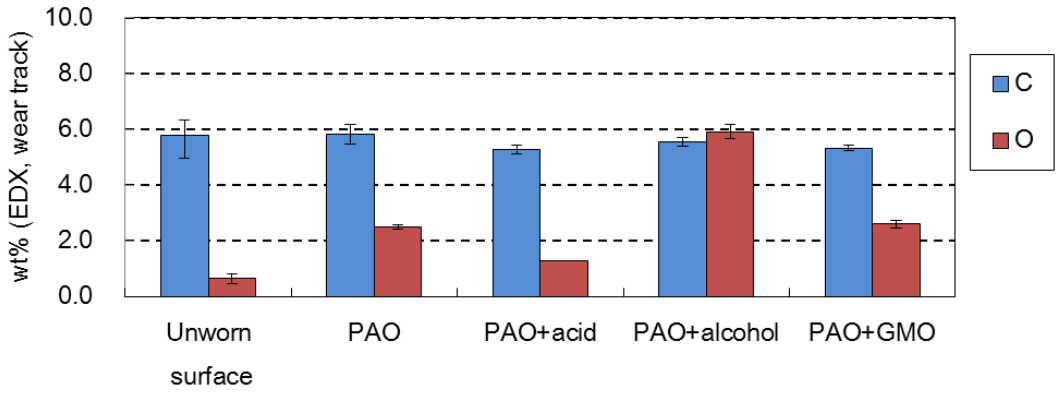

Fig. 4-32. EDX analysis on the post-test plates for the PAO oils (40 °C, 60 minutes)

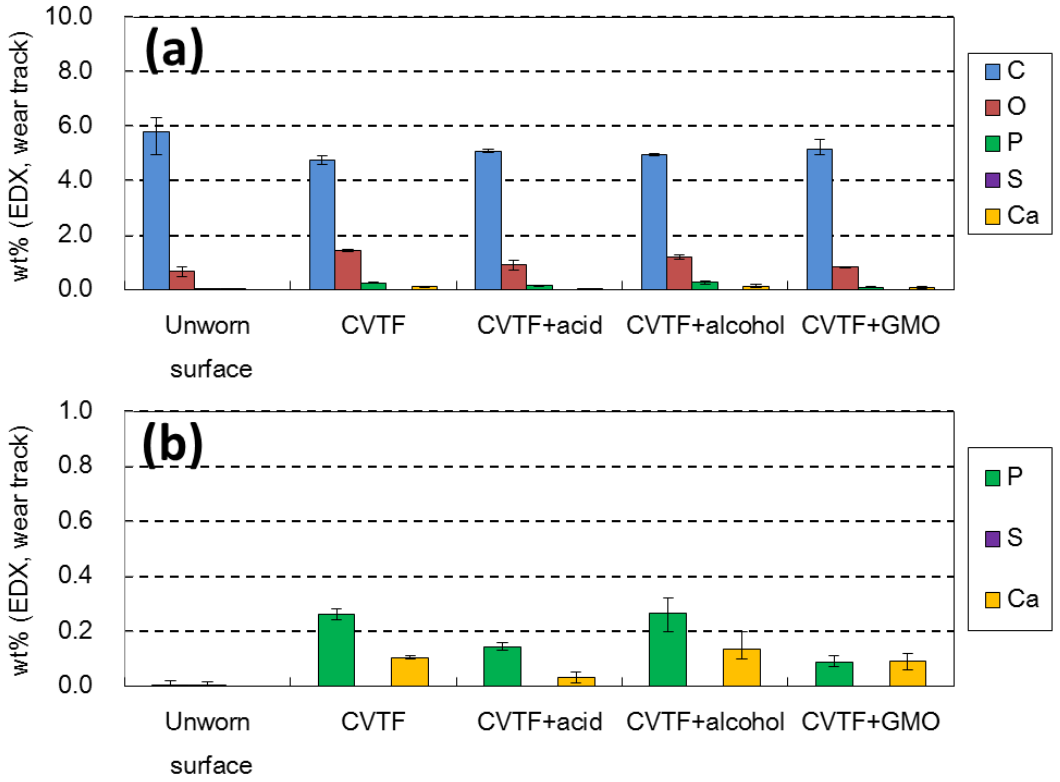

Fig. 4-33. EDX analysis on the post-test plates for the CVTF oils (40 °C, 60 minutes)
(a) showing all the elements except for Fe, (b) focusing on P, S and Ca

4.2.5. XPS Analysis

The XPS analysis was carried out to collect survey scans, and C 1s and O 1s spectra. Because the available slots for XPS were limited, the samples showing severe wear (PAO, PAO+alcohol and PAO+GMO) and without the friction reduction effect (CVTF+alcohol) were not analysed as it was known that the tribofilm presence would be minimised.

Table 4-5 shows the mass fraction of the elements on the wear track of the steel plates calculated from the peak areas in the XPS survey spectra.

- The result of PAO+acid was comparable to that at 100°C (Table 4-2).
- CVTF base fluid showed the oxygen concentration that did not change from 100°C, while CVTF+acid and CVTF+GMO showed more than 5 mass% increase from the 100°C results (Table 4-3).
- The other elements derived from the additives (N, Ca and P) presented the lower fraction than the 100°C results, indicating that the interaction between the additives and steel was weaker at 40°C as shown in the EDX analysis (Fig. 4-33).

Table 4-5. XPS survey spectra inside the wear track on the post-test TE77 steel plates (40 °C, after 60 minutes sliding test)

Element, % mass	PAO + acid	CVTF	CVTF + acid	CVTF+ GMO
C 1s	67.7	64.9	55.8	53.7
O 1s	29.1	25.7	31.3	35.7
N 1s	-	1.4	1.7	0.3
Ca 2p	-	2.1	4.5	4.6
P 2p	-	4.5	5.5	4.3
Fe 2p	3.2	1.4	1.2	1.4

The XPS C 1s and O 1s spectra for PAO+acid are shown in Fig. 4-34.

- The peak positions for the both C 1s and O 1s spectra were comparable to those at 100°C (Fig. 4-15 and Fig. 4-16).
- The C 1s detailed scan showed the stronger peak intensities derived from the oxygen compounds (C-O, O-C-O and O=C-O) compared to 100°C, while the O 1s spectrum presented a higher peak intensity for MBO at 530.3 eV. This result implies that the amount of oleic acid on the steel surface was larger at 40°C.

However, it was not able to form a highly effective FM film with the C-O-Fe bond.

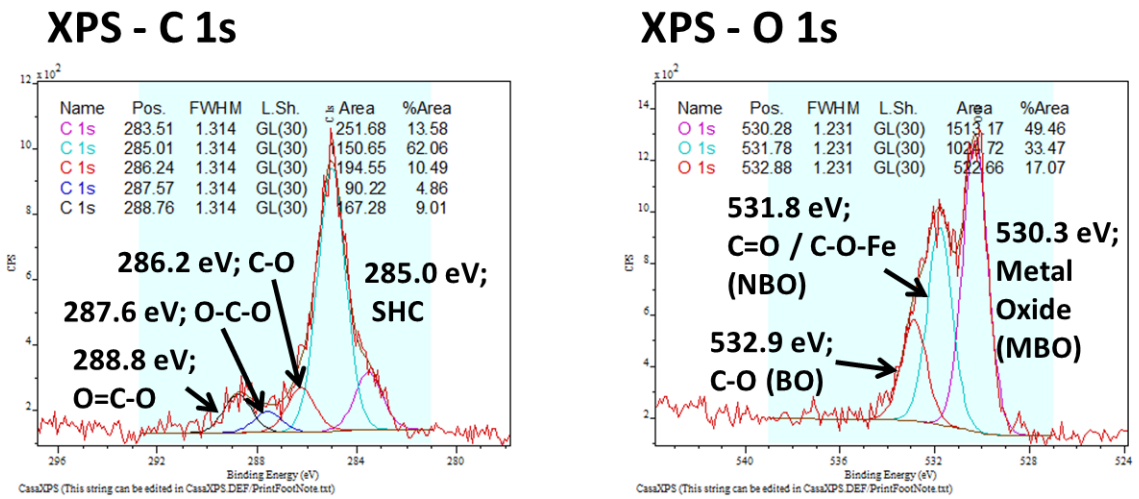

Fig. 4-34. XPS C 1s and O 1s spectra for the PAO with oleic acid on the wear track after the 40 °C TE77 test

The XPS C 1s and O 1s spectra for the CVTF formulations are shown in Fig. 4-35 and Fig. 4-36. The trend of each test oils is as follows;

- CVTF showed a similar trend to the 100°C results for both the C 1s and the O 1s spectra. The peak positions and the intensities were almost the same except that the MBO peak in the O 1s spectrum had a higher intensity. It implies that the interaction between the additives and the surface became weaker at 40°C, resulting in the thinner reaction film as observed by EDX (Fig. 4-33).
- CVTF+acid showed the stronger peaks derived from the oxygen structures in the C 1s spectrum compared with those at 100°C (Fig. 4-17). The peak at the highest energy shifted to upwards to 288.7 eV, which indicates the presence of carboxylate (O=C-O) on the steel surface. It should be the reason that CVTF+acid showed the friction reduction effect only at 40°C. In addition, the O 1s spectrum had a peak derived from MBO at 530.2 eV which was not observed at 100°C. This result supports the assumption that the interaction among the FM, the additives and the steel surface was different between 40°C and 100°C.

- CVTF+GMO had also the stronger intensities derived from the oxygen structures in the C 1s spectrum, while the peak at around 289 eV attributed to carboxylate was observed both at 40°C and 100°C.

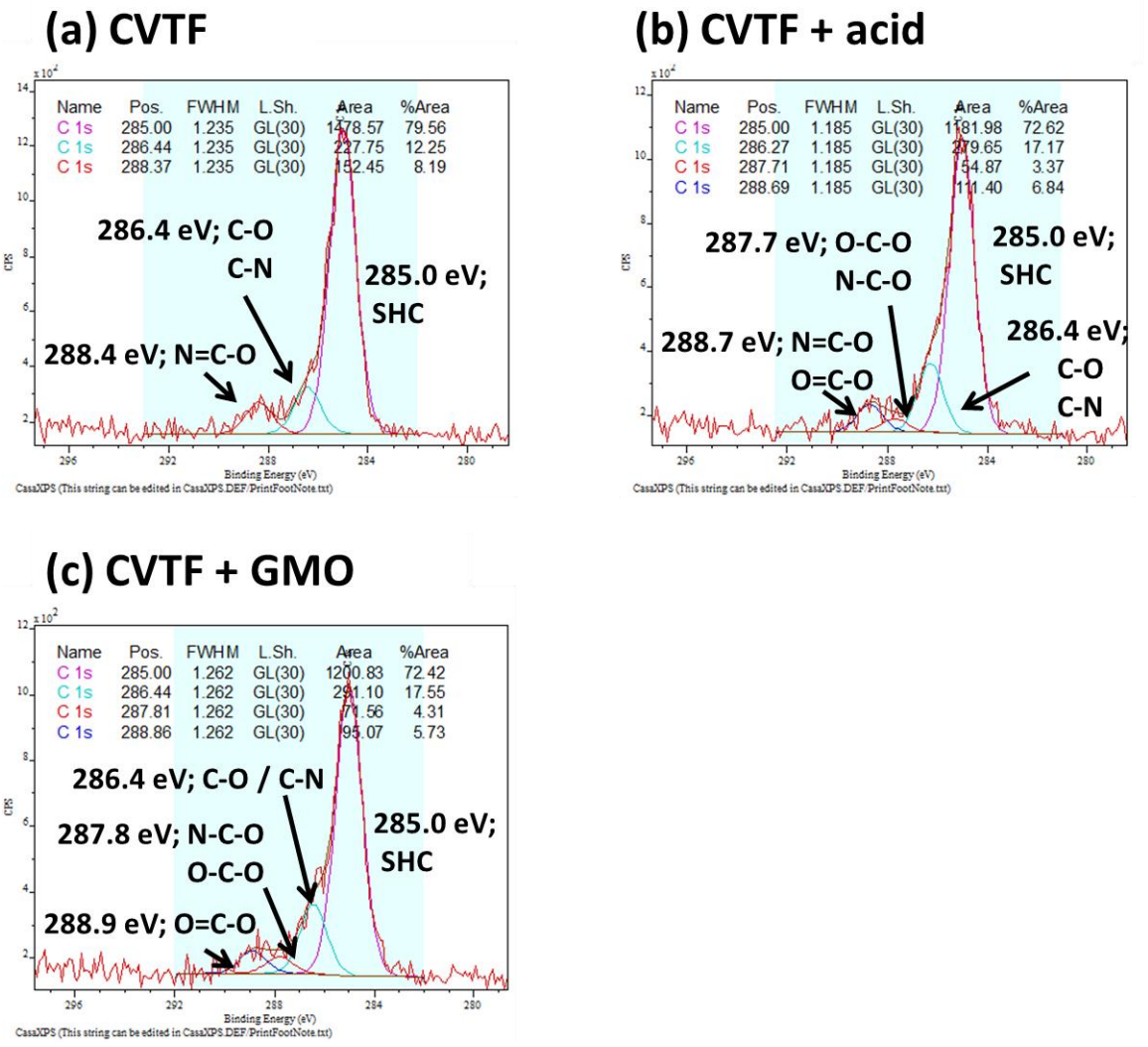

Fig. 4-35. XPS C 1s spectra for the CVTF formulations on the wear track after the 40 °C TE77 test, a) CVTF, b) CVTF + oleic acid, c) CVTF + GMO

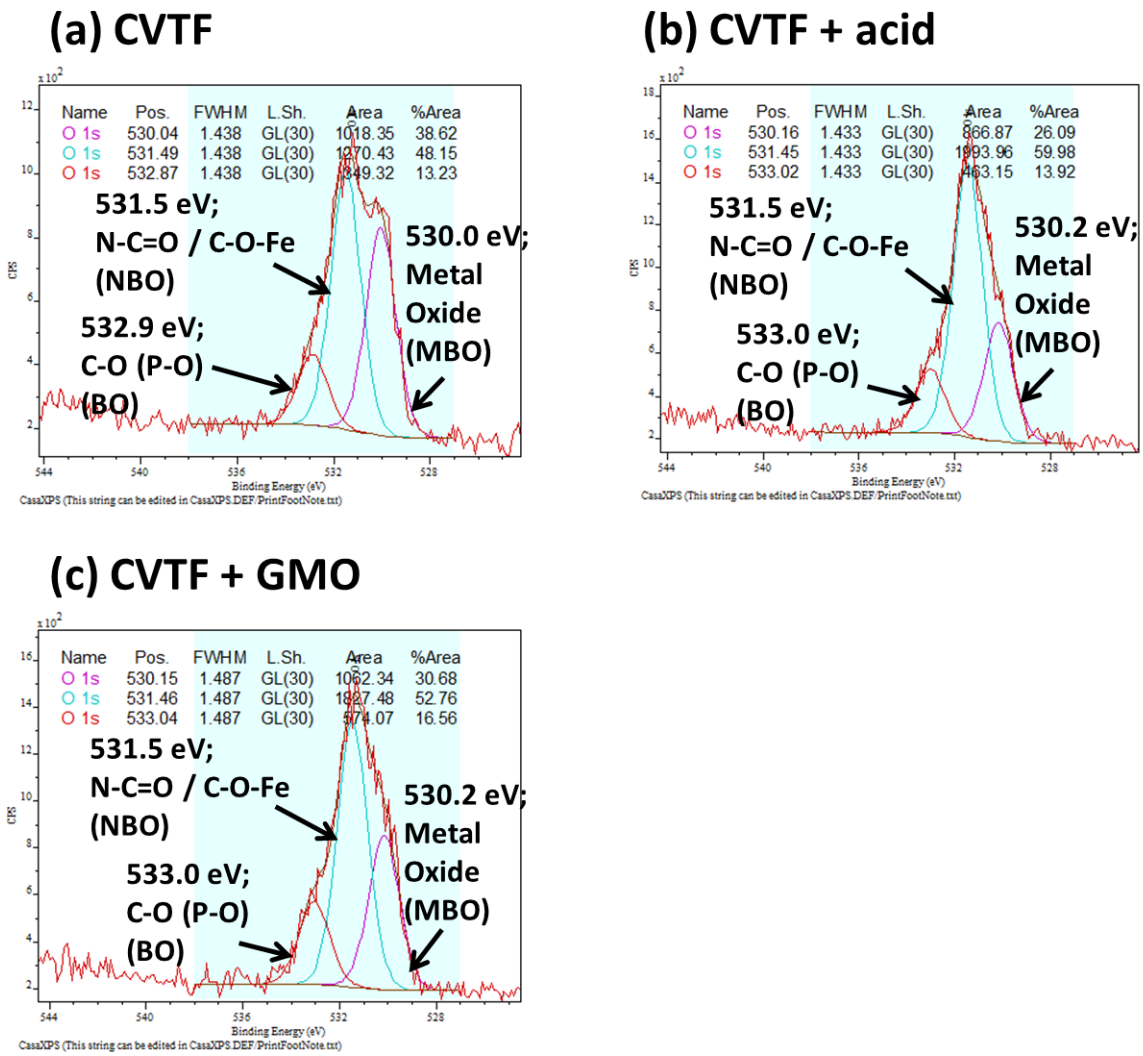

Fig. 4-36. XPS O 1s spectra for the CVTF formulations on the wear track after the 40 °C TE77 test, a) CVTF, b) CVTF + oleic acid, c) CVTF + GMO

4.2.6. ATR-FTIR Analysis

The chemical nature on the wear track was assessed using ATR-FTIR. The spectra of the PAO and the CVTF formulations are shown in Fig. 4-37 and Fig. 4-38, respectively. All the PAO formulations did not present any specific peaks similar to the 100°C results. The spectra of the CVTF oils had a broad peak at around 1,150 cm^{-1} identified to P-O bonding derived from phosphate. The peak intensity was stronger for (a) CVTF, though, the peak position was the same among the CVTF oils. In addition, (b) CVTF+acid did not show the peak shift to lower wave number which was observed at 100°C (Fig. 4-20). The reason should be the weak interaction between oleic acid and the additives as assumed from the other analysis.

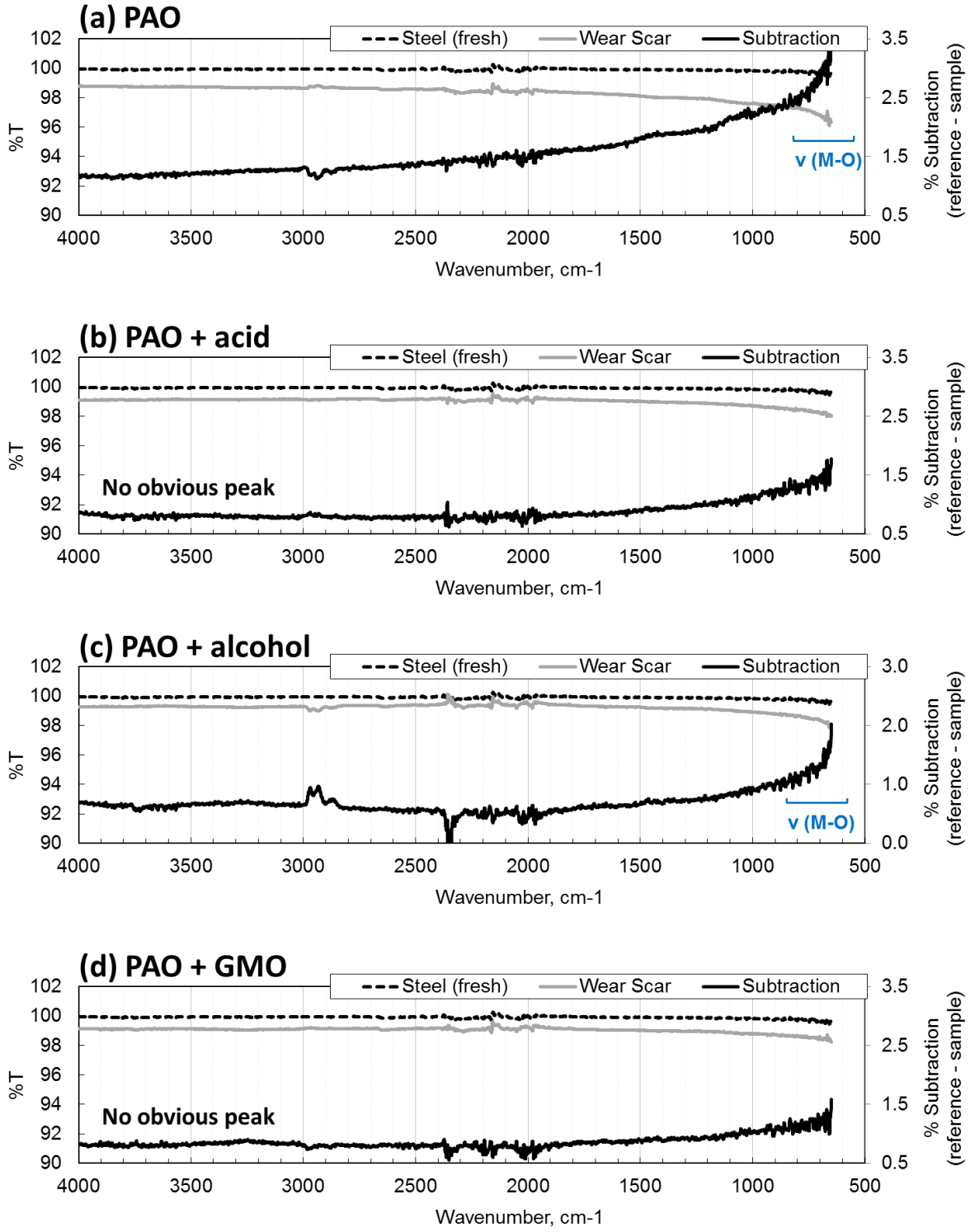

Fig. 4-37. ATR-FTIR spectra for the PAO formulations on the wear track after the 40°C TE77 test, a) PAO, b) PAO + oleic acid, c) PAO + oleyl alcohol, d) PAO + GMO

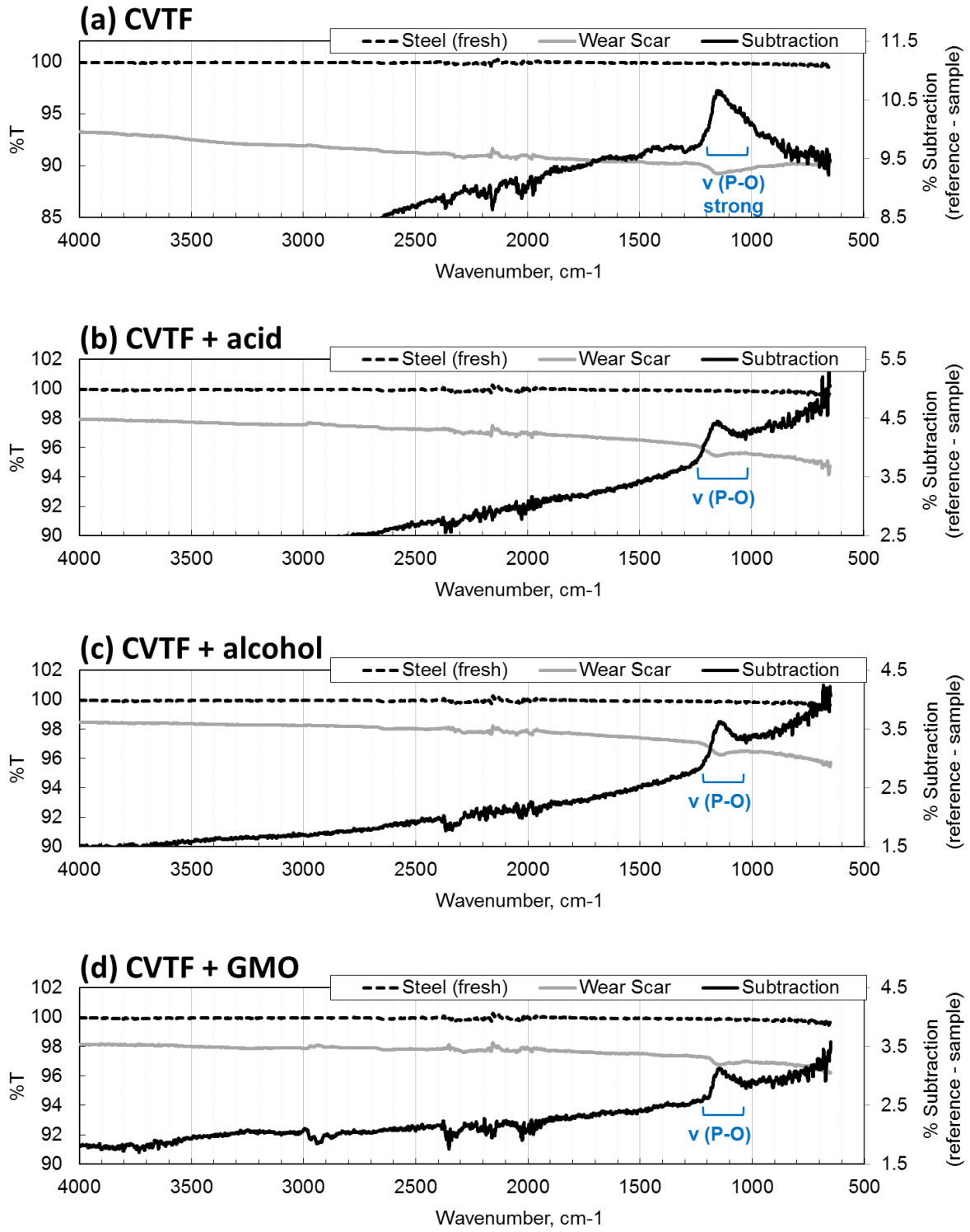

Fig. 4-38. ATR-FTIR spectra for the CVTF formulations on the wear track after the 40°C TE77 test,

a) CVTF, b) CVTF + oleic acid, c) CVTF + oleyl alcohol, d) CVTF + GMO

4.2.7. Summary of TE77 Steel Contact Tests at 40 °C

The features of the TE77 steel sliding tests at 40°C are summarised in Table 4-6.

In terms of the PAO formulations, PAO, PAO+alcohol and PAO+GMO caused severe wear, so that the XPS analysis was not performed. Their friction results were possibly influenced by the huge wear volume. In contrast, oleic acid showed low wear as well as low friction. The oxygen structures (O-C-O / O=C-O) were detected by XPS, therefore, it is considered that oleic acid was capable of forming an effective film even at 40°C comparable to 100°C.

The CVTF oils had the reaction film with lower P and Ca concentrations at 40°C, which implies that the interaction was inhibited due to the low chemical potential. Interestingly, oleic acid did reduce the friction in contrast to 100°C. The XPS spectrum showed the presence of carboxylate (O=C-O), and EDX and ATR-FTIR indicated the less interaction against the additives. On the other hand, oleyl alcohol did not present any effect, while GMO led to the moderate friction reduction showing carboxylate on the wear track.

Table 4-6. Summary of TE77 paper/steel contact at 40°C

	PAO formulations			
	w/o FM	oleic acid	oleyl alcohol	GMO
CoF	0.085	0.074	0.074	0.074
Wear	Severe	Mild	Severe	Severe
Chemical nature				
Topmost surface (XPS)	-	**O-C-O** **O=C-O**	-	-
Reaction film (EDX and ATR-FTIR)	N/A	N/A	N/A	N/A

	CVTF formulations			
	w/o FM	oleic acid	oleyl alcohol	GMO
CoF	0.102	0.092	0.099	0.085
Wear	Mild	Mild	Mild	Mild
Chemical nature				
Topmost surface (XPS)	C-O / C-N N=C-O	C-O / C-N **O-C-O** / N-C-O N=C-O **O=C-O**	-	C-O / C-N **O-C-O** / N-C-O **O=C-O**
Reaction film (EDX and ATR-FTIR)	Ca compound PO_4	Ca compound PO_4 (less Ca conc)	Ca compound PO_4	Ca compound PO_4 (less P conc)

Chapter 5 – Results – TE77 Paper Contact Tests

The results for the TE77 tests at the paper/steel contact are shown in this chapter. The initial sliding tests for 60 minutes were performed both at 100°C and 40°C in order to consider the influence of the substrates (steel or paper) and the test temperature. The frictional properties, friction coefficient and FFWI (Friction Force Wave Index), and the surface analysis results are shown in "5.1. TE77 Paper Contact Tests at 100°C" and "5.2. TE77 Paper Contact Tests at 40°C".

In addition, long-term sliding tests for 12 or 24 hours were also carried out for some oils with interesting frictional characteristics; these were PAO+GMO, CVTF+acid and CVTF+GMO. Automatic transmission fluids need to maintain the frictional properties for a long duration, sometimes all through the car life of over 100,000 miles of driving. Therefore, the durability performance of the FMs is one of the major concerns for formulating CVTFs. Furthermore, it should be useful to trace the change in the chemical nature on the paper surface for understanding the working mechanism of the FMs.

5.1. TE77 Paper Contact Tests at 100°C

5.1.1. Friction Coefficient

The friction between the paper plates and the steel pin was evaluated using TE77. The paper plate was prepared with JASO (Japanese Automotive Standard Association) M349 clutch material. The sliding condition was comparable to the steel/steel contact tests shown in Chapter 4 except for the contact pressure which was controlled at 6.0 MPa to simulate a lock-up clutch.

The friction coefficient values measured with the PAO formulations are presented in Fig. 5-1. The ranking of the friction after 60 minutes was as follows; (highest) PAO >> PAO+alcohol > PAO+GMO > PAO+acid (lowest). Although the friction of all the test oils appeared to reach the stable value after approximately 30 minutes, the error bar of PAO without FMs looked significantly wider than the other oils. The sliding condition was probably too severe due to a lack of the FMs and the additives, leading to an unstable surface condition.

Fig. 5-2 shows the friction measurement results of the CVTF formulations. The ranking of the friction after 60 minutes was as follows; (highest) CVTF > CVTF+alcohol >> CVTF+GMO = CVTF+acid (lowest). The ranking was the same order between the two base fluids in contrast to the steel/steel sliding tests, though, it appeared that oleyl alcohol worked better in the PAO. All the CVTF oils reached a stable friction coefficient value after around 30 minutes, and also presented good repeatability.

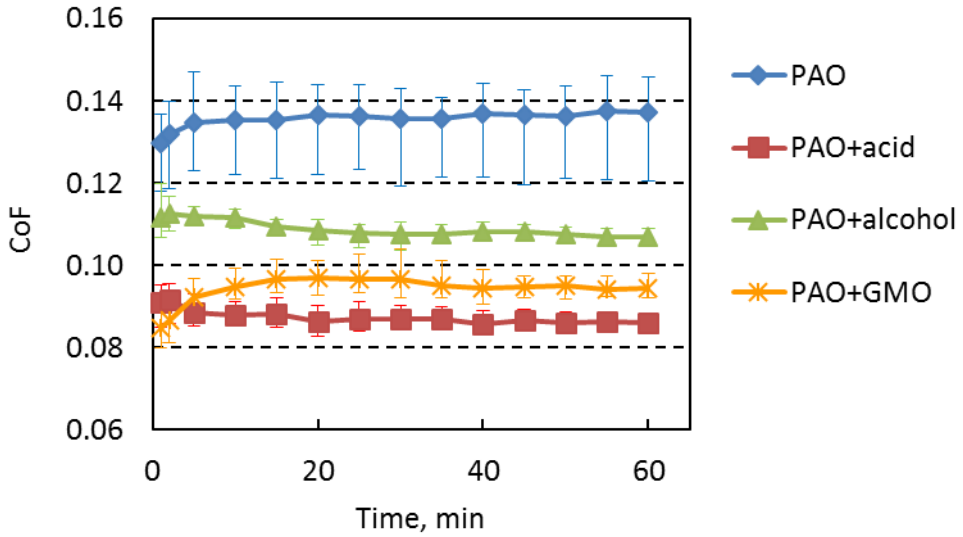

Fig. 5-1. Friction coefficient of paper/steel contact measured by TE77 (PAO formulation, 100°C, 60 min, 0.20 m/s, 6.0 MPa)

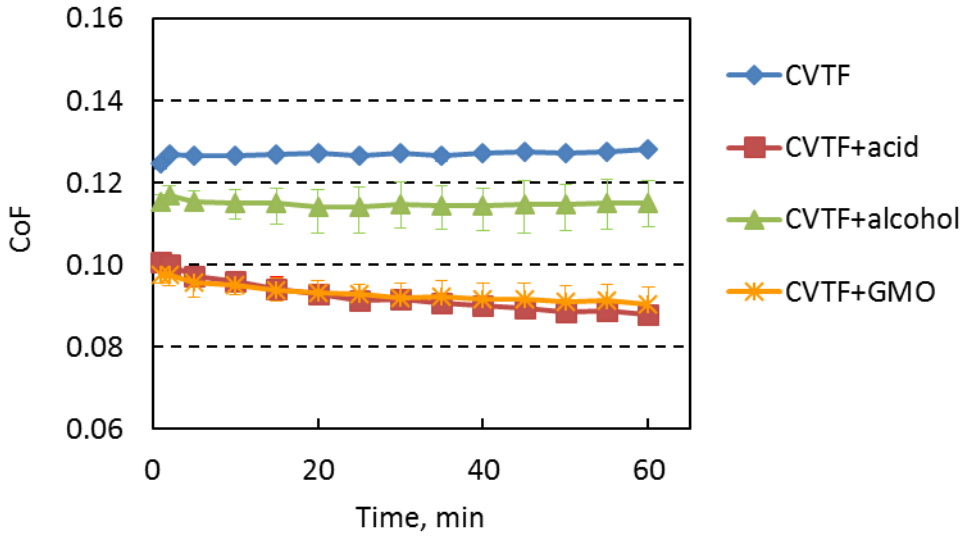

Fig. 5-2. Friction coefficient of paper/steel contact measured by TE77 (CVTF formulation, 100°C, 60 min, 0.20 m/s, 6.0 MPa)

The friction coefficient after 60 minutes of the TE77 test was summarised in Fig. 5-3. Compared with the steel/steel contact results at 100°C (Fig. 4-5), the effect of the FMs on the friction on the paper material appeared to be independent of the base fluid type. Both oleic acid and GMO presented a superior friction modification effect, while oleyl alcohol showed a slight reduction.

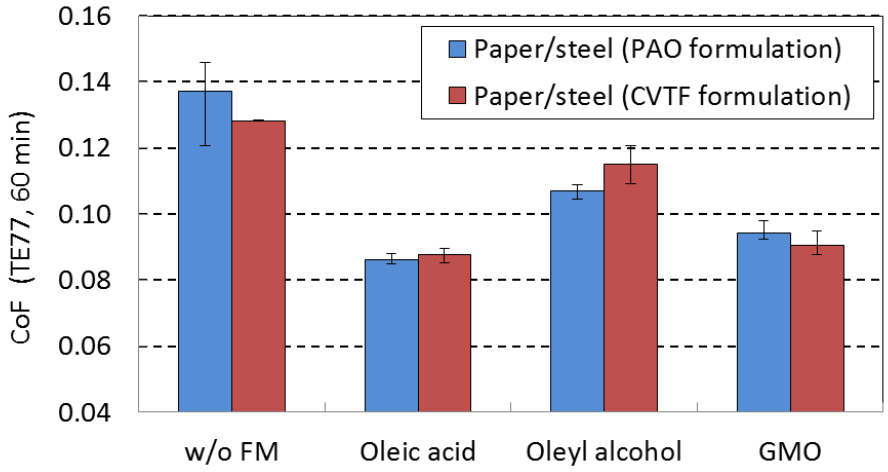

Fig. 5-3. TE77 friction coefficient of paper/steel contact (after 60 minutes)

5.1.2. Friction Force Wave Analysis

The friction force waves during the TE77 paper/steel contact tests are summarised in order to discuss the frictional properties of the FMs. Following the procedure explained in detail in Chapter 3, the wave data from 31 to 60 minutes (the end of the test) were averaged.

The friction force square wave shapes of the PAO formulations are shown in Fig. 5-4. The waves of (a) PAO and (d) PAO+GMO had a spike when the sliding direction changed (at 10 and 35 ms), while the (b) PAO+acid and (c) PAO+alcohol showed a relatively smooth wave shape. For the quantitative comparison, the FFWI (friction force wave index) values are shown in Fig. 5-5. The lower the FFWI, the smaller the spike and the smoother contact as already explained. It is notable that the FFWI of PAO+GMO was almost the same as that of PAO in spite of the good friction reduction effect as shown in Fig 4-5.

The waves and FFWI of the CVTF formulations are presented in Fig. 5-6 and Fig. 5-7. In contrast to the PAO results, (d) CVTF+GMO showed a smooth wave shape with lower FFWI, which implies the working mechanism of GMO was different in the

presence of the CVTF additives. The effect of the oleic acid and oleyl alcohol appeared to be similar to those for PAO.

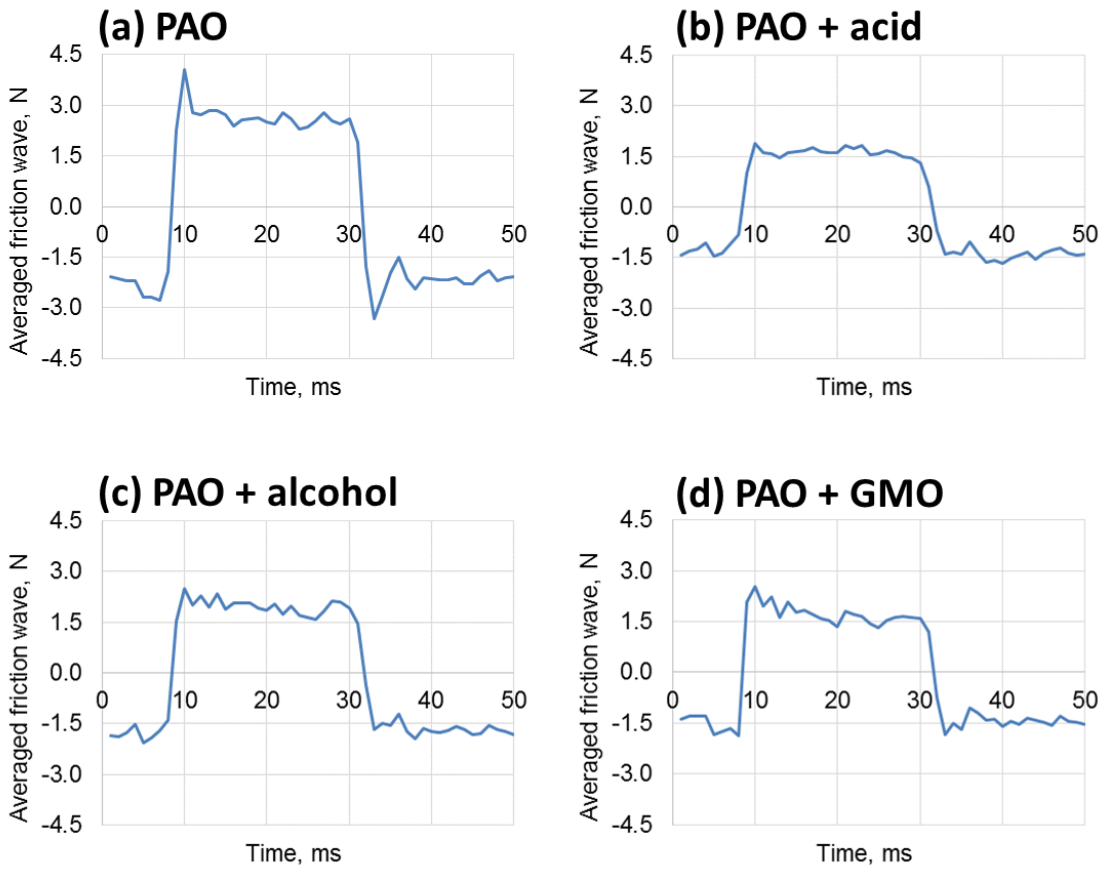

Fig. 5-4. Friction force waves of the PAO formulations during the TE77 paper/steel sliding test at 100°C, a) PAO, b) PAO + oleic acid, c) PAO + oleyl alcohol, d) PAO + GMO

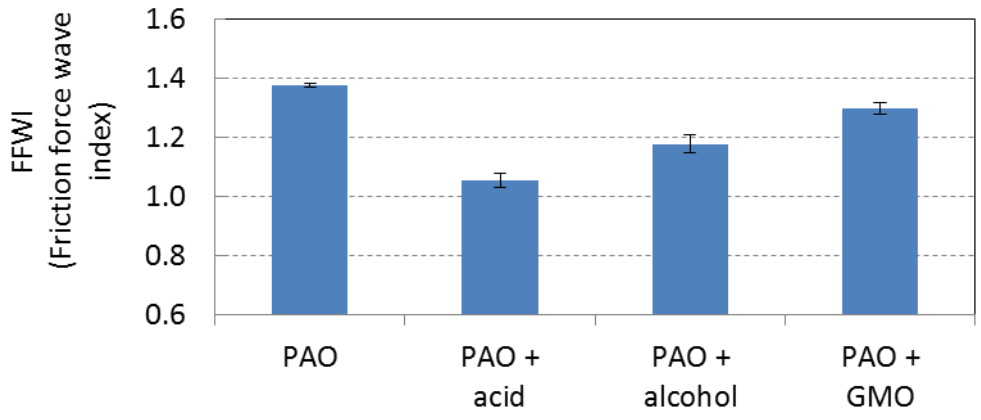

Fig. 5-5. FFWI (friction force wave index) for the PAO formulations at 100°C

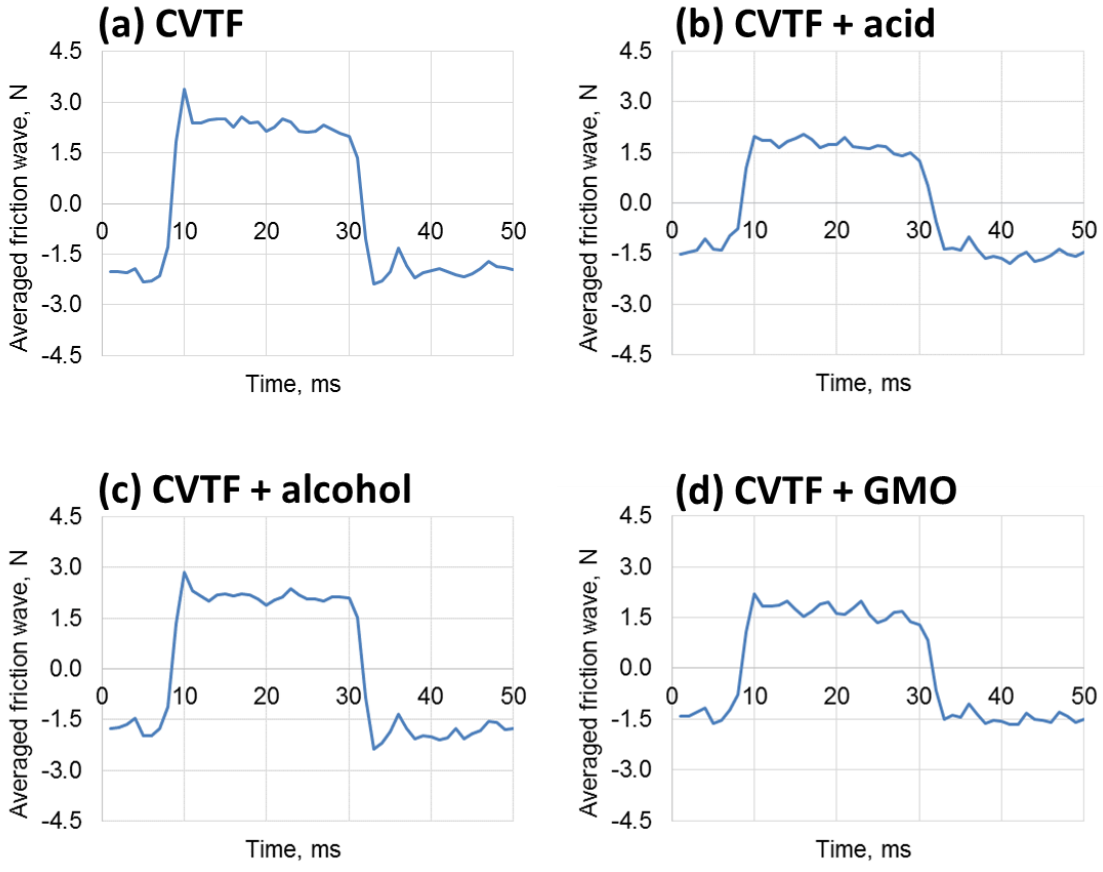

Fig. 5-6. Friction force waves of the CVTF formulations during the TE77 paper/steel sliding test at 100 °C

a) CVTF, b) CVTF + oleic acid, c) CVTF + oleyl alcohol, d) CVTF + GMO

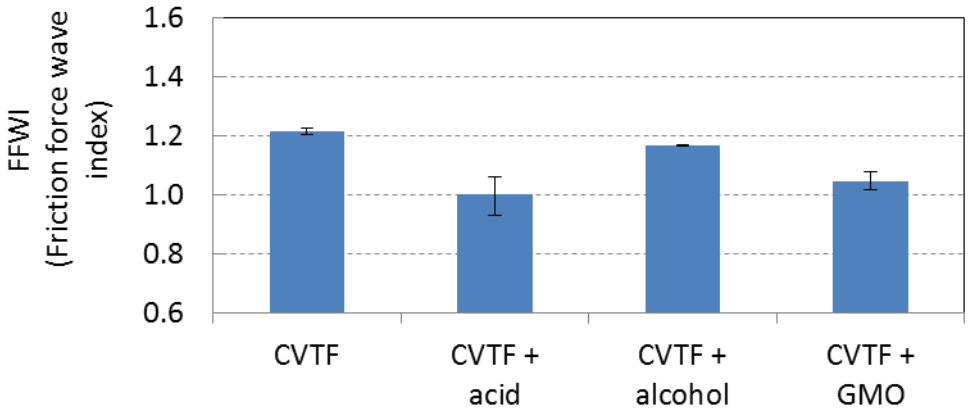

Fig. 5-7. FFWI for the CVTF formulations at 100°C

5.1.3. Wear Track Observation by SEM

The surface topography on the post-test TE77 paper plates was investigated by SEM.

As a reference, a fresh TE77 paper plate was evaluated. The SEM image and EDX mapping results for C Kα and Si Kα are shown in Fig. 5-8. The image presents tangled fibres and small particles, which could be identified as cellulose fibre compacted with resin and diatomite earth (mainly consisting of SiO_2), respectively. The EDX mapping results supports it showing higher carbon concentration at the fibre structure, and higher silicon concentration at the particles. The tangled fibre structure constructed an uneven surface, which plays an important role on managing the frictional properties of the paper clutch by reducing the actual contact area.

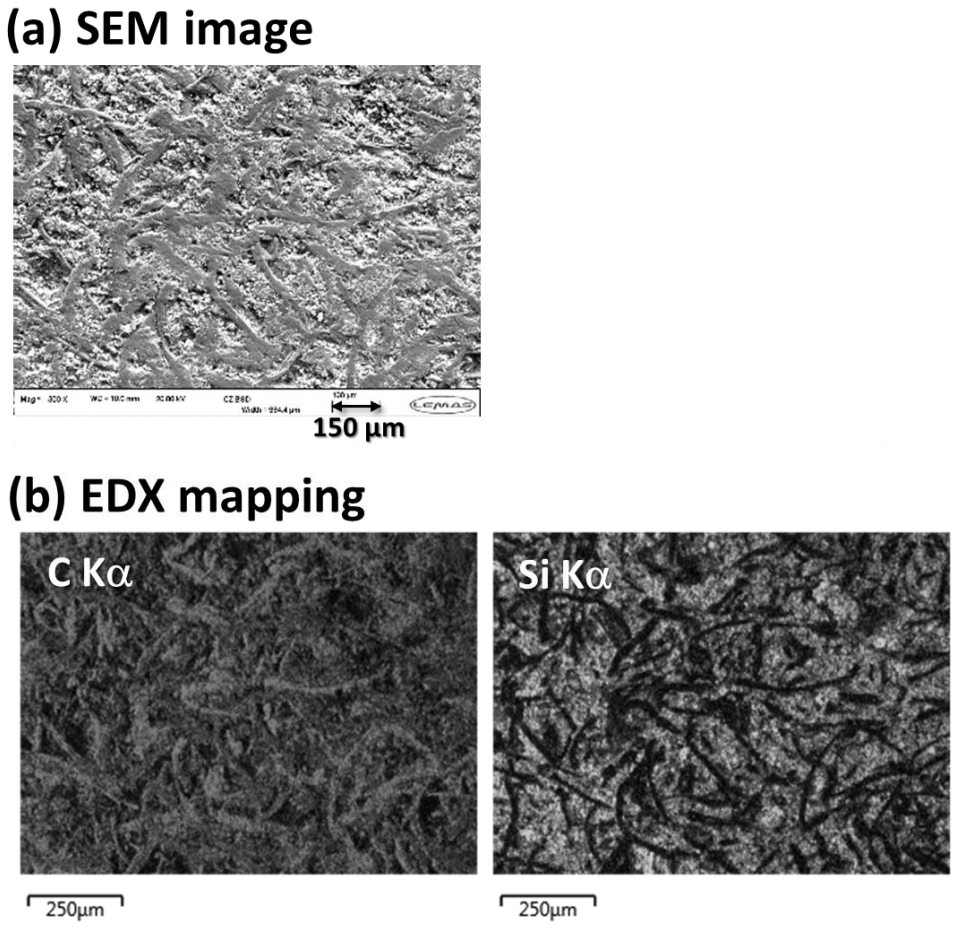

Fig. 5-8. (a) SEM image and (b) EDX mapping (C Kα and Si Kα, white; high concentration, black; low concentration) of a fresh TE77 paper plate

The SEM images of the post-test paper plates after testing PAO formulations are shown in Fig. 5-9. Because of the wide wear track due to the low elasticity of the paper, the paper surface only inside the wear track is shown in the images.

- The paper surface of (a) PAO, (c) PAO+alcohol and (d) PAO+GMO appeared to be flattened compared with the fresh paper. Especially, (d) PAO+GMO likely to be covered with organic material deposited on the paper, which is considered to be GMO.
- (b) PAO+acid kept the uneven surface structure almost the same as the fresh paper. The adsorption film formed by oleic acid might protect the paper surface.

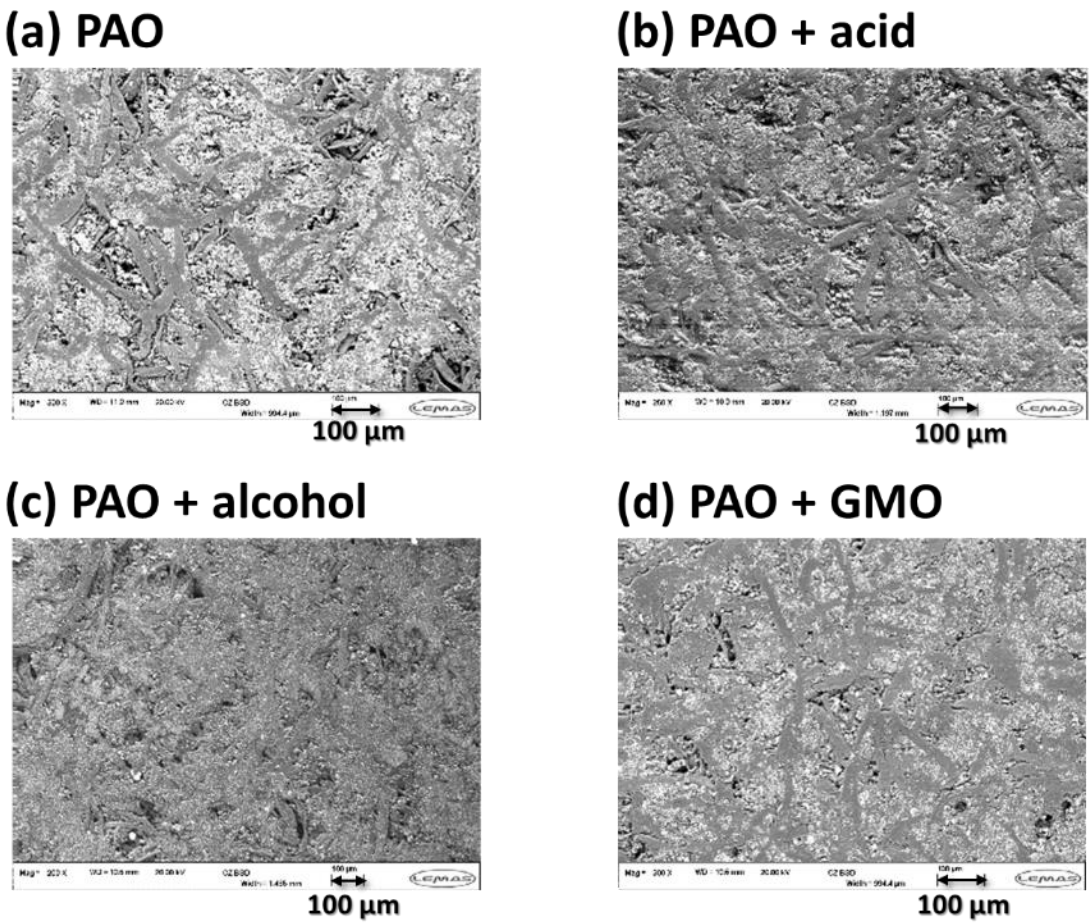

Fig. 5-9. SEM images of the post-test TE77 paper plates
after testing PAO formulations (100 °C, 60 minutes)
a) PAO, b) PAO + oleic acid, c) PAO + oleyl alcohol, d) PAO + GMO

Fig. 5-10 shows the SEM images for the post-test papers after testing the CVTF oils.

- Although the surface topography of all the oils appeared to be flattened by the sliding test, the fibre structure with pores was still kept on the surface.
- The appearance of (d) CVTF+GMO was also showing the features above, and looked different from the image of PAO+GMO (Fig. 5-9 (d)).

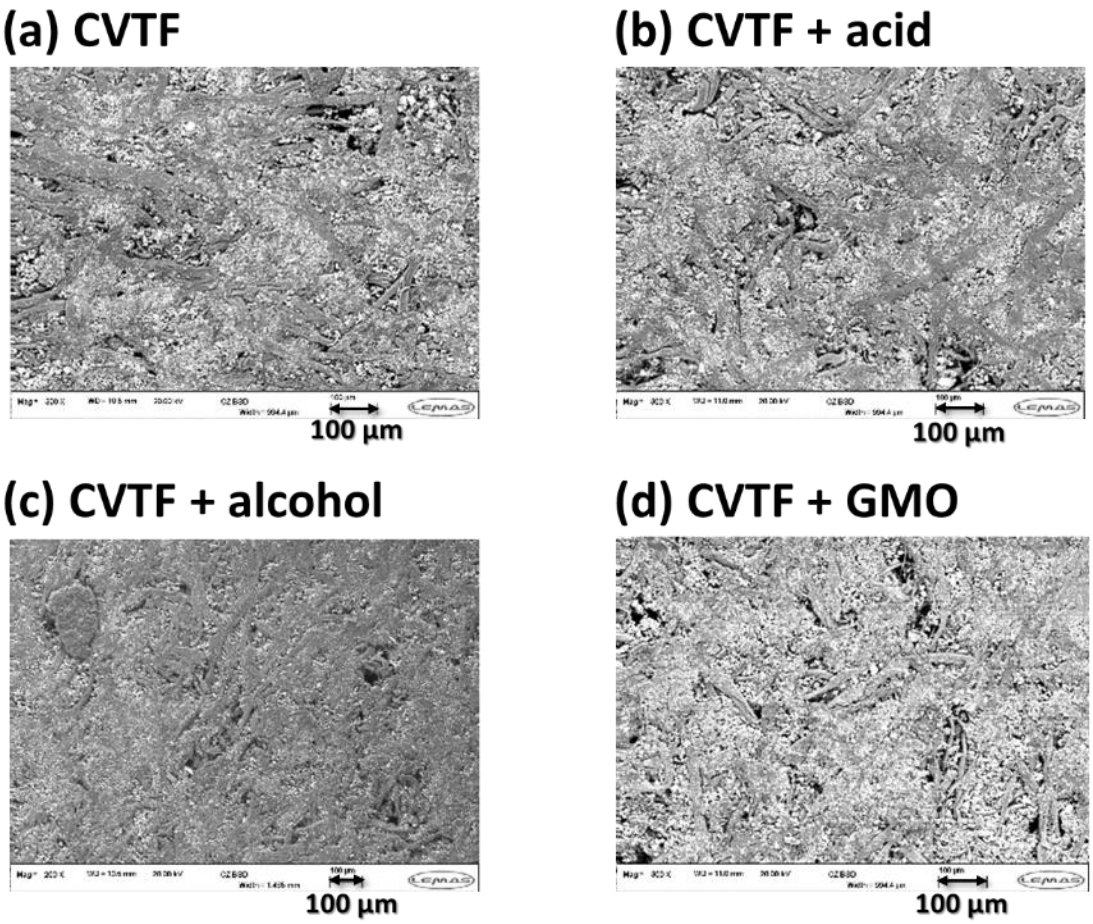

Fig. 5-10. SEM images of the post-test TE77 paper plates
after testing CVTF formulations (100 °C, 60 minutes)
a) CVTF, b) CVTF + oleic acid, c) CVTF + oleyl alcohol, d) CVTF + GMO

5.1.4. EDX Analysis

The wear tracks on the post-test TE77 paper plates were analysed by EDX to assess the elemental information. The mass fraction values on the paper after testing the PAO formulations are shown in Fig. 5-11.

- The fresh paper material showed the presence of 4 elements; carbon and oxygen derived from the cellulose fibre and the resin, silicon and very small quantity of calcium derived from the diatomite earth which is contained in the paper clutch as the filler.
- A comparison among the post-test papers shows that the oils with the FMs had a higher oxygen fraction, which implies the adsorption of the FMs on the surface.
- The oxygen mass fraction was at around 20 mass% for all the PAO+FM formulations. It did not indicate any difference among the oils despite the different frictional performance as shown in Fig. 5-1.

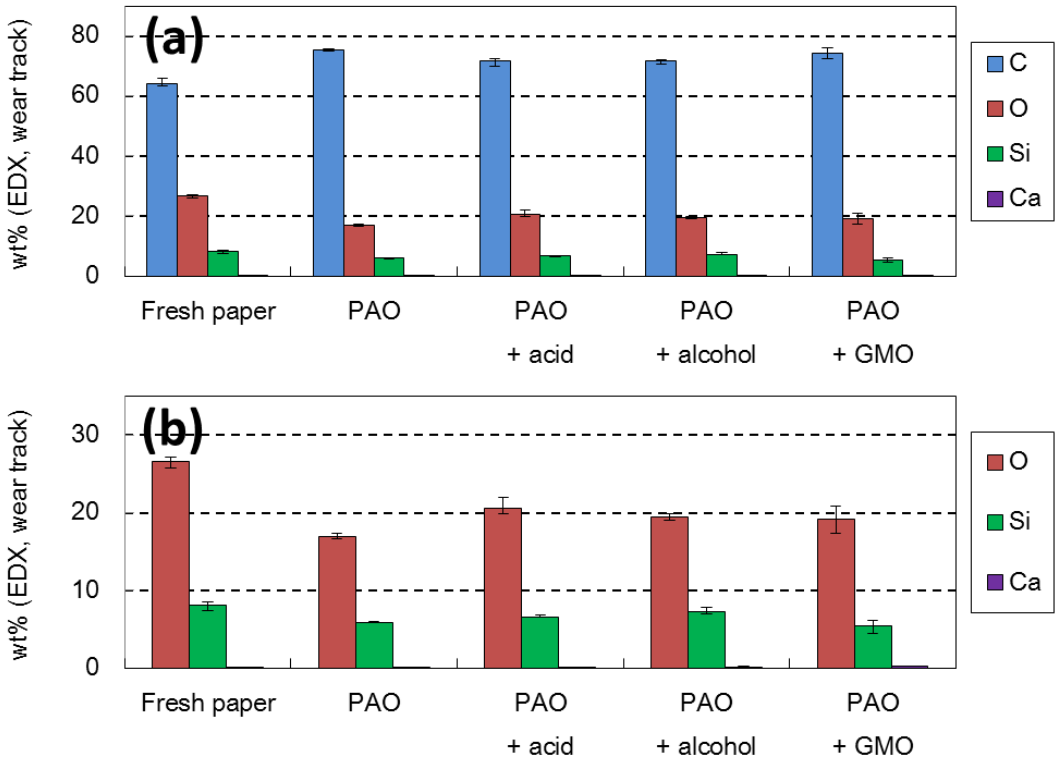

Fig. 5-11. EDX elemental analysis on the fresh TE77 paper plate and on the wear track of the post-test plates after testing the PAO formulations (100 °C, 60 minutes)
(a) whole elements, (b) the elements except for C

The EDX results for the CVTF formulations are shown in Fig. 5-12.

- All the formulations showed a similar oxygen quantity, a little less than 20 mass%. It was independent of the friction results showing the difference among the test oils.
- Focusing on the elements derived from the CVTF additives, the mass fraction of Ca, P and S were much smaller than those observed on the steel plate (Fig. 4-14). The quantitative difference among the oils appeared to be negligible considering the wide error bars.
- The reaction film appeared not to be formed on the paper in contrast to the steel.

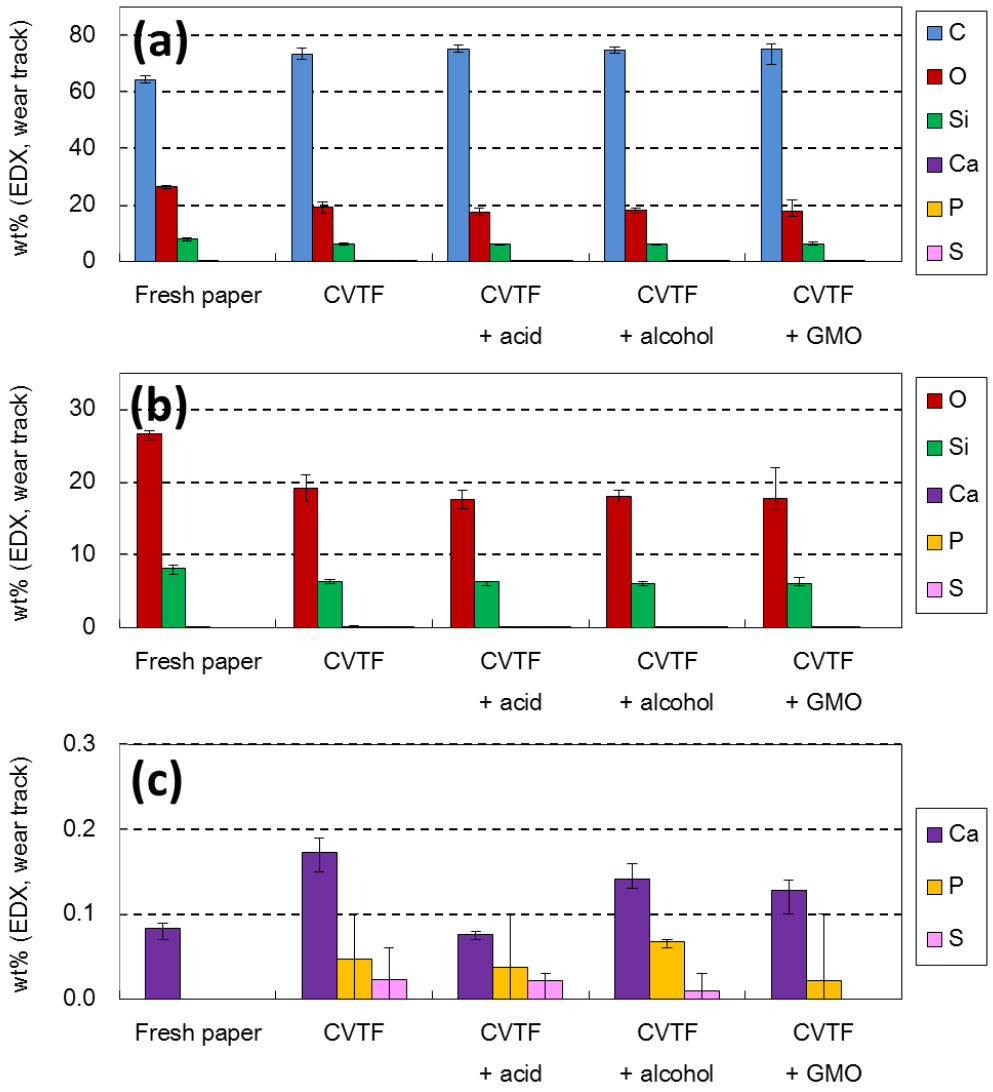

Fig. 5-12. EDX elemental analysis on the fresh TE77 paper plate and on the wear track of the post-test plates after testing the CVTF formulations (100 °C, 60 minutes)
(a) whole elements, (b) the elements except for C, (c) Ca, P and S

5.1.5. XPS Analysis (PAO Formulations)

The chemical nature on the post-test paper plates after testing the PAO formulations was assessed using XPS. Table 5-1 shows the weight fraction of the elements calculated from the XPS survey spectra. The oils with the FM indicated a little higher oxygen weight compared with PAO base oil at 1.1 mass%. Especially, PAO+GMO showed the highest ratio at 2.5 mass%. This result implies the adsorption of the FMs on the paper surface.

Table 5-1. XPS survey spectra on the wear track of the post-test paper plates after testing PAO formulations (100 °C, 60 minutes)

	PAO formulations			
Element, % mass	w/o FM	oleic acid	oleyl alcohol	GMO
C 1s	98.4	98.6	98.2	97.3
O 1s	1.1	1.4	1.8	2.5
N 1s	-	-	-	-
Ca 2p	-	-	-	-
P 2p	-	-	-	-
Si 2p	0.5	-	-	0.2

The XPS C 1s spectra of the PAO formulations are summarised in Fig. 5-13.

- A peak at approximately 285.5 eV was detected in (b) PAO+acid, (c) PAO+alcohol and (d) PAO+GMO, which could be attributed to the secondary shift (C-C-O). This small shift from SHC might appear due to the complicated interactions between the paper material and the FM.
- While (a) PAO showed a peak attributed to C-O at around 286.5 eV, (b) PAO+acid , (c) PAO+alcohol and (d) PAO+GMO had another peak at around 288 eV derived from C=O / O-C-O. Furthermore, (b) and (d) presented the other peak at 289.1 eV derived from carboxylate (O-C=O).
- The results above imply that the adsorption of oleic acid and GMO onto the paper material occurred, and are in good agreement with the friction measurement that shows the favourable friction effect (Fig. 5-1).

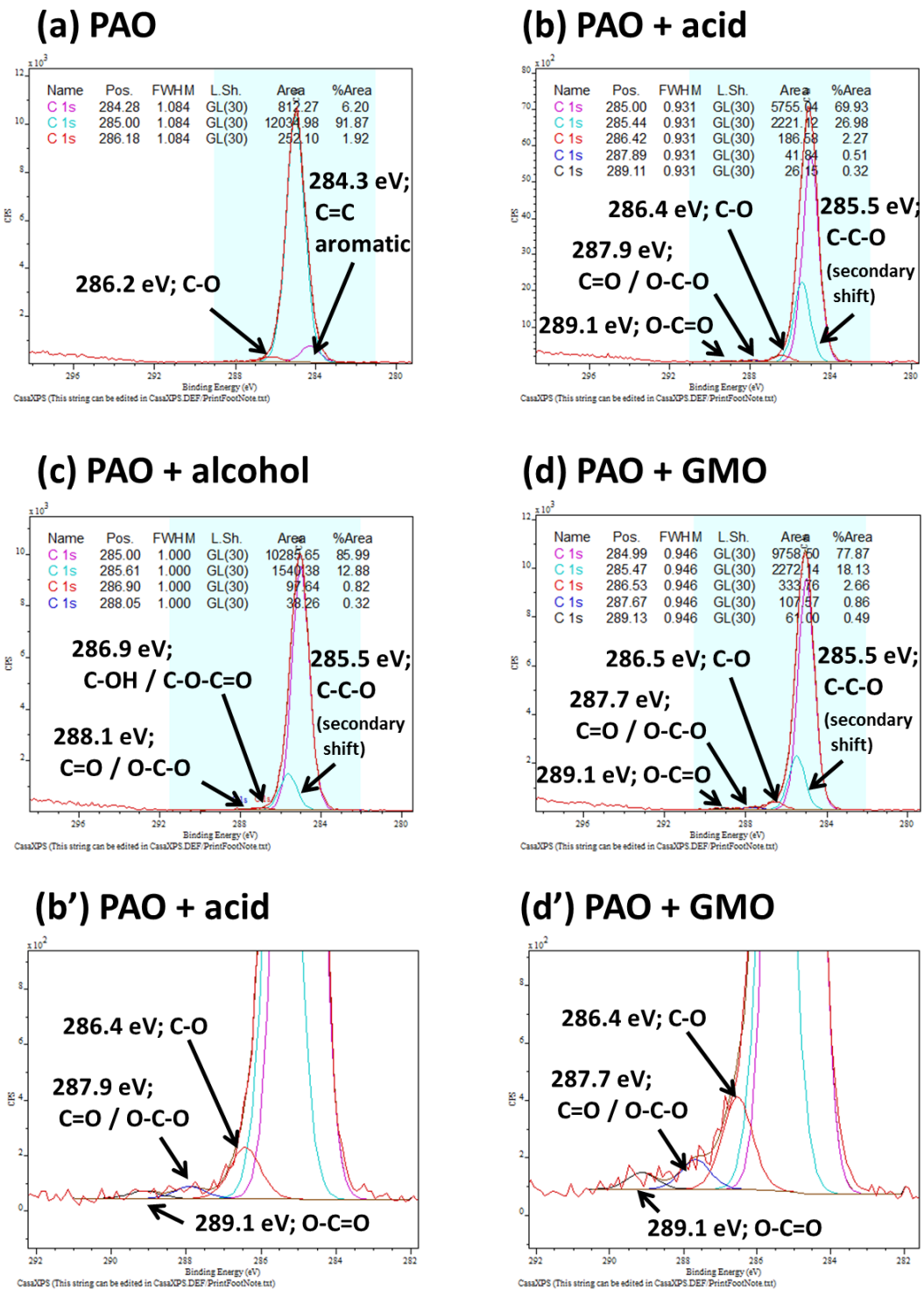

Fig. 5-13. XPS C 1s spectra on the wear track of the post-test paper plates after testing PAO formulations (100 °C, 60 minutes)

a) PAO, b) PAO + oleic acid, c) PAO + oleyl alcohol, d) PAO + GMO

b') and d') are expanded images of b) and d) in Y-axis

5.1.6. XPS Analysis (CVTF Formulations)

Table 5-2 shows the elemental weight fraction on the CVTF post-test paper plates calculated from the XPS survey spectra.

- The CVTF base fluid has almost the same fractions as the PAO base oil.
- CVTF+acid indicated a distinctive trend showing the much higher oxygen fraction, and the presence of Ca and P derived from the CVTF additives. It is considered that oleic acid interacted with the CVTF additives intensively, producing the film consisting of O, Ca and P on the paper surface.
- The oxygen ratio of CVTF+alcohol was almost comparable to the CVTF base oil, while CVTF+GMO showed a slight increase.

Table 5-2. XPS survey spectra on the wear track of the post-test TE77 paper plates after testing CVTF formulations (100 °C, 60 minutes)

	CVTF formulations			
Element, % mass	w/o FM	oleic acid	oleyl alcohol	GMO
C 1s	98.2	80.1	99.0	97.4
O 1s	1.2	12.5	1.0	1.9
N 1s	-	-	-	-
Ca 2p	-	2.4	-	-
P 2p	-	5.0	-	-
Si 2p	0.6	-	-	0.7

The XPS C 1s spectra of the CVTF formulations are shown in Fig. 5-14.

- (a) CVTF and (c) CVTF+alcohol showed the following peaks in common; between 286.0 and 287.1 eV derived from C-O bond and 288.4 eV from C=O / N-C=O bond.
- In contrast, (b) CVTF+acid and (d) CVTF+GMO had a distinctive peak at around 289 eV attributed to carboxylate (O=C-O). This trend corresponds to the tribotest results in which oleic acid and GMO showed the excellent effect.
- (b) CVTF+acid presented much higher peak intensities for C-O at 286.0 and 286.9 eV, which should be related to the film formation detected in Table 5-2.
- The spectrum of (d) CVTF+GMO was similar to that of PAO+GMO. The difference is that the peak at the highest energy shifted to slightly higher (289.3 eV) showing a clear peak shape, which implies the presence of carboxylic acid.

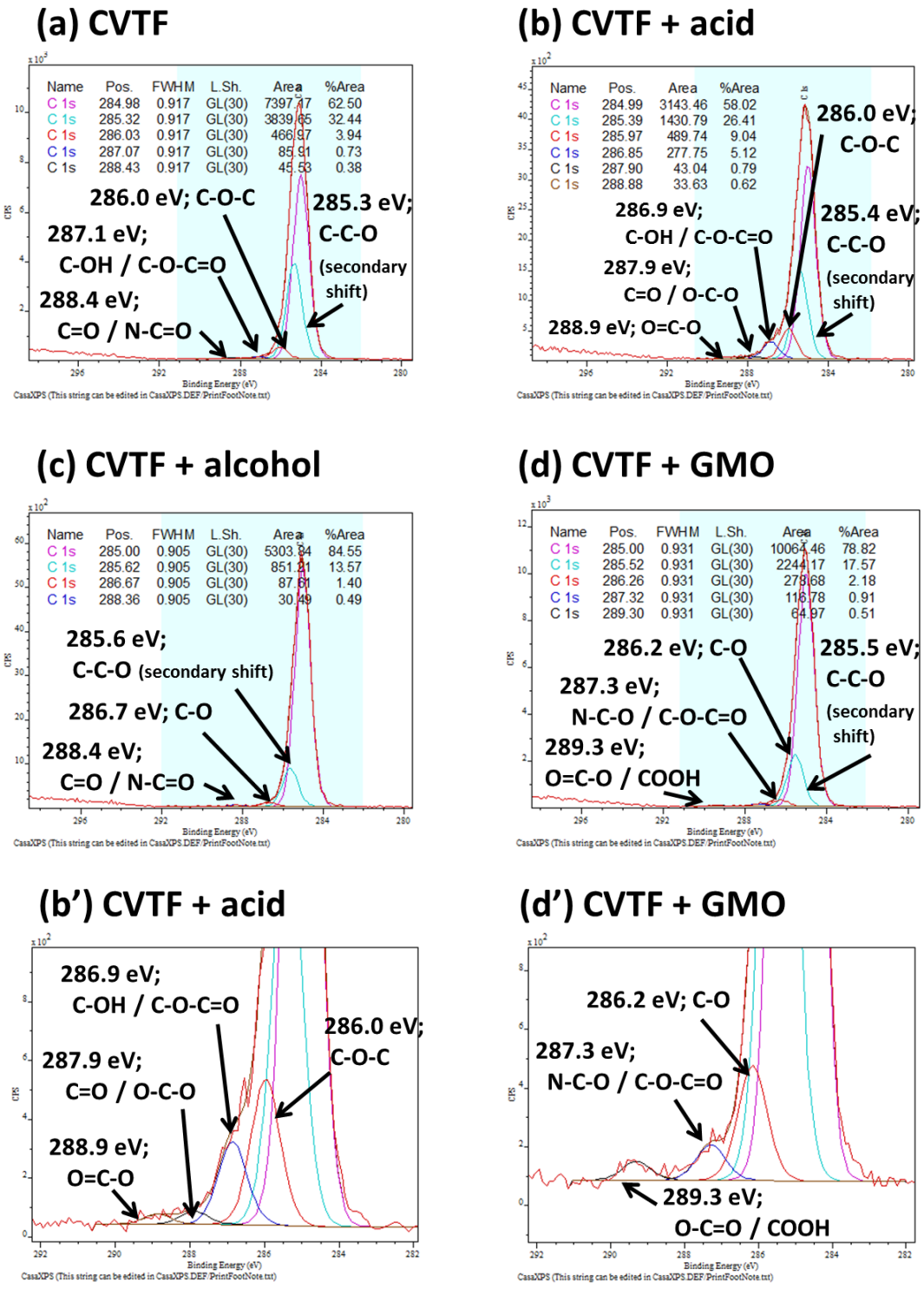

Fig. 5-14. XPS C 1s spectra on the wear track of the post-test paper plates after testing CVTF formulations (100 °C, 60 minutes)

a) CVTF, b) CVTF + oleic acid, c) CVTF + oleyl alcohol, d) CVTF + GMO

b') and d') are expanded images of b) and d) in Y-axis

5.1.7. ATR-FTIR Analysis (PAO Formulations)

ATR-FTIR spectra on the wear track of the post-test paper TE77 plates were measured to investigate the chemical bond formed during the sliding test. Fig. 5-15 shows the IR spectra of the PAO formulations. The difference spectra of the post-test papers subtracted from the fresh paper spectrum were also illustrated in the graphs.

- All the spectra indicated an increase of the peak intensities for hydrocarbon (C-H); ν (C-H) between 3,000 and 2,800 cm^{-1} and σ (C-H) between 1,350 and 1,500 cm^{-1}. They were derived from the adsorption of the test oils on the paper surface.
- Some peaks attributed to the paper material components were observed in the difference spectra. For example, ν (C=O) from aramid fibre at 1,650 cm^{-1}, ν (C-O) from cellulose fibre overlapping with ν_a (Si-O) from the diatomite earth between 1,200 and 900 cm^{-1}. It is considered that the resin material covering the paper clutch surface was removed by the sliding test.
- (b) PAO+acid and (d) PAO+GMO showed the carbonyl peak attributed to oleic acid and GMO at approximately 1,710 and 1,740 cm^{-1}, respectively.

For the comparison among the PAO formulations, the difference spectra were overwritten in Fig. 5-17 focusing on the carbonyl group region. It clearly shows the specific peaks attributed to oleic acid and GMO shown in the spectra for PAO+acid and PAO+GMO.

Furthermore, Fig. 5-17 presents a comparison of the IR spectra for the pure FMs (oleic acid and GMO) and the post-test paper plates. The peak observed in the (a) PAO+acid spectrum was slightly shifted to larger wave number at 5 cm^{-1}, which should be due to the dimer formation of oleic acid. As generally known, the carboxylic acid forms dimer which tends to shift the IR peak position of carboxyl group to lower wave number [176]. On the paper plate, oleic acid appeared to interact with the surface without forming the dimer, resulting in the larger wave number. On the other hand, the peak position of (b) PAO+GMO is comparable to pure GMO. The change in the chemical structure of GMO on the paper was not observed by ATR-FTIR, which implies the deposition of GMO on the surface as shown in the SEM image (Fig. 5-9).

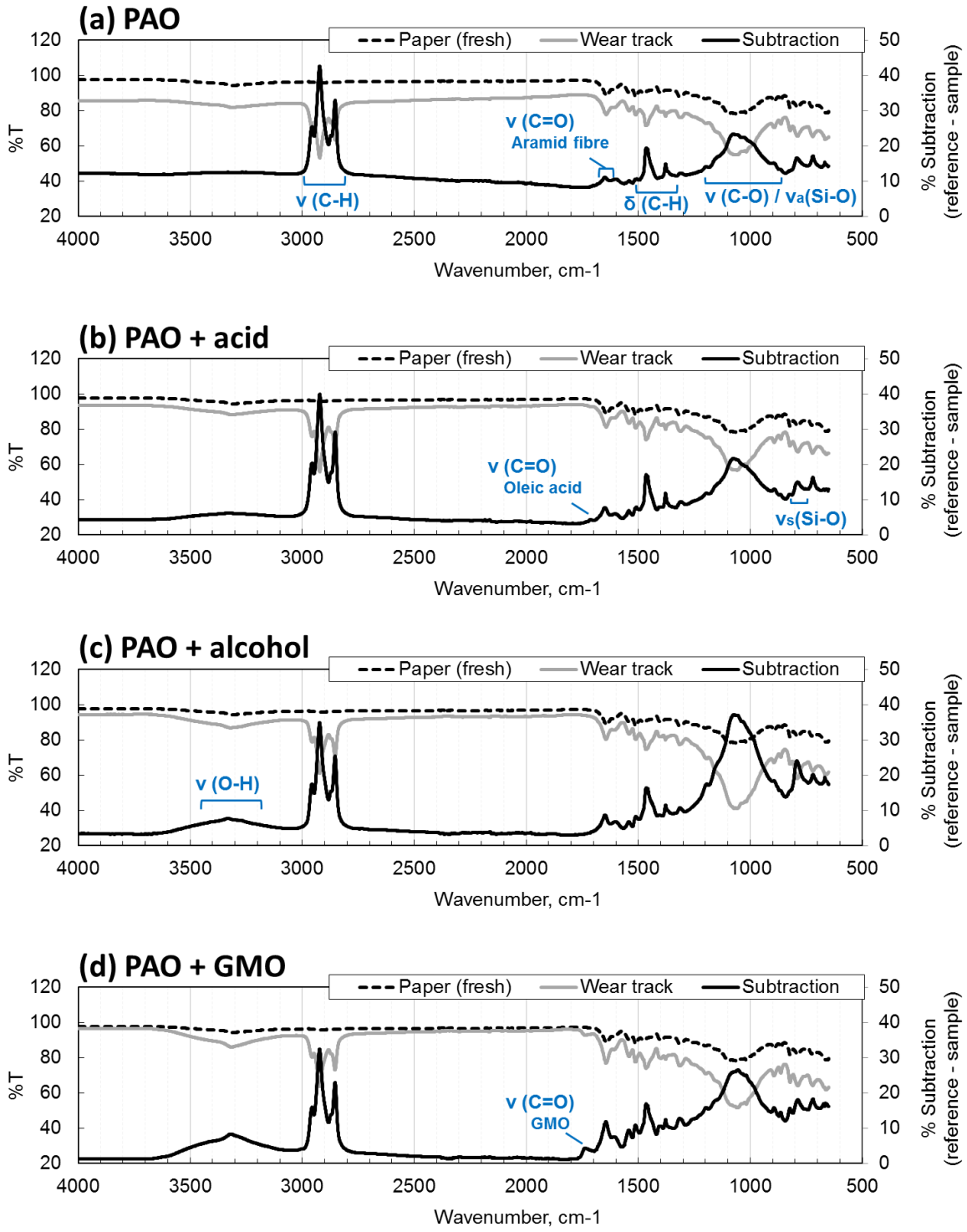

Fig. 5-15. ATR-FTIR spectra on the wear track of the post-test paper plates after testing PAO formulations (100 °C, 60 minutes)

a) PAO, b) PAO + oleic acid, c) PAO + oleyl alcohol, d) PAO + GMO

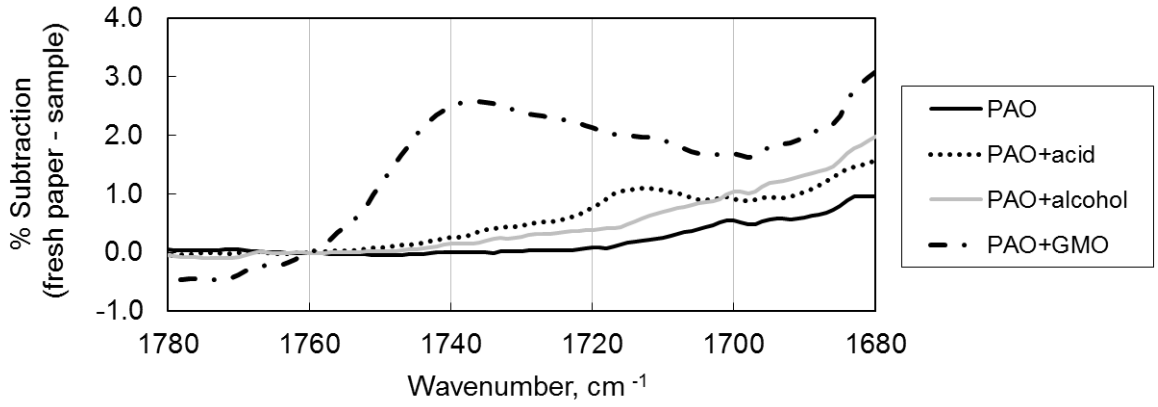

Fig. 5-16. ATR-FTIR difference spectra of the PAO formulations (C=O region)

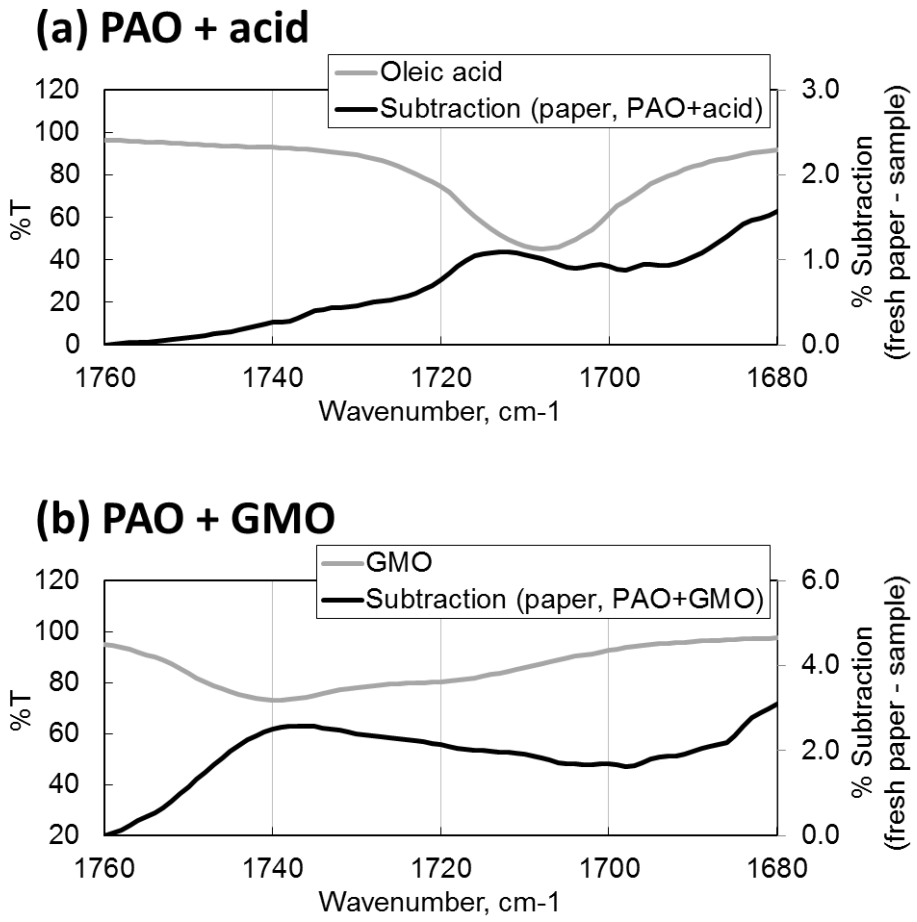

Fig. 5-17. Comparison between the IR peak of the pure FMs and the post-test paper plates, a) PAO + oleic acid, b) PAO + GMO

5.1.8. ATR-FTIR Analysis (CVTF Formulations)

The difference IR spectra for the CVTF formulations are shown in Fig. 5-18.

- The major peaks detected in the difference spectra were similar to those seen in the PAO formulations, which were derived from the test oil and the paper material components; hydrocarbon, cellulose fibre, aramid fibre and diatomite.
- All the formulations presented two carbonyl peaks at 1,730 and 1,700 cm^{-1} that should be attributed to the CVTF additives.

The difference IR spectra are summarised in Fig. 5-19 focusing on the carbonyl groups for the detailed comparison. In contrast to the PAO formulations, the spectra did not show any specific difference attributed to the FMs. In order to identify the observed carbonyl peaks, the post-test paper IR spectrum for the CVTF base fluid was compared with the additives with the carbonyl groups; PMA (polymethacrylate, viscosity modifier) and dispersant (polyisobutylene succineimide) as shown in Fig. 5-20. The graph clearly shows that the peak at 1,730 cm^{-1} could be attributed to the ester bond of PMA, while the peak at 1,700 cm^{-1} to the imide bond of the dispersant.

Based on the ATR-FTIR results for the post-test paper samples, it could be assumed that the CVTF additives inhibited the absorption of the FMs. However, the FM effect of oleic acid and GMO was still obviously shown in the tribotest results even formulated with the CVTF additives. In addition, distinctive peaks were also observed for CVTF+acid and CVTF+GMO when assessed by XPS (Fig. 5-14).

The difference between ATR-FTIR and XPS is considered to be caused by the analysis depth; approximately 1 μm for ATR-FTIR and a few nm for XPS. It means that the ATR-FTIR result mainly reflects the information from the substrate including a reaction film, while the XPS is focusing on the uppermost surface. Thick reaction films could not be formed on the paper clutch surface in contrast to the steel surface as shown in the EDX results (Fig. 5-12), though, the fibrous structure tends to adsorb the polar additives that would be detected by ATR-FTIR. It contrast, the XPS spectra is capable of reflecting the chemical nature on the uppermost rubbed surface, so that it was able to observe the adsorption of oleic acid and GMO. The ATR-FTIR measurement does not seem to be very effective to assess the chemical information on the paper material, especially in the presence of the other additives.

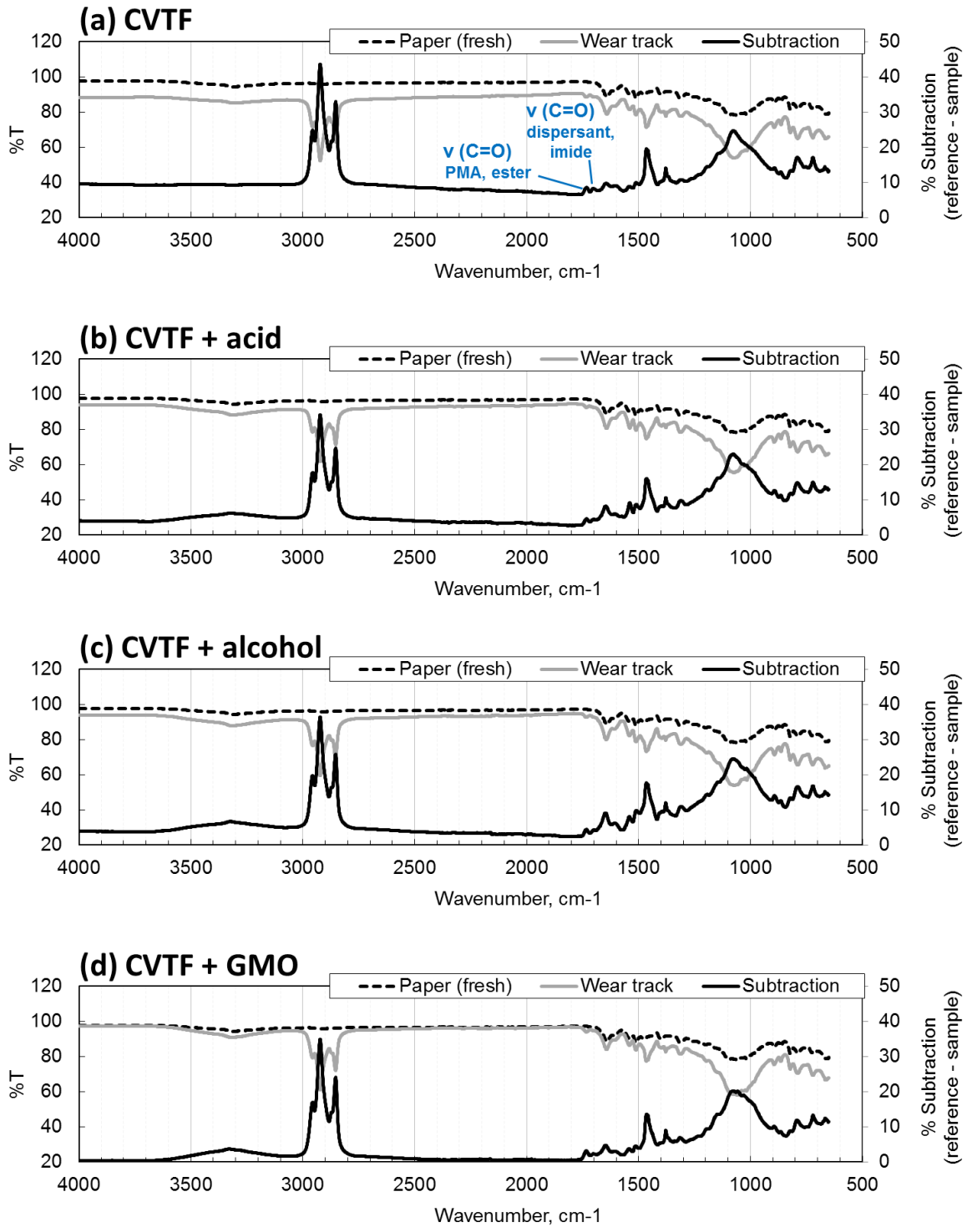

Fig. 5-18. ATR-FTIR spectra on the wear track of the post-test paper plates after testing CVTF formulations (100 °C, 60 minutes)

a) CVTF, b) CVTF + oleic acid, c) CVTF + oleyl alcohol, d) CVTF + GMO

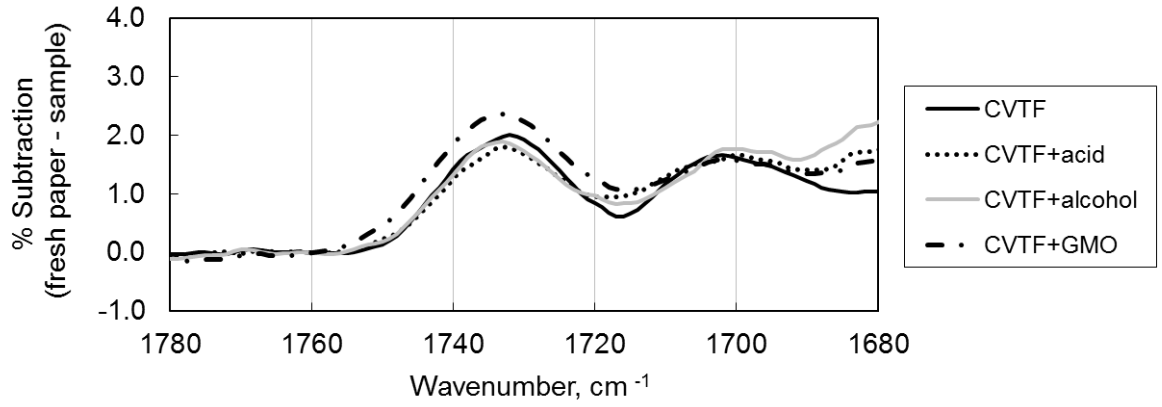

Fig. 5-19. ATR-FTIR difference spectra of the CVTF formulations (C=O region)

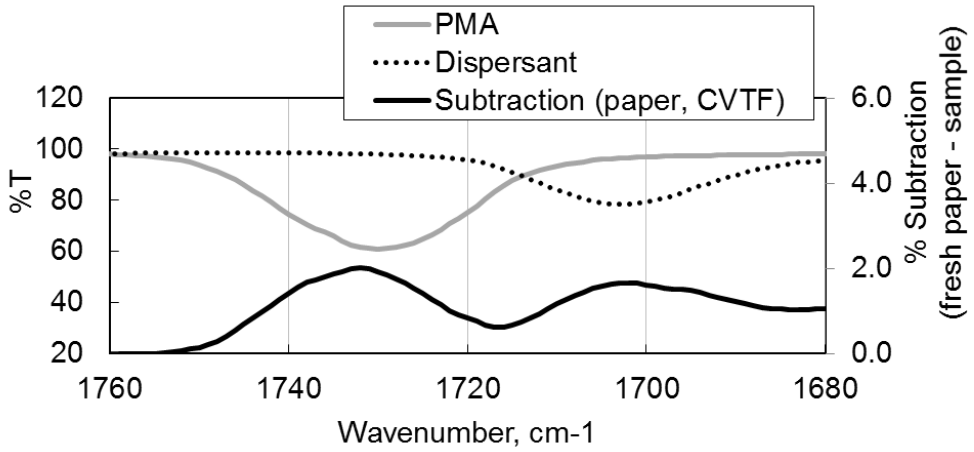

Fig. 5-20. Comparison between the IR peaks of the CVTF additives (PMA and dispersant) and the post-test paper plate after testing the CVTF

5.1.9. Summary of TE77 Paper Contact Tests at 100°C

The results for the TE77 paper/steel sliding tests at 100°C are summarised in Table 5-3.

Among the PAO formulations, oleic acid worked as the most effective FM reducing CoF and FFWI significantly, while oleyl alcohol presented a slight effect. GMO had an interesting trend showing low CoF and high FFWI simultaneously, which would be caused by the GMO deposit on the paper as discussed later. The results of XPS, EDX and ATR-FTIR for PAO+acid or PAO+GMO indicated the presence of the carboxylate

(C=O-O) group derived from the FMs, which means these techniques were capable of detecting the FMs on the paper surface.

In terms of the CVTF formulations, XPS C 1s spectra seemed to be useful to see the correspondence between the frictional performances and the chemical nature on the paper. Although the peaks attributed to the CVTF additives (C-O, C=O and N-C=O) were observed in the spectra for CVTF and CVTF+alcohol, the peak derived from carboxylate (O=C-O) was detected for (b) CVTF+acid and (d) CVTF+GMO. This result implies the formation of the FM film by oleic acid and GMO on the paper surface, and shows good agreement with the friction and FFWI results. On the other hand, EDX and ATR-FTIR seemed not to be effective to discuss the adsorption of the FMs in the presence of the CVTF additives.

Table 5-3. Summary of TE77 paper/steel contact at 100°C

	PAO formulations			
	w/o FM	oleic acid	oleyl alcohol	GMO
CoF	0.137	0.086	0.107	0.094
FFWI	1.38	1.06	1.18	1.30
Paper condition (SEM)	good	good	good	some deposites
Chemical nature				
Topmost surface (XPS)	C-O	C-O C=O / O-C-O **O=C-O**	C-O C=O / O-C-O	C-O C=O / O-C-O **O=C-O**
Surface including unrubbed sublayer (EDX and ATR-FTIR)	-	oleic acid (slight chemical sift)	-	GMO (no chemical shift)

	CVTF formulations			
	w/o FM	oleic acid	oleyl alcohol	GMO
CoF	0.128	0.088	0.115	0.090
FFWI	1.22	1.00	1.17	1.05
Paper condition (SEM)	good	good	good	good
Chemical nature				
Topmost surface (XPS)	C-O C-O-C=O C=O / N-C=O	C-O C-O-C=O C=O / O-C-O **O=C-O**	C-O C=O / N-C=O	C-O C-O-C=O / N-C-O **O=C-O / COOH**
Surface including unrubbed sublayer (EDX and ATR-FTIR)	ester (PMA) imide (dispersant)	ester (PMA) imide (dispersant)	ester (PMA) imide (dispersant)	ester (PMA) imide (dispersant)

5.2. TE77 Paper Contact Tests at 40°C

The behaviour of the FMs was investigated also at 40°C. It is ideal for the automatic transmission fluids to keep the same frictional performances independent on the temperature, however, they are generally influenced from the temperature due to the change of the chemical potential. In this session, the mechanism will be discussed based on the surface analyses.

5.2.1. Friction Coefficient

The friction coefficient values were measured using the TE77. The results for the PAO formulations are shown in Fig. 5-21, while the results for the CVTF formulations are in Fig. 5-22. In addition, the friction values at the end of the 60 minutes tests are summarised in Fig. 5-23.

For both of the formulations, the ranking of the friction coefficient at the end of the test was as follows; (highest) w/o FM > oleic acid = oleyl alcohol > GMO. It appears that oleic acid decreased the effect compared to the results at 100°C, while the effect of oleyl alcohol and GMO was not affected by the temperature condition. It is notable that the friction of the PAO base oil was much lower and more stable than the 100°C result, which implies that the physical damage on the paper surface was prevented at 40°C by the thicker oil film due to the higher viscosity.

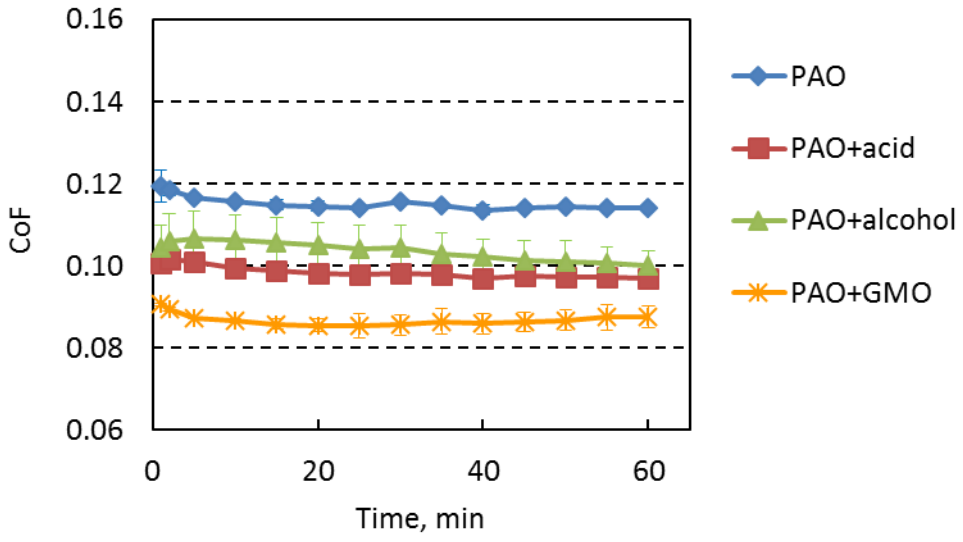

Fig. 5-21. Friction coefficient at the paper/steel contact measured by TE77 (PAO formulation, 40°C, 60 min)

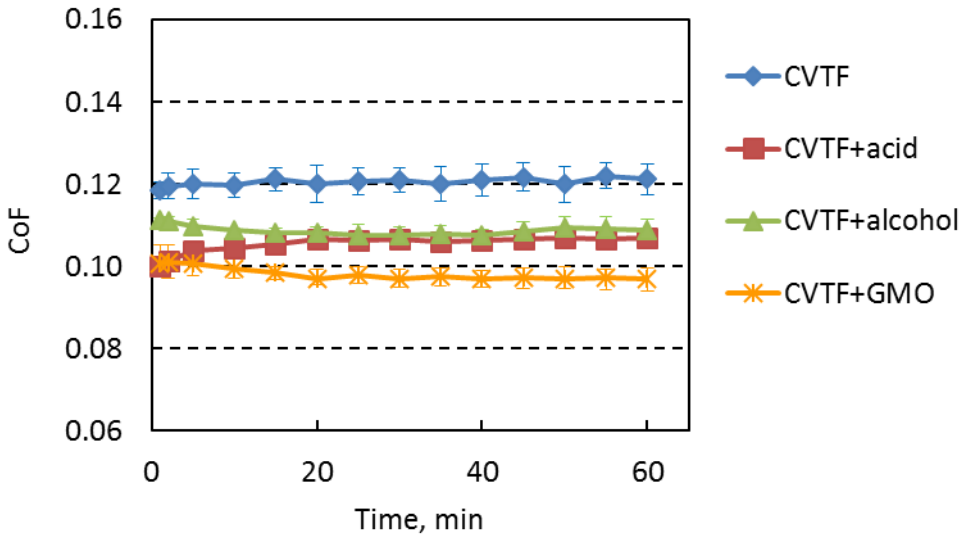

Fig. 5-22. Friction coefficient at the paper/steel contact measured by TE77 (CVTF formulation, 40°C, 60 min)

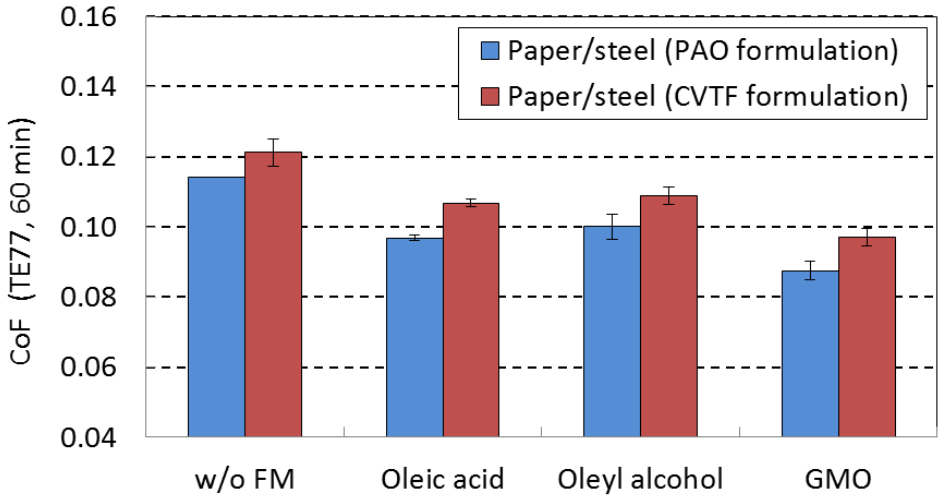

Fig. 5-23. TE77 friction coefficient of paper/steel contact (after 60 minutes)

5.2.2. Friction Force Wave Analysis

The friction force wave shapes during the TE77 tests for the PAO formulations are shown in Fig. 5-24, and the FFWI (friction force wave index) values are summarised in Fig. 5-25. While the wave shapes for (a) PAO, (b) PAO+acid and (c) PAO+alcohol were comparable to the 100°C results (Fig. 5-4), (d) PAO +GMO presented a smoother curve with lower spike height compared with the 100°C curve. The FFWI also enables the quantitative comparison of this trend, presenting a much lower value for PAO+GMO than the 100°C results shown in Fig. 5-5. This trend indicates the different working mechanism of GMO depending on the test temperature.

The results for the CVTF oils are also shown in Fig. 5-26 and Fig. 5-27. The overall trend was not changed from the 100°C results (Fig. 5-6 and Fig. 5-7) except that (b) CVTF+acid had a little higher spike height. It should be noted that the effect of GMO on FFWI was not affected by the test temperature in contrast to PAO+GMO.

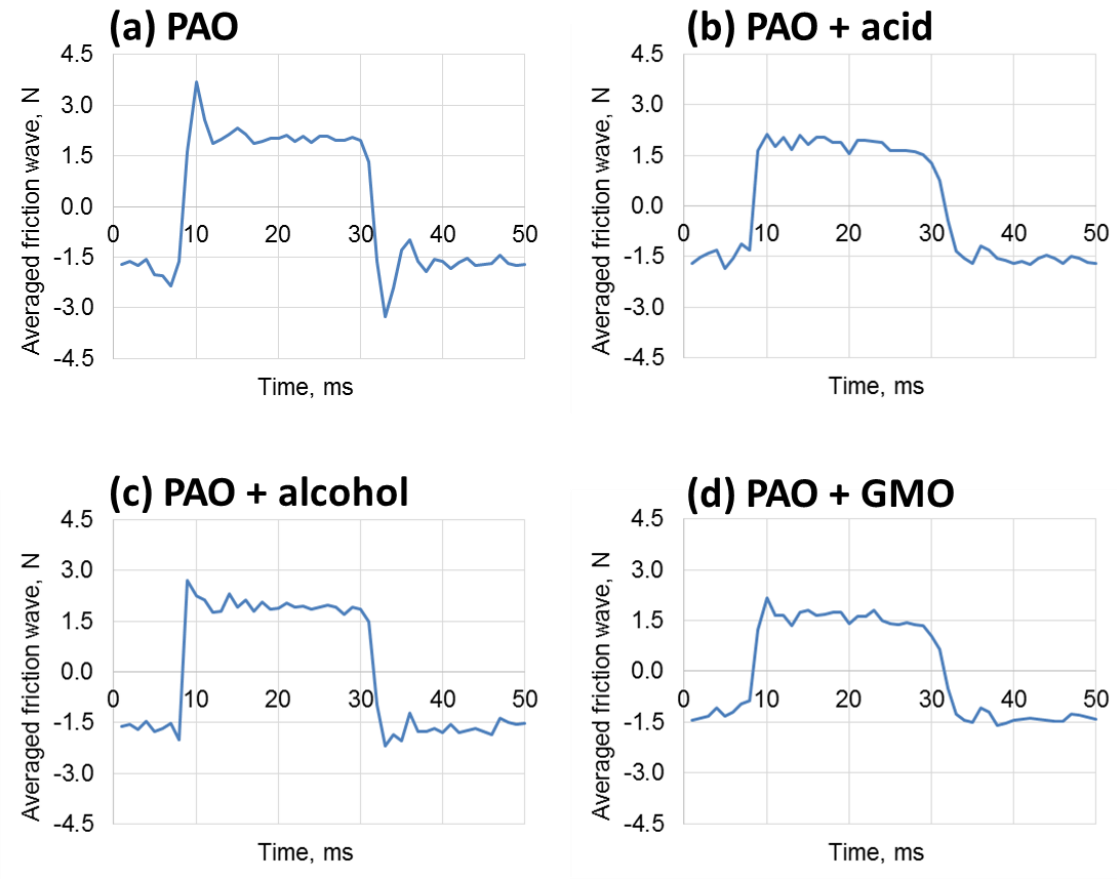

Fig. 5-24. Friction force waves for the PAO formulations at paper/steel sliding test (40 °C, wave data from 30 to 60 minutes were averaged)
a) PAO, b) PAO + oleic acid, c) PAO + oleyl alcohol, d) PAO + GMO

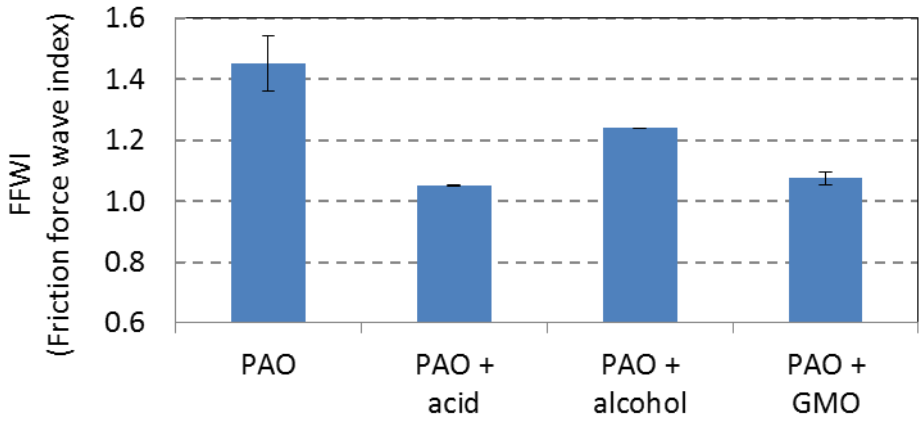

Fig. 5-25. FFWI for the PAO formulations at 40°C

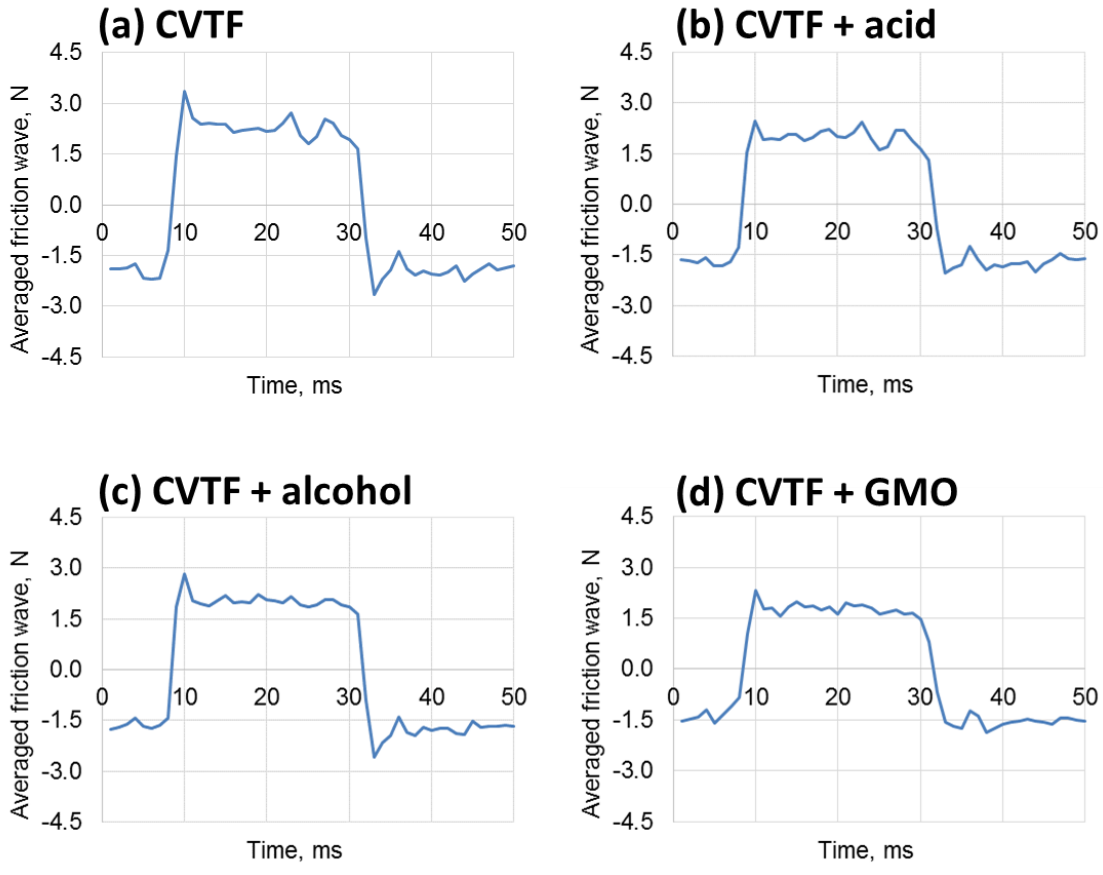

Fig. 5-26. Friction force waves for the CVTF formulations at paper/steel sliding test (40 °C, wave data from 30 to 60 minutes were averaged)

a) CVTF, b) CVTF + oleic acid, c) CVTF + oleyl alcohol, d) CVTF + GMO

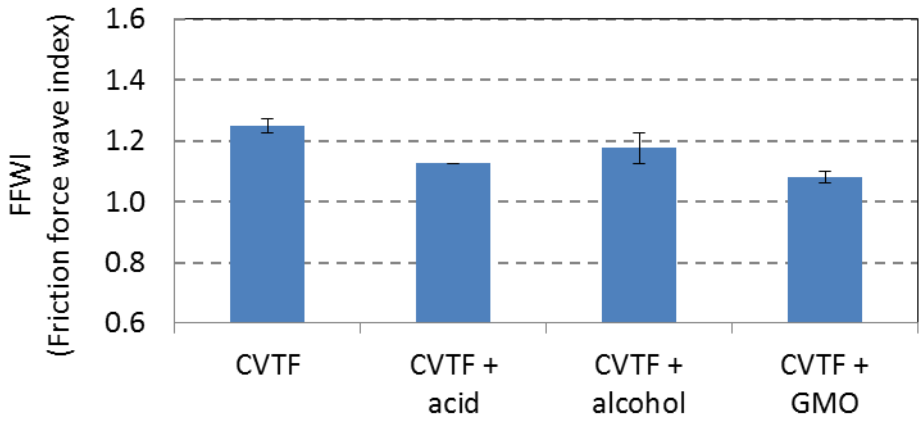

Fig. 5-27. FFWI for the CVTF formulations at 40°C

5.2.3. Wear Track Observation by SEM

The surface images of the post-test papers observed by SEM are shown in Fig. 5-28 for the PAO formulations and in Fig. 5-29 for the CVTF formulations.

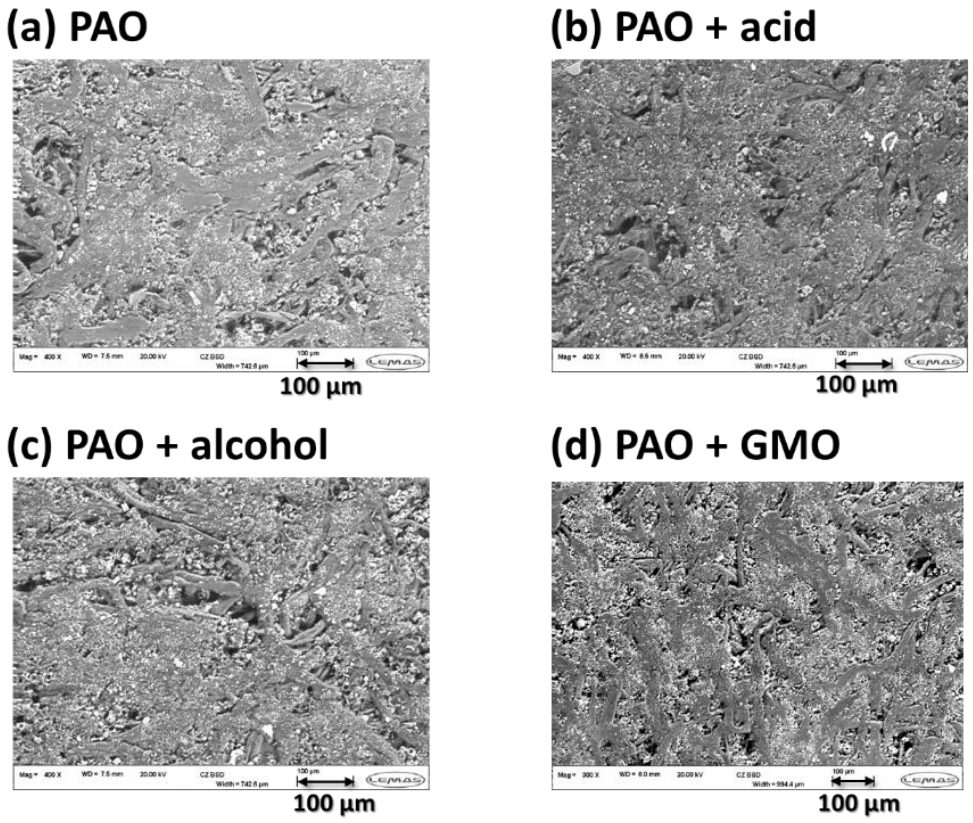

Fig. 5-28. SEM images of the post-test TE77 paper plates for PAO formulations (40°C)
a) PAO, b) PAO + oleic acid, c) PAO + oleyl alcohol, d) PAO + GMO

The tangled fibres with the pores are clearly seen on all the post-test papers, although the PAO surface (Fig. 5-28 (a)) appeared to be a slightly flattened. Interestingly, PAO+GMO (Fig. 5-28 (d)) showed uneven surface in contrast to the 100°C image (Fig. 5-9 (d)). The results indicate that the friction properties of the test oils, except for PAO or PAO+GMO, should be mainly controlled by the surface chemistry rather than the surface topography.

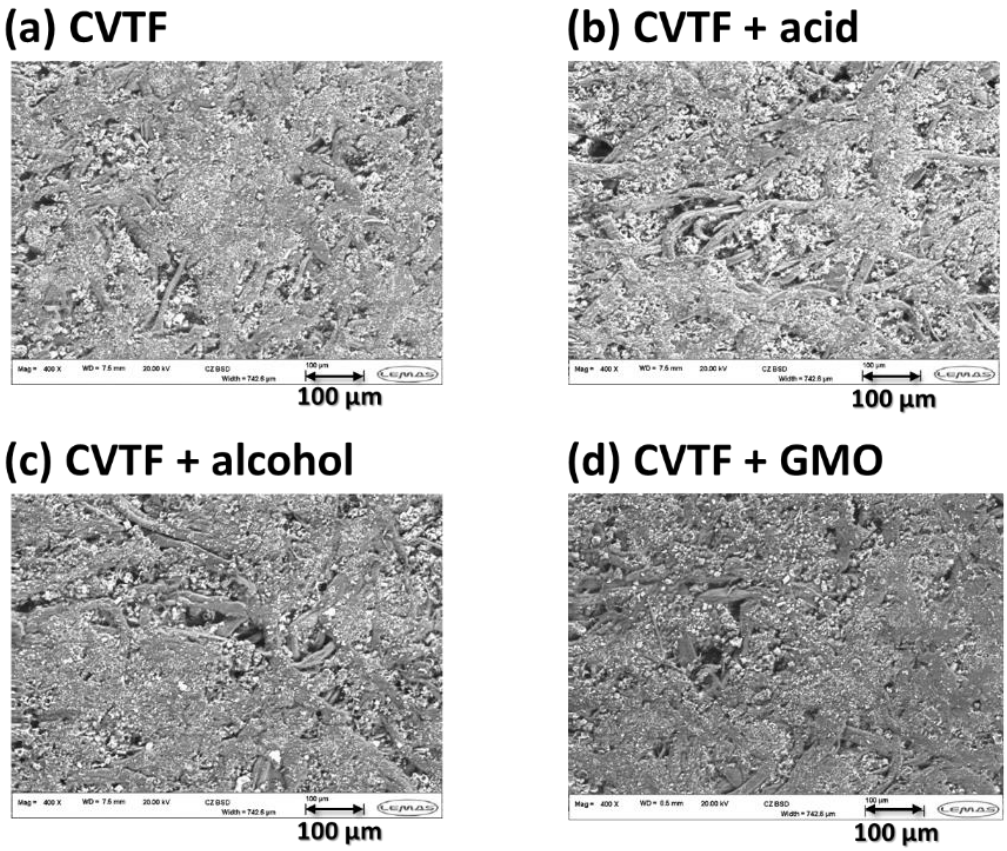

Fig. 5-29. SEM images of the post-test TE77 paper plates for CVTF formulations (40°C)

a) CVTF, b) CVTF + oleic acid, c) CVTF + oleyl alcohol, d) CVTF + GMO

5.2.4. EDX Analysis

EDX analysis was carried out to observe the chemical species on the post-test paper samples. The results for the PAO formulations are summarised in Fig. 5-30. All the post-test plates presented the similar elemental concentration; oxygen approximately at 17 mass% and silicon approximately at 7 mass% despite the significant difference in the frictional properties; the friction coefficient and the FFWI.

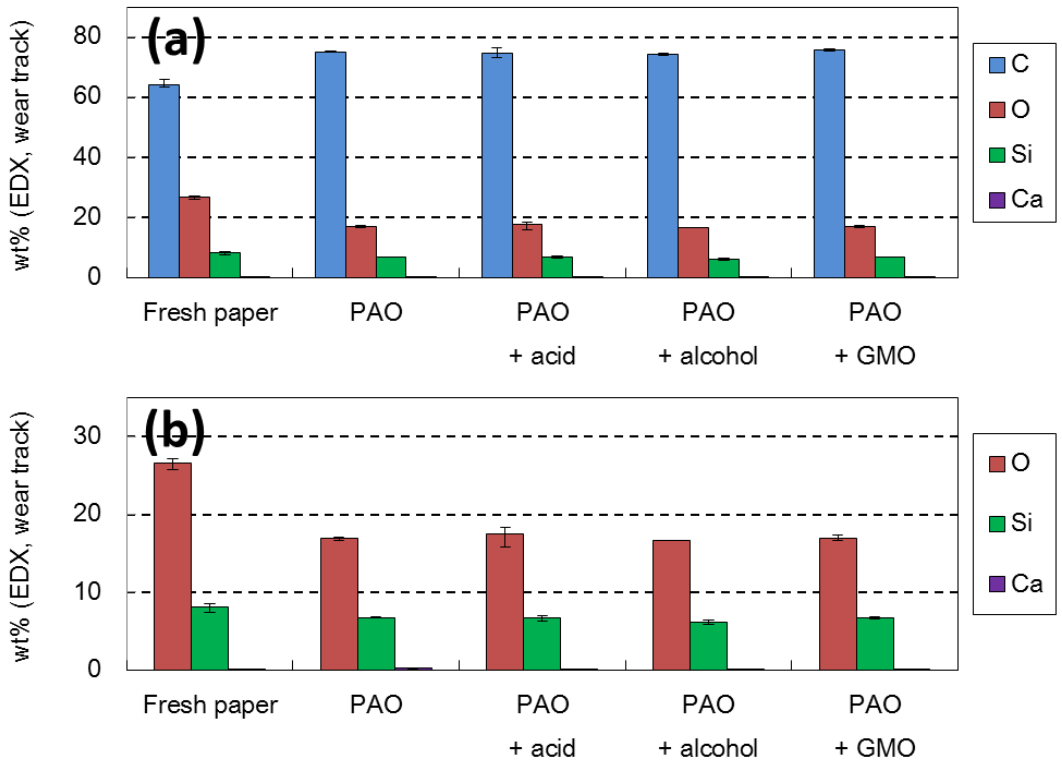

Fig. 5-30. EDX elemental analysis for the fresh TE77 paper plate the post-test plates after testing PAO formulations (40°C, 60 minutes)
(a) all elements, (b) the elements except for C

The EDX results for the CVTF post-test paper plates are shown in Fig. 5-31.

- The oxygen and silicon amount detected on the surface, shown in (b), were approximately at 18 mass% and 7 mass% for all the post-test papers.
- Regarding the elements derived from the CVTF additives (Ca, P and S) shown in (c), CVTF+acid presented a relatively lower Ca concentration less than 0.1 mass%, which was around a half compared with the other post-test samples and almost the same as the fresh paper. Oleic acid probably inhibited the adsorption of the calcium detergent at low temperature condition.
- The results did not show good agreement with the friction coefficient and the FFWI results similar to the PAO formulations. EDX analysis for the paper clutch does not seem to be very useful to obtain information on the surface chemical nature.

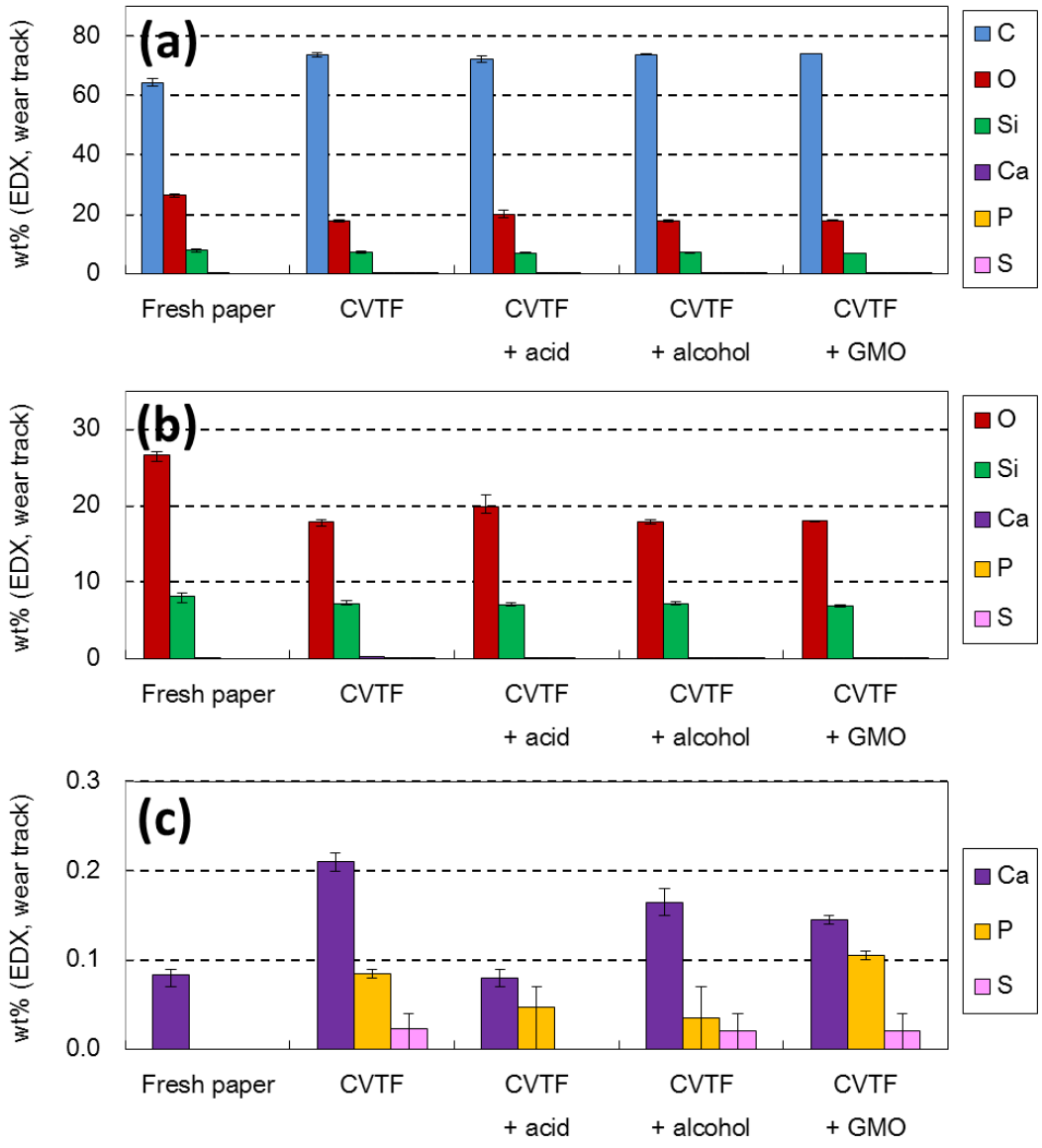

Fig. 5-31. EDX elemental analysis for the fresh TE77 paper plate and the post-test plates after testing the CVTF formulations (40°C, 60 minutes)
(a) all elements, (b) the elements except for C, (c) Ca, P and S

5.2.5. XPS Analysis (PAO Formulations by K-alpha)

The chemical nature on the post-test paper plates were assessed using XPS. As mentioned in Chapter 3, the paper plates after testing the PAO formulation at 40°C were analysed by K-alpha, a different XPS facility at NEXUS, due to the trouble on Theta Probe which was utilised for all the other XPS measurement.

Table 5-4 shows the elemental concentration calculated from the peak area shown in the XPS survey spectra. Oleyl alcohol and GMO increased the oxygen fraction significantly from 0.8 wt% to around 4.0 wt%, while oleic acid showed a slight increase to 1.5 wt%. The C 1s detail scan was performed both inside and outside the wear track. The results are shown in Fig. 5-32. The comments on the results are described below;

- The test oils with the FMs, (b) PAO+acid, (c) PAO+alcohol and (d) PAO+GMO, presented the specific peaks attributed to the oxygen based structure, at around 288 eV derived from C=O or O-C-O and at around 289 eV from 289 eV from O=C-O, which were not detected in the spectrum for (a) PAO.
- (c) PAO+alcohol or (d) PAO+GMO presented the higher peak intensities at approximately 288 and 289 eV than (b) PAO+acid. These results were in good agreement with the oxygen concentration calculated from the XPS survey spectra (Table 5-4).
- No significant difference was observed between the inside and the outside the wear for all the formulations. It implies that the oxygen structures detected in the C 1s spectra were not formed as a result of the sliding action.

Table 5-4. XPS survey spectra on the post-test paper plates after testing PAO formulations (40 °C, 60 minutes)

	PAO formulations			
Element, % mass	w/o FM	oleic acid	oleyl alcohol	GMO
C 1s	99.2	98.1	94.4	94.6
O 1s	0.8	1.5	4.1	3.9
N 1s	-	-	-	-
Ca 2p	-	-	-	-
P 2p	-	-	-	-
Si 2p	-	0.4	1.5	1.5

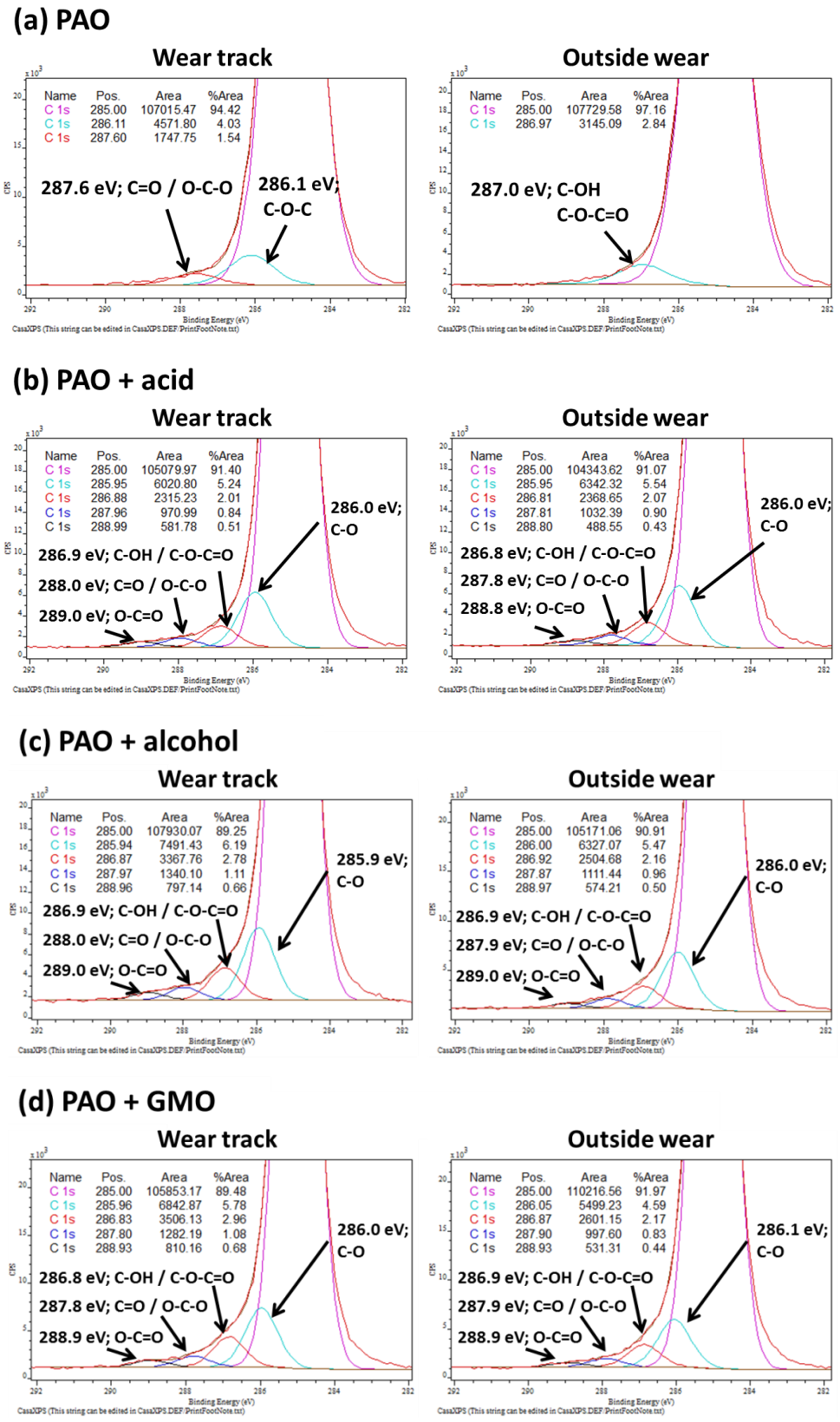

Fig. 5-32. XPS C 1s spectra for the post-test paper plates after testing PAO formulations (40 °C, 60 minutes)

a) PAO, b) PAO + oleic acid, c) PAO + oleyl alcohol, d) PAO + GMO

5.2.6. XPS Analysis (CVTF Formulations)

The post-test paper samples after testing the CVTF formulations were analysed using Theta probe XPS. The elemental analysis results based on the XPS survey spectra is shown in Table 5-5. In contrast to the PAO results, the oxygen concentration did not increased significantly by the addition of the FMs. Furthermore, CVTF+acid did not show the presence of Ca and P, which was different to the 100°C results (Table 5-2).
The C1s detailed spectra of the CVTF formulations are shown in Fig. 5-33.

- Similar to the PAO results, the oils with the FMs, (b) CVTF+acid, (c) CVTF+alcohol and (d) CVTF+GMO, had an additional peak at around 289 eV derived from carboxylate (O=C-O).
- The overall trend of the spectra was comparable between the inside and the outside the wear track for all the test oils, which means that the oxygen compounds appeared to adsorb onto the paper surface without the help of the sliding stress.
- The XPS spectra did not show good correspondence with the frictional performance shown in Fig. 5-22 and Fig. 5-27.

Looking at the XPS results for the post-test papers at 40°C, they did not show the distinctive peaks capable of explaining the frictional properties in contrast to the XPS results at 100°C. The reason should be the type of the interaction between the FM and paper, which depends on the temperature. It is considered that the FMs could not form a strong connection with the paper surface at 40°C, while it could occur at 100°C. The adsorbed FMs on the paper at 40°C would be removed when rinsed with heptane, so that it was not possible to observe the difference among the test oils.

Table 5-5. XPS survey spectra on the post-test paper plates after testing the CVTF formulations (40 °C, 60 minutes)

	CVTF formulations			
Element, % mass	w/o FM	oleic acid	oleyl alcohol	GMO
C 1s	98.8	98.9	98.1	98.9
O 1s	1.2	1.1	1.7	1.1
N 1s	-	-	-	-
Ca 2p	-	-	-	-
P 2p	-	-	-	-
Si 2p	-	-	0.2	-

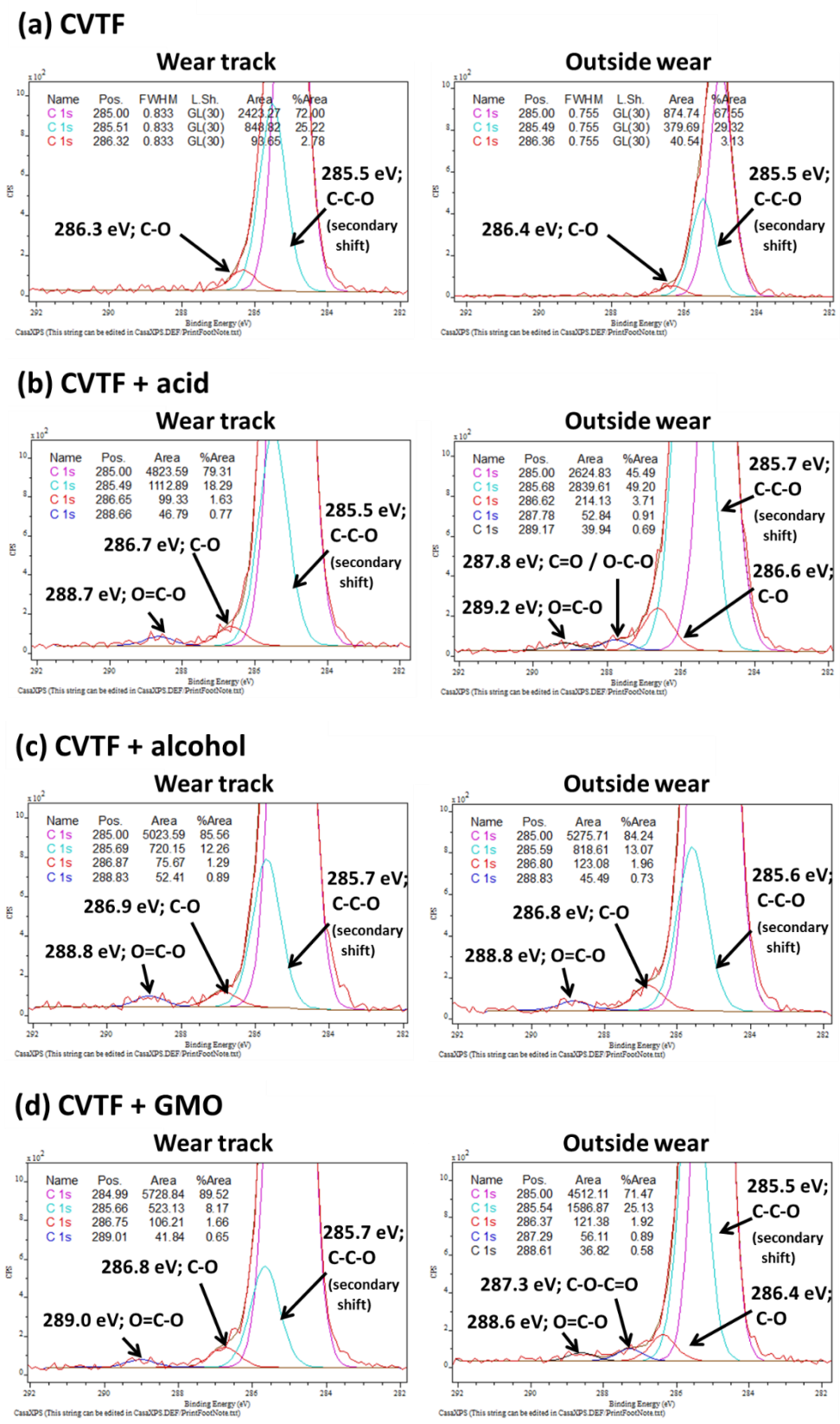

Fig. 5-33. XPS C 1s spectra for the post-test paper plates after testing the CVTF formulations (40 °C, 60 minutes)

a) CVTF, b) CVTF + oleic acid, c) CVTF + oleyl alcohol, d) CVTF + GMO

5.2.7. ATR-FTIR Analysis

ATR-FTIR analysis was carried out to assess the chemical bonds on the post-test paper surface. The results for the PAO formulations are shown in Fig. 5-34. Besides the spectra on the wear track, the difference spectra subtracted from the fresh paper spectrum are presented. The IR peaks derived from the carbonyl groups are compared in Fig. 5-35, and the peak identification for PAO+acid and PAO+GMO is shown in Fig. 5-36. The comments on the results are described as below;

- The overall trend of the spectra was very similar to the 100°C results (Fig. 5-15).
- All the spectra presented the peak increase attributed to hydrocarbons; ν (C-H) between 3,000 and 2,800 cm^{-1} and σ (C-H) between 1,350 and 1,500 cm^{-1}, which should occur due to the remaining oil inside the fibrous structure.
- The peak increase at around 1,050 cm^{-1} could be identified as ν (C-O) derived from the cellulose fibre or ν_a (Si-O) from the diatomite earth contained in the paper material. These results indicate the removal of the resin coating on the paper clutch surface.
- (b) PAO+acid and (d) PAO+GMO had a specific carbonyl peak attributed to the FMs.
- The peak intensity of PAO+GMO shown in Fig. 5-35 is smaller than that at 100°C (Fig. 5-16), while PAO+acid showed the comparable peak strength at both temperature conditions. It could support the assumption about the GMO deposition on the paper at 100°C as expected from the SEM image (Fig. 5-9(d)).
- The peak shown in the difference spectrum of (a) PAO+acid was shifted to the higher wave number at approx. 5 cm^{-1} from pure oleic acid, which is the same trend as the 100°C result (Fig. 5-16). In contrast, the peak position of (b) PAO+GMO was comparable to that of GMO.

The difference spectra for the CVTF formulations are summarised in Fig. 5-37 and Fig. 5-38. The major peaks detected in the difference spectra were derived from the paper material components and two carbonyl peaks at 1,730 and 1,700 cm^{-1} which could be attributed to the ester bond in the PMA and the imide bond in the dispersant. However, a peak which is able to explain the difference in the frictional properties was not observed. All the trends are comparable to those at 100°C.

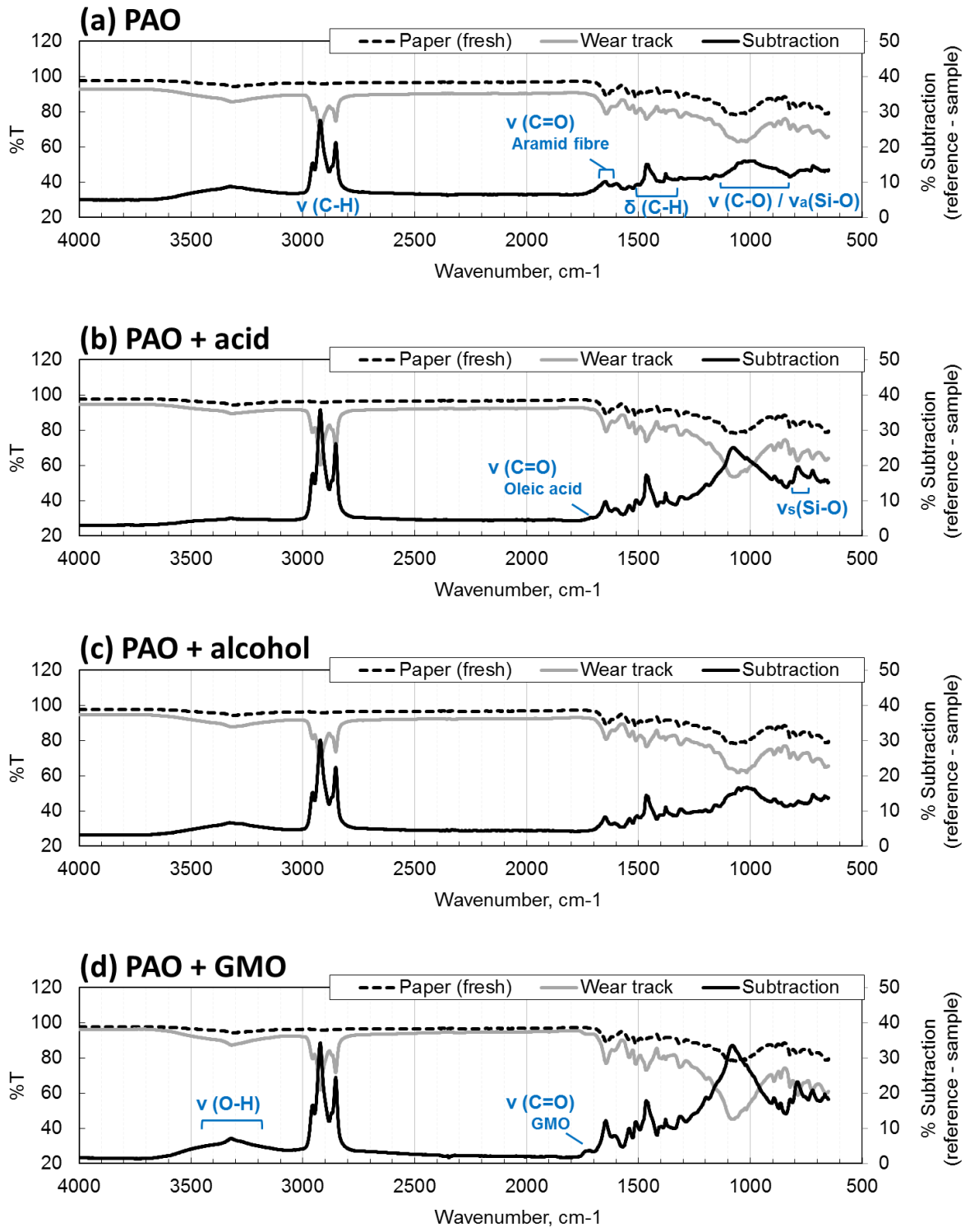

Fig. 5-34. ATR-FTIR spectra for the post-test paper plates after testing PAO formulations (40°C, 60 minutes)

a) PAO, b) PAO + oleic acid, c) PAO + oleyl alcohol, d) PAO + GMO

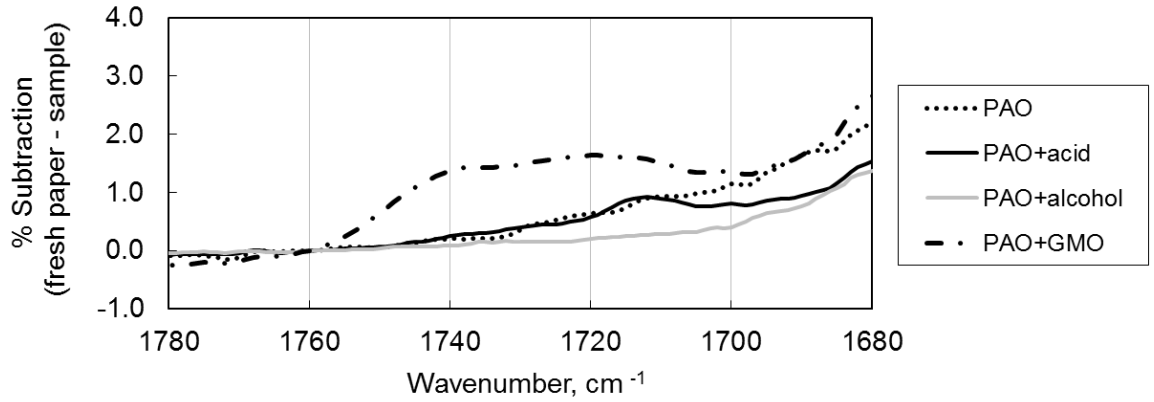

Fig. 5-35. ATR-FTIR difference spectra for the PAO formulations (C=O region)

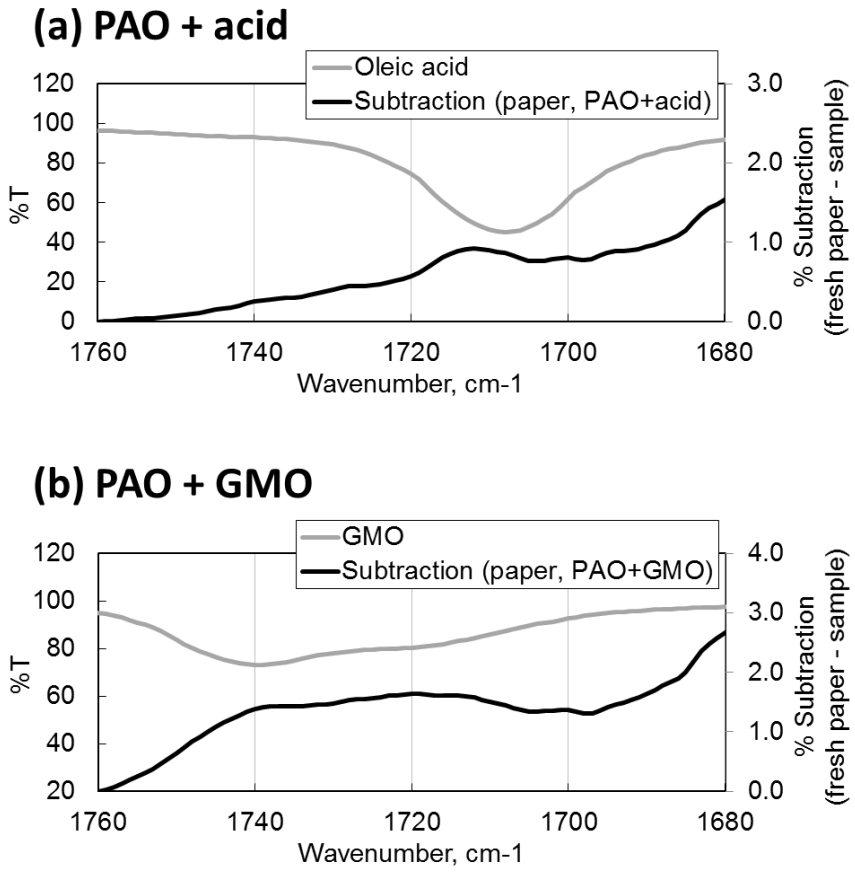

Fig. 5-36. Comparison of the IR spectra for the pure FMs and the post-test paper plates
a) PAO + oleic acid, b) PAO + GMO

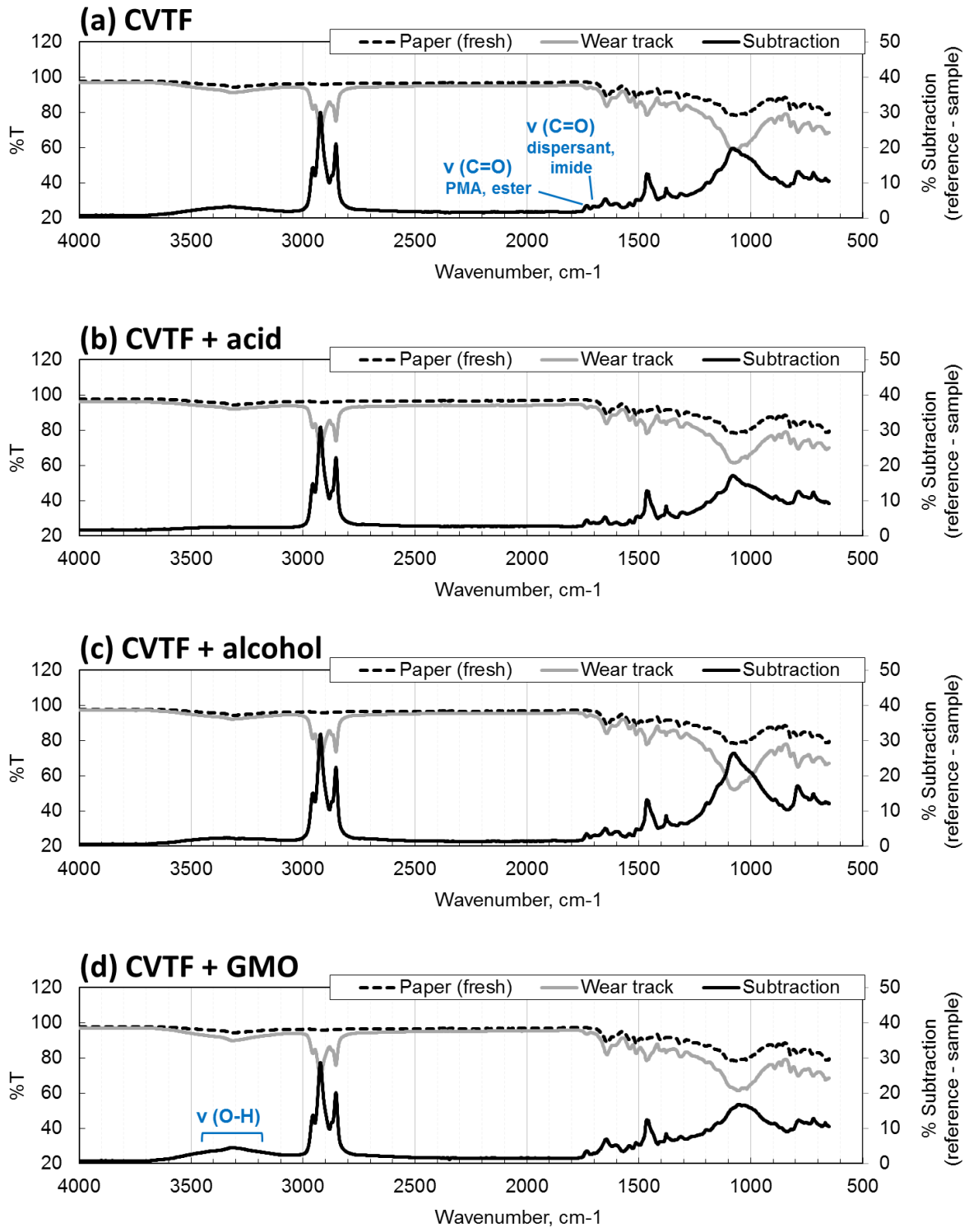

Fig. 5-37. ATR-FTIR spectra for the post-test paper plates after testing CVTF formulations (40 °C, 60 minutes)

a) CVTF, b) CVTF + oleic acid, c) CVTF + oleyl alcohol, d) CVTF + GMO

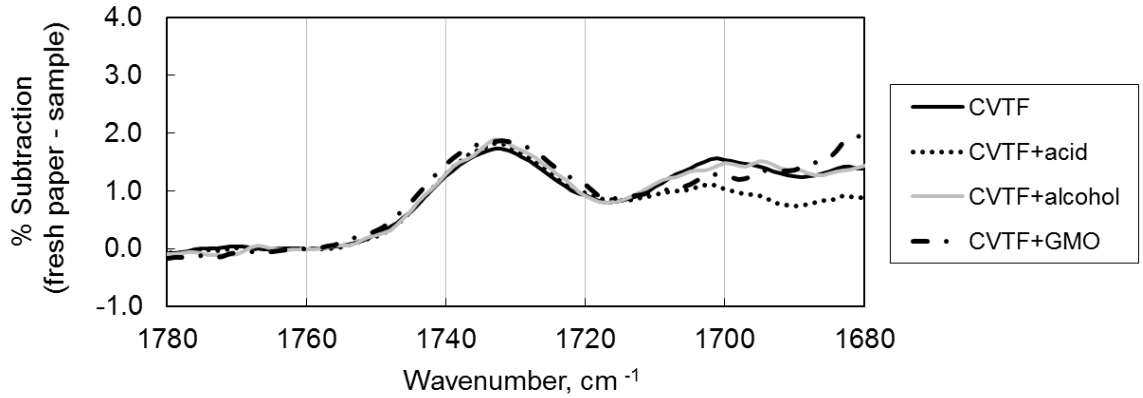

Fig. 5-38. ATR-FTIR difference spectra of the CVTF formulations (C=O region)

5.2.8. Summary of TE77 Paper Contact Tests at 40°C

The results for the TE77 paper/steel sliding test at 40°C are summarised in Table 5-6, and compared with the 100°C results shown Table 5-3.

Comparing the frictional properties of the PAO formulations, while oleyl alcohol showed the friction coefficient and FFWI that were comparable to the 100°C results, oleic acid increased the friction value, and GMO decreased both the friction and the FFWI without forming a deposit on the paper. This result means that the FM effect of oleic acid became weaker at 40°C in contrast to GMO which presented a stronger effect at 40°C. However, the XPS spectra did not show any specific difference to explain these FM effects. The reason should be that the interaction between the FMs and the paper was weaker at 40°C, so that the FM adsorption film on the surface was removed by solvent rinsing. It is considered that the strong interactions, such as chemical bond formation, would not be dominant 40°C. Considering the friction results, GMO was capable of forming the film without making a strong bond with the surface, while oleic acid preferred to interact with the surface making the chemical bonds.

Among the CVTF formulations, oleic acid decreased the performance showing the higher friction coefficient and FFWI than those at 100°C, while oleyl alcohol and GMO presented almost the same effects. The C 1s spectra did not show significant difference among the test oils, and the paper surface film consisting of Ca and P was not formed by CVTF+acid in contrast to the 100°C test. It also implies the dependence of oleic acid effect on the test temperature.

Table 5-6. Summary of the TE77 paper/steel contact at 40°C

	PAO formulations			
	w/o FM	oleic acid	oleyl alcohol	GMO
CoF	0.114	0.097	0.100	0.088
FFWI	1.45	1.05	1.24	1.08
Paper condition (SEM)	some deposites	good	good	good
Chemical nature				
Topmost surface (XPS)	C-O C=O / O-C-O	C-O C=O / O-C-O O=C-O	C-O C=O / O-C-O O=C-O	C-O C=O / O-C-O O=C-O
Surface including unrubbed sublayer (EDX and ATR-FTIR)	-	oleic acid (slight chemical sift)	-	GMO (no chemical shift)

	CVTF formulations			
	w/o FM	oleic acid	oleyl alcohol	GMO
CoF	0.121	0.107	0.109	0.097
FFWI	1.25	1.13	1.18	1.08
Paper condition (SEM)	good	good	good	good
Chemical nature				
Topmost surface (XPS)	C-O	C-O O=C-O	C-O O=C-O	C-O O=C-O
Surface including unrubbed sublayer (EDX and ATR-FTIR)	ester (PMA) imide (dispersant)	ester (PMA) imide (dispersant)	ester (PMA) imide (dispersant)	ester (PMA) imide (dispersant)

5.3. TE77 Durability Tests at 100°C

Automatic transmission fluids need to maintain the frictional property for a long duration, sometimes all through the car life of over 100,000 miles of driving. Durability of the clutch frictional performance is generally an issue because the FMs tend to be degraded by thermal load or interactions with the other chemicals.

Because some of the results presented in the previous sections in this chapter indicated the presence of chemical interactions between the FM and the other additives or the substrate, long-term TE77 tests were carried out to investigate the durability of the FM effect. The performance of the FMs was evaluated by CoF and FFWI, and the post-test lubricants and the paper plates were analysed to assume whether there is any link between the frictional properties and the surface chemistry.

Three test oils, PAO+GMO, CVTF+acid and CVTF+GMO, which showed the special trend in the frictional properties, were used for the durability test. PAO+GMO showed the low FFWI and the high friction coefficient at 100°C, while CVTF+GMO presented both the low values. The frictional performance of CVTF+acid was also excellent at 100°C forming the film consisting of Ca and P on the paper surface.

5.3.1. Frictional Properties

The test sequence of the TE77 durability test is shown in Fig. 5-39. The TE77 test duration for the results shown in Section 5.1 and 5.2 was 1 hour. The durability tests for 12 hours were carried out for the three test oils, and an additional 24 hours test was performed for CVTF+GMO to confirm an increasing trend of the FFWI shown at 12 hours. The frictional data were sampled every 1 hour, and the friction coefficient and the FFWI were evaluated. Except for the duration, all the other conditions were the same as the paper/steel contact test shown in the previous sections, and the test temperature was selected to be 100°C in order to observe the degradative phenomena.

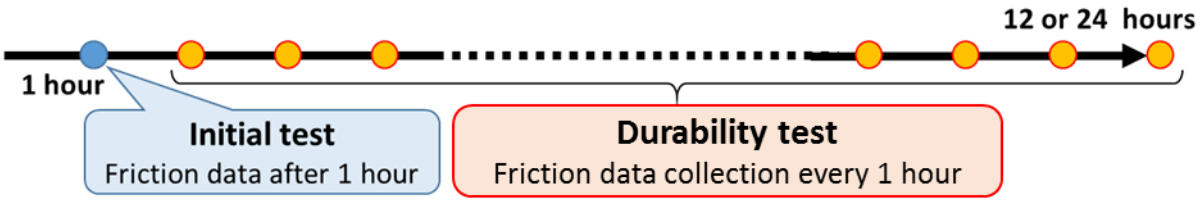

Fig. 5-39. TE77 initial and durability test sequences

The friction coefficient and FFWI values during the durability test are summarised in Fig. 5-40 and Fig. 5-41. The 12 hour tests were carried out twice for PAO+GMO, while both the 12 and the 24 hour tests for CVTF+acid as mentioned above. CVTF+GMO was tested once for 12 hours. The data plotted in Fig. 5-40 and Fig. 5-41 are the average values.

- PAO+GMO experienced a sharp decrease of CoF and FFWI between 60 and 240 minutes. After 240 minutes, the friction was kept relatively constant at around 0.07, while the FFWI continued to decrease to 1.0 at the end of the test. The CoF value was not normal considering the test conditions under the

boundary lubrication regime. It should therefore be considered that the paper plate was mechanically damaged or flattened.

- In contrast to PAO+GMO, CVTF+GMO kept the stable CoF at around 0.09 through the 12 hour test. The FFWI was gradually improved from around 1.1 to 1.0.
- The CoF of CVTF+acid was gradually decreased until 300 minutes from 0.095 to 0.090, then started to increase to 0.094 at the end of 24 hour test. The FFWI value also followed the trend, reached the minimum value at 0.95 after 240 minutes, then increased up to 1.06. It implies that oleic acid lost the effect gradually as the running time increased.

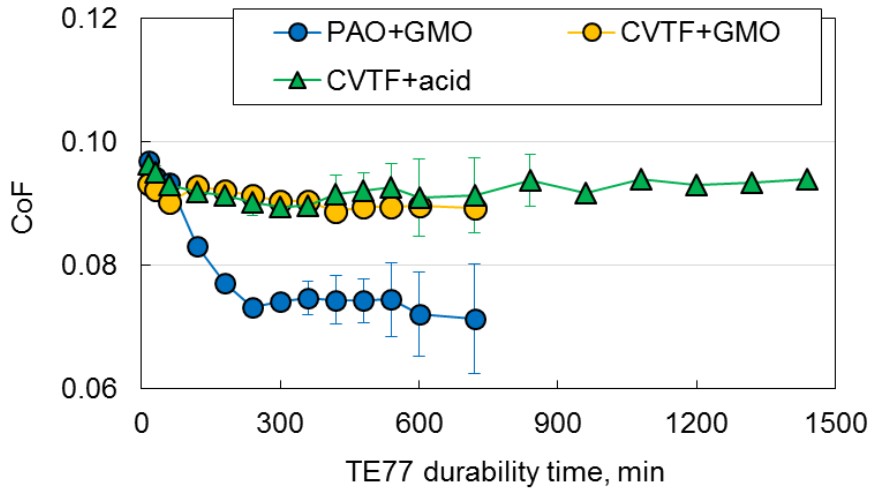

Fig. 5-40. Friction coefficient during the TE77 durability test at paper/steel contact at 100°C

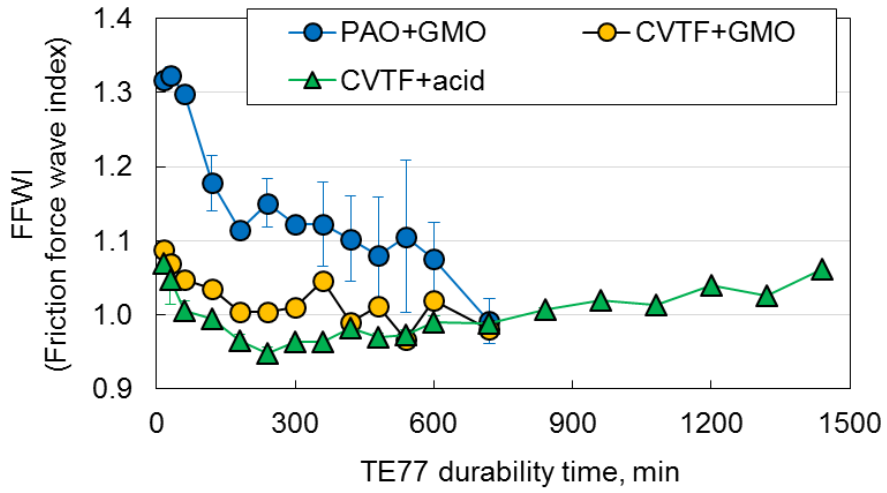

Fig. 5-41. FFWI during the TE77 durability test at paper/steel contact at 100°C

5.3.2. Wear Track Observation by SEM

The surface of the post-test paper samples were observed by SEM. The images are shown in Fig. 5-42.

The surface of (a) PAO+GMO appeared to be flat and covered by some organic deposit that should be GMO. The flattened surface was also observed in the 60 minutes test (Fig. 5-9), however, it appeared to be much obvious after the durability test. The surface appearance looks to be covered by a thick film clogging the pore structure, indicating the accumulation of GMO through the durability test. The flat surface is potentially the reason for the sharp drop of the CoF and the FFWI, which increased the contact area and decreased the actual contact pressure. In contrast, (b) CVTF+acid and (c) CVTF+GMO kept the morphology of the fresh paper material showing the tangled fibres and the pore structures. Therefore, the change in the friction properties should be attributed to the surface chemical nature.

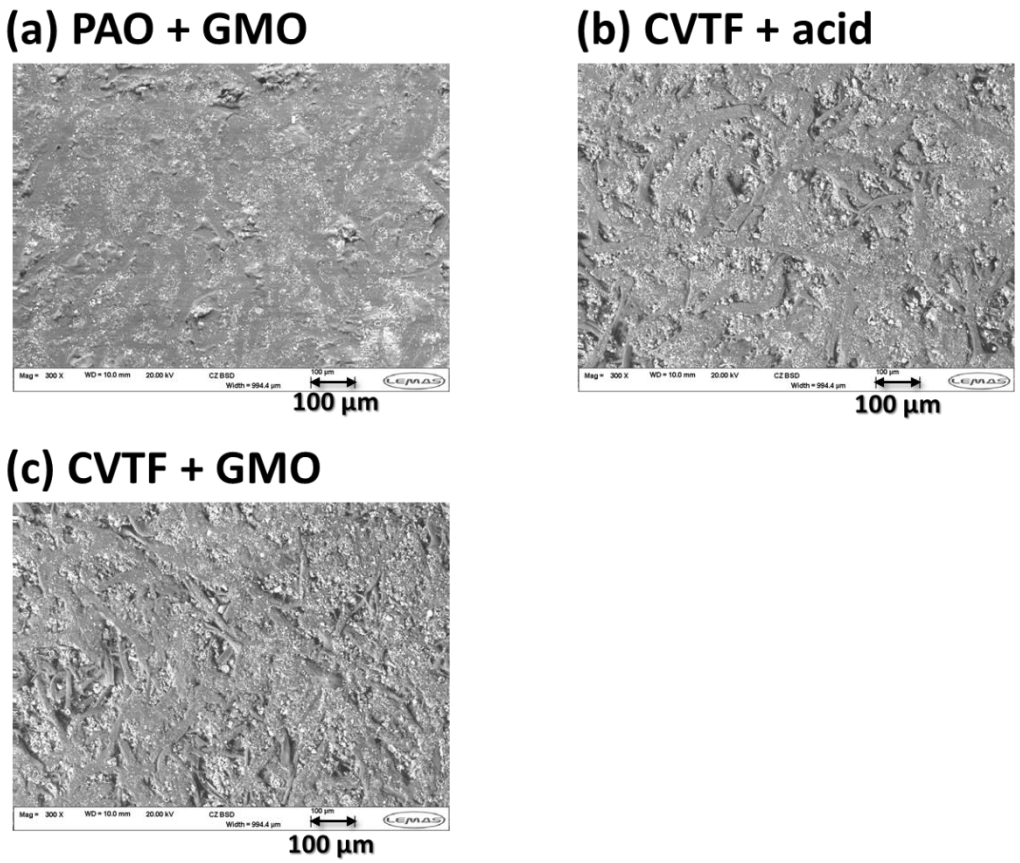

Fig. 5-42. SEM images of the post-test paper plates after the 100°C durability test
a) PAO + GMO (12 hrs), b) CVTF + oleic acid (24 hrs), c) CVTF + GMO (12hrs)

5.3.3. EDX Analysis

The post-test paper plates after the durability test were analysed by EDX to evaluate the elemental concentration on the paper surface.

The result for PAO+GMO after the 12 hours durability test is shown in Fig. 5-43 together with the 60 minute initial test result presented in Fig. 5-11. The oxygen concentration showed an increase at around 8 wt% from the initial value, which supports the assumption that a deposit derived from GMO covered the paper surface during the long-term sliding.

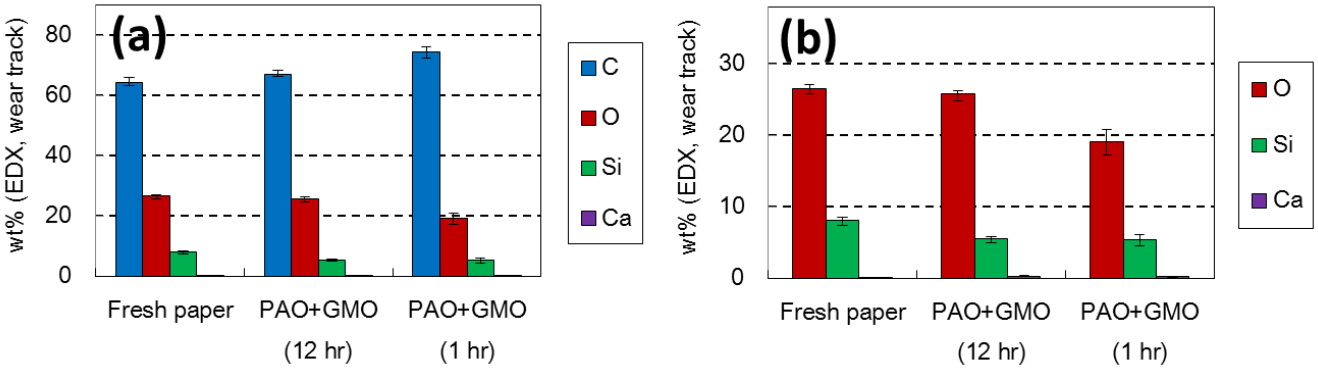

Fig. 5-43. EDX elemental analysis for the post-test paper plates after the durability test of PAO+GMO at 100°C, a) all elements, b) except for C

The results for the CVTF formulations are summarised in Fig. 5-44. Similar to the PAO+GMO result, the oxygen concentration was increased at around 6 wt% from the initial value for both CVTF+acid and CVTF+GMO, although the SEM image did not show any change in the surface topography after the durability test. Interestingly, the concentration of Ca and P did also increase significantly during the durability. For example, CVTF+acid showed the increase for Ca from 0.08 to 0.45 wt%, and for P from 0.04 to 0.44 wt%. This result indicates that the phosphorous anti-wear agent and the calcium detergent were accumulated on the paper surface through the durability test probably due to the thermal or oxidative degradation of these additives. In order to discuss their chemical nature, the results were compared to the elemental analysis results acquired by XPS which show the information on the uppermost paper surface.

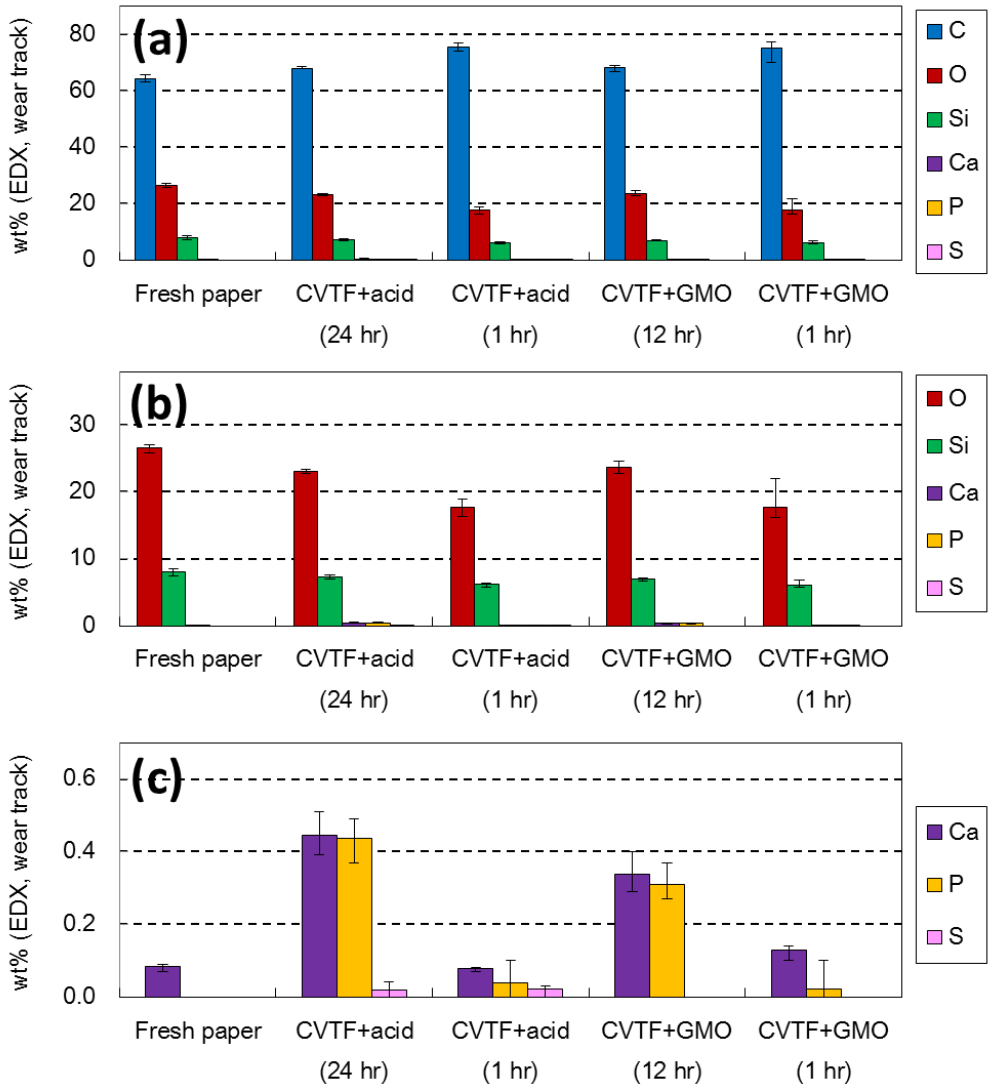

Fig. 5-44. EDX elemental analysis, the post-test paper plates after the durability test for CVTF+acid and CVTF+GMO at 100°C

a) all elements, b) except for C, c) Ca, P and S attributed to the CVTF additives

5.3.4. XPS Analysis

The post-test paper surfaces were analysed by XPS. The elemental fractions obtained from the XPS survey spectra are shown in Table 5-7 with the results for the 60 minute initial tests as a reference.

CVTF+acid presented a significantly different trend from the initial test. Ca and P detected on the paper in the initial test disappeared completely after the 24 hours of the durability. In addition, the concentration for O also sharply decreased to 1.0 wt%. This

result implies that the surface film initially formed by oleic acid and the additives was removed during the long-term sliding at high temperature, which shows good agreement with the increase of the FFWI in the latter half of the test (Fig. 5-41). On the other hand, the two GMO oils did not show any significant difference from the initial results despite the decrease in the FFWI.

Table 5-7. XPS survey spectra on the paper plates after the durability test at 100°C

Element, % mass	Durability test			Initial test (reference)		
	PAO + GMO (12 hrs)	CVTF + acid (24 hrs)	CVTF + GMO (12 hrs)	PAO+ GMO	CVTF + acid	CVTF + GMO
C 1s	97.6	99.0	98.5	97.3	80.1	97.4
O 1s	2.4	1.0	1.4	2.5	12.5	1.9
N 1s	-	-	-	-	-	-
Ca 2p	-	-	-	-	2.4	-
P 2p	-	-	-	-	5.0	-
Si 2p	-	-	0.1	0.2	-	0.7

The XPS C 1s spectra are shown in Fig. 5-45. The spectra are compared with the results for the initial tests (Fig. 5-13 and Fig. 5-14) as shown below;

- (a) PAO+GMO had the peaks derived from oxygen compounds (O=C-O / COOH at 289.3 eV and C=O / O-C-O at 279.9 eV) on the wear track. They were weak or negligible outside the track, so that it is considered that they were formed by the sliding. The peak positions were comparable to those for the initial test, though, the peak intensity (%Area) was improved after the durability, especially for the carboxylate bond.
- The spectrum of (b) CVTF+acid changed from the initial spectra showing a significant peak decrease at 286.9 eV (C-OH / C-O-C=O) as expected from the XPS survey results. Considering the increase in the CoF and FFWI in the latter half of the durability test, the oxygen compositions seemed to play an important role for improving the frictional performance.
- The C 1s spectrum of (c) CVTF+GMO was quite similar to that of the initial test, showing the similar peak intensities as well as the peak positions. Because the initial CoF and FFWI of CVTF+GMO were already close to those after the durability, the surface chemical nature did not show any significant difference.

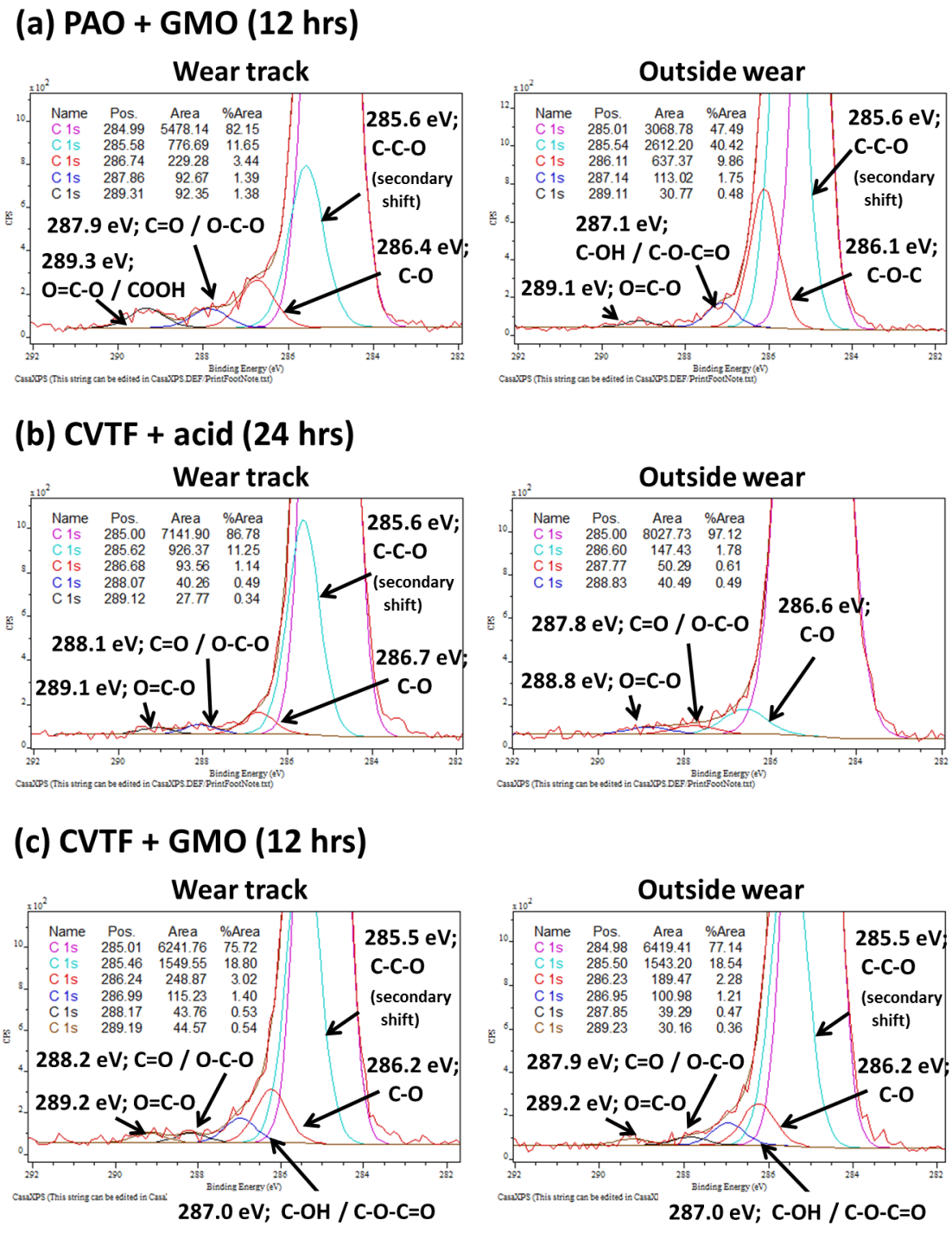

Fig. 5-45. XPS C 1s spectra for the paper plates after the durability test at 100°C (left; inside wear track, right; outside wear)

a) PAO + GMO (12 hrs), b) CVTF + oleic acid (24 hrs), c) CVTF + GMO (12hrs)

5.3.5. ATR-FTIR Analysis for the Paper Plates

The post-test paper surface after 12 hours of durability test with PAO+GMO was analysed using ATR-FTIR. The IR spectrum and the difference spectrum subtracted from the fresh TE77 paper are summarised in Fig. 5-46. In addition, the comparison with the initial test difference spectrum is shown in Fig. 5-47.

The peak intensity at around 1,730 cm^{-1} attributed to the C=O bond in GMO increased clearly after the durability test, and the peak strength seen in the subtraction was around 10 times higher than that for the initial plate. For the detailed identification of the peak, it was compared with the pure GMO spectrum as shown in Fig. 5-48. The spectrum shape as well as the peak positon was exactly the same as the pure GMO, indicating that the GMO was just accumulated on the paper without changing into the other chemical composition. This result met the previous assumption about the working mechanism of GMO in PAO.

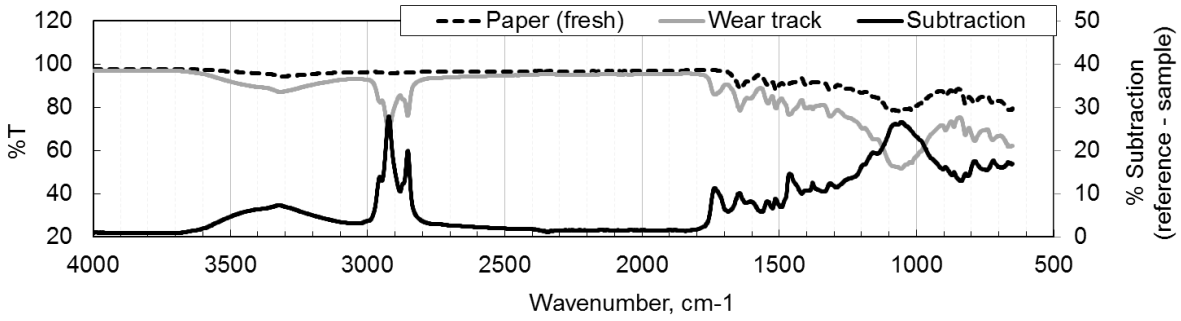

Fig. 5-46. ATR-FTIR analysis on the paper plate after the durability test for PAO+GMO

(IR spectrum on the wear track and difference spectrum subtracted from the fresh paper)

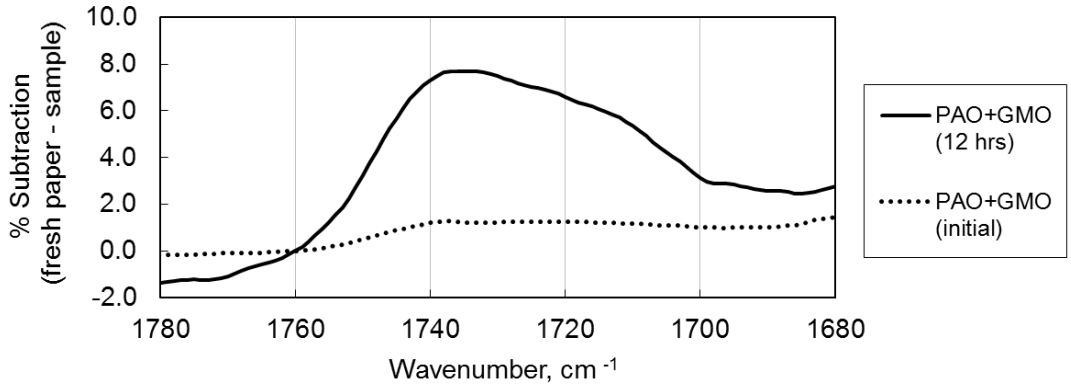

Fig. 5-47. Comparison of the ATR-FTIR spectra on the post-test paper plate after the initial and the durability test of PAO+GMO

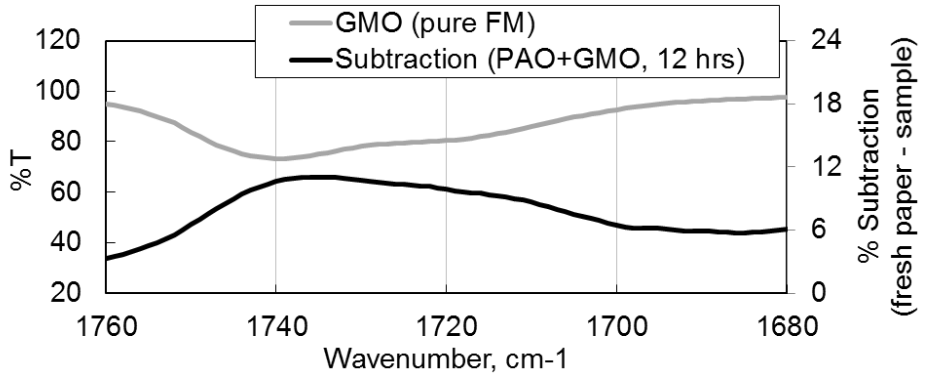

Fig. 5-48. Peak identification of PAO+GMO post-test paper plate after durability test

5.3.6. ATR-FTIR Analysis for the Lubricants

The post-test oils after the durability test were also investigated by ATR-FTIR in order to examine the extent of the additive degradation; the information should be useful to understand the behaviour of the FMs during the long-term sliding test. The spectra of the used oils were subtracted from each of the fresh oil spectra as shown in Fig. 5-49. The positive peak means that the chemical bond was produced during the durability test, while the negative means that the bond disappeared.

(a) PAO+GMO showed an almost flat difference spectra with a slight decrease of alcohol at around 1,050 cm^{-1} probably derived from GMO. On the other hand, (c) CVTF+GMO had stronger alcohol peak intensity, and the peak between 1,200 and 1,150 cm^{-1} attributed to ester was also detected. It implies that the structure of GMO did not change significantly when formulated in PAO, while the ester structure was modified in the presence of the CVTF additives. The modification of the ester bond, probably the decomposition, should be the reason for the good frictional performances of CVTF+GMO.

(b) CVTF+acid presented the increase of ester bond at 1,150 cm^{-1} and carboxylic acid bond at 1,710 cm^{-1}. Considering that CVTF+acid gradually decreased the FM effect, the ester should be identified as the degraded oleic acid, while the acid as the oxidative degradation products. Because the phosphorous (C-O-P) peak at 970 cm^{-1} was weakened, the P anti-wear agent was considered to have an influence on this degradation process.

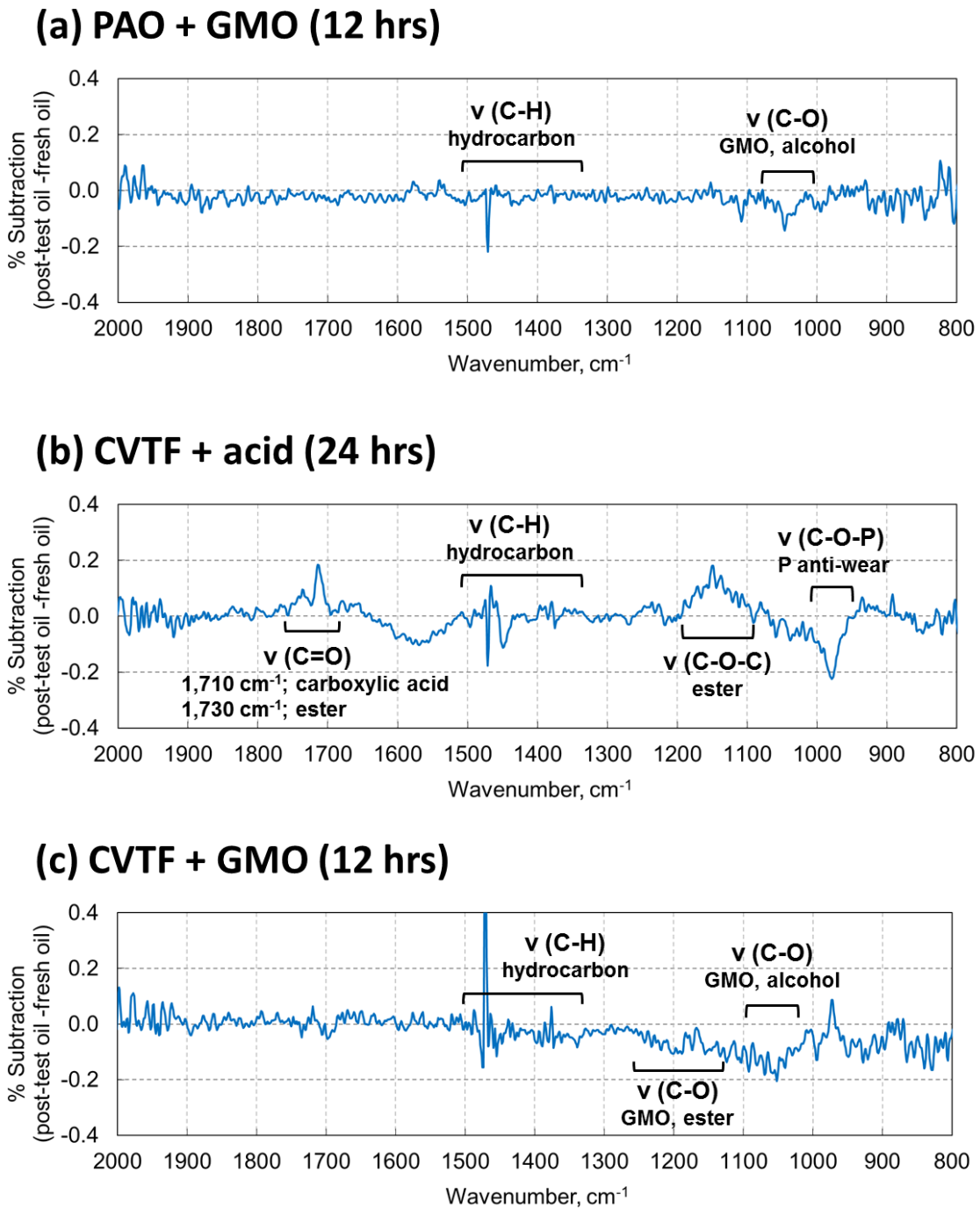

Fig. 5-49. ATR-FTIR difference spectra of the post-test oils subtracted from the fresh oils, a) PAO+GMO (after 12 hr durability),
b) CVTF + oleic acid (after 24 hr durability), c) CVTF + GMO (after 12 hr durability)

5.3.7. Summary of TE77 Paper Durability Tests at 100°C

A brief summary of this section is shown in Table 5-8. The durability tests were carried out in order to observe the changes in the frictional properties and the chemistry for the paper clutch surface and the test oils during the long-term sliding.

PAO+GMO experienced the significant decrease in both the CoF and the FFWI. The paper plate surface was thickly covered by a deposit which was estimated to be GMO. Taking into account that the XPS C1s spectra on the paper did not change from the initial test result, the smooth surface formed by the accumulation of GMO played a main role on the improvement of the frictional performance.

CVTF+GMO showed a slight decrease of the FFWI, although the XPS C 1s spectrum did not change significantly from the initial result. The difference from the PAO+GMO result was the decomposition of the ester bond that was detected by the ATR-FTIR analysis for the post-test lubricants. The interaction between GMO and the additives prevented GMO accumulating on the surface, and seemed to decompose GMO at the ester bond turning into the other chemical structure effective as FM.

Finally, CVTF+acid presented the increase of the CoF and the FFWI after the durability test in contrast to the GMO formulations. Because the XPS analysis showed the significant decrease of the O, Ca and P on the post-test paper surface from the initial results, it is considered that the long-term sliding removed or degraded these surface films, resulting in the degraded frictional performance. The ATR-FTIR difference spectrum of the post-test oil detected the increase of ester bond, which was assumed to be the degradation product of oleic acid. As a decrease of the IR peak derived from P-O-C bond was also observed, it was assumed that the phosphorous anti-wear agent had an influence on this mechanism.

The results will be compared with the MTM results shown in the next chapter. The MTM measurement is useful to evaluate the clutch frictional performance, however, the post-test specimens were difficult to be analysed due to the size issue. The TE77 paper/steel contact tests had an important role to bridge these two tribotests.

Table 5-8. Summary of TE77 durability test under paper/steel contact at 100°C

	Durability test		
	PAO + GMO (12 hrs)	CVTF + acid (24 hrs)	CVTF + GMO (12 hrs)
CoF	0.710	0.094	0.089
FFWI	0.99	1.06	0.98
Paper condition (SEM)	severe deposites	good	good
Chemical nature			
Topmost surface (XPS)	C-O C=O / O-C-O O=C-O	**C-O** **C=O / O-C-O** **(much weaker than initial)** O=C-O	C-O C=O / O-C-O O=C-O
Surface including unrubbed sublayer (EDX and ATR-FTIR)	**GMO** **(Significant increase from initial test)**	Increase of P and Ca	Increase of P and Ca
Lubricant (IR)	Decreased; - Alcohol (GMO)	Increased; - **Ester (degraded oleic acid)** - Carboxylic acid (degradation product) Deceased; - C-O-P (P anti-wear agent)	Decreased; - Alcohol (GMO) **- Ester (GMO)**

	Initial test (reference)		
	PAO + GMO	CVTF + acid	CVTF + GMO
CoF	0.094	0.088	0.090
FFWI	1.30	1.00	1.05
Paper condition (SEM)	some deposites	good	good
Chemical nature			
Topmost surface (XPS)	C-O C=O / O-C-O O=C-O	C-O C-O-C=O C=O / O-C-O O=C-O	C-O C-O-C=O / N-C-O O=C-O / COOH
Surface including unrubbed sublayer (EDX and ATR-FTIR)	GMO (no chemical shift)	ester (PMA) imide (dispersant)	ester (PMA) imide (dispersant)

Chapter 6 – Results – MTM Paper Clutch Tests

Smoothness of the lock-up clutch engagement is generally evaluated by the use of μ-V characteristics, a relationship between the sliding speed and the friction coefficient. Since it is necessary to measure the friction coefficient at various speed conditions for the evaluation of the μ-V characteristics, the TE77 reciprocating tester is not suitable for collecting the friction data as a function of the sliding speed.

In order to deal with the issue, MTM (Mini Traction Machine) tests were carried out using a combination of a standard steel ball and a special paper coated disc as the test specimens. As the paper material, JASO M349 clutch which is the same material as the TE77 paper plate was applied. The pure sliding condition was applied to simulate the actual clutch engagement, and the μ-V performance was evaluated. Firstly, the initial performance and the effect of the FMs and test temperature are discussed in "6.1. MTM Initial Performance", and then the long-term effect of the FMs is shown in "6.2. MTM Durability Performance".

6.1. MTM Initial Performance

Initial μ-V characteristics were measured at 3.0 N load (P_{max}; 4.8 MPa) between 0.01 and 2.4 m/s, which are in the standard range of conditions for the lock-up clutch sliding control. At each of the sliding speed conditions, the friction data were collected for 3 minutes under pure sliding configuration at constant speed, and the data during the last 1 minute were averaged to obtain the friction at each sliding speed. Furthermore, the measurement started from the lowest speed (0.01 m/s) to the highest (2.4 m/s), then went back to the lowest speed again. It means that the friction was evaluated twice at each sliding speed. These two data were averaged, and finally adopted as the result shown in the μ-V characteristics graph. No hysteresis between the increasing and the decreasing speed conditions was observed except for the GMO formulations in a specific durability condition as discussed later.

The tests were performed at both 100°C and 40°C to consider the effect of temperature. Additionally, before starting the measurement, 30 minutes of the running-in process at 3.5 MPa, 1.0 m/s and 100°C/40°C (depending on the test temperature) was carried out.

6.1.1. Frictional Properties

The μ-V characteristics at 100°C measured by MTM are summarised in Fig. 6-1 for the PAO formulations and in Fig. 6-2 for the CVTF formulations. Each of the results shows two graphs consisting of (a) showing full sliding speed range between 0.01 and 2.4 m/s and (b) an enlarged view in the speed range below 1.0 m/s. Looking at the Fig. 6-1(a) and Fig. 6-2(a), the μ-V slope tended to reach to a plateau over 1.0 m/s, so that the μ-V property is able to be compared in detail with the graphs focusing on the low sliding speed region. Hence, only the graphs in the speed range below 1.0 m/s are shown for the later results.

In terms of the PAO formulations, only the PAO+acid presented a positive slope, while the others had negative slopes. PAO without the FM showed obviously the worst shape with CoF more than 0.2 below 0.04 m/s. The curve of PAO+alcohol and PAO+GMO was still negative; however, the friction at low speed region was reduced by the effect of the FMs.

The CVTF without the FM also had a negative slope, though, much better than PAO. This is probably due to the effect of the CVTF additives with polar groups, such as the dispersant. The slope of the CVTF+alcohol was similar to the CVTF, indicating that oleyl alcohol was not able to work well on the paper in the presence of the other additives as expected from the TE77 results. On the other hand, CVTF+acid and CVTF+GMO presented positive μ-V characteristics. It is notable that GMO changed the effect in the presence of the additives, while oleic acid worked consistently in both PAO and the CVTF base fluid. It could be assumed that the CVTF additives assisted GMO in improving the μ-V property.

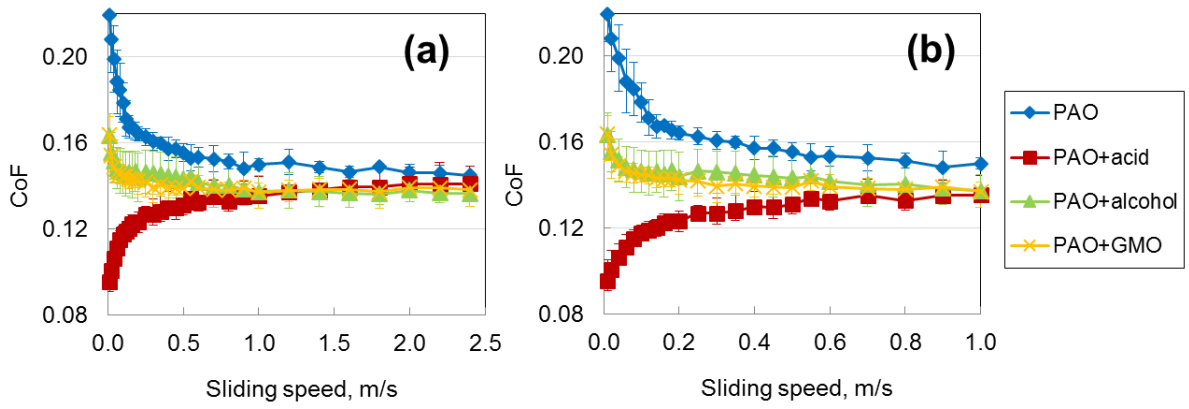

Fig. 6-1. μ-V characteristics of the PAO formulations at 100°C measured by MTM
a) full sliding speed range (~2.5 m/s), b) enlarged view below 1.0 m/s

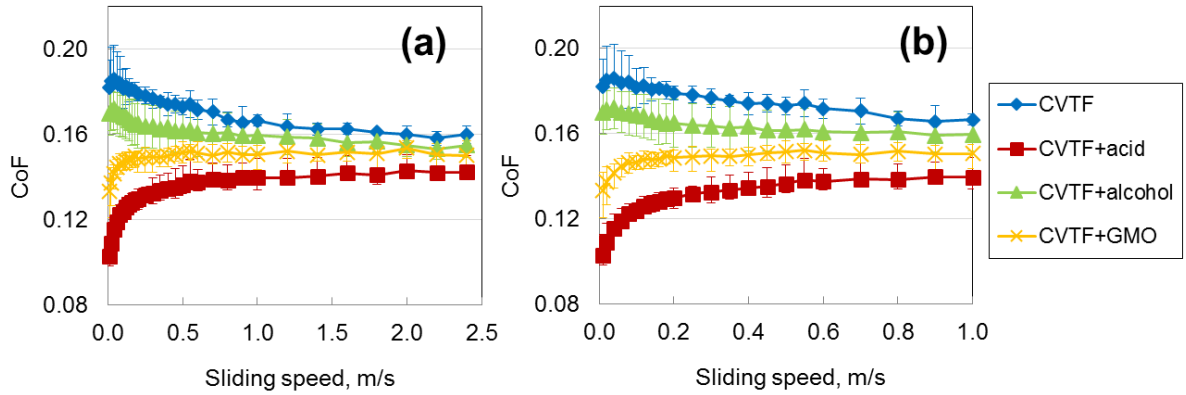

Fig. 6-2. μ-V characteristics of the CVTF formulations at 100°C measured by MTM
a) full sliding speed range (~2.5 m/s), b) enlarged view below 1.0 m/s

For the quantitative comparison of the μ-V characteristics, a factor "μ ratio" was introduced as explained in Chapter 3. It was calculated as a division of μ at 0.01 m/s by μ at 0.50 m/s, so that the lower the μ ratio, the better the μ-V characteristics with a positive slope. The μ ratio at 100°C is shown in Fig. 6-3.

Although the overall trend is the same as discussed with the μ-V graphs, the μ ratio values clearly show that only GMO indicated the dependence on the base fluid formulation, while the effect of oleic acid and oleyl alcohol was consistent with both PAO and the CVTF base fluids.

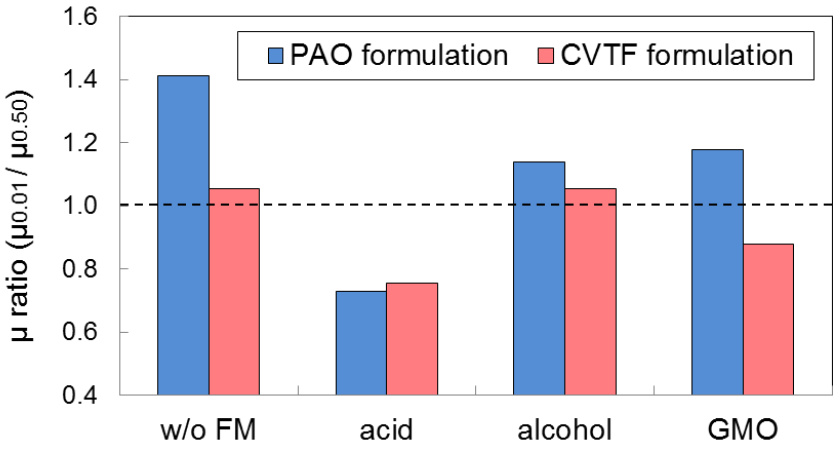

Fig. 6-3. μ ratio (μ at 0.01 m/s divided by μ at 0.50 m/s)
calculated from MTM results at 100°C

The MTM pure sliding test was also carried out at 40°C. The μ-V characteristics are summarized in Fig. 6-4, and the μ ratio in Fig. 6-5.

PAO and the CVTF base fluid without the FM showed an obviously negative curve comparable to the 100°C results. Oleic acid kept a positive slope even at 40°C in both formulations, though the μ ratio slightly increased from those at 100°C. Oleyl alcohol also presented a similar trend to the 100°C results, showing some friction modification effect with PAO while a negative slope with the CVTF additives. Interestingly, GMO indicated a good positive μ-V property in both base fluids in contrast to the 100°C results. It implies that the working mechanism of GMO was different between 100°C and 40°C.

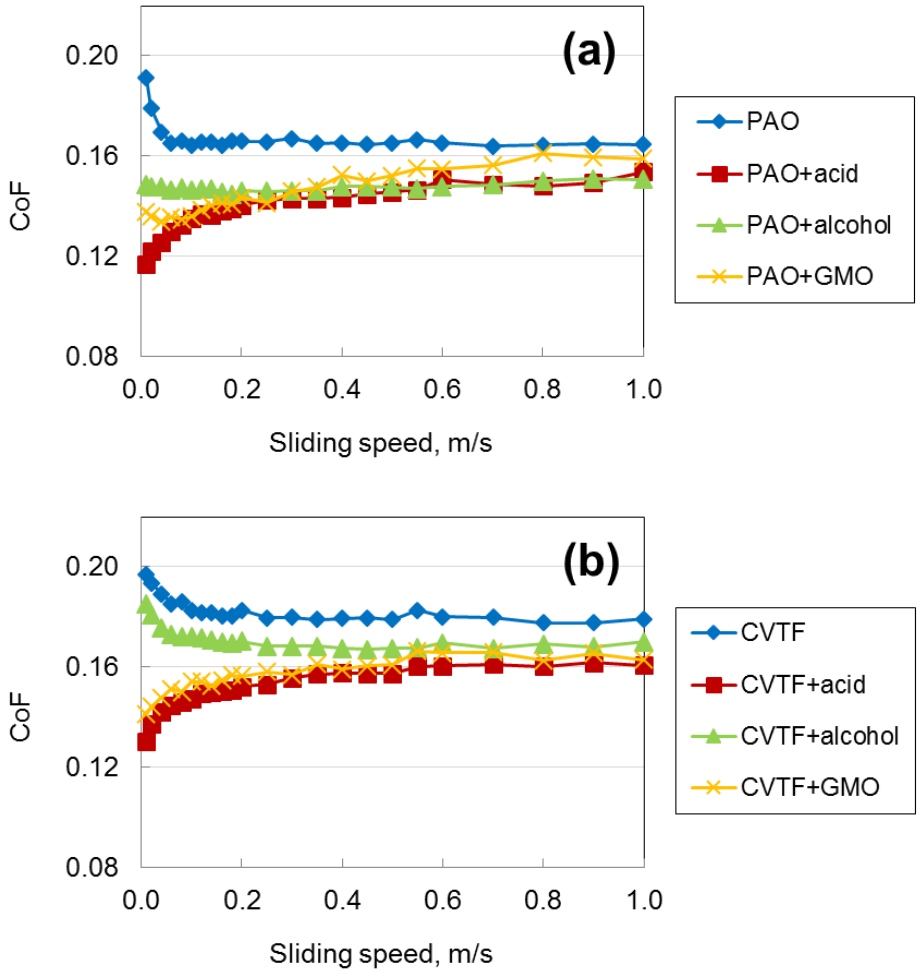

Fig. 6-4. μ-V characteristics at 40°C measured by MTM for (a) the PAO formulations and (b) the CVTF formulations

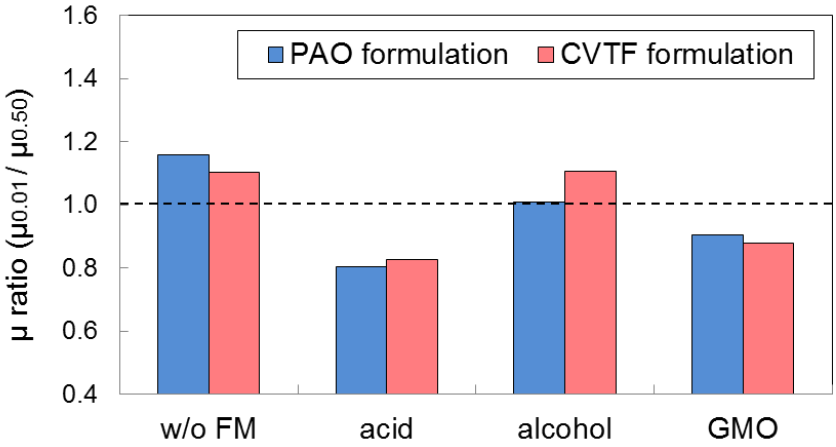

Fig. 6-5. μ ratio (μ at 0.01 m/s divided by μ at 0.50 m/s) calculated from MTM results at 40°C

6.1.2 ATR-FTIR Analysis for the MTM Paper Plates

The post-test MTM paper plates after the initial μ-V measurement at 100°C were analysed using ATR-FTIR for the purpose of comparing the chemical nature between the MTM and TE77 paper surface. Since it was difficult to process the MTM post-test paper for the high-vacuum analysis (such as SEM/EDX or XPS) due to the disc size, ATR-FTIR was a good tool to confirm if the FMs would work on the MTM paper in the same way as on the TE77 paper.

ATR-FTIR difference spectra of the post-test papers after testing the PAO formulations are shown in Fig. 6-6. The difference spectra were obtained by subtraction of the fresh MTM paper plate spectrum from the acquired spectrum on the post-test paper wear track. The range of the wave number focuses at the carbonyl group adsorption between 1,780 and 1,680 cm^{-1} because the specific peaks attributed to the FMs were not observed in the other region comparable to the TE77 post-test paper analysis. Looking at the spectra, while PAO and PAO+alcohol did not present any peaks, PAO+acid and PAO+GMO showed a carbonyl peak probably derived from the each of the FM.

In order to identify the peak observed in the spectra of PAO+acid and PAO+GMO, each spectrum was compared with that of the corresponding FM as shown in Fig. 6-7 and Fig. 6-8. The peak position of PAO+acid was similar to the carbonyl bond of oleic acid, however, shifted slightly to higher wavenumber from 1,708 to 1,715 cm^{-1}. The reason

should be the same as the TE77 post-test paper sample analysis result; the dimer oleic acid structure in the bulk FM fluid was changed into the adsorption film on the paper surface. On the other hand, the spectrum shape of the PAO+GMO was almost the same as pure GMO, which indicates that GMO formed the adsorption film without making any chemical connection against the paper surface. These ATR-FTIR results observed for the PAO formulations have good agreement with the TE77 results as expected.

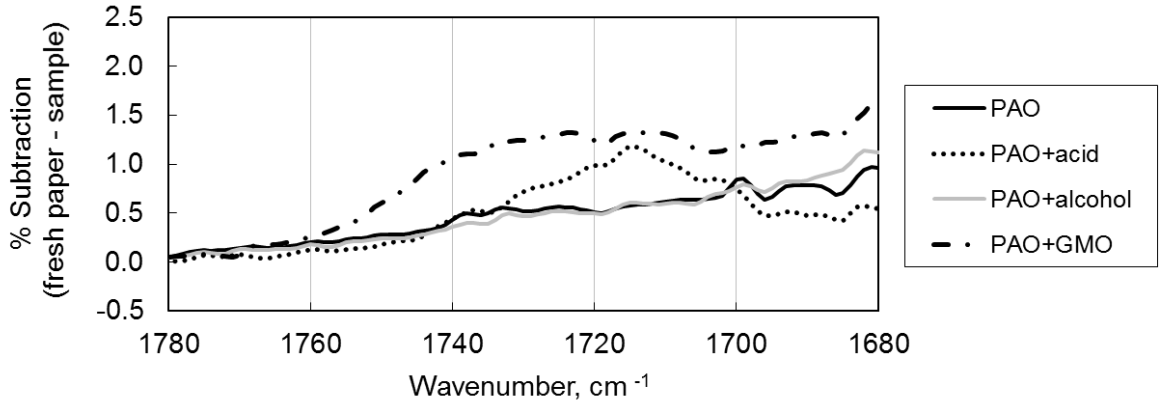

Fig. 6-6. ATR-FTIR difference spectra of the post-test MTM paper plates after the 100°C initial measurement (PAO formulations)

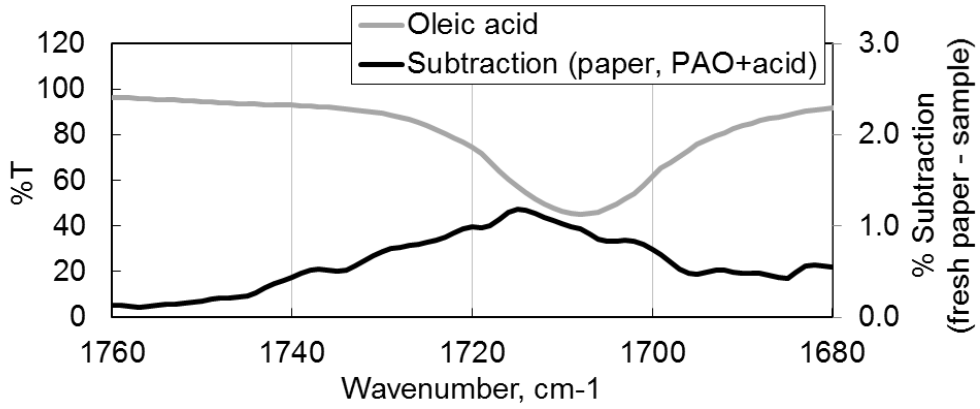

Fig. 6-7. ATR-FTIR spectra comparison between the PAO+acid post-test plate and pure oleic acid

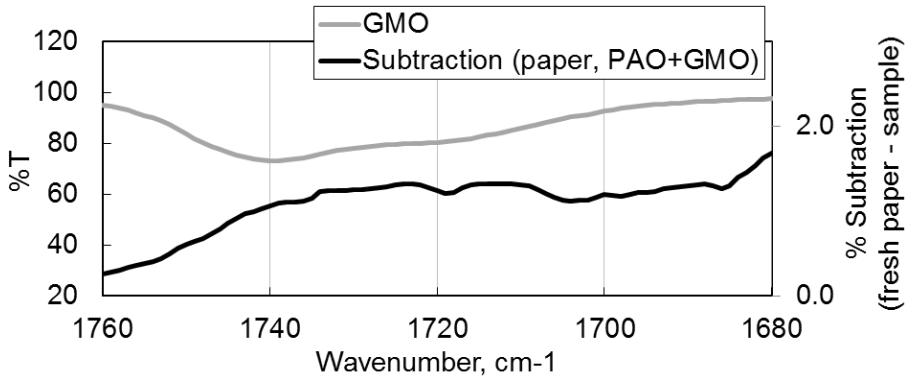

Fig. 6-8. ATR-FTIR spectra comparison between the PAO+GMO post-test plate and pure GMO

The difference spectra for the CVTF formulations are summarised in Fig. 6-9. All the spectra showed two peaks; a strong and wide peak at around 1,730 cm^{-1} derived from the ester bond in PMA and a weak peak at around 1,705 cm^{-1} from the imide bond of the dispersant. CVTF+acid appeared to have an additional very weak peak at 1,712 cm^{-1} derived from carboxylic acid.

The obscure IR peaks of oleic acid or GMO in the presence of the CVTF additives are also comparable to the TE77 results. It indicates the competitive effect between the FM and the additives, and also implies that the chemical nature on the paper was similar between the TE77 and the MTM friction test in spite of the different sliding configuration.

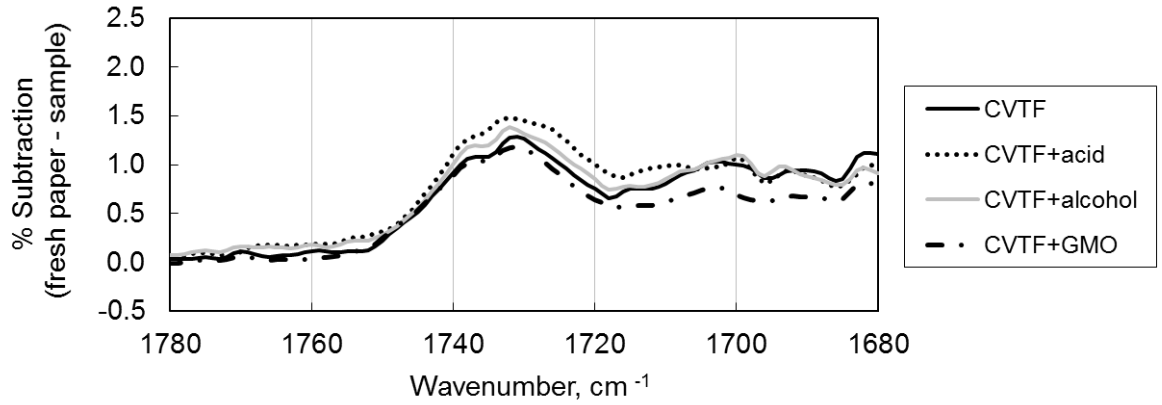

Fig. 6-9. ATR-FTIR difference spectra of the post-test MTM paper plates after the 100°C initial measurement (CVTF formulations)

6.2. MTM Durability Performance

The transmission fluids are required to maintain their performance for a long time as mentioned in the previous chapter. In this subchapter, the long-term test is performed using MTM to evaluate the durability of the FMs and the paper clutch.

The test sequences are summarised in Fig. 6-10. A standard sequence is performed at the constant temperature at 100°C or 40°C. Following the running-in and the initial μ-V measurement, the durability step was carried out. The condition is the same as the running-in (3.5 MPa, 1.0 m/s and 100°C/40°C), and the lubricant and the paper were aged through the step. Then, the μ-V performance was measured again, and the durability step and the μ-V measurement were repeated. The duration of the durability step was 2 or 4 hours, and the μ-V performance was evaluated at 2, 4, 8, 12 and 16 hours. On the other hand, in the combined sequence, while the running-in and the durability step were controlled at 100°C, the μ-V property was investigated at both 100°C and 40°C in order to observe an effect of the degradation at high temperature on the frictional properties at low temperature. The durability test is useful for assessing the working mechanism of the FMs as well as for evaluating their long-term effects.

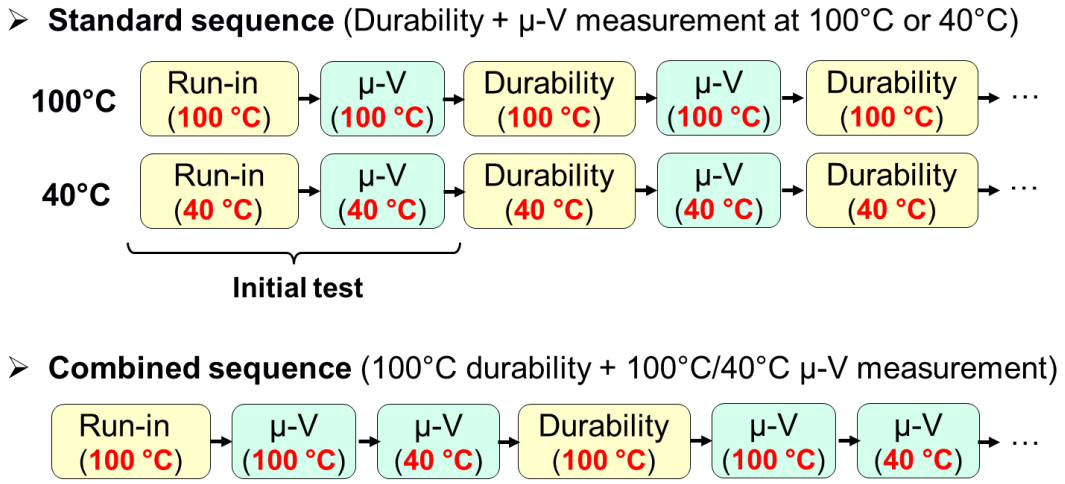

Fig. 6-10. Sequences for the MTM paper clutch durability test

6.2.1. Friction Performance at the Standard Sequence

The MTM durability tests were carried out for the four formulations which showed specific trends in the TE77 tests or the MTM initial sliding tests; PAO+acid, CVTF+acid, PAO+GMO and CVTF+GMO. The friction performance at the standard sequence is shown in this section.

The μ-V characteristics for the oleic acid formulations through the durability tests are presented in Fig. 6-11 and Fig. 6-12. The tests at the different temperature conditions were performed separately for all the standard sequence results as explained.

Regarding PAO+acid results shown in Fig. 6-11, the μ-V curve was relatively stable through the 16 hours of the durability steps. Especially at 40°C, the curves were almost overlapped and the frictional properties did not change during the test. When it comes to the 100°C results, the performance appeared to become worse slightly as the test time increased by dropping the friction coefficient at high sliding speed region, however, the relationship was still positive after 16 hours. As for the reason for the friction decrease at high speed, the damage on the clutch paper (the clogged pore structure and/or the flattened surface) caused by the long-term sliding under the severe condition can be considered.

In terms of the CVTF formulation shown in Fig. 6-12, although the friction performance at 100°C was excellent at the beginning of the durability test, it became worse after 8 hours. The trend finally turned into an almost flat μ-V relationship at the end of the test. In contrast, the curves were stable at 40°C, which was similar to PAO+acid. Considering the TE77 initial test that implied the presence of the interaction between oleic acid and the CVTF additives only at 100°C, it can be assumed that oleic acid continued to be consumed due to the interaction through the long-term test, and finally lost the FM effect when most of the oleic acid was degraded into less effective chemical structure. At 40°C, the interaction would not be significant, so that oleic acid was able to maintain its effect through the test.

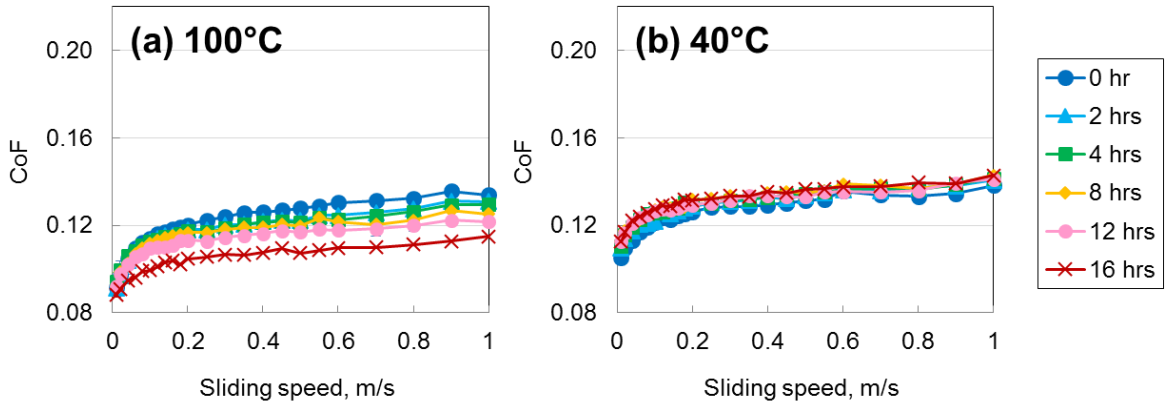

Fig. 6-11. μ-V characteristics during the MTM durability test for PAO+acid under the standard sequence at (a) 100°C and (b) 40°C

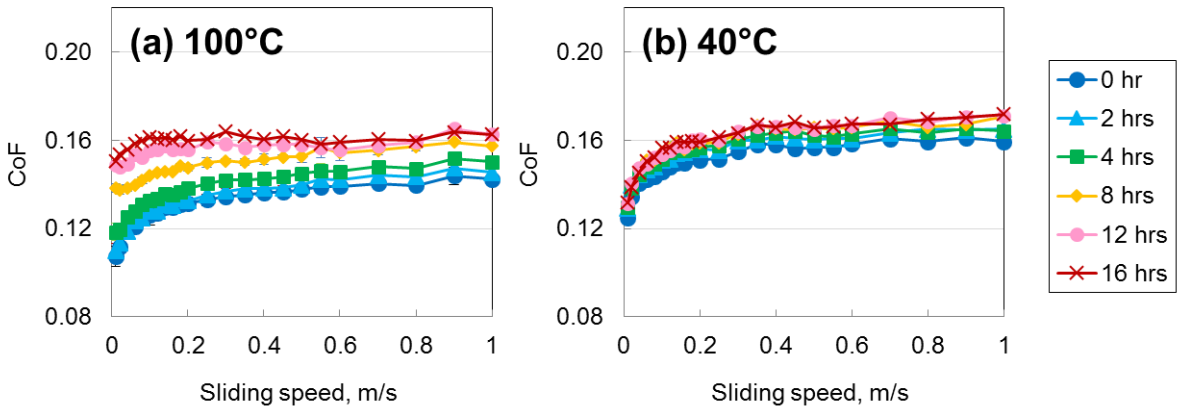

Fig. 6-12. μ-V characteristics during the MTM durability test for CVTF+acid under the standard sequence at (a) 100°C and (b) 40°C

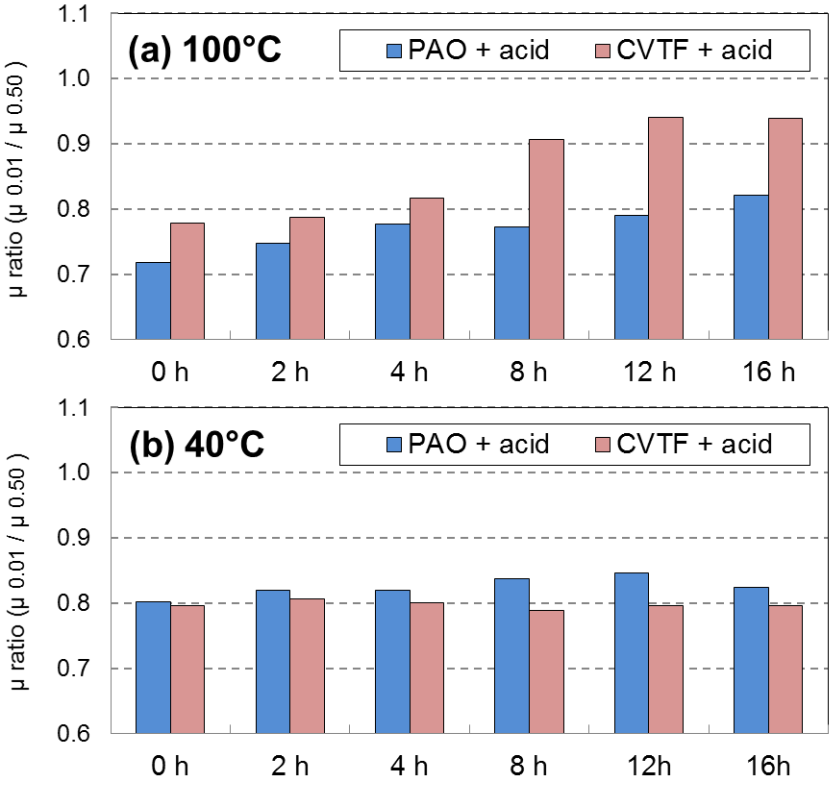

Fig. 6-13. μ ratio during the MTM durability test for the oleic acid formulations under the standard sequence at (a) 100°C and (b) 40°C

For the quantitative discussion, the μ ratio of the oleic acid formulations was summarised in Fig. 6-13. The graph for the 100°C results clearly shows a sharp increase of the μ ratio of CVTF+acid indicating that the CVTF additives accelerated the degradation of oleic acid. In contrast, the FM effect of oleic acid was consistent at 40°C

through the durability test even formulated with the additives, which implies that the high temperature and the presence of the additives should be the key factors to inactivate oleic acid.

The results of the PAO+GMO were shown in Fig. 6-14. It had a negative curve at the beginning of the (a) 100°C test, then became better, and finally reached a slightly positive relationship. However, it is notable that the friction was decreased in all the range of the sliding speed. It is considered that the physical deposition of GMO onto the paper led to the flat surface as the similar to that observed in the TE77 durability test with PAO+GMO. In contrast, the friction property was positive and stable at (b) 40°C all through the durability test. It agrees well with the TE77 initial test at 40°C showing a good FFWI, and indicates that GMO was not stuck on the paper at 40°C and the working mechanism was different from 100°C.

Interestingly, GMO improved the effect during the 100°C durability test when formulated with the CVTF additives as shown in Fig. 6-15(a). As the durability time increased, the friction at low speed region became lower resulting in a better μ ratio. A similar trend was also observed in the TE77 durability test, and it can be considered that GMO was changed into more effective chemical structure by an interaction with the additives. Since the (b) 40°C graph shows a stable relationship and the curve shapes were not pretty good through the test, it is possible to support the assumption that the high temperature test condition helped the reaction of GMO with the CVTF additives.

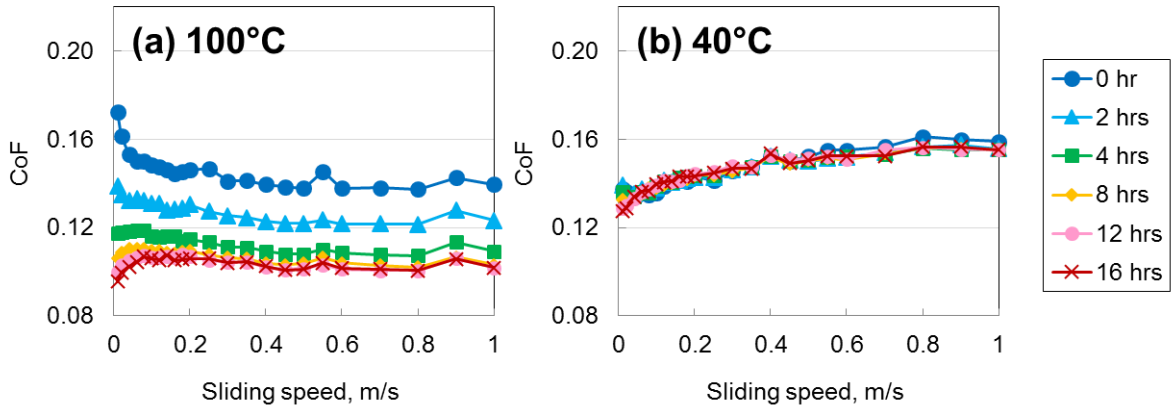

Fig. 6-14. μ-V characteristics during the MTM durability test for PAO+GMO under the standard sequence at (a) 100°C and (b) 40°C

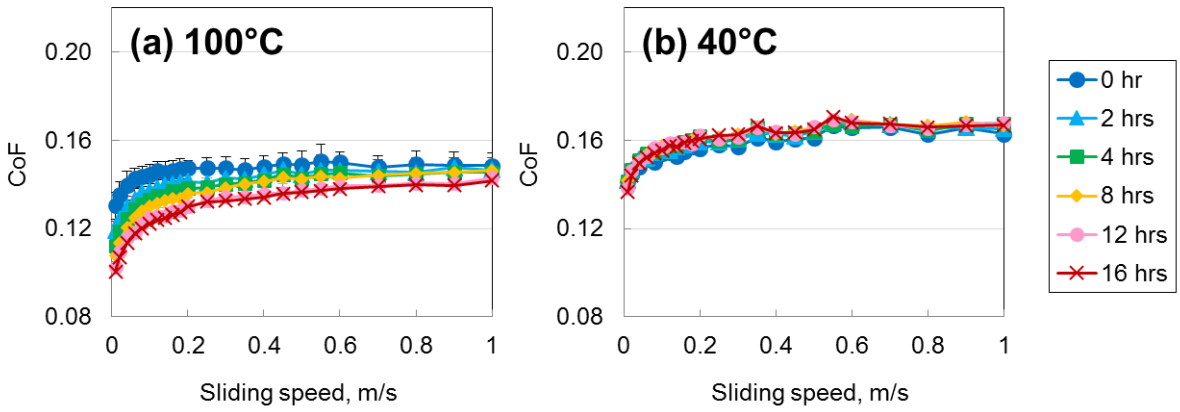

Fig. 6-15. μ-V characteristics during the MTM durability test for CVTF+GMO under the standard sequence at (a) 100°C and (b) 40°C

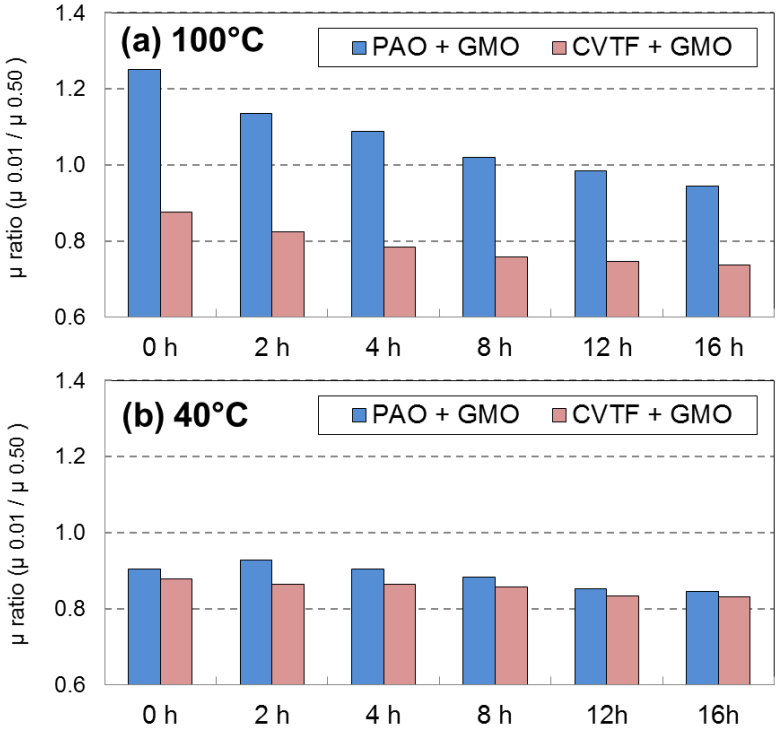

Fig. 6-16. μ ratio during the MTM durability test for the GMO formulations under the standard sequence at (a) 100°C and (b) 40°C

Finally, the μ ratio of the GMO formulations is summarised in Fig. 6-16. From the 100°C results showing the μ ratio getting better as the durability time increases, it is possible to say that the high temperature condition assisted GMO changing into the chemical structure with a better friction modification effect. In addition, the presence of the CVTF additives was also helpful for the GMO decomposition because CVTF+GMO

presented good μ-V characteristics from the beginning of the test. The interaction of GMO seemed to be inhibited at 40°C probably due to the low chemical activity at low temperature.

6.2.2. Friction Performance at the Combined Sequence

The μ-V characteristics measured by the combined sequence are shown in this section. In the combined sequence, the frictional performance was evaluated firstly at 100°C, then the 40°C test was followed at the end of each durability step at 100°C as explained in Fig. 6-10. The purpose for applying this method is to assume the reason of the specific frictional trend observed in the standard sequence tests. In addition, a procedure similar to this combined sequence is adopted in some industrial standards, such as JASO M349, for evaluating the paper clutch performance of lubricants.

The μ-V characteristics of the oleic acid formulations are shown in Fig. 6-17 and Fig. 6-18, and the μ ratio is summarised in Fig. 6-19. While the μ-V properties of PAO+acid showed a similar trend to the standard sequence keeping the positive curve all through the durability steps, CVTF+acid showed a different result at 40°C. In the case of the standard sequence, the μ-V property of CVTF+acid became worse after 16 hours only at 100°C, though, the poor performance was observed both at 100°C and 40°C in the combined sequence. This result indicates that the performance decrease was attributed to the irreversible degradation of oleic acid caused at the high temperature condition. Once the oleic acid was degraded into the less effective structure at 100°C, it was not able to work at 40°C as well.

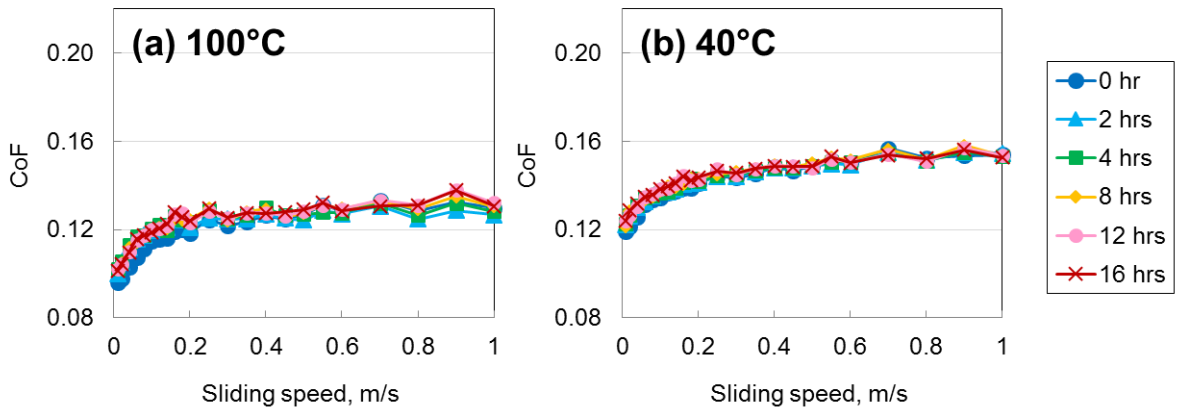

Fig. 6-17. μ-V characteristics during the MTM durability test for PAO+acid under the combined sequence at (a) 100°C and (b) 40°C

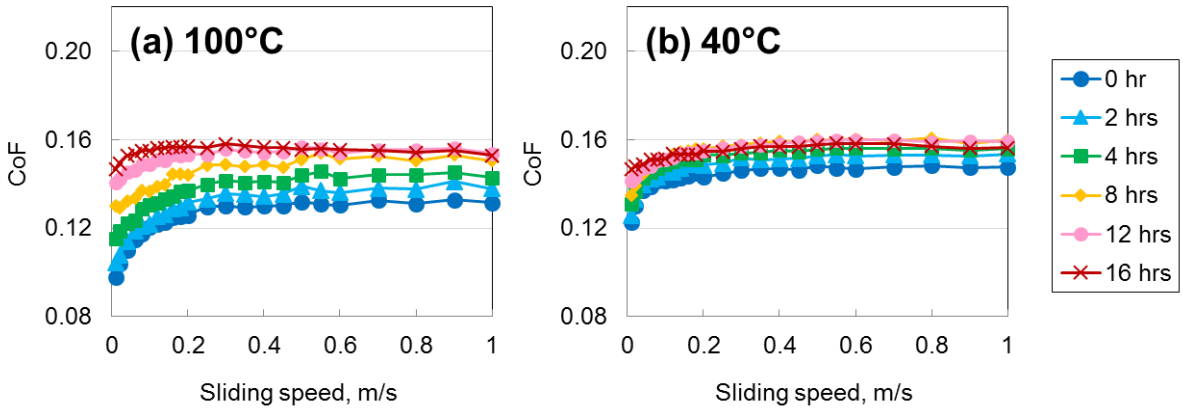

Fig. 6-18. μ-V characteristics during the MTM durability test for CVTF+acid under the combined sequence at (a) 100°C and (b) 40°C

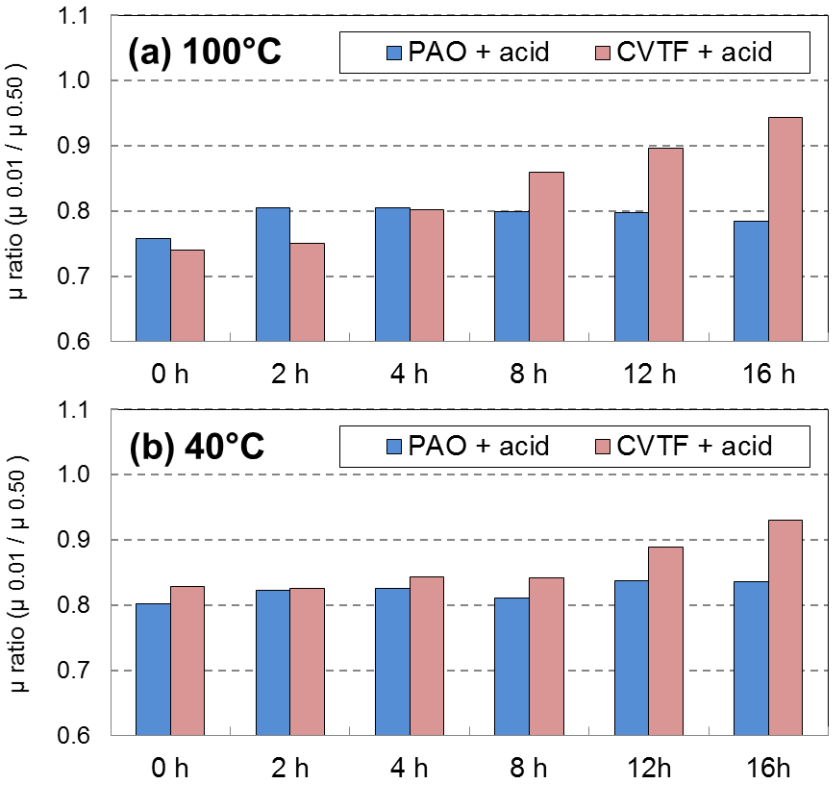

Fig. 6-19. μ ratio during the MTM durability test for the oleic acid formulations under the combined sequence at (a) 100°C and (b) 40°C

The μ-V characteristics of the GMO formulations during the combined sequence durability test are shown in Fig. 6-20 and Fig. 6-21, and the μ ratio is summarised in Fig. 6-22.

Both formulations presented the trend comparable to those under the standard sequence at 100°C, while the μ ratio values at 40°C were better than the standard sequence keeping less than 0.8 thorough the test. This result implies that the working mechanism of GMO should be different between at 40°C and 100°C. It is assumed that the decomposition of GMO is important at 100°C while the physical adsorption is dominant at 40°C. Therefore, the decomposed GMO produced at 100°C durability could enhance the μ-V characteristics at 40°C in addition to the physical adsorption effect when the combined sequence was carried out.

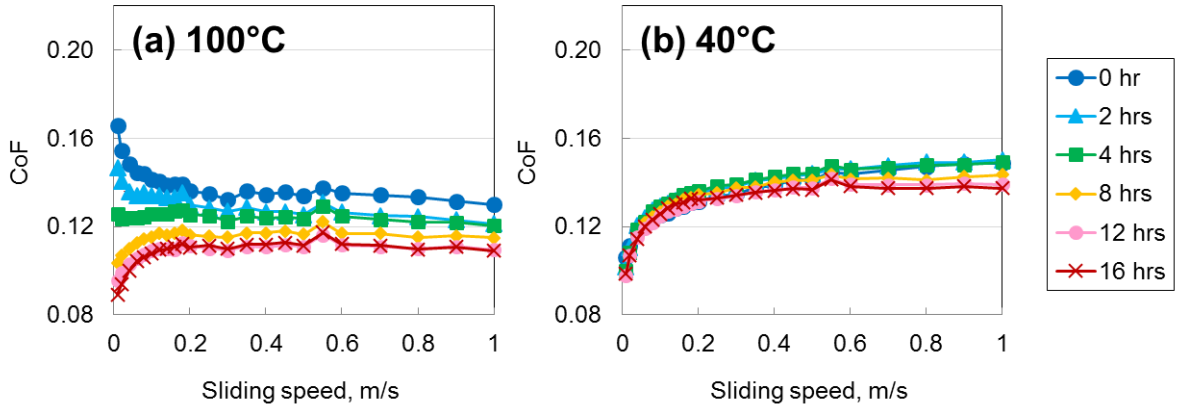

Fig. 6-20. μ-V characteristics during the MTM durability test for PAO+GMO under the combined sequence at (a) 100°C and (b) 40°C

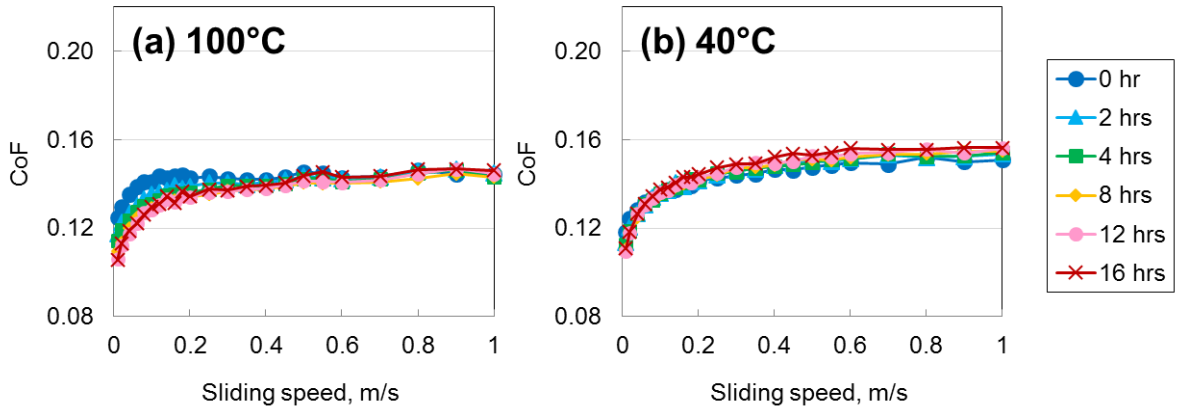

Fig. 6-21. μ-V characteristics during the MTM durability test for CVTF+GMO under the combined sequence at (a) 100°C and (b) 40°C

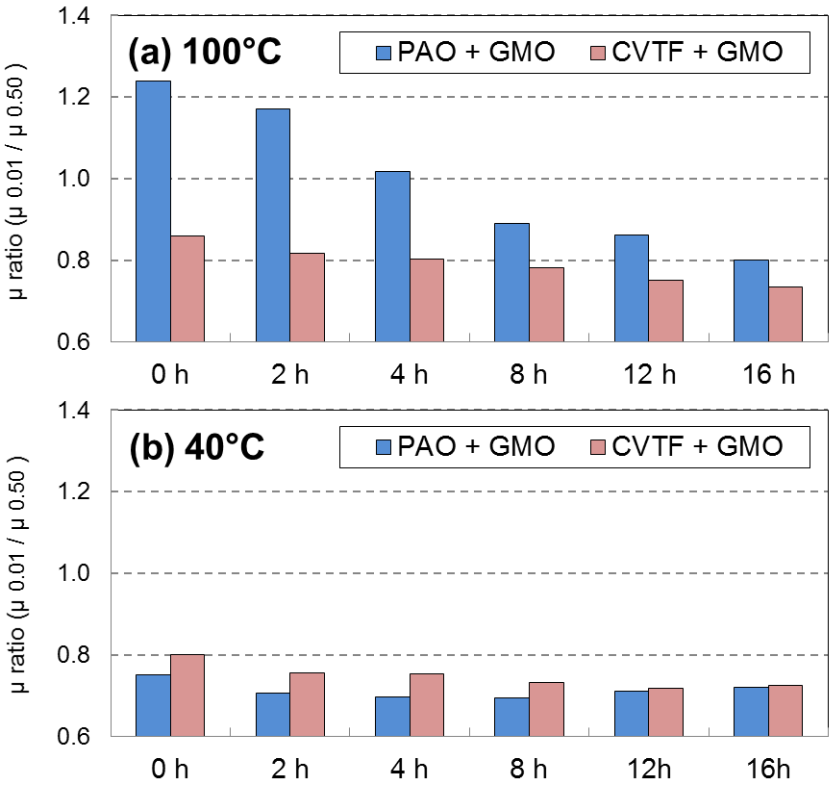

Fig. 6-22. μ ratio during the MTM durability test for the GMO formulations under the combined sequence at (a) 100°C and (b) 40°C

6.2.3. ATR-FTIR Analysis for Lubricants after Durability Test

The post-test lubricants after the MTM durability tests were analysed using ATR-FTIR in order to discuss the change in the chemical structure of the FMs and the additives caused by the long-term sliding load. The IR spectra are summarised as the difference spectra subtracted from each of the fresh oil, therefore, a positive peak means that a corresponding chemical bond was increased during the durability test, while a negative peak means the reduction of the chemical bond.

Fig. 6-23 shows the difference spectra of the post-test PAO+acid oils. As all the spectra do not have any specific peaks, it is considered that the oleic acid did not change the chemical structure through the test even at 100°C. This result is in good agreement with the μ-V characteristics of PAO+acid, which showed the consistent and excellent properties in all the durability test conditions.

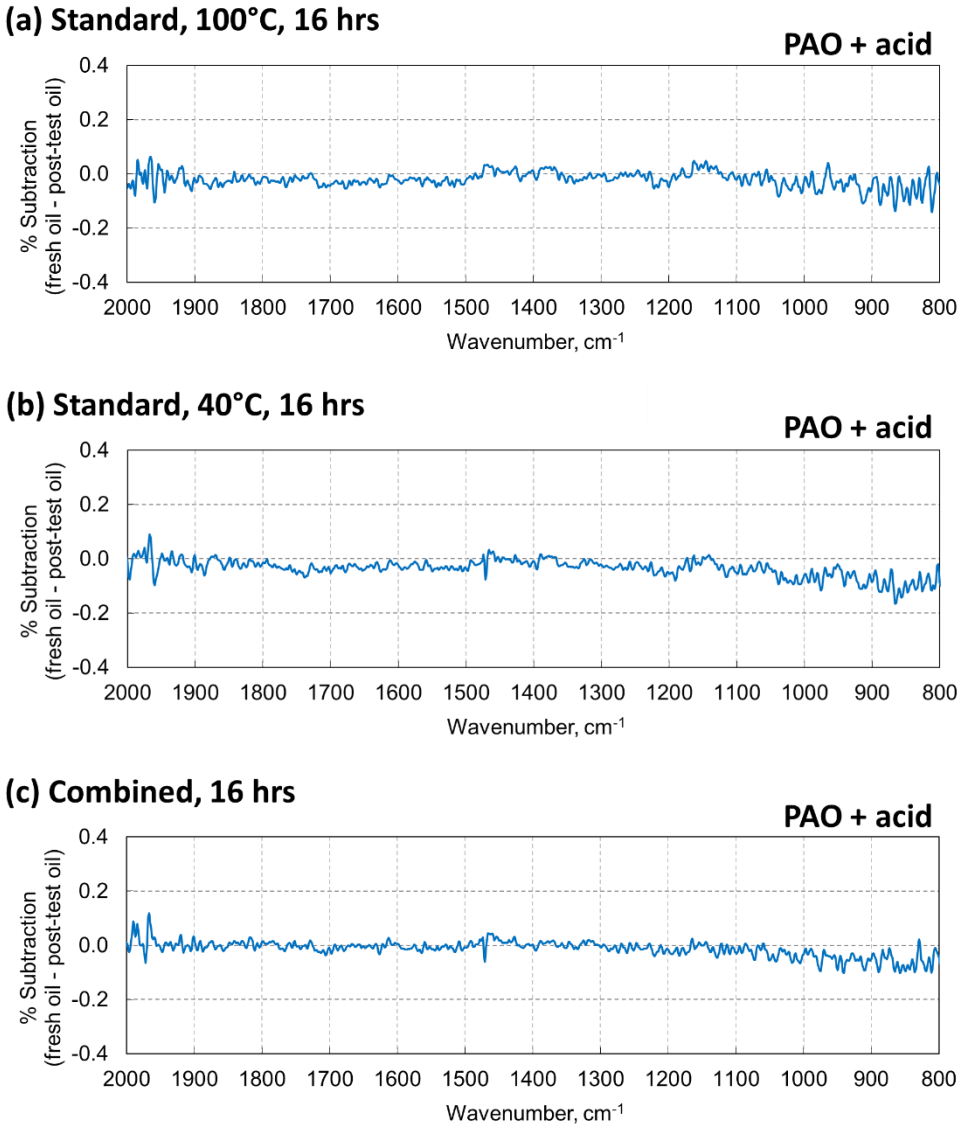

Fig. 6-23. Difference ATR-IR spectra of the post durability test lubricants (PAO+acid) subtracted from the fresh oil spectrum, (a) Standard sequence at 100°C for 16 hrs, (b) Standard sequence at 40°C for 16hrs, (c) Combined sequence for 16 hrs

Interestingly, the degradation of oleic acid was detected when formulated with the CVTF additives as shown in Fig. 6-24. In the spectra of (a) the standard sequence at 100°C and (c) the combined sequence, the following peaks appeared in common; a positive broad peak from C-O-C (ester) between 1,200 and 1,100 cm^{-1}, a positive peak derived from C=O at around 1,710 cm^{-1} and a negative peak from C-O-P bond at around 970 cm^{-1}. The ester peak should be attributed to the degradation products of oleic acid, taking into account that the oleic acid lost the FM effect at the end of the durability test in the both conditions. On the other hand, the carbonyl peak would be derived from the

degradation of the other additives, which was possibly not effective for improving the μ-V performance due to the hydrocarbon chain structure. It is notable that the negative peak of C-O-P bond attributed to the phosphorous anti-wear agent was detected, which means the anti-wear agent might have influence on the degradation of oleic acid. In contrast, at (b) 40°C standard durability test, no specific peak was observed except for a slight increase of the ester bond. It also agrees with the μ-V performance that was stable through the durability steps at 40°C.

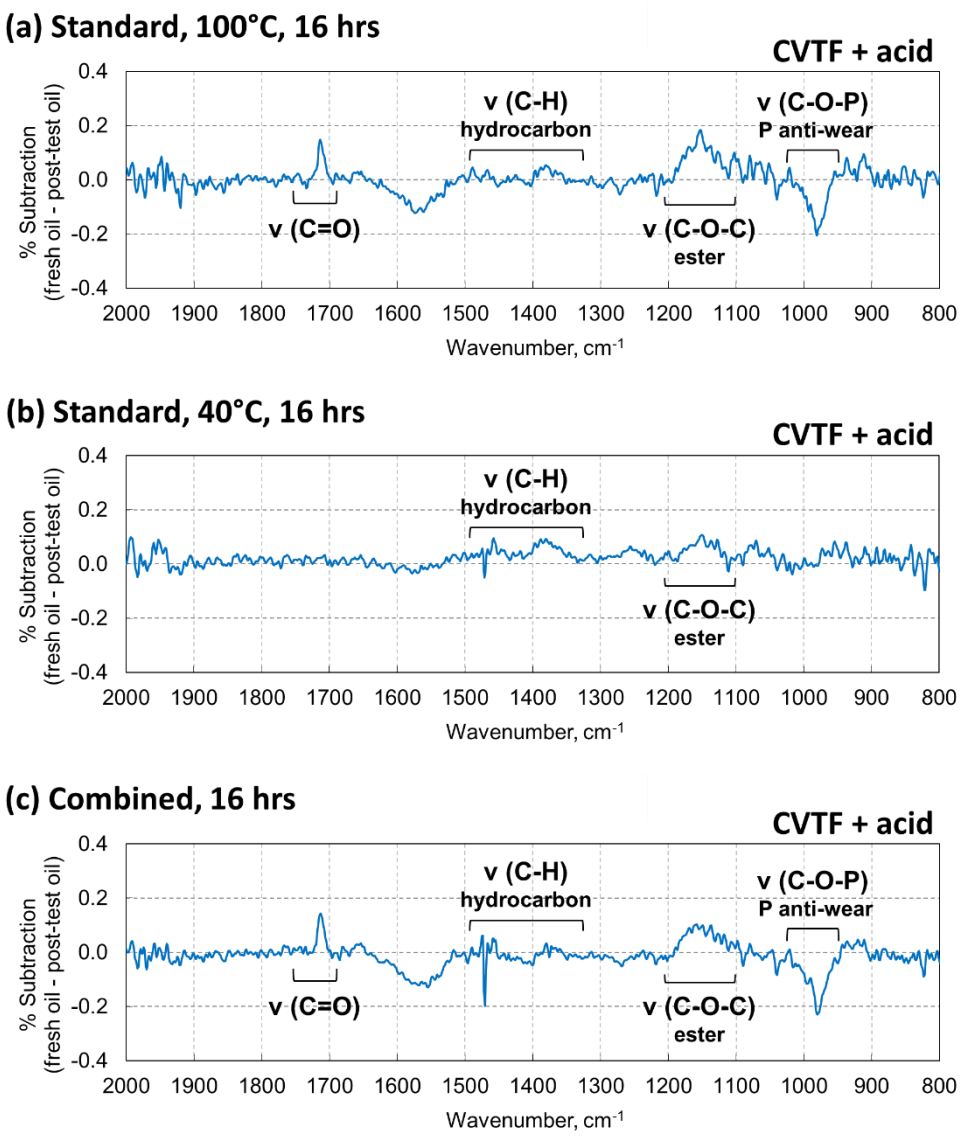

Fig. 6-24. Difference ATR-IR spectra of the post durability test lubricants (CVTF+acid) subtracted from the fresh oil spectrum, (a) Standard sequence at 100°C for 16 hrs, (b) Standard sequence at 40°C for 16hrs, (c) Combined sequence for 16 hrs

The spectra of the post-test PAO+GMO are shown in Fig. 6-25. All the difference spectra presented a similar trend showing the weak negative peaks derived from an ester and an alcohol bond. These peaks should be attributed to the decomposition of GMO, however, each peak intensity was not strong. It is considered that GMO did not change the structure significantly through the durability test.

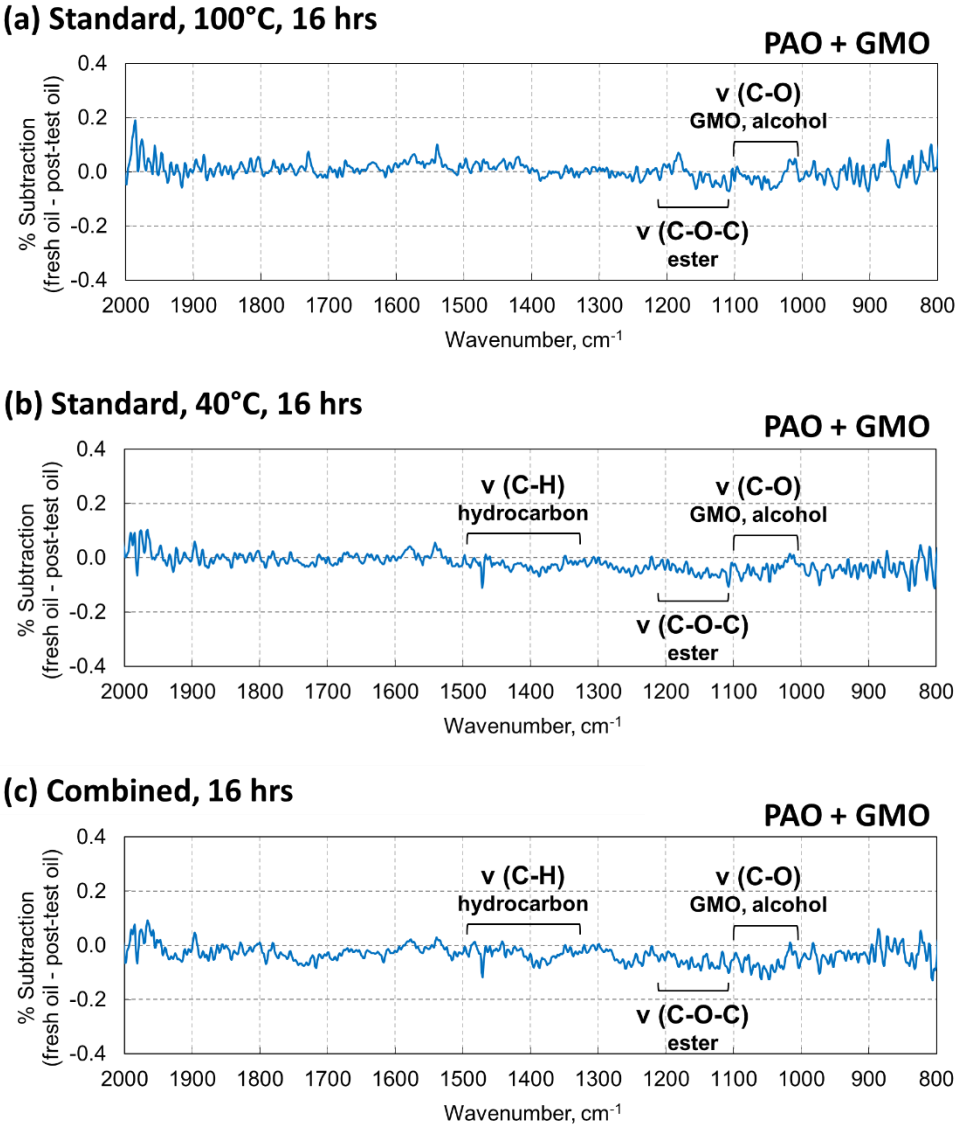

Fig. 6-25. Difference ATR-IR spectra of the post durability test lubricants (PAO+GMO) subtracted from the fresh oil spectrum, (a) Standard sequence at 100°C for 16 hrs, (b) Standard sequence at 40°C for 16hrs, (c) Combined sequence for 16 hrs

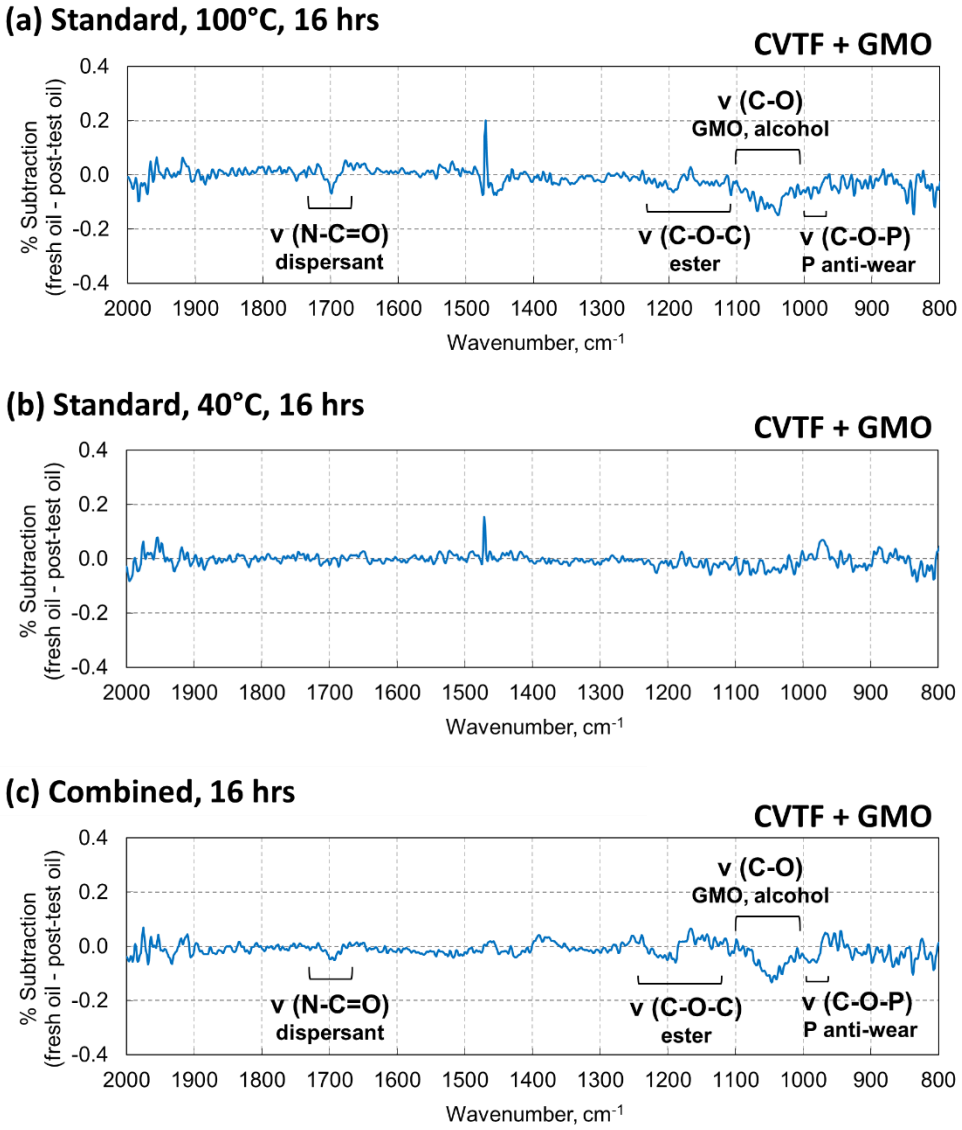

Fig. 6-26. Difference ATR-IR spectra of the post durability test lubricants (CVTF+GMO) subtracted from the fresh oil spectrum, (a) Standard sequence at 100°C for 16 hrs, (b) Standard sequence at 40°C for 16hrs, (c) Combined sequence for 16 hrs

Finally, the spectra of the post-test CVTF+GMO are summarised in Fig. 6-26. The shape of the spectra for (a) standard sequence at 100°C and (c) combined sequence appeared to be quite similar showing the negative peaks derived from the ester bond at around 1,200 cm^{-1}, the alcohol bond between 1,100 and 1,000 cm^{-1}, the C-O-P bond at 970 cm^{-1} and the amide bond at 1,700 cm^{-1}. The decrease of the ester and alcohol peak should be attributed the decomposition of GMO, and the intensity was stronger than those observed in the PAO+GMO spectra. It implies that the CVTF additives assisted

the GMO decomposition into the effective FM structure as assumed from the μ-V performance results. Since the small decrease of the phosphorous bond was also detected, the anti-wear agent might help the decomposition process. On the other hand, any specific peak was not detected in the spectrum (b) standard sequence at 40°C. The high temperature should be one of the key factors to promote the reaction as the CVTF+acid spectra also indicated.

6.2.4. ATR-FTIR analysis for Paper Plates after Durability Test

The wear tracks on the post durability test MTM paper plates were analysed using ATR-FTIR in order to estimate the chemical nature on the paper surface. The acquired spectra were subtracted from the fresh paper spectrum, and the difference spectra were summarised between 1,780 and 1,680 cm^{-1}, which is the specific wavenumber of carbonyl bonds derived from the FMs and the additives. In each graph, the spectrum for the paper plate after the initial performance test is also shown together for the comparison.

The difference spectra for the oleic acid formulations are shown in Fig. 6-27. Among the PAO results, no significant change was observed, though, the spectra of the standard 100°C test and the combined test had a slight increase between 1,760 and 1,730 cm^{-1}. This region corresponds to the carbonyl group for ester bonds, therefore, it implies slight degradation of oleic acid through the 100°C durability steps. It also agrees with the μ ratio of PAO+acid experienced a slight increase during the 100°C durability test.

On the other hand, the spectra for the CVTF formulations presented a peak increase at around 1,700 cm^{-1} after the standard 100°C and combined sequence tests, while the 40°C durability spectrum was almost the same as the initial test result. The wavenumber at around 1,710 cm^{-1} is identified as carboxylic acid, which is corresponding to the post-test lubricant IR analysis that detected the increase of carboxylic acid as the degradation products. In addition, the increase at 1,700 cm^{-1} should be attributed to imide group of the dispersant. It implies the adsorption of the dispersant on the paper surface in the high temperature condition.

The results for the GMO formulations are summarised in Fig. 6-28. In terms of the PAO+GMO, the papers after 100°C durability tests, the standard sequence at 100°C and the combined sequence, showed a significant peak increase at around 1,730 cm^{-1}

attributed to GMO. This results corresponds to the TE77 durability test of PAO+GMO at 100°C, which showed a similar post-test paper ATR-FTIR spectrum due to the GMO deposit on the paper surface. It is considered that the GMO deposition would be accelerated at 100°C, leading to the friction reduction at all the sliding speed.

In contrast, the significant increase of the GMO peak was not observed among the CVTF+GMO spectra. The trend for all the post durability test spectra was similar to the initial result, except for showing a slight increase around 1,700 cm^{-1} derived from the imide bond for the dispersant. Since the peak intensity is much smaller than that of the CVTF+acid spectra (Fig. 6-27 (b)), the increase should be derived from a simple adsorption without a specific interaction caused during the durability test.

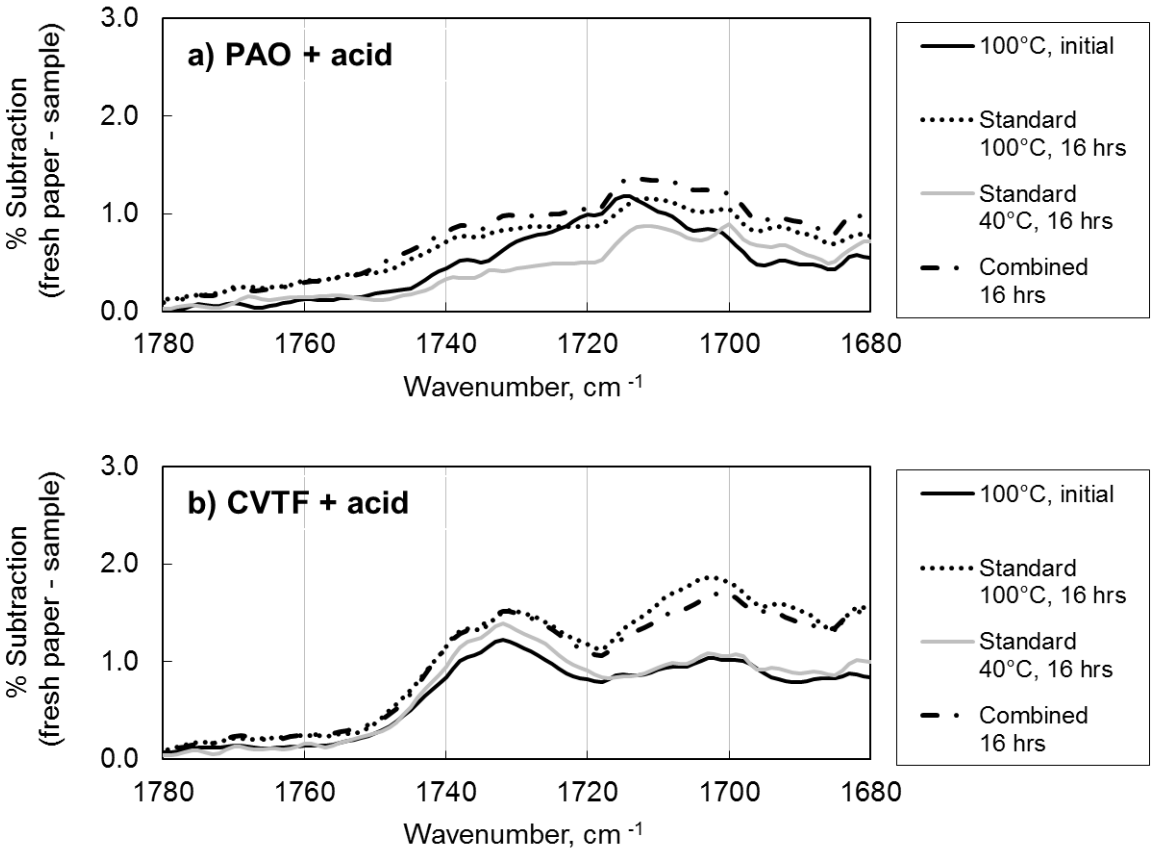

Fig. 6-27. Difference ATR-IR spectra for the post-test MTM paper plates after testing the oleic acid formulations (subtraction by the fresh paper spectrum)
(a) the PAO formulations, (b) the CVTF formulations

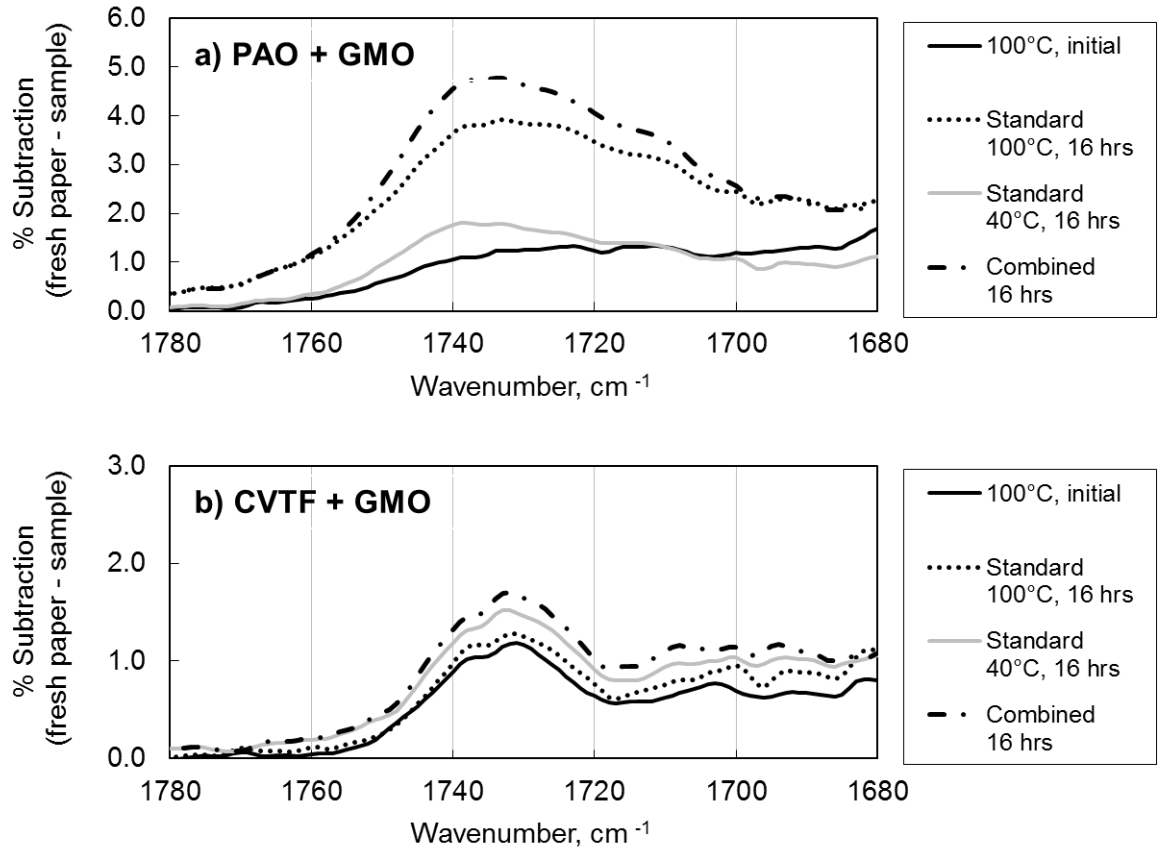

Fig. 6-28. Difference ATR-IR spectra for the post-test MTM paper plates after testing the GMO formulations (subtraction by the fresh paper spectrum)
(a) the PAO formulations, (b) the CVTF formulations

6.3. Summary (MTM Tribotests)

In this chapter, the μ-V characteristics of the FMs were investigated using the MTM under the paper/steel contact configuration. The initial frictional performance was evaluated for all the formulations, and then the durability test was carried out for the oleic acid and GMO formulations.

Firstly, the results for the base fluids and oleyl alcohol are summarised in Table 6-1. Oleyl alcohol showed a slight improvement on the μ-V performance when added in PAO, while this effect disappeared in the presence of the CVTF additives probably due to the competitive adsorption with the other additives.

Table 6-1. Summary of MTM friction tests (Base fluids and oleyl alcohol)

	PAO (base)		CVTF (base)	
	100°C	40°C	100°C	40°C
Initial performance				
μ ratio	1.41	1.16	1.05	1.10
ATR-FTIR (paper)	N/A	-	Dispersant PMA	-

	PAO + alcohol		CVTF + alcohol	
	100°C	40°C	100°C	40°C
Initial performance				
μ ratio	1.14	1.01	1.05	1.11
ATR-FTIR (paper)	N/A	-	Dispersant PMA	-

The results for the oleic acid formulations are summarised in Table 6-2. Oleic acid initially presented an excellent μ-V property in all the test conditions independent of the base fluid or the test temperature. While the μ-V performance could be kept under the 40°C durability test condition, it became worse after the 100°C durability tests. This trend was significant when formulated with the CVTF additives, and the μ ratio was increased from 0.75 to 0.94 in the case of the standard sequence at 100°C. The reason for the μ-V performance reduction is considered to be the degradation of oleic acid, and the high temperature condition and the CVTF additives seemed to be the factors to accelerate the process. The IR spectra of the post-test lubricants after the 100°C durability test showed a peak increase of ester bonds, which should be attributed to the degraded products of oleic acid. Additionally, decomposition of the phosphorous anti-wear agent and the adsorption of the dispersant onto the post-test paper were observed. These additives might play an important role on the μ-V performance degradation at 100°C.

Finally, the MTM results for the GMO formulations are summarised in Table 6-3. In terms of the 100°C condition, although the effect of GMO was not significant initially, especially when added into PAO, the μ-V performance became better through the 100°C durability steps; from 1.18 to 0.94 for PAO+GMO and from 0.88 to 0.74 for CVTF+GMO. It is considered that GMO was decomposed into the effective chemical structure by the thermal and sliding load, and the CVTF additives could assist the process. However, PAO+GMO showed a very strong IR peak attributed to GMO on the

post-test paper, which is considered to be the GMO deposit comparable to the TE77 results. The flattened paper clutch surface by the deposit would be another factor for the μ ratio reduction; it is not preferable for the clutch performance because of the friction decrease at high speed region.

On the other hand, at the 40°C condition, the μ ratio was good and consistent at around 0.85 all through the durability test. It is notable that the μ ratio presented further reduction down to around 0.7 at the combined sequence, the working mechanism of GMO is considered to be different between 100°C and 40°C. The GMO decomposition seems to be a key factor at 100°C, while GMO appeared to be capable of forming the effective adsorption film without the decomposition at 40°C. In the combined sequence, the decomposed GMO produced during the 100°C test could work effectively at the μ-V measurement at 40°C in addition to the simple GMO adsorption, resulting in the further μ ratio reduction.

Table 6-2. Summary of MTM friction tests (Oleic acid)

	PAO + acid		CVTF + acid	
	100°C	40°C	100°C	40°C
Initial performance				
μ ratio	0.73	0.80	0.75	0.83
ATR-FTIR (paper)	- Oleic acid	-	- Oleic acid (weak) - Dispersant - PMA	-
Standard sequence (16 hrs)				
μ ratio	0.82	0.82	**0.94**	0.80
ATR-FTIR (paper)	- Oleic acid - C=O increase (weak, ester bond)	- Oleic acid	- Carboxylic acid - Dispersant (very strong) - PMA	- Dispersant - PMA
ATR-FTIR (lubricant)	N/A	N/A	- C=O increase degradation products - C-O-C increase degraded oleic acid - C-O-P decrease P anti-wear degradation	- C-O-C increase (weak) degraded oleic acid
Combined sequence (16 hrs)				
μ ratio	0.78	0.84	**0.94**	**0.93**
ATR-FTIR (paper)	- Oleic acid - C=O increase (weak, ester bond)		- Carboxylic acid - Dispersant (very strong) - PMA	
ATR-FTIR (lubricant)	N/A		- C=O increase, degradation products - C-O-C increase, degraded oleic acid - C-O-P decrease, P anti-wear degradation	

Table 6-3. Summary of MTM friction tests (GMO)

	PAO +GMO		CVTF + GMO	
	100°C	40°C	100°C	40°C
Initial performance				
μ ratio	**1.18**	0.90	**0.88**	0.88
ATR-FTIR (paper)	- GMO	-	- Dispersant - PMA	-
Standard sequence (16 hrs)				
μ ratio	**0.94**	0.85	**0.74**	0.83
ATR-FTIR (paper)	- GMO (very strong, deposit)	- GMO	- Carboxylic acid (weak) - Dispersant (weak) - PMA	- Carboxylic acid (weak) - Dispersant (weak) - PMA
ATR-FTIR (lubricant)	- C-O decrease (very weak, GMO) - C-O-C decrease (very weak, GMO)	- C-O decrease (very weak, GMO) - C-O-C decrease (very weak, GMO)	- C-O decrease - C-O-C decrease - C-O-P decrease (very weak, P anti-wear)	N/A
Combined sequence (16 hrs)				
μ ratio	0.80	**0.72**	0.73	**0.72**
ATR-FTIR (paper)	- GMO (very strong, deposit)		- Carboxylic acid (weak) - Dispersant (weak) - PMA	
ATR-FTIR (lubricant)	- C-O decrease (very weak, GMO) - C-O-C decrease (very weak, GMO)		- C-O decrease - C-O-C decrease - C-O-P decrease (very weak, P anti-wear)	

Chapter 7 – Discussion

The behaviour of the FMs on the substrate surface and the influence of factors such as the polar group of the FMs, the substrate material, the CVTF additives and test temperature are discussed based on the experimental results presented between Chapters 4 and 6.

Firstly, the uniqueness of the frictional requirements at the CVT system is briefly reviewed in “7.1. Frictional Requirement at the CVT”, and the methodology of this study is confirmed in “7.2. Appropriateness of the Methodology”. Then, the friction test results are summarised in “7.3. An Overview of Distinctive FM Effects”, and the specific behaviour of oleic acid and GMO is discussed in “7.4. Working Mechanism of Oleic Acid at 100°C” and “7.5. Working Mechanism of GMO”. Finally, the practical application of the FMs to the CVTFs is proposed in “7.6. Application of FMs to CVTF”.

7.1. Frictional Requirements of the CVT

The uniqueness of the CVT is the steel belt-pulley system which enables the energy efficient engine control. The overview of the CVT system is shown in Fig. 7-1. The engine torque is transferred through the steel/steel contact between the belt and the pulley, so that the steel friction needs to be kept higher to prevent a macro slip of the steel belt. The issue is that the CVT also equips the torque converter, and the friction at the paper lock-up clutch also has to be controlled appropriately using only one lubricant.

The frictional requirements at the lock-up clutch and the steel belt-pulley are summarised in Fig. 7-2. At the lock-up clutch, the μ-V characteristics, a relationship between the sliding speed and the friction coefficient, should be managed to be a positive curve in order to prevent a self-induced vibration, so called shudder. Therefore, regarding the friction at low sliding speed region, each component prefers an opposite property; low friction at the lock-up clutch and high friction at the belt-pulley system.

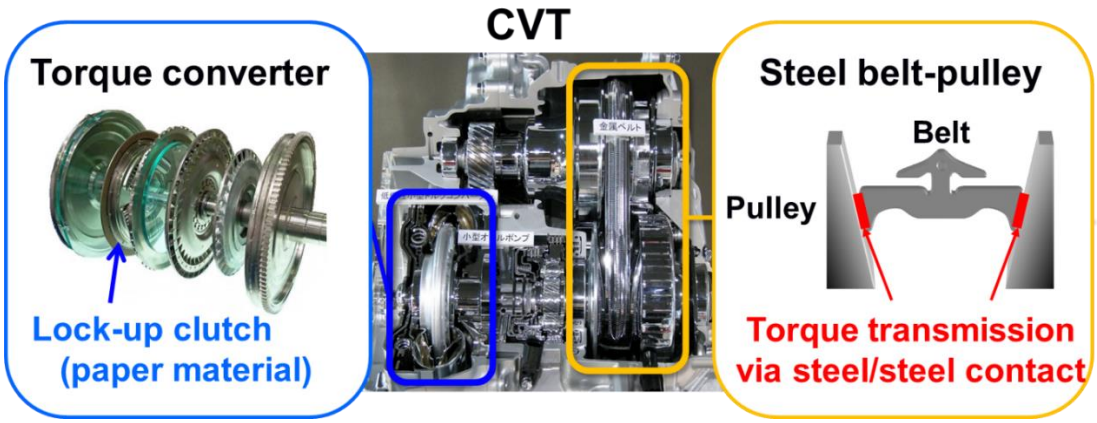

Fig. 7-1. Overview of the CVT components (photos are reproduced from [177, 178])

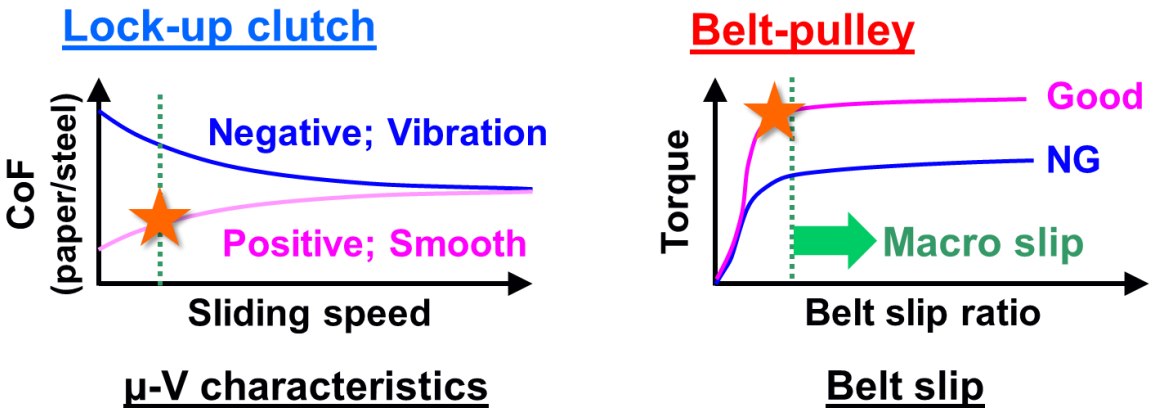

Fig. 7-2. Frictional requirements at the lock-up clutch and the belt-pulley at CVT

Organic FMs play an important role to control the low speed friction. In order to satisfy the challenging requirements, it is necessary to manage the behaviour of the FMs as to adsorb onto the paper material selectively as shown in Fig. 7-3. It seems to be difficult to realise this ideal control when the FM adsorbs onto the surface simply based on the electrostatic interactions between the FM and the substrate. The adsorption force should be determined by the polarity of the FM and the substrate, so that the ranking of the FM effect would not be different between the steel and the paper surface. Therefore, the interactions among the FM and the other additives are considered to be a key factor for the sophisticated FM adsorption control, which has not been studied sufficiently especially at the paper surface.

This study aims to elucidate the behaviour of the FMs and the interactions with the additives for the purpose of designing the next generation CVTFs with sophisticated friction control.

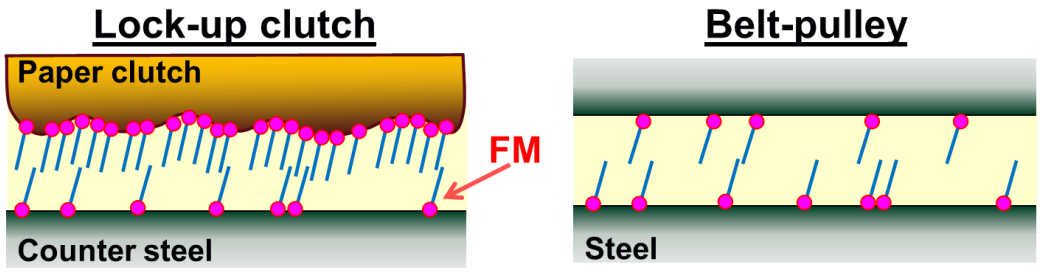

Fig. 7-3. Schematic images of ideal behaviour of the FMs on the steel and paper surface

7.2. Appropriateness of the Methodology

7.2.1. Novelty

In this study, TE77 and MTM were utilised to evaluate the effect of the FMs at the CVTF components; the lock-up clutch and the steel belt-pulley mechanism. The TE77 reciprocating test was performed at both the steel/steel and paper/steel contact conditions in order to simulate the belt-pulley and the lock-up clutch, respectively. On the other hand, the MTM was applied to evaluate the paper clutch performance in pure sliding conditions.

As described in Chapter 3, TE77 is widely used to evaluate the friction at metal/metal contact configurations [113-116]. It is applicable to simulate the belt-pulley system, and Narita [96, 97] reported good agreement between the TE77 friction values and the torque capacity at the actual belt-pulley. In contrast, TE77 has been less utilised to simulate the paper clutch engagement due to the difference in the sliding motion; the TE77 motion is reciprocating, while the actual clutch works in pure sliding conditions. The validity for the application of TE77 for the paper contact is discussed in the next section because some of the surface analysis results were obtained from the post-test TE77 paper plates. On the other hand, MTM is used to evaluate the paper clutch performance, and Ingram [85, 87] investigated the effect of FMs by MTM using the plate coated with the paper clutch material. Therefore, the tribotest procedures to evaluate the frictional performance at the belt-pulley or at the paper clutch system have been established. The issue is that the CVT requires that the frictional performance at

both systems is simultaneously satisfied due to the unique system. The working mechanism of the additives needs to be discussed on both steel and paper using the same test oils; only a few studies have focused on it [94].

Furthermore, the surface analyses of the post-test specimens are also important to understand the working mechanism of additives for the purpose of designing CVTFs with excellent performance. While the various techniques are utilised for observing the metal surface, the chemistry on the paper clutch material has not been studied in great detail due to the fibrous structure that is not easily applied in a high vacuum condition, such as is seen in XPS or SEM/EDX. Only the exception is the studies by Zhao [51, 92, 93], which investigated the effect of the FMs on the paper clutch material. The post-test paper clutches were analysed by EDX, XPS, EDX and TOF-SIMS, and it appeared that XPS is useful to assume the chemistry on the uppermost surface of the paper clutch. However, the studies by Zhao focused on ATFs, so that the effect at the steel component was not discussed.

The novelty of this study is the investigation of the FM's behaviour on the steel and paper clutch systems based on the surface analyses. Each of the tribotest or the surface analysis procedure has been established, however, the combination of them is essential to discuss the better formulation of CVTFs.

7.2.2. Comparison between TE77 and MTM

The frictional performance of the paper clutch material was investigated using both TE77 and MTM. For the quantitative evaluation of the μ-V characteristics, FFWI (Friction Force Wave Index) was introduced for the TE77 measurements, while μ ratio for the MTM. The comparison between the factors is discussed in this section for the purpose of considering the mechanism of μ-V characteristics on the paper material.

The FFWI and μ ratio after the initial performance test are summarised in Fig. 7-4. The horizontal axis represents the FFWI values measured by the TE77 paper/steel contact tests, while the vertical axis shows the μ ratio values obtained from the MTM initial performance measurements. Interestingly, the graphs show an excellent linear relationship between the two factors in spite of the completely different sliding configurations between the TE77 and the MTM. Only the exception is the rightmost blue plot that represents the PAO base oil result at 40°C, which presented an unstable

friction values as the wide error bar shows. The details of the sliding condition of the both tests are summarised in Table 7-1. The major difference is attributed to the sliding motions; the FFWI for TE77 was calculated from the force data during dynamic reciprocating motion, while the μ ratio for MTM was based on the friction measurement at constant speed. Especially, the maximum acceleration of the TE77 test reached at 39 m/s^2 due to the high frequency.

These results imply the independence of the FM behaviour on the sliding configuration; the motion or the acceleration. The FM effect reducing the friction at low speed region could be detectable even at the highly frequent reciprocating motion. It also insists that the FMs could form a stable and regenerative film instantly because the μ-V result of the TE77 plate rubbed 40 times/sec agrees with that of the MTM plate rubbed only 3 times/sec even at 0.50 m/s. In summary, the surface chemistry on the post-test paper plate should be comparable between TE77 and MTM. It is valid to utilise the post-test TE77 paper plate for the surface analyses to discuss the effect of the FMs on the μ-V characteristics.

In addition, this is a unique approach to evaluate the clutch μ-V performance based on the frictional force wave in a reciprocating motion, and showed good correspondence with that measured by the standard clutch test method conducted under the pure sliding conditions. It is useful to develop a new clutch performance tester which enables quicker and easier investigation using a low amount of test oil, which must be helpful to accelerate the development of transmission fluids.

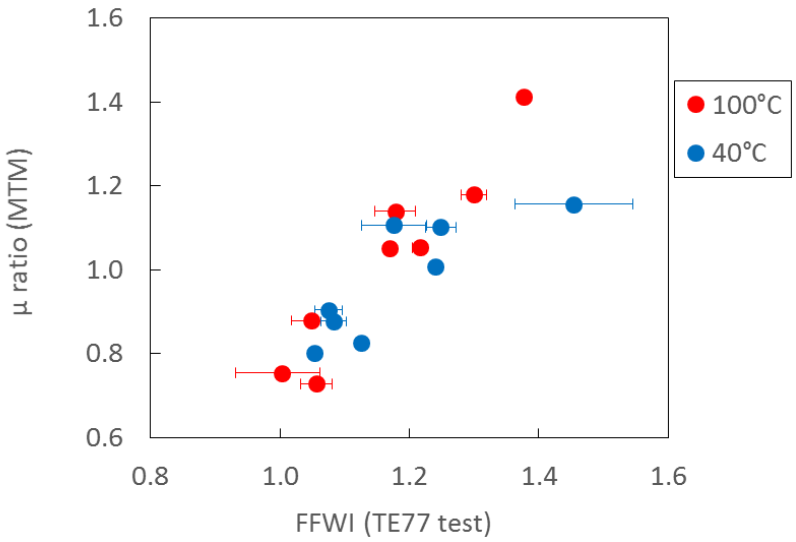

Fig. 7-4. Comparison between FFWI and μ ratio for the initial performance tests at 100°C and 40°C

Table 7-1. TE77 and MTM sliding test conditions for the paper plate

	TE77	MTM
Test specimens	Steel pin (AISI 52100) Paper plate (JASO M349)	Steel ball (AISI 52100) Paper plate (JASO M349)
Load	16.5 N	3.0 N
Pressure (P_{max})	6.0 MPa	4.8 MPa
Sliding motion	Reciprocating (20Hz, 5 mm)	Pure sliding
Measuement conditon	**Dynamic** **(varying speed)**	Static (constant speed)
Sliding speed	Average; 0.20 m/s Maximum; 0.34 m/s	beween 0.01 and 0.50 m/s (μ ratio calculation)
Acceleration	**Maximum; 39 m/s^2**	0 m/s^2
Temperature	100°C or 40°C	

7.3. An Overview of the Distinctive FM Effects

Friction modification effect of the FMs is given in Table 7-2. As the effect on steel, the friction reduction at the TE77 tests is summarised, while the μ ratio evaluated by MTM is also shown to represent the effect on the paper clutch. For the purpose of comparing the results visually, each cell is coloured in response to the FM effect as follows;

Orange; Strong effect (friction reduction at steel; ≤ -0.03, μ ratio; ≤ 0.8)
Yellow; Intermediate effect (friction reduction at steel; -0.02, μ ratio; 0.9)
Green; Weak effect (friction reduction at steel; -0.01, μ ratio; 1.0)
Blue; Negligible effect (friction reduction at steel; 0.00 ≤, μ ratio; 1.1 ≤)

	Friction	μ ratio
	≤ - 0.03	≤ 0.8
	- 0.02	0.9
	- 0.01	1.0
	0.00 ≤	1.1 ≤

Table 7-2. Overview of the FM effect evaluated by the tribotests

		Oleic acid		Oleyl alcohol		GMO	
		100°C	40°C	100°C	40°C	100°C	40°C
PAO formulations	TE77 Steel friction reduction	-0.02	-0.01	0.00	-0.01	-0.03	-0.01
	MTM μ ratio (initial)	0.7	0.8	1.1	1.0	1.2	0.9
	MTM μ ratio (standard, 16h)	0.8	0.8	-	-	0.9	0.9
CVTF formulations	TE77 Steel friction reduction	0.00	-0.01	0.00	0.00	-0.02	-0.02
	MTM μ ratio (initial)	0.8	0.8	1.1	1.1	0.9	0.9
	MTM μ ratio (standard, 16h)	1.0	0.8	-	-	0.7	0.8

If the effect of the FM would be independent of the surrounding factors, the presence of the other additives, test temperature or substrates, the cells should be filled with the same colour. Oleyl alcohol is a good example of this trend showing all the cells are coloured with blue or green, which means a weak FM effect in all the test conditions. The low effect of alcohol FMs was reported by Kalin [68] for the steel contact and Kugimiya [54] for the paper clutch contact. In addition, Kalin also revealed the effect of the alcohol FM was promoted on the DLC surface by forming hydrogen bonds. Therefore, it is considered that the hydroxyl group of oleyl alcohol worked simply making the adsorption film without any significant influence from the factors.

In contrast, oleic acid had a significant dependence on the substrate materials, steel or paper. It showed the good μ-V performance on the paper material, while the friction reduction effect on steel was weak especially at 100°C in the presence of the CVTF additives. In addition, the μ-V performance of CVTF+acid diminished after the durability test only at 100°C. These results indicate that effect of oleic acid was strongly influenced by the factors. This should the first topic whose mechanism will be discussed.

GMO also shows interesting results. The effect on the paper clutch appeared to be excellent when formulated with the CVTF additives, while the initial μ ratio of PAO+GMO was poor at 1.2. It is notable that the paper properties became better as the durability time increased in contrast to oleic acid, which means the mechanism of GMO seems to be different from that of oleic acid. This point also needs to be highlighted.

In summary, the following two points will be discussed in this chapter. This approach will be able to reveal the interactions between the FMs and the other factors, which must be useful to consider the appropriate chemical structures for the FMs applied in CVTFs;

1) The working mechanism of oleic acid at 100°C
   - Why did it not work on steel in the presence of the CVTF additives
   - Why did it lose the FM effect at the paper clutch after the durability when formulated with the additives?

2) The working mechanism of GMO
   - Why did it not work well on paper at 100°C when the CVTF additives were absent?
   - Why did it improve the FM effect on the paper after the durability test?

7.4. Working Mechanism of Oleic Acid at 100°C

7.4.1. Interaction between Oleic Acid and the Additives on Steel Surface

Oleic acid is one of the most historical friction modifiers [59, 60], and the mechanism of the adsorption film formation has been examined using optical interferometry [66] or computational simulations [179].

In this study, oleic acid showed excellent anti-wear performance even in PAO (Fig. 4-7), and the XPS C 1s spectra of PAO+acid (Fig. 4-15) presented the peaks derived from O=C-O (carboxylate) and O-C-O at both 100°C and 40°C. In terms of the chemical nature of carboxylic acids on the steel surface, Sahoo [180] studied the adsorption of stearic acid and linoleic acid using XPS, and concluded that there are two (symmetric and asymmetric) mechanisms as shown in Fig. 7-5. In this study, it is considered that oleic acid worked on the steel surface following the same mechanisms, because the shape of the XPS C 1s spectrum is comparable to that reported by Sahoo. The result of the XPS O 1s spectra (Fig. 4-16) supports this assumption. The peak intensity for non-bridging oxygens (NBO) at around 531.5 eV was higher at 100°C than that at 40°C. Since the NBO peak is derived from C=O (carbonyl) or C-O-Fe (connection with metal substrate) [132, 181, 182], it indicates that the formation of the oleic acid adsorption film following the mechanism shown in Fig. 7-5 was promoted at 100°C due to the high chemical potential. It is in good agreement with the TE77 friction results that PAO+acid presented less effect at 40°C.

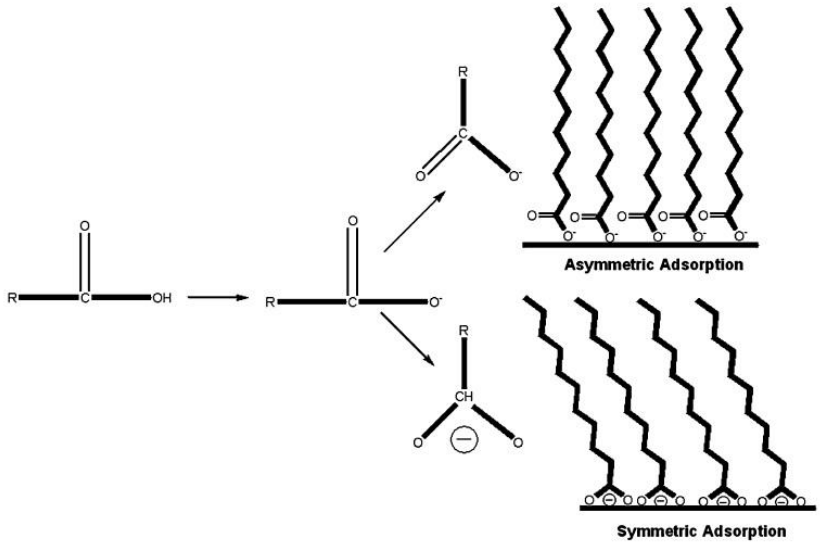

Fig. 7-5. Two mechanisms for the adsorption of fatty acids onto steel (reprinted from [180])

The steel friction of oleic acid presented the opposite trend when formulated with the CVTF additives showing no effect at 100°C. The reason could be assumed from the XPS C 1s spectrum of CVTF+acid at 100°C (Fig. 4-17) that shows only the peaks derived from the nitrogen bond from the dispersant. The peak attributed to oleic acid was not detected, and the spectra shape was almost the same as that of the CVTF base fluid. This result implies that the adsorption of oleic acid was inhibited by the CVTF additives. The clue to understand the mechanism could be found in the XPS survey spectra (Table 4-3). The CVTF+acid showed different trend for the mass fraction of calcium and phosphorous; lower Ca and higher P concentration compared with the other CVTF test oils. The EDX results (Fig. 4-14) also presented the significantly lower Ca concentration in the reaction film, and the ATR-FTIR result (Fig. 4-20) confirmed that only CVTF+acid formed phosphate (PO_4) reaction film probably because of the different ratio between Ca and P on steel surface.

The carboxylic acid is relatively chemically active due to the chemical structure, and some reports mentioned the interaction with the other additives [54, 83]. In this study, the surface analysis results suggest the interaction against the overbased Ca detergent. The $CaCO_3$ (Ca carbonate), the core of the detergent, prefers to adsorb onto steel surface [171], and tends to react with the other additives forming the reaction film [96, 97]. Therefore, oleic acid could interact with $CaCO_3$ on the steel surface and neutralised it as follows;

$$2RCOOH + CaCO_3 \rightarrow Ca(RCOO)_2 + H_2O + CO_2 \quad (R = C_{17}H_{33})$$

Oleic acid was changed into calcium oleate by the reaction which could not form the adsorption film on steel due to losing the carboxylic acid structure as reported by Ratoi [64]. In addition, this reaction appears to be dominant only at 100°C as the TE77 results shown in Fig. 4-25. The study reported by Hone [183] regarding mechanism of acid neutralisation by overbased detergent supports this assumption. The interaction between the acid and the detergent tends to become weaker at low temperature.

7.4.2. Chemical Nature of Oleic Acid on Paper Surface

Oleic acid presented the consistent FM effect with PAO or the CVTF additives, however, the surface analysis results and the durability test results indicate the presence of different working mechanisms. The chemical interaction seems to be present when formulated with the additives. In terms of the PAO formulation, the XPS C 1s detailed

scan detected the peaks derived from O-C=O and O-C-O / C=O bonds on the post-test TE77 paper clutch plate after the TE77 test at 100°C (Fig. 5-13). These peak positions are comparable to those observed at steel/steel contact. However, the surface adsorption should be also controlled by the hydrogen bonds onto the cellulose fibre because the reaction between carboxylic acid and hydroxyl groups of the cellulose fibre requires the severe condition [150, 184-186]. The number of previous works that assessed the chemical nature on the paper clutch surface is quite limited, though, Zhao [51, 92] proposed the adsorption mechanism of the amine or amide FMs on the paper clutch by the electrostatic interaction. Taking into account that PAO+acid slightly decreased the effect after the MTM durability tests at 100°C (Fig. 6-13), it suggests that small amount of oleic acid was chemically adsorb on paper only at 100°C because the decomposition temperature of oleic acid is higher than 200°C [187].

The behaviour of oleic acid appeared to be different in the presence of the CVTF additives. Interestingly, Ca and P were detected on the post-test paper by XPS only for CVTF+acid at 100°C (Table 5-2). The adsorption of Ca or P additives on the paper clutch material was also reported by Zhao [92, 93]. Zhao evaluated the μ-V performance of the FMs using the clutch tester at severe condition (121°C, 16 hours durability test), and Ca ($CaCO_3$) and P were detected by XPS on the post-test paper clutches. In this study, the intensive interaction between oleic acid and the additives formed the tribochemical film consisting of Ca and P only in this condition. The XPS survey result also shows the higher concentration of O for CVTF+acid, which should be attributed to $CaCO_3$ and the phosphite as well as oleic acid on the paper surface. In the XPS C 1s spectrum of CVTF+acid at 100°C (Fig. 5-14), the peaks derived from O=C-O, O-C-O and C-O bonds were detected, which implies the adsorption of oleic acid on the surface. In addition, the peak intensity of C-O at 286.9 eV was much stronger than the other samples. It is considered that the peak would be partially attributed to C-O-Ca or C-O-P bonds [182, 188] formed by the tribochemical reaction. The reaction between oleic acid and the detergent did not occur on the paper clutch probably due to the much lower contact pressure at the paper/steel contact (6.0 MPa) compared to the steel/steel contact (1.0 GPa). The dependence of the contact pressure on the chemical interactions and the friction properties was reported by Derevjanik [94].

Interestingly, the effect of oleic acid diminished after the durability test in the presence of the CVTF additives (Fig. 5-41). In contrast to the initial test result, the XPS survey

scan did not detect Ca or P on the surface (Table 5-7), and the C-O peak intensity in the C 1s spectrum got much weaker than that of the initial test (Fig. 5-45). These results indicate that the Ca/P film initially formed on the paper was removed during the durability test. The ATR-FTIR spectrum of the post-test lubricant shows the increase of the ester bond indicating thermal oxidation of oleic acid. On the other hand, the increase of the carboxylic acid was also detected, which should be produced by the degradation of the other additives [189, 190] and possibly inhibited oleic acid by disrupting the formation of the ordered film structure [85]. The ATR-FTIR spectrum of the post-test MTM plate showed the higher peaks derived from carboxylic acid and imide (dispersant) compared with the initial test (Fig. 6-28). It implies that the interaction between oleic acid and the dispersant accelerated the adsorption of the dispersant on the surface, though, further study is necessary to understand the detailed mechanism.

7.4.3. Summary on the Working Mechanism of Oleic Acid

Oleic acid experienced the strong interaction with the additives, which potentially diminish its effect. There would be three factors, the high contact pressure, the presence of the additives and the long-term sliding, which could be the trigger to degrade oleic acid (Table 7-3). Schematic representation of the surface chemistry is shown in Fig. 7-6. The interaction with the calcium carbonate ($CaCO_3$) inhibited the friction reduction on steel (Fig. 7-6(b)), while it did not occur on the paper clutch due to the low contact pressure (Fig. 7-6(d)). This property is ideal for the CVTF since it enables to satisfy the opposite requirement; high friction coefficient at steel belt-pulley and a good μ-V property at the paper clutch system, by controlling the interaction with the other additives. The drawback is that oleic acid tends to lose the effect after the long-term sliding due to the thermal and oxidative degradation. It is necessary to compensate the long-term effect with the other FMs.

Table 7-3. Factors that affect the effect of oleic acid at 100°C

	PAO+acid			CVTF+acid		
	Steel /steel	Paper/steel		Steel /steel	Paper/steel	
		Initial	durability		Initial	durability
High contact pressure	✓			✓		
CVTF additives				✓	✓	✓
Long-term sliding			✓			✓
FM effect*	✓	✓	✓		✓	

* Friction reduction at steel/steel contact, and μ-V performance at paper/steel contact

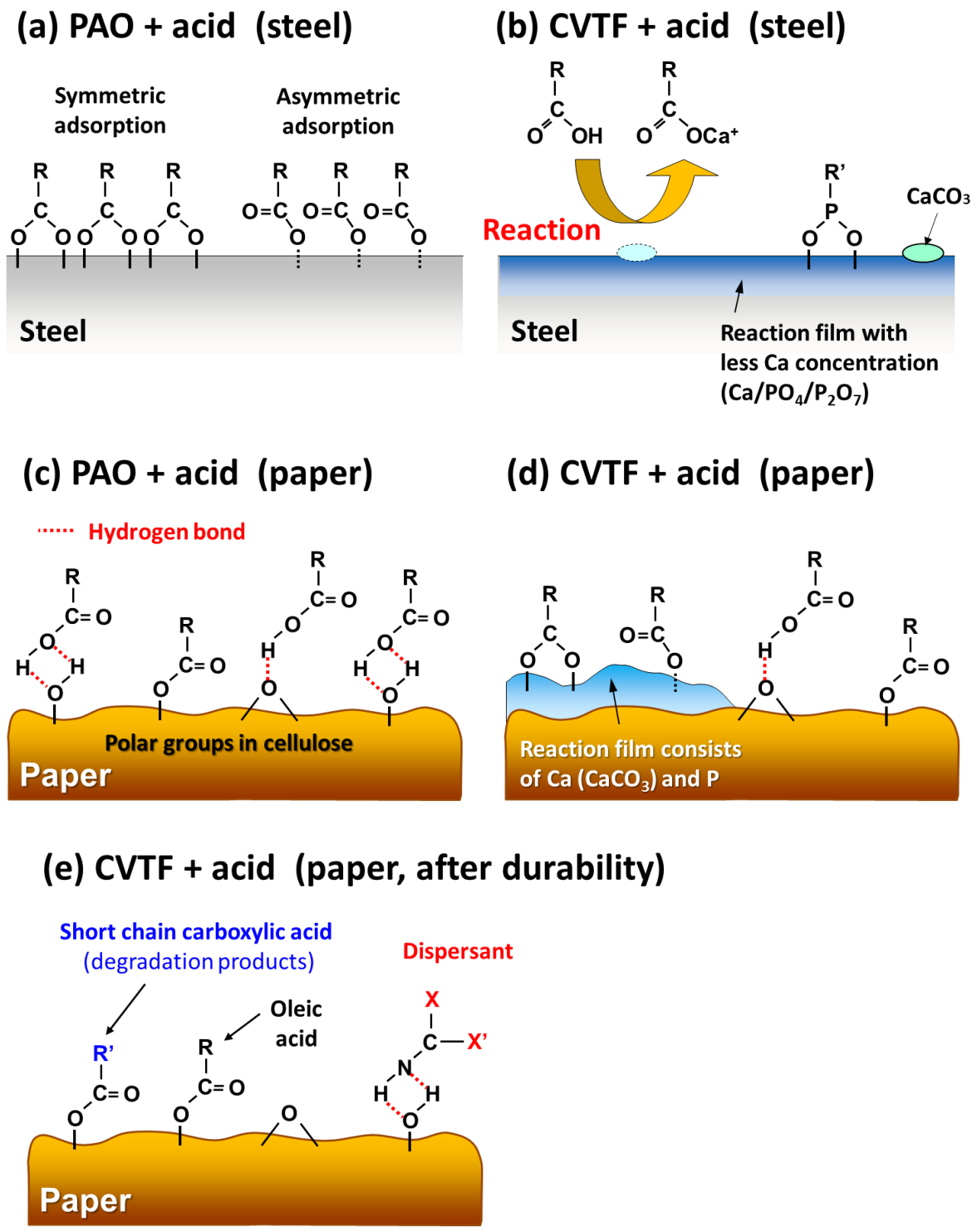

Fig. 7-6. Schematic representation of the chemical nature of the oleic acid at the 100°C (a) PAO+acid on steel, (b) CVTF+acid on steel, (c) PAO+acid on paper, (d) CVTF+acid on paper, (e) CVTF+acid on paper after the 16 hours durability test

7.5. Working Mechanism of GMO

7.5.1. Activation Mechanism of GMO

The effect of GMO appeared to be enhanced in the severe sliding conditions; at the high pressure on the steel, in the presence of the additives or the long-term sliding. These results imply that GMO could be changed into an effective FM structure during the sliding test in contrast to oleic acid that was degraded.

When added into PAO, GMO showed a significant friction reduction effect at the TE77 steel/steel contact at 100°C (Fig. 4-1). Considering the electrical contact resistance close to the maximum value (Fig. 4-2) and the good anti-wear performance (Fig. 4-6), GMO could form a stable adsorption film as oleic acid. Looking at the XPS C 1s spectrum with exactly the same peak positions as oleic acid, GMO appeared to be able to adsorb on steel as the symmetric or the asymmetric coordination (Fig. 7-5), which means some of GMO molecules were decomposed into carboxylic acid. Kano [69] confirmed the GMO decomposition into acid by the tribochemical reaction on DLC using TOF-SIMS. The high test temperature seems to be necessary to activate GMO since the very severe wear (Fig. 4-21) and the low electrical contact resistance (Fig. 4-22) were observed at 40°C. The minor friction modification effect of GMO at 40°C was also reported by Tasdemir [81].

Interestingly, GMO showed the excellent friction reduction effect at 100°C and 40°C conditions when formulated with the CVTF additives (Fig. 4-3 and Fig. 4-23). Looking at the XPS C 1s spectrum, the peaks derived from O=C-O and O-C-O bond were detected (Fig. 4-15 and Fig. 4-35) comparable to the spectrum of PAO+GMO at 100°C, which implies the decomposition of GMO. This result means that the polar additives, such as the detergent or the phosphorous anti-wear agent, interacted with GMO helping the decomposition. There are a large number of reports regarding synergetic or antagonistic interactions between the FM and the other additives [83, 94, 118].

The test temperature and the additives are the key factors to decompose and activate GMO changing it into the carboxylic acid structure. The schematic images for the assumed chemistry of GMO on the steel surface are summarised in Fig. 7-7.

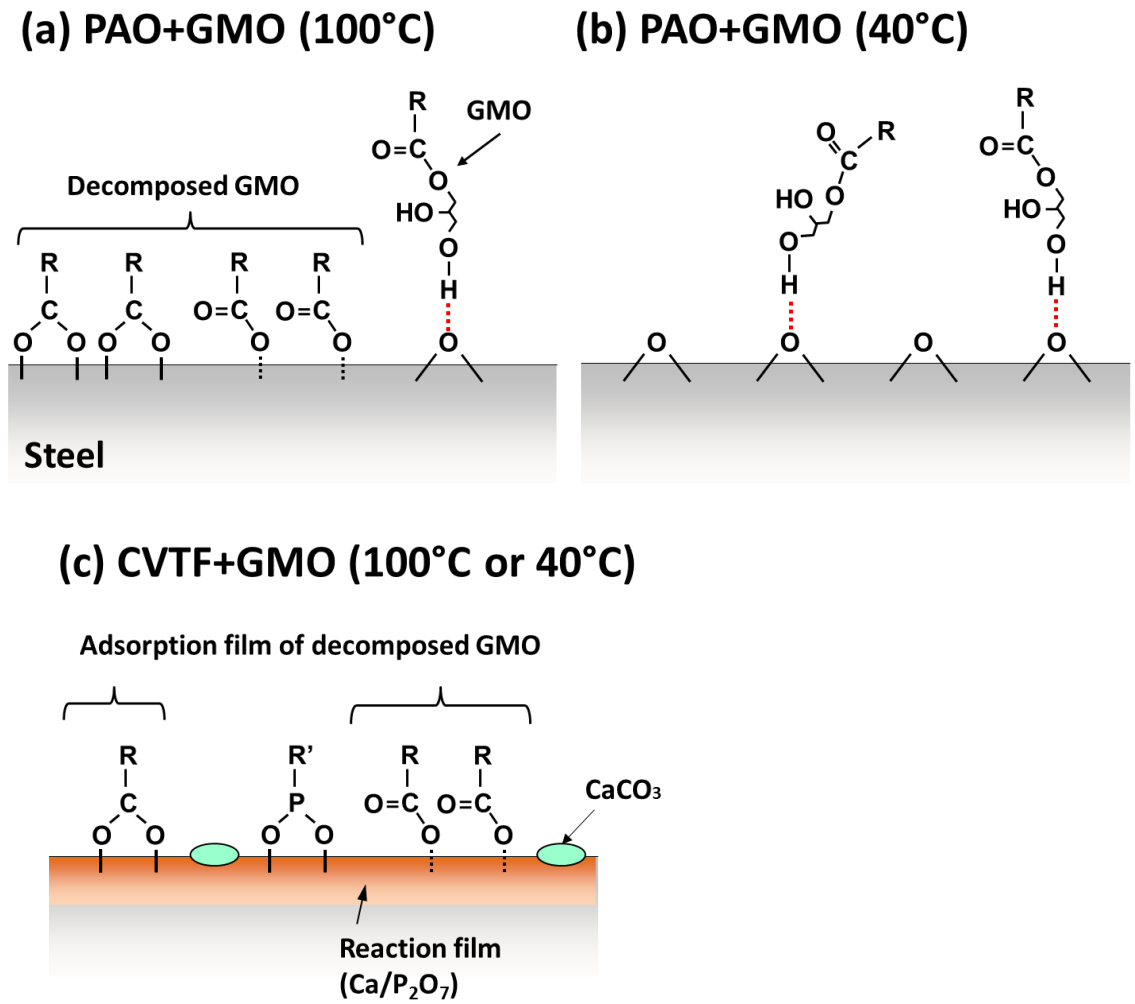

Fig. 7-7. Schematic representation of the chemical nature of GMO on steel
(a) PAO+GMO at 100°C, (b) PAO+GMO at 100°C, (c) CVTF+GMO at 100°C or 40°C

7.5.2. Chemical Nature of GMO on Paper Surface at 100°C

The distinctive tribotest result at the paper contact is the MTM μ-V characteristics of PAO+GMO at 100°C that showed a negative relationship (Fig. 6-1), while GMO showed an excellent μ-V performance in all the other conditions. It is interesting the TE77 results for PAO+GMO presented the friction reduction effect (Fig. 5-1) and the poor FFWI (Fig. 5-5) simultaneously at 100°C. The reason is considered to be the deposition of GMO onto paper surface as expected from the SEM image of the post-test paper plate (Fig. 5-9). The deposit made the paper surface flat leading to the lower friction, however, it could not improve the μ-V characteristics because the surface roughness is one of the key factors to achieve the positive relationship [84, 86, 87].

Although a large amount of GMO would be present on the surface as shown in the ATR-FTIR result (Fig. 5-16), it was not able to work effectively due to the surface topography. In addition, it seems that the decomposition of GMO did not occur in contrast to the steel contact due to the low contact pressure. Since the μ-V performance of PAO+GMO became better after the 100°C durability test (Fig. 5-41 and Fig. 6-20), the long-term thermal load could gradually decompose GMO into carboxylic structure that is effective for the friction modification. The ATR-FTIR spectra of the post-test PAO+GMO oil after the durability tests presented a minor decrease of peaks attributed to the alcohol and the ester groups (Fig. 6-25), which should be the evidence of the GMO decomposition by the tribochemical reaction on the clutch surface.

The behaviour of GMO seems to change in the presence of the CVTF additives. While the friction reduction effect was comparable to PAO+GMO, the improvement of the μ-V property was confirmed both by the FFWI of TE77 (Fig. 5-7) and μ ratio of MTM (Fig. 6-2). In addition, the deposit of GMO on the paper was not observed in the SEM image (Fig. 5-10). These results imply existence of the interaction between GMO and the additives, and it is assumed that GMO was decomposed into carboxylic acid by the tribochemical reaction as assumed at the steel/steel contact (Fig. 7-7) with the help of the additives, resulting in the better μ-V performance. The decomposition appeared to be accelerated during the durability test. The friction results evaluated using TE77 (Fig. 5-41) and MTM (Fig. 6-15) showed the improvement of the μ-V properties as the test time increased, which implies that the formation of the tribochemical reaction film of GMO. The XPS C 1s spectrum of the post-test TE77 plate (Fig. 5-14) showed an additional peak derived from O-C-O bond at 288.2 eV compared with the initial spectrum possibly due to the film formation during the durability. In addition, the ATR-FTIR difference spectra of CVTF+GMO after the durability test showed the decrease of the peaks derived from alcohol and ester bond (Fig. 6-26), which is able to support this assumption.

In summary, the decomposition of GMO also plays an important role on the paper, and the presence of the CVTF additives or the long-term sliding appeared to be the key factors to promote the reaction. PAO+GMO could not improve the μ-V property initially due to the low contact pressure in contrast to the steel contact. The schematic images for the chemical nature of GMO on the paper surface at 100°C are summarised in Fig. 7-8.

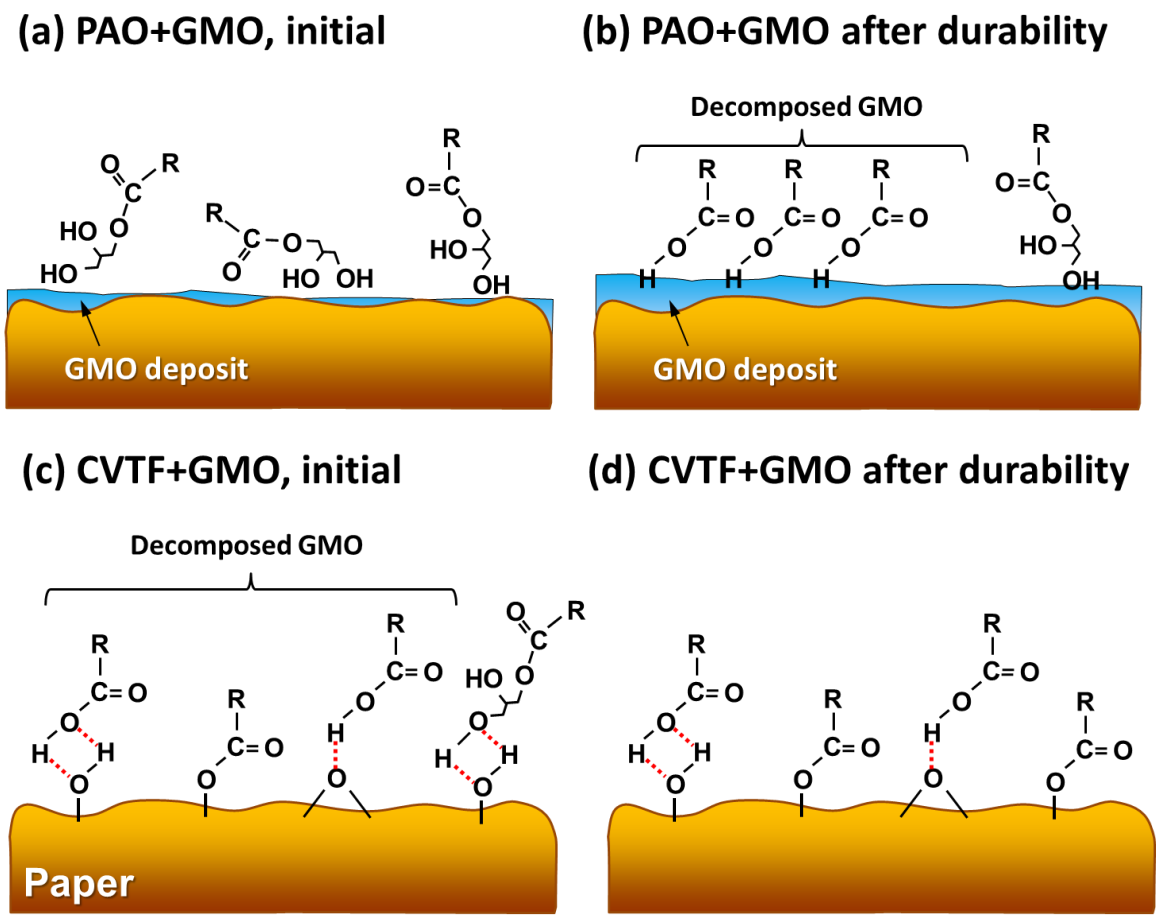

Fig. 7-8. Schematic representation of the chemical nature of GMO on paper at 100°C (a) PAO+GMO, initial (b) PAO+GMO after durability (c) CVTF+GMO, initial (d) CVTF+GMO after durability

7.5.3. Dependence of GMO Behaviour on Temperature

The effect of GMO on the paper material seems to have a different working mechanism at 40ºC because PAO+GMO presented showed a good μ-V performance at 40ºC in contrast to the 100ºC result. The decomposition of GMO should not occur on paper at 40ºC since it did not at 100ºC considering the chemical potential. Therefore, the GMO film at 40ºC appears to be the adsorption film of GMO itself, which could be formed by the hydrogen bonds against the cellulose fibre and more stable than at 100ºC due to the low molecular activity.

The MTM durability test result using the combined sequence showed good agreement with the assumption. The μ-V characteristics of the GMO formulation at 40°C measured with the combined sequence (Fig. 6-22) presented much better performance

than those measured with the standard sequence at 40°C (Fig. 6-16). In order to consider the reason, the hysteresis of the μ-V characteristics of PAO+GMO after 16 hours of the MTM durability test with the combined sequence is checked as shown in Fig. 7-9. As mentioned in Chapter 3, the measurement starts at the lowest speed (0.01 m/s), increasing to the highest speed (2.4 m/s), then, coming back to the lowest speed (0.01 m/s). Basically, the μ-V property did not show any hysteresis as shown in Fig. 7-9(b), however, only the exceptions were the GMO formulations at 40°C measured with the combined sequence. The friction at the start of the measurement was lower than that at the end, and the overall friction at the up speed region was also lower than the down speed region as shown in Fig. 7-9(a). The combined sequence would cause the hysteresis of the GMO because the 40°C μ-V measurement was performed after the 100°C measurement. Although the decomposed GMO film formed on the paper during the 100°C measurement was capable of working effectively at the start of the 40°C measurement, it would be removed gradually since the new film could not be regenerated at 40°C. This result indicates the GMO film was mainly formed by the tribochemical reaction of the decomposed GMO at 100°C, while the adsorption film formed by the hydrogen bonds was dominant at 40ºC.

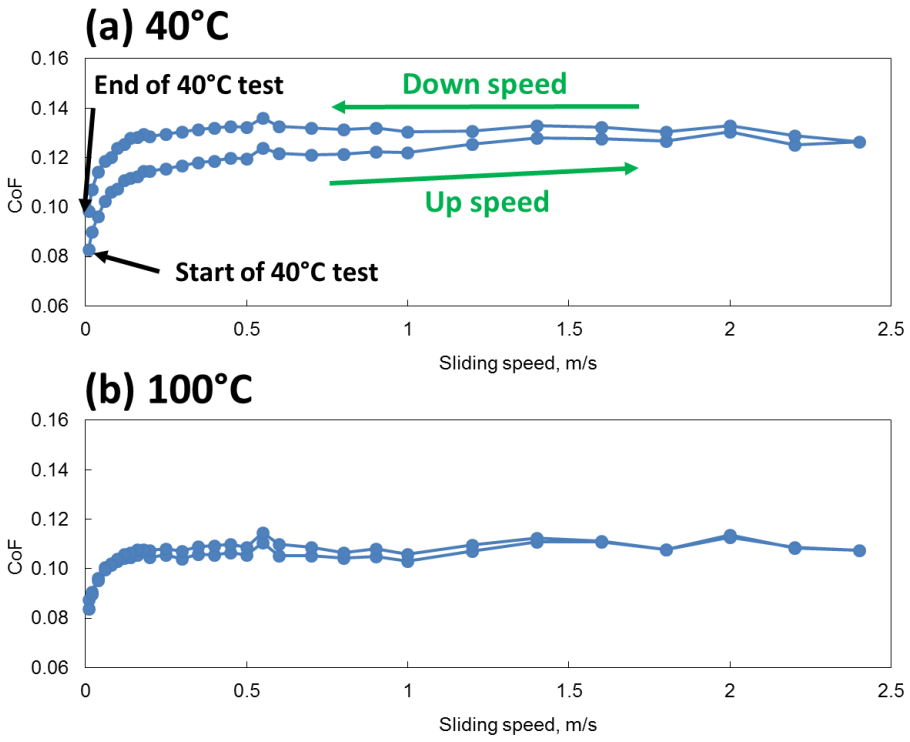

Fig. 7-9. Hysteresis of μ-V property of PAO+GMO at (a) 40°C and (b) 100°C after 16 hours of MTM durability test with the combined sequence

7.5.4. Summary on the Working Mechanism of GMO

There are three factors to explain the effect of GMO at 100°C; the high contact pressure, the presence of the additives and the long-term sliding. They are exactly the same as the factors for oleic acid to promote the degradation, however, they works opposite way for GMO activating it to enhance the FM effect. As a result, only PAO+GMO did not show the FM effect on the paper material. The difference is reasonable considering the chemical structure of GMO synthesised by esterification between oleic acid and glycerine. The carboxylic acid structure in GMO is protected as the ester bond. It could be decomposed gradually by the thermal load with the help of the CVTF additives, resulting in the long-term effect at the paper clutch keeping the excellent μ-V performance for a long time. In addition, GMO is capable of forming the adsorption film on the paper at 40°C without the decomposition due to the lower molecular motility. The mechanism appears to be independent of the film formation by the decomposed GMO at 100°C.

Table 7-4. Factors that affect the effect of GMO at 100°C

	PAO+GMO			CVTF+GMO		
	Steel /steel	Paper/steel		Steel /steel	Paper/steel	
		Initial	durability		Initial	durability
High contact pressure	✓			✓		
CVTF additives				✓	✓	✓
Long-term sliding			✓			✓
FM effect*	✓		✓	✓	✓	✓

* Friction reduction at steel/steel contact, and μ-V performance at paper/steel contact

7.6. Application of FMs to CVTF

Oleic acid presented the ideal performance for the application to the CVTFs; it is possible to improve the μ-V characteristics at the paper clutch system, while keeping the high friction at steel belt-pulley mechanism. This property is attributed to the interaction between oleic acid and the overbased calcium detergent, one of the CVTF additives. Oleic acid is capable of reacting with the detergent only on the steel contact condition assisted by the tribochemical reaction at the high contact pressure, leading to the less friction reduction effect. The main parameters which controls this interaction is

the polar group type of the FM and the detergent structure. As the FM polar group, it is considered that the carboxylic acid structure appears to be a key structure because the hydroxyl group (oleyl alcohol or GMO) or the ester group (GMO) did not show this phenomena. In addition, the minor FM effect of the metal oleate was reported by Ratoi [64, 191]. Therefore, the carboxylic acid is essential to induce this interaction. In contrast, there would be some options for the detergent structure. As reported by Derevjanik [94], types of the detergents could be categorised by the metal species (generally Ca or Mg), the metal carbonate core size or the alkyl dispersant structure (generally sulfonate, salicylate or phenate), and they affects the interaction with the FM. Further study is necessary to recognise the detailed effect from the detergent structure, though, the combination of the carboxylic acid FM and the appropriate detergent should be the key factor to satisfy the frictional requirements of the CVT.

The drawback of oleic acid is the long-term durability. The carboxylic acid structure was degraded gradually under the thermal load due to the high chemical activity, losing the effect after the long-term sliding. GMO is capable of compensating the performance, which is able to decompose into the carboxylic acid structure by the thermal load in contrast to oleic acid. This performance is attributed to the chemical structure of GMO synthesised by the esterification between oleic acid and glycerine. GMO could be decompose at the ester bond by the thermal load with the help of the CVTF additives, turning into the carboxylic acid structure showing the excellent FM effect. The decomposition of GMO due to the tribochemical reaction on DLC surface was reported by Kano [69], and Zhao [51, 92] proposed the similar mechanism on the durability of paper clutch performance using the amide FM, in which the decomposition at the amide bond was essential to maintain the μ-V performance. It would be possible to control the decomposition speed of GMO by replacing the ester bond with the other structure such as amide bond, or changing the surrounding chemical environment to modify the bond dissociation energy for the ester bond.

In summary, the combination of oleic acid and GMO should be appropriate for the application to CVTF. The high friction coefficient on steel, the μ-V performance at the paper clutch and the long-term effect can be satisfied simultaneously by controlling the interactions between the FMs and the CVTF additives. Further research is necessary in order to recognise the detailed interaction mechanisms, which will be useful to customise the CVTF formulation optimum for the CVT mechanism.

Chapter 8 – Conclusions and Future Work

8.1. Conclusions

This study aim was to elucidate the behaviour of the FMs in CVTFs and reveal the appropriate chemical structure to satisfy the frictional requirements.

The number of cars which are equipped with the CVT is increasing due to the excellent fuel efficiency in order to achieve the legislative targets for CO_2 emissions. The CVT requires the complicated friction control for the lubricant; high torque capacity at the steel belt-pulley mechanism and a positive μ-V relationship at the lock-up clutch system. It means the friction coefficient at low speed needs to be controlled at a high value at the steel/steel contact, while at a low value at the paper/steel contact. It is ideal if the FM could work only on the paper surface for satisfying these opposite requirements, and the interaction between the FM and the other factors, such as the type of the substrate, the presence of the other additives or temperature, is considered to be essential to realise the selective behaviour of the FM. There have been a large number of reports investigating the working mechanism of FMs on metal surface, while only a few studies have focused on the effect on the paper clutch material. In addition, the studies tried to assess the chemical nature of the additives on the paper surface are quite rare, although it seems to be necessary to understand the exact behaviour of the FMs. The novelty of this work is that the working mechanism of the FMs on the steel and the paper surface were discussed based on the chemical nature assessed by the surface analyses as well as the frictional properties evaluated by the tribometers.

Three types of the FMs were chosen for this study; oleic acid, oleyl alcohol and glycerol monooleate (GMO). They are commonly used in the commercial transmission fluids, and their simple chemical structure was useful to consider the working mechanism. The FMs were formulated in two types of the base fluids; PAO and the model CVTF. The pure effect was investigated when added in PAO, while the interactions of the FMs with the other additives could be observed using the model CVTF formulations. Two types of the tribometers were utilised to evaluate the frictional properties of the test lubricants; TE77 and MTM. The TE77 reciprocating test was performed at both the steel/steel and paper/steel configuration to simulate the lubrication at the belt-pulley and the lock-up

clutch in the CVT, respectively. The correspondence between the TE77 steel friction and the belt-pulley had been confirmed by previous literature, and the small test specimen size was also an advantage considering the surface analyses. The disadvantage of TE77 was on the reciprocating motion at the paper/steel contact test, which was different from the actual clutch engagement motion. In order to deal with the issue, the MTM pure sliding test was also performed to evaluate the μ-V characteristics at the paper/steel contact. The tribotests were conducted at both 100°C and 40°C in order to investigate the effect of temperature, and the long-term sliding test at the paper/steel contact was performed for some lubricants for the detailed estimation on the working mechanism of the FMs. In summary, the effect of the following factors on the frictional properties and the interactions were investigated in this study;

- Type of the polar group in the FMs
  – Carboxylic acid (oleic acid), alcohol (oleyl alcohol and GMO) or ester (GMO)
- Base fluid – PAO or the model CVTF
- Type of the substrates – Steel or the paper clutch material
- Test temperature – 100°C (high temperature) or 40°C (low temperature)
- Test duration – Initial (TE77 60 mins tests or MTM initial performance tests)
  or Long-term (TE77 durability tests or MTM durability tests)

The post-test specimens were investigated using the following surface analysis techniques; WLI, SEM, EDX, XPS and ATR-FTIR. WLI and SEM were applied to observe the surface topography, while EDX, XPS and ATR-FTIR were utilised to assess the chemical nature on the substrate surface.

The results for the TE77 steel contact condition are shown in Chapter 4. The following friction reduction effects were observed for each of the FMs;

- Oleic acid – Friction reduction in all the conditions except for the 100°C test with the CVTF additives
- Oleyl alcohol – Negligible effect in all the conditions
- GMO – Friction reduction in all the conditions, though the 40°C test with PAO showed severe wear on the post-test steel pin

Since the XPS C 1s detailed scan detected the O=C-O (carboxylate) or O-C-O on the post-test steel plates that showed the friction reduction effect, the FM film on the steel surface was considered to consist of these structures effective to reduce the friction. In

addition, GMO appeared to be decomposed into the carboxylic acid at 100°C or in the presence of the CVTF additives. The steel contact results indicate that the behaviour of oleic acid is useful for formulating the CVTF because it did not reduce the friction at steel in the presence of the additives. The surface analysis results implied the interaction between oleic acid the calcium detergent on the steel surface, which inactivated the oleic acid losing its friction reduction effect. This process occurred only when the following factors were satisfied; high contact pressure (steel/steel contact), high temperature (100°C) and the presence of the CVTF additives.

The FM effect at the paper clutch material was investigated in Chapter 5 using TE77 and in Chapter 6 using MTM. The initial performance was evaluated for all the FMs, and in addition, the durability tests were performed for oleic acid and GMO. The overall frictional trends were summarised as below.

Initial performance;

- Oleic acid – Excellent μ-V performance in all the conditions
- Oleyl alcohol – Slight effect in PAO, and negligible effect with the CVTF additives
- GMO – Excellent performance when formulated with the CVTF additives, while negligible effect in PAO at 100°C

Long-term performance;

- Oleic acid – The μ-V performance gradually became worse at the 100°C with the additives, while it was almost stable in the other conditions
- GMO – The performance gradually became better in all the conditions except for the 40°C durability test with PAO

Oleic acid showed the good μ-V characteristics in all the initial test conditions, though, the XPS results revealed that the mechanism was different depending on the conditions. The interaction among the oleic acid and the other additives played an important role at 100°C test for the CVTF formulation, while the adsorption film formation on the cellulose fibre based on the hydrogen bond seemed to be dominant in the other conditions. This mechanism should be the reason why CVTF+acid lost the FM effect after the 100°C durability test. The interaction degraded oleic acid into the ester structure with less FM effect as assumed from the ATR-FTIR results for the post-test oil.

This process did not occur in the other conditions due to the absence of the CVTF additives or the less chemical potential at low temperature.

In contrast, the long-term μ-V performance of GMO at 100°C became better gradually during the durability steps, especially formulated with the CVTF additives. This result indicates that the decomposed GMO was capable of forming the effective adsorption film on the paper surface comparable to the steel contact results, and the following factors could promote the process; high temperature (100°C), the CVTF additives and the long-term thermal and sliding load. The assumed mechanism was confirmed by the XPS C 1s spectra showing the strong peaks derived from carboxylate (O=C-O) or carboxylic acid (COOH) on the post-test papers as well as the ATR-FTIR spectra of CVTF+GMO oils after the 100°C durability test showing a significant decrease of the ester bond peak. Interestingly, the working mechanism of GMO was different at 40°C. It appeared to be able to form the effective adsorption film without the decomposition as assumed from the MTM durability test results using the combined sequence. Therefore, it is considered that the behaviour of GMO was controlled by the decomposition at 100°C, while the adsorption film formation was dominant at 40°C.

The weak FM effect of oleyl alcohol should be attributed to the hydroxyl polar group whose adsorption was inhibited by the CVTF additives. Comparing with the effect of GMO which has two hydroxyl groups in its chemical structure, the ester bond played an important role for the distinctive performance of GMO.

This study revealed that the interaction between the FMs and the other additives is the key factor to achieve the friction control required for the CVTF. The effect of the FMs on steel could be inhibited by the interaction with the other additives, as seen between oleic acid and the calcium detergent, which could be essential to satisfy the opposite requirements at the CVT components; higher friction at the steel belt-pulley and lower friction at the paper clutch systems. The drawback of this approach is that the FM needs to be chemically active to induce the interaction, therefore, the FM tends not to be robust for the degradation caused during the long-term use. The interaction could be utilised to deal with the issue. As the example of GMO, it is possible to design the FM structure to be decomposed into the effective chemical structure gradually during the long-term sliding by the interaction with the other CVTF additives. In summary, the FM effect could be controlled by the interaction with the additives as well as the type of the polar group of the FMs. Therefore, it could be possible to optimise the effect by

modifying the chemical structure of the other additives. The other parameters such as temperature or the type of substrates have an influence on the possibility of the interaction.

The behaviour of the FMs elucidated through this study will be able to contribute significantly to the development of the CVTFs suggesting the appropriate formulation of the FMs. In addition, the gained knowledge on the working mechanism of the FMs must be useful for designing all types of the lubricants.

8.2. Future Work

8.2.1. Interaction Mechanism between Oleic Acid and the Other Additives

This study indicates the importance of the interactions between the FMs and the other additives in order to manage the frictional properties. Particularly, it was revealed that the reaction between oleic acid and the calcium detergent on steel inactivates oleic acid, which is capable of achieving the high friction value on the steel components. However, the other CVTF additives, the phosphorous anti-wear agent or the dispersant, might also affect this process because they were detected on the post-test steel surface by XPS and the phosphate structure was observed in the reaction film only in this condition. In addition, the molecular structure of the detergent also has an influence on the interaction. Further investigation on the detailed mechanism about the interactions between oleic acid and the other additives will be helpful to realise the precise friction management on the steel surface. The friction tests and the surface analyses using the oleic acid test oils formulated with the different types of the detergents, the dispersants or the phosphorous anti-wear agents will be able to give good suggestions on the mechanism. Regarding the surface analysis techniques, Raman spectroscopy would be useful to assess the further information on the chemical structure of the reaction film [192, 193].

8.2.2. Activation Mechanism of GMO

The durability test results for the paper/steel contact indicated the improvement of the μ-V performance of GMO during the long-term sliding load. Although the IR spectra of the post-test oils and the XPS C 1s spectra could give the assumption that GMO turned into an active chemical structure such as carboxylic acid, further study should be necessary to elucidate the detailed mechanism. There would be two topics to be

discussed; the exact chemical structure of the decomposed GMO and the detailed interaction mechanism between GMO and the other additives. Schematic representation is shown in Fig. 8-1.

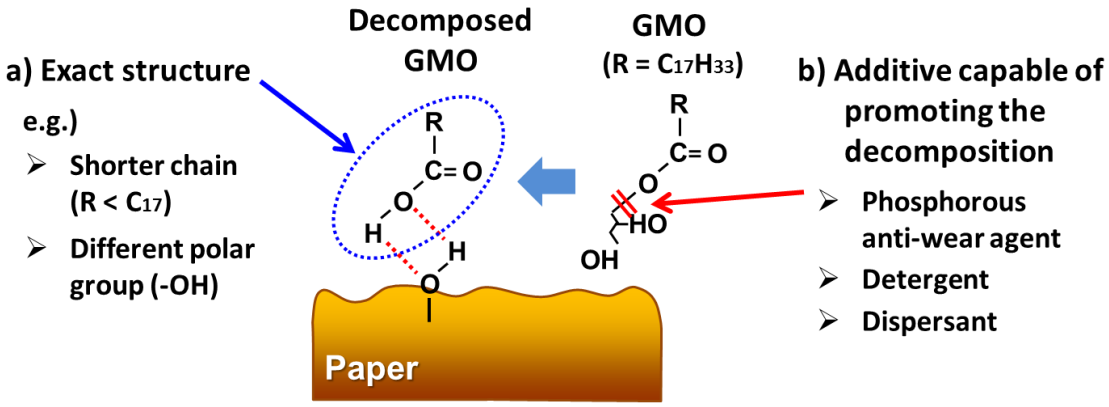

Fig. 8-1. Schematic representation about the GMO activation mechanism to be discussed

The information on the exact chemical structure of the activated GMO is essential in order to understand the mechanism of the long-term friction modification effect. Although it was estimated that the ester bond of GMO was decomposed, the exact chemical structure is still unclear. TOF-SIMS analysis of the post-test plate surface or mass spectroscopy of the post-test oils will give a good suggestion on it.

Furthermore, the interaction between GMO and the other additives played an important role on this process considering that the activation of GMO was accelerated in the presence of the additives at 100°C. Based on the IR spectra of the post-test oil showing a slight peak decrease derived from the P-O-C bond, the phosphorous anti-wear agent possibly related with the decomposition of GMO. However, the detailed behaviour should be investigated to gain the knowledge for the control of the long-term FM activity. Some clues could be given through the tribotests using the simple formulation with GMO (e.g. GMO only with the phosphorous additive, the detergent or the dispersant).

These studies will be able to reveal the mechanism of the long life FMs, which will be useful to design the novel FMs with a superior durability.

8.2.3. Effect of the Polar Group Structure of the FMs

The effectiveness of the ester group as the polar group of the FMs was recognised by the comparison between oleyl alcohol and GMO. However, there would be a possibility that the two hydroxyl groups in GMO did have a contribution to the distinctive FM effect of GMO. The investigation of methyl oleate and ethylene glycol monooleate (Fig. 8-2) will give a good suggestion if the hydroxyl groups in GMO would have the effect on the friction modification. This approach will be also useful to design new FMs capable of improving the clutch performance.

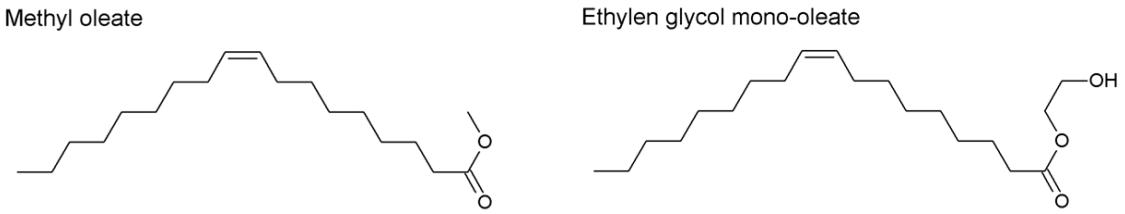

Fig. 8-2. Molecular structures of methyl oleate and ethylene glycol monooleate

8.2.4. Effect of the Hydrocarbon Chain Structure of the FMs

In this study, the hydrocarbon chain of the FMs was oleic structure in common. As generally known, the length or the structure of the hydrocarbon chain have an influence on the FM performance [85]. Hence, it should be worth to confirm their effect on the additive interactions as well as the frictional properties. For example, stearic acid, lauric acid or caprylic acid could be applied in order to estimate the effect of the hydrocarbon structure of carboxylic acid. If some of the results show the different trend from oleic acid, it would be possible to arrange the frictional properties by controlling the chemical interactions with the use of the FM with a different hydrocarbon chain structure.

8.2.5. FMs' Behaviour on the Paper Material at Low Temperature

While the chemistry of the FMs on the paper could be well understood by the XPS analysis at 100°C, the XPS results at 40°C showed a similar trend among the FMs despite the different friction values. The reason should be the different working mechanism of the FMs between 100°C and 40°C; the FMs were capable of forming the consistent bonds against the paper surface at 100°C, while the physical adsorption was

dominant at 40°C. It is considered that the adsorption film formed at 40°C was washed out by the rinsing with heptane. Therefore, a new surface analysis technique is necessary in order to discuss the adsorption film structure at the low temperature condition.

An ideal procedure should be the adsorption film analysis in the liquid phase, which does not need to wash the post-test specimen. Although there have been several attempts of the liquid phase analysis using *in-situ* ATR-FTIR [194, 195] or AFM [68], these methods could not be applied for the paper material since the smooth or reflective surface is required. In terms of the discussion on the affinity between the FMs and the paper material without considering the tribochemical reaction, a column chromatography using the cellulose fibre will give a good suggestion. The longer retention time means the stronger affinity, so that it is possible to discuss the correspondence between the physical adsorption strength and the friction value. Since the chemical nature of the FMs on the paper clutch material has not been investigated in great detail, it has a significant impact on the transmission fluid development to establish the analysis techniques.

References

1. European Commission. *Reducing CO_2 emissions from passenger cars*. [cited 2014 27th Nov.]; Available from:http://ec.europa.eu/clima/policies/transport/vehicles/cars/index_en.htm.
2. Mock, P. *EU CO_2 standards for passenger cars and light-commercial vehicles*. ICCT - policy update, 2014.
3. Tseregounis, S.I., M.L. McMillan, and R.M. Olree, *Engine Oil Effects on Fuel Economy in GM Vehicles -- Separation of Viscosity and Friction Modifier Effects.* SAE Technical Paper Series, 1998: 982502.
4. Hayden, T.E., C.A. Ropes, and M.G. Rawdon, *The Performance of a Gasoline Friction Modifier Fuel Additive.* SAE Technical Paper Series, 2001: 2001-01-1961.
5. Ishikawa, M., K. Yamamori, S. Hirano, T. Kowalski, and J. Linden, *Introduction of Fuel Economy Engine Oil Performance Target with New SAE Viscosity Grade.* SAE International Journal of Fuels and Lubricants, 2016. **9**(2): p. 374-382.
6. Covitch, M.J., M. Brown, C. May, T. Selby, I. Goldmints, and D. George, *Extending SAE J300 to Viscosity Grades below SAE 20.* SAE International Journal of Fuels and Lubricants, 2010. **3**(2): p. 1030-1040.
7. Spearot, J.A., *Friction, wear, health, and environmental impacts - tribology in the new millennium*, in *A keynote lecture at the STLE Annual Meeting*. 2000: Nashville, Tennessee.
8. Fraser, N., H. Blaxill, G. Lumsden, and M. Bassett, *Challenges for Increased Efficiency through Gasoline Engine Downsizing.* SAE International Journal of Engines, 2009. **2**(1): p. 991-1008.
9. Zaccardi, J.-M., A. Pagot, F. Vangraefschepe, C. Dognin, and S. Mokhtari, *Optimal Design for a Highly Downsized Gasoline Engine.* SAE Technical Paper Series, 2009: 2009-01-1794.
10. Onodera, K., T. Kato, S. Ogano, K. Fujimoto, K. Kato, and T. Kaneko, *Engine Oil Formulation Technology to Prevent Pre-ignition in Turbocharged Direct Injection Spark Ignition Engines.* SAE Technical Paper Series, 2015: 2015-01-2027.
11. Ritchie, A., D. Boese, and A.W. Young, *Controlling Low-Speed Pre-Ignition in Modern Automotive Equipment Part 3: Identification of Key Additive Component Types and Other Lubricant Composition Effects on Low-Speed Pre-Ignition.* SAE International Journal of Engines, 2016. **9**(2): p. 832-840.
12. Luo, X., H. Teng, T. Hu, R. Miao, and L. Cao, *An Experimental Investigation on Low Speed Pre-Ignition in a Highly Boosted Gasoline Direct Injection Engine.* SAE International Journal of Engines, 2015. **8**(2): p. 520-528.
13. Kurashina, H., Y. Ito, H. Isomura, and K. Yamaguchi, *A Study of Transmission fluid Performance on Fuel Economy.* SAE Technical Paper Series, 2007. **1**: p. 2007-01-1980.

14. Inukai, K., A. Shibahara, T. Uchino, N. Keiichi, Y. Murakami, and M. Kojima, *Development of High-Efficiency New CVT for Midsize Vehicle.* SAE International, 2013: 2013-01-0365.

15. Cha, S.Y., D. Whitticar, A. Gajanayake, and M. Ikeda, *Development of Next-Generation Continuously Variable Transmission Fluid Technology.* SAE International, 2012. **1**: p. 2012-01-1670.

16. Greiner, J., M. Grumbach, A. Dick, and C. Sasse, *Advancement in NVH- and Fuel-Saving Transmission and Driveline Technologies.* SAE International, 2015: 2015-01-1087.

17. Li, S., M.T. Devlin, J. Milner, R. Iyer, T.-C. Jao, M.R. Hoeprich, and T.M. Cameron, *Investigation of Pitting Mechanism in the FZG Pitting Test.* SAE Technical Paper Series, 2003: 2003-01-3233.

18. Dowson, D., *History of tribology*. 1979, London : Longman

19. Bhushan, B., *Introduction to tribology*. 2002, New York: John Wiley & Sons

20. Jost, H.P., *Economical Impact of Tribology.* Mechanical Engineering, 1975. **97**(8): p. 26-33.

21. Jost, H.P., *Tribology - Origin and Future.* Wear, 1990. **136**(1): p. 1-17.

22. Jamison, W.E., *INTRODUCTION TO TRIBOLOGY.* Journal of Vacuum Science & Technology, 1976. **13**(1): p. 76-81.

23. Neale, M.J., *The tribology handbook*. 2nd ed. 1995, Oxford ; Butterworth-Heinemann.

24. Bhushan, B., *Modern tribology handbook*. Mechanics and materials science series. 2001, Boca Raton ; CRC Press.

25. Mortier, R.M., M.F. Fox, and S.T. Orszulik, *Chemistry and technology of lubricants*. 3rd ed. 2010, Dordrecht ; New York: Springer

26. Jacobson, B., *The Stribeck memorial lecture.* Tribology International, 2003. **36**(11): p. 781-789.

27. Fuwa, Y., *Do you know the tribology for automobiles .1. Automobile and tribology.* Journal of Japanese Society of Tribologists, 1996. **41**(3): p. 223-226. (written in Japanese)

28. Goto, T., *Do you know the tribology for automobiles? .2. Engine.* Journal of Japanese Society of Tribologists, 1996. **41**(4): p. 328-331. (written in Japanese)

29. Hoshino, M., *Engine oil.* Journal of Japanese Society of Tribologists, 1996. **41**(5): p. 391-394. (written in Japanese)

30. Priest, M. and C.M. Taylor, *Automobile engine tribology - approaching the surface.* Wear, 2000. **241**(2): p. 193-203.

31. Johnson, E.R., R.M. Olree, M.L. McMillan, and S.L. Clark, *Gasoline Engine Oil Specifications, Past, Present and Global.* SAE Technical Paper Series, 2009: 2009-01-2664.

32. Murakami, Y., *Half a century of automatic transmissions for vehicles - The tribology for friction materials and fluids.* Journal of Japanese Society of Tribologists, 2005. **50**(9): p. 665-670. (written in Japanese)

33. Wagner, G., *Application of Transmission Systems for Different Driveline Configurations in Passenger Cars.* SAE Technical Paper Series, 2001: 2001-01-0882.

34. Fletcher, I., *World: In Gear: Present and Future Trends in the Global Light Vehicle Transmission Market* in *IHS Automotive: Automotive Forecasting*. 2010, IHS Automotive.

35. Prasad, M., A. Sardar, and S. Mubashir, *Transmission Technologies : An Indian Perspective.* SAE International, 2011 (2011 SIAT, India): 2011-26-0083.

36. Urquhart, T., *World: In Gear: Present and Future Trends in the Global Light Vehicle Transmission Market* in *IHS Automotive: Automotive Forecasting*. 2013, IHS Automotive.

37. Newcomb, T., C. Tipton, and T. C. Jao, *Automatic Transmission and Driveline Fluids.* SAE Technical Paper Series, 2007: 2007-01-3988

38. Yoshimura, N., *Automatic transmission.* Journal of Japanese Society of Tribologists, 1996. **41**(8): p. 659-662. (written in Japanese)

39. Ryo Ashikawa, Hideo Kurashina, Tohru Matsuoka, Takao Adachi, Takeo Nakayama, *ATF Characteristics Required for the Latest Automatic Transmissions.* SAE Technical Paper Series, 1993: 932849.

40. Takanori Kugimiya, J.i.M., Narihiko Yoshimura, Hiroyuki Kaneko, Hideaki Akamatsu, Fumio Ueda, Takanori Nakada, Shoji Akiyama, *Development of Automatic Transmission Fluid for Slip-Controlled Lock-Up Clutch Systems* SAE Technical Paper Series, 1995: 952348.

41. T. M. Camero, M. Devlin, S. Tersigni, T. C. Jao, *ATF Friction Properties and Shift Quality.* SAE Technical Paper Series, 2004: 2004-01-3027.

42. Ost, W., P. De Baets, and J. Degrieck, *The tribological behaviour of paper friction plates for wet clutch application investigated on SAE#II and pin-on-disk test rigs.* Wear, 2001. **249**(5-6): p. 361-371.

43. Kugimiya, T., N. Yoshimura, and J. Mitsui, *Tribology of automatic transmission fluid.* Tribology Letters, 1998. **5**(1): p. 49-56.

44. Abo, K. and M. Kobayashi, *Development of a New Metal Belt CVT for High Torque Engines.* SAE Technical Paper Series, 2000 : 2000-01-0829.

45. Sato, T., *Recent Trend of Metal Pushing Belt Type Continuously Variable Transmission Fluids.* Journal of Japanese Society of Tribologists, 2009. **54**(4): p. 248-253. (written in Japanese)

46. Mitsui, H., *Trends and requirements of fluids for metal pushing belt type CVTs.* Journal of Japanese Society of Tribologists, 2000. **45**(6): p. 435-440. (written in Japanese)

47. Ando, T., T. Yagasaki, S. Ichijo, K. Sakagami, and S. Sumida, *Improvement of Transmission Efficiency in CVT Shifting Mechanism Using Metal Pushing V-Belt.* SAE International Journal of Engines, 2015. **8**(3): p. 1391-1397.

48. Rudnick, L.R., *Lubricant Additives: Chemistry and Applications, Second Edition*. 2009: CRC Press.

49. Kurihara, I. and O. Kurosawa, *Design and Performance of Low-Viscosity ATF.* SAE Technical Paper Series, 2007: 2007-01-3974.

50. Spikes, H., *The history and mechanisms of ZDDP.* Tribology Letters, 2004. **17**(3): p. 469-489.

51. Zhao, H.Y., A. Morina, A. Neville, and R. Vickerman, *Tribochemistry on Clutch Friction Material Lubricated by Automatic Transmission Fluids and the Link to Frictional Performance.* Journal of Tribology-Transactions of the Asme, 2013. **135**(4): p. 041801.

52. Rudnick, L.R., *Lubricant additives : chemistry and applications*. 2nd ed. Chemical industries. 2009, Boca Raton: CRC Press.

53. Kugimiya, T., *Relationship between chemical structures of dispersant and metallic detergent and mu-nu characteristics.* Journal of Japanese Society of Tribologists, 2000. **45**(5): p. 396-405. (written in Japanese)

54. Kugimiya, T., *Effects of additives of ATF and components of friction material for AT on mu-nu characteristics.* Journal of Japanese Society of Tribologists, 2000. **45**(5): p. 387-395. (written in Japanese)

55. Gellman, A.J. and N.D. Spencer, *Surface chemistry in tribology.* Proceedings of the Institution of Mechanical Engineers Part J-Journal of Engineering Tribology, 2002. **216**(J6): p. 443-461.

56. Allen, C.M. and E. Drauglis, *Boundary Layer Lubrication . Monolayer or Multilayer.* Wear, 1969. **14**(5): p. 363

57. Spikes, H., *Friction Modifier Additives.* Tribology Letters, 2015. **60**(5). *in press*

58. Wilson, R.E. and D.P. Barnard, *The mechanism of lubrication - II Methods of measuring the property of oiliness.* Journal of Industrial and Engineering Chemistry-Us, 1922. **14**: p. 683-695.

59. Hardy, W.B. and I. Doubleday, *Boundary lubrication - The temperature coefficient.* Proceedings of the Royal Society of London Series a-Containing Papers of a Mathematical and Physical Character, 1922. **101**(713): p. 487-492.

60. Hardy, W. and I. Bircumshaw, *Bakerian Lecture - Boundary lubrication - Plane surfaces and the limitations of Amontons' law.* Proceedings of the Royal Society of London Series a-Containing Papers of a Mathematical and Physical Character, 1925. **108**(745): p. 1-27.

61. Bowden, F.P. and L. Leben, *The friction of lubricated metals.* Philosophical Transactions of the Royal Society of London Series a-Mathematical and Physical Sciences, 1940. **239**(799): p. 1-10.

62. Hutchings, I.M., *Tribology: Friction and Wear of Engineering Materials* 1992: Elsevier Limited.

63. Fuks, G.I., *The properties of solutions of organic acids in luquid hydrocarbons at solid surfaces, in B. V. Deryaguin (e.d.).* Research in Surface Forces; Translation by Consultants Bereau, New York (1966), 1964. **2**.

64. Ratoi, M., C. Bovington, and H. Spikes, *In situ study of metal oleate friction modifier additives.* Tribology Letters, 2003. **14**(1): p. 33-40.

65. Anghel, V., C. Bovington, and H.A. Spikes, *Thick-boundary-film formation by friction modifier additives.* Lubrication Science, 1999. **11**(4): p. 313-335.

66. Ratoi, M., V. Anghel, C. Bovington, and H.A. Spikes, *Mechanisms of oiliness additives.* Tribology International, 2000. **33**(3-4): p. 241-247.

67. Yoshida, K., M. Kano, and M. Masuko, *Effect of polar groups in lubricants on sliding speed dependent friction coefficients of DLC coatings.* Tribology - Materials, Surfaces & Interfaces, 2015. **9**(1): p. 54-61.

68. Kalin, M. and R. Simic, *Atomic force microscopy and tribology study of the adsorption of alcohols on diamond-like carbon coatings and steel.* Applied Surface Science, 2013. **271**: p. 317-328.

69. Kano, M., Y. Yasuda, Y. Okamoto, Y. Mabuchi, T. Hamada, T. Ueno, J. Ye, S. Konishi, S. Takeshima, J.M. Martin, M.I.D. Bouchet, and T. Le Mogne, *Ultralow friction of DLC in presence of glycerol mono-oleate (GMO).* Tribology Letters, 2005. **18**(2): p. 245-251.

70. Simic, R., M. Kalin, T. Hirayama, P. Korelis, and T. Geue, *Fatty Acid Adsorption on Several DLC Coatings Studied by Neutron Reflectometry.* Tribology Letters, 2014. **53**(1): p. 199-206.

71. Kalin, M., R. Simic, T. Hirayama, T. Geue, and P. Korelis, *Neutron-reflectometry study of alcohol adsorption on various DLC coatings.* Applied Surface Science, 2014. **288**: p. 405-410.

72. Koshima, H., H. Kamano, Y. Hisaeda, H. Liu, and S. Ye, *Analysis of the Adsorption Structures of Friction Modifiers by Means of Quantitiative Structure-Property Relationship Method and Sum Frequency Generation Spectroscopy.* Tribology Online, 2010. **5**(3): p. 165-172.

73. Li, Z.J. and W.T. Tysoe, *The adsorption of acetic acid on clean and oxygen-covered Au/Pd(100) alloy surfaces.* Surface Science, 2012. **606**(23-24): p. 1934-1941.

74. Morina, A., H.Y. Zhao, and J.F.W. Mosselmans, *In-situ reflection-XANES study of ZDDP and MoDTC lubricant films formed on steel and diamond like carbon (DLC) surfaces.* Applied Surface Science, 2014. **297**: p. 167-175.

75. Morina, A. and A. Neville, *Understanding the composition and low friction tribofilm formation/removal in boundary lubrication.* Tribology International, 2007. **40**(10-12): p. 1696-1704.

76. Zhang, J., E. Yamaguchi, and H. Spikes, *The Antagonism between Succinimide Dispersants and a Secondary Zinc Dialkyl Dithiophosphate.* Tribology Transactions, 2014. **57**(1): p. 57-65.

77. Martin, J.M., T. Onodera, C. Minfray, F. Dassenoy, and A. Miyamoto, *The origin of anti-wear chemistry of ZDDP*. Faraday Discussions, 2012. **156**: p. 311-323.

78. Belin, M., J.M. Martin, G. Tourillon, B. Constans, and C. Bernasconi, *Local order in surface ZDDP reaction films generated on engine parts, using EXAFS and related techniques.* Lubrication Science, 1995. **8**(1): p. 1-14.

79. Miklozic, K.T., T.R. Forbus, and H.A. Spikes, *Performance of friction modifiers on ZDDP-Generated surfaces.* Tribology Transactions, 2007. **50**(3): p. 328-335.

80. Ratoi, M., V.B. Niste, H. Alghawel, Y.F. Suen, and K. Nelson, *The impact of organic friction modifiers on engine oil tribofilms.* Rsc Advances, 2014. **4**(9): p. 4278-4285.

81. Tasdemir, H.A., M. Wakayama, T. Tokoroyama, H. Kousaka, N. Umehara, Y. Mabuchi, and T. Higuchi, *Ultra-low friction of tetrahedral amorphous diamond-like carbon (ta-C DLC) under boundary lubrication in poly alpha-olefin (PAO) with additives.* Tribology International, 2013. **65**: p. 286-294.

82. Tasdemir, H.A., M. Wakayama, T. Tokoroyama, H. Kousaka, N. Umehara, Y. Mabuchi, and T. Higuchi, *The effect of oil temperature and additive concentration on the wear of non-hydrogenated DLC coating.* Tribology International, 2014. **77**: p. 65-71.

83. Murase, A. and T. Ohmori, *TOF-SIMS study on the adsorption behavior of mixtures of a phosphite and a friction modifier onto ferrous material.* Applied Surface Science, 2003. **203**: p. 586-589.

84. Tohyama, M., T. Ohmori, and F. Ueda, *Anti-Shudder Mechanism of ATF Additives at Slip-Controlled Lock-Up Clutch.* SAE Technical Paper Series, 1999: 1999-01-3616.

85. Ingram, M., J. Noles, R. Watts, S. Harris, and H.A. Spikes, *Frictional Properties of Automatic Transmission Fluids: Part I-Measurement of Friction-Sliding Speed Behavior.* Tribology Transactions, 2011. **54**(1): p. 145-153.

86. Ingram, M., H. Spikes, J. Noles, and R. Watts, *Contact properties of a wet clutch friction material.* Tribology International, 2010. **43**(4): p. 815-821.

87. Ingram, M., J. Noles, R. Watts, S. Harris, and H.A. Spikes, *Frictional Properties of Automatic Transmission Fluids: Part II-Origins of Friction-Sliding Speed Behavior.* Tribology Transactions, 2011. **54**(1): p. 154-167.

88. Li, S., M.T. Devlin, S.H. Tersigni, T.-C. Jao, K. Yatsunami, and T.M. Cameron, *Fundamentals of Anti-shudder Durability: Part I - Clutch Plate Study.* SAE Technical Paper, 2003: 2003-01-1983.

89. Devlin, M.T., S.H. Tersigni, J. Senn, T.L. Turner, T.-C. Jao, and K. Yatsunami, *Effect of Friction Material on the Relative Contribution of Thin-Film Friction to Overall Friction in Clutches.* SAE Technical Paper Series, 2004: 2004-01-3025.

90. Nyman, P., R. Maki, R. Olsson, and B. Ganemi, *Influence of surface topography on friction characteristics.* Wear, 2006. **261**(1): p. 46-52.

91. Zhao, H.Y., A. Morina, A. Neville, J. Durham, and R. Vickerman, *Understanding Friction Behavior in Automatic Transmission Fluid LVFA Test: A New Positive Curve Parameter to Friction Coefficient Ratio Index Evaluation.* Journal of Tribology-Transactions of the Asme, 2011. **133**(2): p. 021802.

92. Zhao, H.Y., A. Neville, A. Morina, R. Vickerman, and J. Durham, *Improved Anti-shudder Performance of ATFs-Influence of a New Friction Modifier and Surface Chemistry.* Tribology International, 2012. **46**(1): p. 62-72.

93. Zhao, H.Y., A. Morina, A. Neville, and R. Vickerman, *Anti-Shudder Properties of ATFs-Investigation into Tribofilm Composition on Clutch Friction Material and Steel Surfaces and the Link to Frictional Performance.* Tribology Transactions, 2012. **55**(6): p. 782-797.

94. Derevjanik, T.S., *Detergent and Friction Modifier Effects on Metal/Metal and Clutch Material/Metal Frictional Performance.* SAE Technical Paper Series, 2001: 2001-01-1993.

95. Narita, K. and M. Priest, *Friction characteristics between metal contacting surfaces from anti-wear additives with application to metal V-belt type continuously variable transmission lubricants.* Proceedings of the Institution of Mechanical Engineers Part J-Journal of Engineering Tribology, 2007. **221**(J3): p. 195-207.

96. Narita, K. and M. Priest, *Boundary lubrication film formation from phosphorus antiwear additives with application to metal V-belt type continuously variable transmission lubricants.* Proceedings of the Institution of Mechanical Engineers Part J-Journal of Engineering Tribology, 2008. **222**(J3): p. 343-356.

97. Narita, K. and M. Priest, *Friction Characteristics and Topography of Tribofilms from Anti-Wear Additives Applied to Metal V-Belt Type CVT Fluids.* Tribology Letters, 2009. **35**(1): p. 45-56.

98. Narita, K. and M. Priest, *Friction characteristics and topography of tribofilms from antiwear additives applied to metal V-belt type CVT fluids.* Proceedings of the Asme/Stle International Joint Tribology Conference, 2008: p. 89-91.

99. Okamura, M., *Trends of metal pushing belt type CVTs.* Journal of Japanese Society of Tribologists, 2000. **45**(6): p. 423-428. (written in Japanese)

100. Fujii, T. and S. Kanehara, *Power transmitting mechanisms for, and the future of, metal pushing belt type CVTs.* Journal of Japanese Society of Tribologists, 2000. **45**(6): p. 441-448. (written in Japanese)

101. Kono, K., H. Itoh, S. Nakamura, K. Yoshizawa, and M. Osawa, *Torque Converter Clutch Slip Control System.* SAE Technical Paper Series, 1995: 950672.

102. Robinette, D., M. Grimmer, J. Horgan, J. Kennell, and R. Vykydal, *Torque Converter Clutch Optimization: Improving Fuel Economy and Reducing Noise and Vibration.* SAE International Journal of Engines, 2011. **4**(1): p. 94-105.

103. Oshidari, T., *Trends of development in CVTs and their tribology.* Journal of Japanese Society of Tribologists, 2001. **46**(3): p. 201-208. (written in Japanese)

104. Srivastava, N. and I. Haque, *A review on belt and chain continuously variable transmissions (CVT): Dynamics and control.* Mechanism and Machine Theory, 2009. **44**(1): p. 19-41.

105. Yakabe, F. and M. Yoshida, *Technical Trends and Tribological Aspects of Belt CVT.* Journal of Japanese Society of Tribologists, 2008. **53**(9): p. 574-579. (written in Japanese)

106. Ohishi, K., T. Uehara, and I. Kishigami, *Development of High Fatigue Strength Maraging Steel for CVT Belt.* SAE International, 2015: 2015-01-1102

107. Yagasaki, T., S. Hanehara, H. Aoyama, K. Ishii, and Y. Okada, *Development of Metal Pushing V-Belt for Continuously Variable Transmission - Investigation for Clearance Between Elements, Strength of Element and Strength of Ring Material.* SAE Technical Paper Series, 2003: 2003-01-0969

108. Yoshida, M., A. Ikeda, S. Takekawa, and S. Kuroda, *Improvement in wear resistance of belt-CVT pulleys by fine particle peening.* Journal of Japanese Society of Tribologists, 2002. **47**(12): p. 901-907. (written in Japanese)

109. Soyama, H., M. Shimizu, Y. Hattori, and Y. Nagasawa, *Improving the fatigue strength of the elements of a steel belt for CVT by cavitation shotless peening.* Journal of Materials Science, 2008. **43**(14): p. 5028-5030.

110. Zhang, X., K.Z. Li, H.J. Li, Y.W. Fu, and J. Fei, *Influence of compound mineral fiber on the properties of paper-based composite friction material.* Proceedings of the Institution of Mechanical Engineers Part J-Journal of Engineering Tribology, 2013. **227**(11): p. 1241-1252.

111. Society of Automotive Engineers of Japan, *JASO Standards: M349-12*. 2012.

112. Murakami, Y., J.L. Linden, J.E. Flaherty, J.W. Sprys, T.E. King, H. Kurashina, M. Furumoto, S.-i. Iwamoto, M. Kagawa, and F. Ueda, *Anti-Shudder Property of Automatic Transmission Fluids - A Study by the International Lubricants Standardization and Approval Committee (ILSAC) ATF Subcommittee.* SAE Technical Paper Series, 2000: 2000-01-1870.

113. Kalin, M. and I. Velkavrh, *Non-conventional inverse-Stribeck-curve behaviour and other characteristics of DLC coatings in all lubrication regimes.* Wear, 2013. **297**(1-2): p. 911-918.

114. Blau, P.J. and C.E. Devore, *Sliding Friction and Wear Behavior of Several Nickel Aluminide Alloys under Dry and Lubricated Conditions.* Tribology International, 1990. **23**(4): p. 226-234.

115. Sheasby, J.S., T.A. Caughlin, A.G. Blahey, and K.F. Laycock, *A Reciprocating Wear Test for Evaluating Boundary Lubrication.* Tribology International, 1990. **23**(5): p. 301-307.

116. Lin, Y.C. and J.N. Chen, *Tribological behavior of* $(Cu_{42}Zr_{42}Al_8Ag_8)_{99.5}Si_{0.5}$ *bulk metallic glass.* Wear, 2012. **280**: p. 5-14.

117. Neville, A., A. Morina, T. Haque, and Q. Voong, *Compatibility between tribological surfaces and lubricant additives - How friction and wear reduction can be controlled by surface/lube synergies.* Tribology International, 2007. **40**(10-12): p. 1680-1695.

118. Greenall, A., A. Neville, A. Morina, and M. Sutton, *Investigation of the interactions between a novel, organic anti-wear additive, ZDDP and overbased calcium sulphonate.* Tribology International, 2012. **46**(1): p. 52-61.

119. Eguchi, M. and T. Yamamoto, *Shear characteristics of a boundary film for a paper-based wet friction material: friction and real contact area measurement.* Tribology International, 2005. **38**(3): p. 327-335.

120. Shi, J. and C.R. Liu, *On predicting chip morphology and phase transformation in hard machining.* International Journal of Advanced Manufacturing Technology, 2006. **27**(7-8): p. 645-654.

121. Miyazaki, T., T. Matsumoto, and T. Yamamoto, *Effect of visco-elastic property on friction characteristics of paper-based friction materials for oil immersed clutches.* Journal of Tribology-Transactions of the Asme, 1998. **120**(2): p. 393-398.

122. Gao, H. and G.C. Barber, *Engagement of a rough, lubricated and grooved disk clutch with a porous deformable paper-based friction material.* Tribology Transactions, 2002. **45**(4): p. 464-470.

123. Ito, K., K.A. Barker, M. Kubota, and S. Yoshida, *Designing Paper Type Wet Friction Material for High Strength and Durability.* SAE Technical Paper Series, 1998: 982034.

124. Nakagawa, H., *The Influence of Fillers on Paper-Based Friction Materials Relative to Wet Clutch Slip Characteristics.* SAE Technical Paper, 1997: 970975.

125. Matsumoto, T., *A Study of the Influence of Porosity and Resiliency of a Paper-Based Friction Material on the Friction Characteristics and Heat Resistance of the Material.* SAE Technical Paper, 1993: 932924.

126. Kimura, Y. and C. Otani, *Contact and wear of paper-based friction materials for oil-immersed clutches - wear model for composite materials.* Tribology International, 2005. **38**(11-12): p. 943-950.

127. Fadley, C.S., R.J. Baird, W. Siekhaus, T. Novakov, and Bergstro.Sa, *SURFACE ANALYSIS AND ANGULAR-DISTRIBUTIONS IN X-RAY PHOTOELECTRON-SPECTROSCOPY.* Journal of Electron Spectroscopy and Related Phenomena, 1974. **4**(2): p. 93-137.

128. Beamson, G. and D. Briggs, *High Resolution XPS of Organic Polymers: The Scienta ESCA300 Database*. 1992: Wiley.

129. Briggs, D., *Surface Analysis of Polymers by XPS and Static SIMS*. Cambridge Solid State Science Series. 1998.

130. Briggs, D. and G. Beamson, *PRIMARY AND SECONDARY OXYGEN-INDUCED C1S BINDING-ENERGY SHIFTS IN X-RAY PHOTOELECTRON-SPECTROSCOPY OF POLYMERS.* Analytical Chemistry, 1992. **64**(15): p. 1729-1736.

131. Shih, P.Y., S.W. Yung, and T.S. Chin, *Thermal and corrosion behavior of P2O5-Na2O-CuO glasses.* Journal of Non-Crystalline Solids, 1998. **224**(2): p. 143-152.

132. Singh, A., R.T. Gandra, E.W. Schneider, and S.K. Biswas, *Lubricant Degradation and Related Wear of a Steel Pin in Lubricated Sliding Against a Steel Disc.* Acs Applied Materials & Interfaces, 2011. **3**(7): p. 2512-2521.

133. Singh, A., R.T. Gandra, E.W. Schneider, and S.K. Biswas, *Studies on the Aging Characteristics of Base Oil with Amine Based Antioxidant in Steel-on-Steel Lubricated Sliding.* Journal of Physical Chemistry C, 2013. **117**(4): p. 1735-1747.

134. Velkavrh, I., F. Ausserer, S. Klien, J. Brenner, P. Foret, and A. Diem, *The effect of gaseous atmospheres on friction and wear of steel-steel contacts.* Tribology International, 2014. **79**: p. 99-110.

135. Zubir, N.A., C. Yacou, J. Motuzas, X.W. Zhang, and J.C.D. da Costa, *Structural and functional investigation of graphene oxide-Fe_3O_4 nanocomposites for the heterogeneous Fenton-like reaction.* Scientific Reports, 2014. **4**.

136. Hua, W., L. Jing, H.L. Yi, X.Q. Zeng, L.B. Lv, and T.H. Ren, *The tribological behavior of diester-containing polysulfides as additives in mineral oil.* Tribology International, 2007. **40**(8): p. 1246-1252.

137. Eglin, M., A. Rossi, and N.D. Spencer, *X-ray photoelectron spectroscopy analysis of tribostressed samples in the presence of ZnDTP: a combinatorial approach.* Tribology Letters, 2003. **15**(3): p. 199-209.

138. Crobu, M., A. Rossi, F. Mangolini, and N.D. Spencer, *Chain-length-identification strategy in zinc polyphosphate glasses by means of XPS and ToF-SIMS.* Analytical and Bioanalytical Chemistry, 2012. **403**(5): p. 1415-1432.

139. Ma, W.Y., P. Yang, J.G. Li, S.Q. Li, P.C. Li, Y.C. Zhao, and N. Huang, *Immobilization of poly(MPC) brushes onto titanium surface by combining dopamine self-polymerization and ATRP: Preparation, characterization and evaluation of hemocompatibility in vitro.* Applied Surface Science, 2015. **349**: p. 445-451.

140. Jiang, S.S., S.Z. Li, L.X. Liu, L. Wang, and N. Mominou, *The tribological properties and tribochemical analysis of blends of poly alpha-olefins with neopentyl polyol esters.* Tribology International, 2015. **86**: p. 42-51.

141. Martin, J.M., C. Grossiord, K. Varlot, B. Vacher, and J. Igarashi, *Synergistic effects in binary systems of lubricant additives: a chemical hardness approach.* Tribology Letters, 2000. **8**(4): p. 193-201.

142. Nicholls, M.A., G.M. Bancroft, P.R. Norton, M. Kasrai, G. De Stasio, B.H. Frazer, and L.M. Wiese, *Chemomechanical properties of antiwear films using X-ray absorption microscopy and nanoindentation techniques.* Tribology Letters, 2004. **17**(2): p. 245-259.

143. Willermet, P.A., J.M. Pieprzak, D.P. Dailey, R.O. Carter, N.E. Lindsay, L.P. Haack, and J.E. Devries, *The Composition of Surface-Layers Formed in a Lubricated Cam Tappet Contact.* Journal of Tribology-Transactions of the Asme, 1991. **113**(1): p. 38-47.

144. Dalby, K.N., H.W. Nesbitt, V.P. Zakaznova-Herzog, and P.L. King, *Resolution of bridging oxygen signals from O 1s spectra of silicate glasses using XPS: Implications for O and Si speciation.* Geochimica Et Cosmochimica Acta, 2007. **71**(17): p. 4297-4313.

145. Guo, F., Z.Z. Zhang, W.M. Liu, F.H. Su, and H.J. Zhang, *Effect of plasma treatment of Kevlar fabric on the tribological behavior of Kevlar fabric/phenolic composites.* Tribology International, 2009. **42**(2): p. 243-249.

146. Charlier, J., V. Detalle, F. Valin, C. Bureau, and G. Lecayon, *Study of ultrathin polyamide-6,6 films on clean copper and platinum.* Journal of Vacuum Science & Technology a-Vacuum Surfaces and Films, 1997. **15**(2): p. 353-364.

147. Pereira, C., A.M. Pereira, P. Quaresma, P.B. Tavares, E. Pereira, J.P. Araujo, and C. Freire, *Superparamagnetic gamma-Fe_2O_3@SiO_2 nanoparticles: a novel support for the immobilization of [$VO(acac)_2$]*. Dalton Trans, 2010. **39**(11): p. 2842-54.

148. Titirici, M.M., A. Thomas, and M. Antonietti, *Aminated hydrophilic ordered mesoporous carbons.* Journal of Materials Chemistry, 2007. **17**(32): p. 3412-3418.

149. Shabtai, K., I. Rubinstein, S.R. Cohen, and H. Cohen, *High-resolution lateral differentiation using a macroscopic probe: XPS of organic monolayers on composite Au-SiO_2 surfaces.* Journal of the American Chemical Society, 2000. **122**(20): p. 4959-4962.

150. Darie, R.N., S. Vlad, N. Anghel, F. Doroftei, T. Tamminen, and I. Spiridon, *New PP/PLA/cellulose composites: effect of cellulose functionalization on accelerated weathering behavior (accelerated weathering behavior of new PP/PLA/cellulose composites).* Polymers for Advanced Technologies, 2015. **26**(8): p. 941-952.

151. Ross, S.D., *Inorganic infrared and Raman spectra*. McGraw-Hill European chemistry series. 1972, London, New York,: McGraw-Hil.

152. Nakanishi, K.j., *Infrared absorption spectroscopy, practical*. 1962, San Francisco,: Holden-Day.

153. Roeges, N.P.G., *A guide to the complete interpretation of infrared spectra of organic structures*. 1994, Chichester ; New York: Wiley.

154. Colthup, N.B., L.H. Daly, and S.E. Wiberley, *Introduction to infrared and Raman spectroscopy*. 2d ed. 1975, New York: Academic Press.

155. Nakamoto, K., *Infrared and Raman spectra of inorganic and coordination compounds*. 6th ed. 2009, Hoboken, N.J.: Wiley.

156. Efimov, A.M., *IR fundamental spectra and structure of pyrophosphate glasses along the 2ZnO P_2O_5-2Me_2O P_2O_5 join (Me being Na and Li).* Journal of Non-Crystalline Solids, 1997. **209**(3): p. 209-226.

157. Bargar, J.R., J.D. Kubicki, R. Reitmeyer, and J.A. Davis, *ATR-FTIR spectroscopic characterization of coexisting carbonate surface complexes on hematite.* Geochimica Et Cosmochimica Acta, 2005. **69**(6): p. 1527-1542.

158. Upritchard, H.G., J. Yang, P.J. Bremer, I.L. Lamont, and A.J. McQuillan, *Adsorption of Enterobactin to Metal Oxides and the Role of Siderophores in Bacterial Adhesion to Metals.* Langmuir, 2011. **27**(17): p. 10587-10596.

159. Lefevre, G., *In situ Fourier-transform infrared spectroscopy studies of inorganic ions adsorption on metal oxides and hydroxides.* Advances in Colloid and Interface Science, 2004. **107**(2-3): p. 109-123.

160. Li, W.J., S.Y. Gao, T.F. Liu, L.W. Han, Z.J. Lin, and R. Cao, *In Situ Growth of Metal-Organic Framework Thin Films with Gas Sensing and Molecule Storage Properties.* Langmuir, 2013. **29**(27): p. 8657-8664.

161. Elzinga, E.J. and R. Kretzschmar, *In situ ATR-FTIR spectroscopic analysis of the co-adsorption of orthophosphate and Cd(II) onto hematite.* Geochimica Et Cosmochimica Acta, 2013. **117**: p. 53-64.

162. Guan, X.H., C. Shang, and G.H. Chen, *ATR-FTIR investigation of the role of phenolic groups in the interaction of some NOM model compounds with aluminum hydroxide.* Chemosphere, 2006. **65**(11): p. 2074-2081.

163. Ebbesen, S.D., B.L. Mojet, and L. Lefferts, *In situ attenuated total reflection infrared (ATR-IR) study of the adsorption of NO_2^-, NH_2OH, and NH_4^+ on Pd/Al_2O_3 and Pt/Al_2O_3.* Langmuir, 2008. **24**(3): p. 869-879.

164. Hug, S.J., *In situ Fourier transform infrared measurements of sulfate adsorption on hematite in aqueous solutions.* Journal of Colloid and Interface Science, 1997. **188**(2): p. 415-422.

165. Miller, F.A. and C.H. Wilkins, *INFRARED SPECTRA AND CHARACTERISTIC FREQUENCIES OF INORGANIC IONS - THEIR USE IN QUALITATIVE ANALYSIS.* Analytical Chemistry, 1952. **24**(8): p. 1253-1294.

166. Corbridge, D.E.C. and E.J. Lowe, *THE INFRA-RED SPECTRA OF SOME INORGANIC PHOSPHORUS COMPOUNDS.* Journal of the Chemical Society, 1954(FEB): p. 493-502.

167. Hunt, J.M., M.P. Wisherd, and L.C. Bonham, *INFRARED ABSORPTION SPECTRA OF MINERALS AND OTHER INORGANIC COMPOUNDS.* Analytical Chemistry, 1950. **22**(12): p. 1478-1497.

168. Piras, F.M., A. Rossi, and N.D. Spencer, *In situ Attenuated Total Reflection (ATR) spectroscopic analysis of tribological phenomena*. Boundary and Mixed Lubrication: Science and Applications, ed. D. Dowson, et al. Vol. 40. 2002, Amsterdam: Elsevier Science Bv : p. 199-206.

169. Oblonsky, L.J. and T.M. Devine, *A SURFACE-ENHANCED RAMAN-SPECTROSCOPIC STUDY OF THE PASSIVE FILMS FORMED IN BORATE BUFFER ON IRON, NICKEL, CHROMIUM AND STAINLESS-STEEL.* Corrosion Science, 1995. **37**(1): p. 17-41.

170. Gu, R.A., P.G. Cao, J.L. Yao, B. Ren, Y. Xie, B.W. Mao, and Z.Q. Tian, *Surface Raman spectroscopic studies on the adsorption of pyridine at bare iron electrodes.* Journal of Electroanalytical Chemistry, 2001. **505**(1-2): p. 95-99.

171. Roonasi, P. and A. Holmgren, *An ATR-FTIR study of carbonate sorption onto magnetite.* Surface and Interface Analysis, 2010. **42**(6-7): p. 1118-1121.

172. Westerfield, C. and S. Agnew, *IR Study of the Chemistry of Boundary Lubrication with High-Temperature and High-Pressure Shear*. Wear, 1995. **181**: p. 805-809.

173. Cann, P.M. and H.A. Spikes, *In Lubro Studies of Lubricants in Ehd Contacts Using Ftir Absorption-Spectroscopy.* Tribology Transactions, 1991. **34**(2): p. 248-256.

174. Sasaki, K., N. Inayoshi, and K. Tashiro, *In Situ FTIR-ATR Observation of Phase Transition Behavior of n-Alkane Molecules Induced by Friction Motion on a Metal Interface.* Journal of Physical Chemistry C, 2009. **113**(8): p. 3287-3291.

175. Mangolini, F., A. Rossi, and N.D. Spencer, *Chemical Reactivity of Triphenyl Phosphorothionate (TPPT) with Iron: An ATR/FT-IR and XPS Investigation.* Journal of Physical Chemistry C, 2011. **115**(4): p. 1339-1354.

176. Florio, G.M., T.S. Zwier, E.M. Myshakin, K.D. Jordan, and E.L. Sibert, *Theoretical modeling of the OH stretch infrared spectrum of carboxylic acid dimers based on first-principles anharmonic couplings.* Journal of Chemical Physics, 2003. **118**(4): p. 1735-1746.

177. Wikipedia. *Continuously variable transmission*. [cited 2016 6th July]; Available from: https://en.wikipedia.org/wiki/Continuously_variable_transmission.

178. Wikipedia. *Torque converter*. [cited 2016 6th July]; Available from: https://ja.wikipedia.org/wiki/%E3%83%88%E3%83%AB%E3%82%AF%E3%82%B3%E3%83%B3%E3%83%90%E3%83%BC%E3%82%BF.

179. Doig, M., C.P. Warrens, and P.J. Camp, *Structure and Friction of Stearic Acid and Oleic Acid Films Adsorbed on Iron Oxide Surfaces in Squalane.* Langmuir, 2014. **30**(1): p. 186-195.

180. Sahoo, R.R. and S.K. Biswas, *Frictional response of fatty acids on steel.* Journal of Colloid and Interface Science, 2009. **333**(2): p. 707-718.

181. Makowska, M., C. Kajdas, and M. Gradkowski, *Interactions of n-hexadecane with 52100 steel surface under friction conditions.* Tribology Letters, 2002. **13**(2): p. 65-70.

182. Tosatti, S., R. Michel, M. Textor, and N.D. Spencer, *Self-assembled monolayers of dodecyl and hydroxy-dodecyl phosphates on both smooth and rough titanium and titanium oxide surfaces.* Langmuir, 2002. **18**(9): p. 3537-3548.

183. Hone, D.C., B.H. Robinson, D.C. Steytler, R.W. Glyde, and J.R. Galsworthy, *Mechanism of acid neutralization by overbased colloidal additives in hydrocarbon media.* Langmuir, 2000. **16**(2): p. 340-346.

184. Heinze, T. and T. Liebert, *Unconventional methods in cellulose functionalization.* Progress in Polymer Science, 2001. **26**(9): p. 1689-1762.

185. Pavan, F.A., M.S.P. Francisco, R. Landers, and Y. Gushikem, *Adsorption of phosphoric acid on niobium oxide coated cellulose fiber: Preparation, characterization and ion exchange property.* Journal of the Brazilian Chemical Society, 2005. **16**(4): p. 815-820.

186. Edgar, K.J., C.M. Buchanan, J.S. Debenham, P.A. Rundquist, B.D. Seiler, M.C. Shelton, and D. Tindall, *Advances in cellulose ester performance and application.* Progress in Polymer Science, 2001. **26**(9): p. 1605-1688.

187. Ataei, S., R. Yahya, S.N. Gan, and A. Hassan, *Study of Thermal Decomposition Kinetics of Palm Oleic Acid-Based Alkyds and Effect of Oil Length on Thermal Stability.* Journal of Polymers and the Environment, 2012. **20**(2): p. 507-513.

188. Voigts, F., F. Bebensee, S. Dahle, K. Volgmann, and W. Maus-Friedrichs, *The adsorption of CO_2 and CO on Ca and CaO films studied with MIES, UPS and XPS.* Surface Science, 2009. **603**(1): p. 40-49.

189. Tan, K.H., H. Awala, R.R. Mukti, K.L. Wong, B. Rigaud, T.C. Ling, H.A. Aleksandrov, I.Z. Koleva, G.N. Vayssilov, S. Mintova, and E.P. Ng, *Inhibition of Palm Oil Oxidation by Zeolite Nanocrystals.* Journal of Agricultural and Food Chemistry, 2015. **63**(18): p. 4655-4663.

190. Macian, V., B. Tormos, Y.A. Gomez, and J.M. Salavert, *Proposal of an FTIR Methodology to Monitor Oxidation Level in Used Engine Oils: Effects of Thermal Degradation and Fuel Dilution.* Tribology Transactions, 2012. **55**(6): p. 872-882.

191. Ratoia, M., C. Bovington, and H. Spikes, *In situ study of metal oleate friction modifier additives.* Tribology Letters, 2003. **14**(1): p. 33-40.

192. Yablon, D.G., P.H. Kalamaras, D.E. Deckman, and M.N. Webster, *Atomic force microscopy and Raman spectroscopy investigation of additive interactions responsible for anti-wear film formation in a lubricated contact.* Tribology Transactions, 2006. **49**(1): p. 108-116.

193. Yang, L.Q., A. Neville, A. Brown, P. Ransom, and A. Morina, *Effect of Lubricant Additives on the WDLC Coating Structure When Tested in Boundary Lubrication Regime.* Tribology Letters, 2015. **57**(2). *in press*

194. Mangolini, F., A. Rossi, and N.D. Spencer, *Tribochemistry of Triphenyl Phosphorothionate (TPPT) by In Situ Attenuated Total Reflection (ATR/FT-IR) Tribometry.* Journal of Physical Chemistry C, 2012. **116**(9): p. 5614-5627.

195. Rossi, A., M. Eglin, F.M. Piras, K. Matsumoto, and N.D. Spencer, *Surface analytical studies of surface-additive interactions, by means of in situ and combinatorial approaches.* Wear, 2004. **256**(6): p. 578-584.